Exploring the Antimicrobial and Antifouling Properties of Secondary Metabolites Produced by *Serratia marcescens*

by

Tanya Lee Clements

Dissertation presented for the degree of Doctor of Philosophy in the Faculty of Science at Stellenbosch University

Promoter: Prof Wesaal Khan

Co-Promoter: Dr Thando Ndlovu

Faculty of Science

Department of Microbiology

March 2021

DECLARATION

By submitting this dissertation electronically, I declare that the entirety of the work contained therein is my own, original work, that I am the sole author thereof (save to the extent explicitly otherwise stated), that reproduction and publication thereof by Stellenbosch University will not infringe any third party rights and that I have not previously in its entirety or in part submitted it for obtaining any qualification.

This dissertation includes two original papers published in peer-reviewed journals, one South African patent application and one unpublished publication. The development and writing of the papers (published and unpublished) were the principal responsibility of myself and, for each of the chapters where this is not the case, the authors are indicated in each research chapter.

March 2021

Signature: …… Date: ……

SUMMARY

The emergence of multi- (MDR) and extensive drug-resistant (XDR) bacterial and fungal pathogens constitutes a major public health concern and has led to the prioritisation of research into the discovery of novel bioactive compounds. Microbial secondary metabolites serve as promising alternative antimicrobial and antifouling agents, with *Serratia* species representing a potential untapped source of novel and structurally diverse bioactive compounds. **Chapter one** (abbreviated version published in Applied Microbiology and Biotechnology) focused on the classification, biosynthesis, production and application of secondary metabolites produced by *Serratia* species. The primary focus of this dissertation was subsequently to identify secondary metabolites produced by environmental *Serratia* species that display antimicrobial and antifouling activity, and elucidate the secondary metabolic profiles and chemical structures of these compounds.

In **Chapter two** (published in Microbiological Research), various environmental sources were screened for *Serratia* isolates capable of biosurfactant production during secondary metabolism. A total of 569 presumptive *Serratia* strains were subsequently isolated from wastewater treatment plants, an oil refinery, winery and olive oil estates, river water and rainwater samples. Preliminary screening methods (i.e. oil spreading method, emulsification assay and surface tension measurements) and molecular typing identified twenty-two pigmented (*n* = 11; P1 to P11) and non-pigmented (*n* = 11; NP1 to NP11) *Serratia marcescens* (*S. marcescens*) presumptive biosurfactant producers. Based on the physico-chemical analysis, molecular analysis and preliminary antimicrobial testing, ultra-performance liquid chromatography (UPLC) linked to electrospray ionisation mass spectrometry (ESI-MS) was used to identify the secondary metabolites produced by *S. marcescens* strains P1, NP1 and NP2. Strains P1 and NP1 produced serrawettin W1 homologues (also known as serratamolides) as well as prodigiosin (P1) and glucosamine derivative A (NP1). In contrast, serrawettin W2 analogues were predominantly identified in the NP2 extract. Antimicrobial analysis then indicated that the P1 and NP1 crude extracts exhibited broad-spectrum antimicrobial activity against opportunistic pathogens, such as MDR *Pseudomonas aeruginosa* (*P. aeruginosa*), methicillin-resistant *Staphylococcus aureus* and a clinical *Cryptococcus neoformans* strain. While an XDR *Acinetobacter baumannii* strain was susceptible to the NP2 extract, a narrower spectrum of antimicrobial activity was observed in comparison to the other two strains. The compounds produced by the P1 (pigmented) and NP1 (non-pigmented) *S. marcescens* strains could thus serve as a promising source of antimicrobial agents for therapeutic application.

An integrated approach involving the use of reverse-phase high-performance liquid chromatography (RP-HPLC), ESI-MS, UPLC linked to tandem mass spectrometry (UPLC-MS^e) and molecular networking (using the Global Natural Products Social molecular network platform), was applied in **Chapter three** to unravel the secondary metabolic profiles and structures of the bioactive compounds produced by *S. marcescens* P1 and NP1. The mass spectrometry-based molecular

networking guided the structural elucidation of 18 compounds for the P1 strain (including 6 serratamolides, 10 glucosamine derivatives, prodigiosin and serratiochelin A) and 15 compounds for the NP1 strain (including 8 serratamolides, 6 glucosamine derivatives and serratiochelin A) using the UPLC-MS^e fragmentation profiles. It was proposed that the serratamolide homologues consisted of two L-serine residues (cyclic or open-ring) linked to two fatty acyl chains (lengths of C_{10}, C_{12} or $C_{12:1}$). The glucosamine derivative homologues consisted of four residues, including glucose / hexose, valine, butyric acid (or oxo-hexanoic acid for derivative at *m/z* 627.4192) and a saturated or unsaturated fatty acyl chain (lengths of C_{13} to C_{17}). The putative structures of a novel open-ring serratamolide homologue and eight novel glucosamine derivative congeners were described. The minimum inhibitory and bactericidal concentrations revealed that prodigiosin exhibited potent activity against *Enterococcus faecalis* (*E. faecalis*), followed by glucosamine derivative A and serratamolides A, B and C. The integrated approach thus provided insight into the secondary metabolic profile and structures of novel congeners produced by the *S. marcescens* strains.

In **Chapter four**, the biofilm disruption and antiadhesive potential of the P1 and NP1 crude extracts was evaluated using the Minimum Biofilm Eradication Concentration (MBEC) Assay® against single- and dual-species biofilms. Plate count and viability-quantitative polymerase chain reaction indicated that the P1 and NP1 extracts significantly reduced (≥ 2 logs) biofilms formed by *E. faecalis*, while the single-species *P. aeruginosa* biofilm was more susceptible (≥ 2 logs) to the P1 extract. The P1 and NP1 extracts significantly reduced the dual-species *P. aeruginosa* and *E. faecalis* biofilm; however, in comparison to the single-species *E. faecalis* biofilm, increased concentrations of both extracts were required to reduce *E. faecalis* by ≥ 2 logs. Moreover, pre-absorption of the P1 and NP1 extracts (at 50 mg/mL) onto the pegs of the MBEC Assay® reduced the adhesion of mono-culture *P. aeruginosa* and *E. faecalis* cells by ≥ 80% based on cell counts and gene copies. In contrast, for the co-culture experiments, significant reductions (≥ 90% based on cell counts and gene copies) in the adhesion of only *E. faecalis* to the P1 and NP1 coated pegs were observed. Serratamolides and glucosamine derivatives present in the P1 and NP1 extracts were subsequently covalently immobilised onto high-density polyethylene (HDPE) and polyvinyl chloride (PVC) discs. The P1 and NP1 coated HDPE reduced the adhesion of *P. aeruginosa* cells by ≥ 87% based on plate counts and ≥ 64% based on gene copies, while the *E. faecalis* cells were reduced by ≥ 96% based on plate counts and ≥ 87% based on gene copies. The P1 and NP1 coated PVC also effectively reduced the adhesion of *P. aeruginosa* cells by ≥ 81% based on plate counts and ≥ 99% based on gene copies however, minor reductions in *E. faecalis* adhesion were observed. While it is recommended that the antifouling potential of the biomaterials be tested against mixed microbial communities and that the serratamolides and glucosamine derivatives be immobilised onto various other piping materials frequently used in the water, food and medical industries; this preliminary analysis indicates that the P1 and NP1 extracts could potentially be applied as a preventative strategy to delay the onset of biofilm formation on polymeric materials.

OPSOMMING

Die ontstaan van multi- (MDR) en ekstensiewe (XDR) antibiotika weerstandige bakterieë en swamme is ‘n groot bekommernis vir gemeenskapsgesondheid. Dit het dus gelei tot die prioritisering van navorsing wat fokus op die ontdekking van nuwe bio-aktiewe verbindings. Sekondêre metaboliete van mikrobiese oorsprong is belowende alternatiewe antimikrobiese en antibesoedelings verbindings en *Serratia* spesies dien as ’n ongetapte bron van nuwe en struktureel diverse bio-aktiewe verbindings. **Hoofstuk een** (verkorte weergawe gepubliseer in “Applied Microbiology and Biotechnology”) het dus op die klassifikasie, biosintese, produksie en toepassing van sekondêre metaboliete wat deur *Serratia* spesies geproduseer word, gefokus. Daaropvolgend was die primêre doel van hierdie dissertasie om die sekondêre metaboliete wat deur omgewingstamme van *Serratia* spesies geproduseer word, en antimikrobiese en antibesoedeling aktiwiteit toon, te identifiseer, om die stamme se sekondêre metaboliet profiele te bepaal en die chemiese samestelling van die metaboliete te ontleed.

In **Hoofstuk twee** (gepubliseer in “Microbiological Research”), is verskeie bronne in die omgewing ondersoek vir *Serratia* isolate wat biosurfaktante tydens sekondêre metabolisme kan produseer. In totaal is 569 voornemende *Serratia* stamme uit water van riool aanlegte, ’n olieraffinadery, wyn- en olyf-plase, asook rivier- en reënwater, geïsoleer. Voorlopige toetse (soos die olieverspreidingstoets, emulsifikasie toets en oppervlak spanning metings) en molekulêre tipering het twee-en-twintig gepigmenteerde (*n* = 11; P1 tot P11) en ongepigmenteerde (*n* = 11; NP1 tot NP11) *Serratia marcescens* (*S. marcescens*) stamme, wat moontlike biosurfaktant produseerders is, geïdentifiseer. Na aanleiding van die fisiese en chemiese analises, die molekulêre analises en voorlopige antimikrobiese toetse, is ultraprestasie vloeistofchromatografie (UPVC) wat aan elektronsproei ionisasie massaspektrometrie (ESI-MS) gekoppel is, gebruik om die voornemende sekondêre metaboliete wat deur *S. marcescens* P1, NP1 en NP2 geproduseer word, te identifiseer. Die P1 stam het serrawettin W1 homoloë (wat ook bekend staan as serratamoliedes) en prodigiosien geproduseer, terwyl NP1 serrawettin W1 homoloë en glukosamien afstammelinge geproduseer het. In teenstelling hiermee, is serrawettin W2 analoë hoofsaaklik in die NP2 ekstrakte geïdentifiseer. Die antimikrobiese analises het aangedui dat die P1 en NP1 kru-ekstrakte breë spektrum antimikrobiese aktiwiteit teen opportunistiese patogene soos *Pseudomonas aeruginosa* (*P. aeruginosa*), metisillien weerstandige *Staphylococcus aureus* en ‘n kliniese *Cryptococcus neoformans* stam gehad het. Daarteenoor was ’n XDR *Acinetobacter baumannii* stam sensitief vir die NP2 ekstrak, waarvoor ‘n nouer spektrum van antimikrobiese aktiwiteit opgemerk is. Die verbindings wat deur die P1 (gepigmenteerd) en NP1 (ongepigmenteerd) *S. marcescens* stamme geproduseer word, kan dus as belowende bron van antimikrobiese middels vir terapeutiese verbruik dien.

'n Geïntegreerde benadering wat omgekeerde fase hoëprestasie vloeistofchromatografie (OF-HPVC), ESI-MS, UPVC gekoppel aan tandem massaspektrometrie (UPVC-MS^e) en molekulêre netwerking (deur gebruik van die "Global Natural Products Social" molekulêre netwerk) insluit, is toegepas in **Hoofstuk drie** om die sekondêre metaboliese profiel en die strukture van die bio-aktiewe verbindings wat deur *S. marcescens* P1 en NP1 geproduseer word, te ontrafel. Die massaspektrometrie gebaseerde molekulêre netwerking het die ontleding van 18 verbindings wat deur P1 geproduseer word (insluitend 6 serratamoliedes, 10 glukosamien verwantes, prodigiosien en serratiochelin) en 15 verbindings wat deur NP1 geproduseer word (insluitend 8 serratamoliedes, 6 glukosamien verwantes, prodigiosien en serratiochelin) begelei met die gebruik van die UPVC-MS^e fragmentasie profiele. Dit is voorgestel dat die serratamoliede homoloë uit twee L-serienreste (siklies of oop-ring) wat aan twee vet asielkettings (met lengtes van C_{10}, C_{12} en $C_{12:1}$) gekoppel is, bestaan. Dit is ook voorgestel dat die glukosamien verwante homoloë uit vier reste wat glukose/heksose, valien, bottersuur (of okso-heksanoësuur vir die verwante verbinding by m/z 627.4192) en 'n versadigde of onversadigde vet asielketting (met lengtes van C_{13} tot C_{17}), bestaan. Die voorlopige struktuur van 'n nuwe oop-ring serratamolied homoloog en agt nuwe glukosamine verwante kongenere is ook beskryf. Die minimum inhibitoriese en bakterisidiese konsentrasie is bepaal en het aangedui dat prodigiosien kragtige aktiwiteit teen *Enterococcus faecalis* (*E. faecalis*) toon, gevolg deur glukosamien verwante verbinding A en die serratamolieded (A, B en C). Die geïntegreerde benadering het dus insig gelewer aangaande die sekondêre metaboliese profiel en die strukture van die nuwe kongenere wat deur *S. marcescens* stamme geproduseer word.

In **Hoofstuk vier** is die vermoë van P1 en NP1 om biofilms af te breek en die anti-aanhegtings potensiaal van hierdie kru-ekstrakte geëvalueer deur gebruik te maak van die "Minimum Biofilm Eradication Concentration (MBEC) Assay®" op enkel spesie en tweeledige biofilms. Plaattellings en lewensvatbaarheid-kwantitatiewe polimerase kettingreaksie analises het aangedui dat die P1 en NP1 ekstrakte biofilms wat deur *E. faecalis* gevorm is, beduidend afgebreek het (≥ 2 log vermindering), terwyl die enkel spesie biofilm wat deur *P. aeruginosa* gevorm is, meer sensitief (≥ 2 log vermindering) was vir die P1 ekstrak. Die P1 en NP1 ekstrakte het die tweeledige biofilm wat uit *P. aeruginosa* en *E. faecalis* bestaan beduidend verminder, maar vir die biofilm wat slegs uit *E. faecalis* bestaan, moes hoër konsentrasies van beide ekstrakte gebruik word om *E. faecalis* met ≥ 2 logs te verminder. Verder het die absorpsie van die P1 en NP1 ekstrakte (teen 50 mg/mL) aan die penne van die "MBEC Assay®", die aanhegting van die monokultuur *P. aeruginosa* en *E. faecalis* selle met 80% verminder na aanleiding van die seltellings en geen kopieë wat verkry is. In teenstelling hiermee, vir die tweeledige kultuur eksperimente, is daar 'n beduidende vermindering (≥ 90% gebaseer op seltellings en geen kopieë) in die aanhegting van die *E. faecalis* selle aan die penne wat met die P1 en NP1 ekstrakte bedek is, opgemerk. Serratamoliede en glukosamien verwante verbindings wat in die P1 en NP1 ekstrakte voorgekom het, is kovalent geïmmobiliseer op hoë digtheid poli-etileen (HDPE) en poliviniel chloried (PVC) skyfies. Die P1 en NP1 ekstrakte wat

op die HDPE skyfies aangebring is, het die aanhegting van die *P. aeruginosa* selle met ≥ 87% (plaattellings) en ≥ 64% (geen kopieë) verminder, terwyl die aanhegting van die *E. faecalis* selle met ≥ 96% (plaattellings) en ≥ 87% (geen kopieë) verminder is. Die P1 en NP1 ekstrakte wat op die PVC skyfies aangebring is, het die aanhegting van die *P. aeruginosa* selle met ≥ 81% (plaattellings) en ≥ 99% (geen kopieë) verminder, maar vir *E. faecalis* is daar slegs ‘n minimale vermindering van die selle opgemerk. Terwyl dit aanbeveel word dat biomateriale getoets moet word vir antibesoedeling potensiaal teen gemengde mikrobiese gemeenskappe en dat serratamoliede en glukosamien verwante verbindings geïmmobiliseer moet word op materiaal wat gebruik word in die water, kos en mediese industrie, wys hierdie voorlopige resultate ook dat die P1 en NP1 ekstrakte aangewend kan word as ’n voorkomings maatreël wat moontlik die vorming van biofilms op polimeriese materiaal kan vertraag.

ACKNOWLEDGEMENTS

I would like to express my sincere gratitude to my supervisor, **Prof. Wesaal Khan**, for your invaluable knowledge, guidance and motivation throughout my postgraduate studies. Your passion and drive for microbiology has been such an inspiration to me throughout my time in your laboratory. You have been a great mentor and without whom, this journey would not have been possible.

I would also like to express my gratitude and appreciation to my co-supervisor, **Dr. Thando Ndlovu**, for your continued guidance, support and enthusiasm during my postgraduate studies.

I would like to thank **Prof. Marina Rautenbach** for your enthusiasm, knowledge and guidance in the analytical biochemistry sections of this dissertation.

I would like to thank **Prof. Sehaam Khan** for your support and guidance during my postgraduate studies.

Thank you to my past and present **colleagues in the Water Resource Laboratory** for your continued support and friendship throughout my studies. I consider myself extremely fortunate to have met and worked with such wonderful people.

To my fiancé **Kevin Decker**, words can't express how grateful I am for your immense love, understanding and motivation throughout my studies. Thank you for always being my sounding board and supporting me when I needed you the most.

A special thanks to my parents, **Sandy and Zane Clements**, for your encouragement and love during my studies. Thank you for always believing in me and supporting my decisions to pursue my passion. To my sister, **Monica Clements**, thank you for your continued support and inspiring me to pursue a career in science.

Thank you to the **Department of Microbiology at Stellenbosch University** for accommodating me during my postgraduate studies.

Thank you to the **National Research Foundation** for financial assistance in the form of a scholarship during my postgraduate studies and for travel funding for me to attend national and international conferences.

TABLE OF CONTENTS

LIST OF ABBREVIATIONS AND ACRONYMS

$[M+H]^+$	singly charged protonated ion species
$[M+K]^+$	singly charged potassium adduct
$[M+Na]^+$	singly charged sodium adduct
ABF	analysis base file
ACP	acyl carrier protein
Amu	atomic mass units
APTES	3-triethoxysilylpropan-1-amine
ATCC	american type culture collection
ATP	adenosine triphosphate
ATR-FTIR	attenuated total reflectance fourier transform infrared
BCYE	buffered charcoal yeast extract
BDL	below the detection limit
BLAST	basic local alignment search tool
BSE-EDX	backscattered electron imaging-energy dispersive X-ray spectroscopy
CAF	central analytical facility
CDC	centres for disease control and prevention
CFU	colony forming units
CLSM	confocal laser scanning microscopy
CT	caprylate-thallous
Da	daltons
DMSO	dimethyl sulfoxide
DNA	deoxyribonucleic acid
E_{24}	emulsification index
eDNA	extracellular DNA
EI	emulsification index
EMA-qPCR	ethidium monoazide bromide quantitative polymerase chain reaction
EPS	extracellular polymeric substance
ESI-MS	electrospray ionisation mass spectrometry
GNPS	global natural products social molecular network
HDPE	high-density polyethylene
HPLC	high performance liquid chromatography
HRMS	high resolution mass spectrometry
LC	liquid chromatography
LC-MS	liquid chromatography-mass spectrometry
Lys-PG	lysylphosphatidylglycerol
m/z	mass/charge ratio
MAP	2-methyl-3-n-amyl-pyrrole
MBC	minimum bactericidal concentration
MBEC	minimum biofilm eradication concentration
MDR	multidrug-resistant
mgf	mascot generic format
MHA	mueller hinton agar
MHB	mueller hinton broth
MIC	minimum inhibitory concentration
mN/m	millinewton per meter
MRSA	methicillin-resistant *Staphylococcus aureus*
MS	mass spectrometry
MS/MS	tandem mass spectrometry
n.s	not specified
n/a	not applicable
NA	nutrient agar
NCBI	national centre for biotechnological information
NMR	nuclear magnetic resonance

NP	non-pigmented
NRPS	non-ribosomal peptide synthetase
OD	optical density
ORF	open reading frame
OSMAC	one strain many compounds
P	pigmented
PCP	peptidyl carrier protein
PCR	polymerase chain reaction
PG	phosphatidylglycerol
PKS	polyketide synthases
ppm	parts per million
PPTase	40-phosphopantetheinyl transferase
PVC	polyvinyl chloride
rRNA	ribosomal ribonucleic acid
RP-HPLC	reverse phase-high performance liquid chromatography
Rt	retention time
SEM	scanning electron microscopy
TAE	tris/acetate/ethylenediamine-tetraacetic acid
TFA	trifluoroacetic acid
TOF	time-of-flight
$TSAYE_{0.6\%}$	tryptone soy agar supplemented with 6 g/L yeast extract
$TSBYE_{0.6\%}$	tryptone soy broth supplemented with 6 g/L yeast extract
UPLC	ultra-performance liquid chromatography
$UPLC\text{-}MS^{e}$	ultra-performance liquid chromatography coupled to tandem mass spectrometry
WHO	world health organisation
WWTP	wastewater treatment plant
XDR	extensive drug-resistant
XTT	tetrazolium salt

Chapter 1:

Literature Review

An abbreviated version of the literature review was published in Applied Microbiology and Biotechnology (2019), Volume 103: pages 589-602

(This chapter is compiled in the format of Applied Microbiology and Biotechnology and UK spelling is employed)

1.1. General Introduction

Biosurfactants play important physiological roles in cellular metabolism, motion and the defence mechanisms of microorganisms (Banat et al. 2014). Accordingly, genera, such as *Acinetobacter, Alcanivorax, Arthrobacter, Bacillus, Candida, Corynebacterium, Flavobacterium, Lactobacillus, Mycobacterium, Nocardia, Pseudomonas, Rhodococcus, Rhodotorula, Serratia, Streptomyces* and *Thiobacillus*, amongst others, secrete various classes of biosurfactants as secondary metabolites (Rahman and Gakpe 2008; Zhang et al. 2012; Santos et al. 2016). The production of biosurfactants by microorganisms is often triggered by the presence of hydrophobic substrates and aids in the survival of these microorganisms in nutrient poor or highly contaminated environments (Bodour et al. 2003; Silva et al. 2014). This is achieved by increasing the bioavailability of nutrients, thus promoting the uptake and metabolism of less soluble substrates (Fiechter 1992). Furthermore, it has been hypothesised that anionic biosurfactants are able to protect microbial cells by forming complexes with positively charged toxic heavy metals present in the environment (Mulligan et al. 2001; Ron and Rosenberg 2001). Therefore, biosurfactant producing microorganisms are routinely isolated from highly contaminated sites, such as metal or hydrocarbon contaminated soil and water environments, and wastewater treatment plants (Bodour et al. 2003; Ndlovu et al. 2016).

Of the numerous biosurfactant producing genera isolated from different environments, biosurfactants produced by members of the *Serratia* genus are gaining increased scientific interest as they have been shown to display emulsification-, surface-, antifouling-, antitumor- and antimicrobial activity (Escobar-Díaz et al. 2005; Dusane et al. 2011; Nalini and Parthasarathi 2014; Su et al. 2016). They are also able to modify the hydrophobicity of the cell surface, which plays an important role in the adhesion of these bacteria to various surfaces and contributes to enhancing the surface spreading of bacteria in nutrient poor environments (Bar-Ness et al. 1988; Wei et al. 2004; Matsuyama et al. 2011; Su et al. 2016). Various biosurfactant producing *Serratia marcescens* (*S. marcescens*), *Serratia rubidaea* (*S. rubidaea*) and *Serratia surfactantfaciens* (*S. surfactantfaciens*) strains as well as a *Serratia liquefaciens* (*S. liquefaciens*) strain (recently reclassified as a *S. marcescens* strain) have subsequently been isolated from hydrocarbon contaminated soil and rhizosphere soil, surface water, marine environments and wastewater treatment plants (Matsuyama et al. 1985, 1990; Lindum et al. 1998; Anyanwu et al. 2010; Dusane et al. 2011; Nalini and Parthasarathi 2013, 2014; Ndlovu et al. 2016; Su et al. 2016; Almansoory et al. 2017).

Serratia species predominantly produce various glycolipid and lipopeptide biosurfactants, which have been reported to display antibacterial, antifungal and antiprotozoal activity (Desai and Banat 1997; Dusane et al. 2011; Kadouri and Shanks 2013; Su et al. 2016; Ganley et al. 2018). In addition, glycolipids produced by *Serratia* species display biofilm disrupting and antiadhesive activity

against bacterial and fungal strains (Dusane et al. 2011). The glycolipids and lipopeptides produced by this genus are thus of interest due to their potential biomedical and therapeutic applications (Cameotra and Makkar 2004). Moreover, the robustness and environmentally friendly nature of biosurfactant compounds in general allows for several potential applications in a number of different industrial fields, such as the petroleum, agricultural, food, cosmetic and pharmaceutical industries (Aparna et al. 2012).

The focus of the current study was to identify environmental *Serratia* species that produce antimicrobial secondary metabolites, elucidate their metabolic profiles and metabolite structures, and apply these bioactive compounds as antifouling and biofilm disrupting agents. In the current study, this was achieved by collecting various environmental water samples, and isolating and screening for *Serratia* spp. capable of producing secondary metabolites with broad-spectrum antimicrobial activity and subjecting the crude extracts to ultra-performance liquid chromatography (UPLC) coupled to electrospray ionisation mass spectrometry (ESI-MS) to detect and putatively identified the bioactive secondary metabolites. An integrated approach involving reverse-phase high performance liquid chromatography (RP-HPLC), ESI-MS, ultra-performance liquid chromatography coupled to tandem mass-spectrometry (UPLC-MS^e) and mass spectrometry-based molecular networking was used to identify secondary metabolites and elucidate the putative structures of various congeners produced by pigmented (P1) and non-pigmented (NP1) *S. marcescens* strains. In addition, the susceptibility of a clinical *Enterococcus faecalis* (*E. faecalis*) strain to fractions collected during RP-HPLC analysis was evaluated using disc diffusion assays (all fractions). Broth microdilution assays were also used to determine the minimum inhibitory concentration (MIC) and minimum bactericidal concentration (MBC) of selected fractions. Thereafter, the biofilm disrupting and antiadhesive potential of the crude extracts produced by *S. marcescens* P1 and NP1 strains was investigated against single- and dual-species biofilms of *E. faecalis* S1 and *Pseudomonas* aeruginosa (*P. aeruginosa*) S1 68, using the MBEC™ assay coupled with standard plate count methods and ethidium monoazide bromide quantitative polymerase chain reaction (EMA-qPCR; viability-qPCR) analysis. The secondary metabolites present in the P1 and NP1 crude extracts were then covalently immobilised onto the surface of high-density polyethylene PE300 (HDPE) and polyvinyl chloride (PVC) and subjected to antifouling testing against *E. faecalis* S1 and *P. aeruginosa* S1 68.

1.2. The Genus *Serratia*

Serratia species are Gram-negative, facultative anaerobic bacteria that belong to the Enterobacteriaceae family (Su et al. 2016). The genus is comprised of 22 species, including the type species *S. marcescens* which is used as a biological marker because of its easily distinguishable red colonies (Khanna et al. 2013; Su et al. 2016). Although *S. marcescens* was first

assumed to be non-pathogenic, it was later found to be an opportunistic pathogen associated with nosocomial infections, such as urinary tract, respiratory tract, surgical wound and blood stream infections (Khanna et al. 2013). Other species within the *Serratia* genus such as *Serratia plymuthica* (*S. plymuthica*), *S. rubidaea* and *Serratia nematodiphila* (*S. nematodiphila*), are also capable of producing the non-diffusible red pigment, prodigiosin, during secondary metabolism (Su et al. 2016). Prodigiosin has been reported to display antimalarial, antibacterial, antifungal, antiprotozoal, antitumor and immunosuppressant activities (Stankovic et al. 2014). In addition to prodigiosin, various members of the genus *Serratia* are known to produce other secondary metabolites, such as biosurfactants, glucosamine derivatives, oocydin A, carbapenem, althiomycin, bacteriocins and serratin (Foulds 1972; Srobel et al. 1999; Dwivedi et al. 2008; Matsuyama et al. 2011; Gerc et al. 2012; Wilf and Salmond 2012; Luna et al. 2013).

The primary lipopeptides produced by *Serratia* species, include serrawettins (W1, W2 and W3) and stephensiolides (A to K) (Matsuyama et al. 1985; Dwivedi et al. 2008; Su et al. 2016; Ganley et al. 2018). *Serratia* species have also been reported to produce the glycolipids, rubiwettins (R1 and RG1) and rhamnolipids (Matsuyama et al. 1990; Nalini and Parthasarathi 2014). A few additional glycolipids, including a sucrose lipid, an arabinolipid and a glycolipid composed of a glucose attached to a palmitic acid, have also been detected (Pruthi and Cameotra 2000; Bidlan et al. 2007; Dusane et al. 2011). In addition, a study conducted by Ndlovu et al. (2016) isolated *S. marcescens* ST29 from a wastewater treatment plant sample and found the strain to contain genes encoding for the biosynthesis of both surfactin and iturin. However, the chemical characterisation of the biosurfactant compounds produced by this strain was not investigated. Finally, Dwivedi et al. (2008) reported on the production of bioactive glucosamine derivatives (A to C) by a *Serratia* strain. Although *Serratia* species produce a number of bioactive secondary metabolites, this review will focus on the glycolipid and lipopeptide biosurfactant compounds, as well as prodigiosin and glucosamine derivatives produced by members of this genus.

1.2.1. Lipopeptides Produced by *Serratia* species

Lipopeptides represent a class of low molecular weight compounds composed of a hydrophilic peptide attached to a hydrophobic lipid or fatty acid (Banat et al. 2014). A wide range of lipopeptide structures have been identified which display variation in the length and conformation of the lipid moiety resulting in different homologues, while analogues exist due to variation in amino acid composition within the peptide moiety (Banat et al. 2014). As indicated, lipopeptides produced by *Serratia* species, include serrawettin W1 (initially referred to as serratamolide A) with identified homologues serratamolide B to G (Wasserman et al. 1961; Matsuyama et al. 1985; Dwivedi et al. 2008; Zhu et al. 2018). In addition, studies have identified serrawettin W2 (and its analogues) (Matsuyama et al. 1992; Su et al. 2016) and serrawettin W3 has been partially characterised

(Matsuyama et al. 1986). In addition to serrawettins, Ganley et al. (2018) discovered antimicrobial lipodepsipeptides known as stephensiolides A to K.

1.2.1.1. Serrawettin Family

Serrawettins are solely produced by members of the *Serratia* genus; serrawettin W1 is produced by strains of *S. marcescens*, serrawettin W2 is produced by *S. marcescens* and *S. surfactantfaciens* strains, and the partially characterised serrawettin W3 was also produced by a *S. marcescens* strain (Matsuyama et al. 1985, 1992; Matsuyama and Nakagawa 1996; Su et al. 2016). The first serrawettin was isolated in 1985 from a *S. marcescens* strain and was found to be identical to serratamolide A that was previously identified by Wasserman et al. (1961) (Matsuyama et al. 1985). The general structure of serrawettin W1 (also known as serratamolide A) includes a symmetric dilactone structure composed of two L-serine amino acids linked to two β-hydroxy fatty acids (comprised of 3-hydroxydecanoic acids) (molecular weight is 514.66 Da) (**Fig. 1.1a**) (Eckelmann et al. 2018). The diversity in the structure of serrawettin W1 (serratamolide A) exists due to the variation in the length of the fatty acid chain (C_8 to C_{14}) and the presence or absence of double bonds, resulting in homologues of serrawettin W1 (serratamolide A), namely serratamolide B to G (Dwivedi et al. 2008; Zhu et al. 2018). The molecular weight of the homologues range from 486.61 to 665.40 Da (Dwivedi et al. 2008; Zhu et al. 2018). In contrast to serrawettin W1, the general structure of serrawettin W2 includes five amino acids, (D-leucine/isoleucine-L-serine-L-threonine-D-phenylalanine-L-isoleucine/leucine) bonded to a β-hydroxy fatty acid moiety (molecular weight of 731.93 Da) (**Fig. 1.1b**) (Matsuyama et al. 1992; Motley et al. 2016).

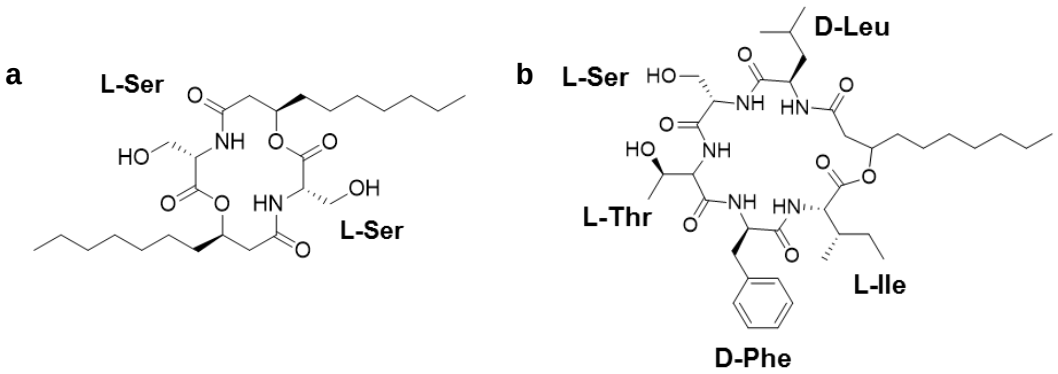

Fig. 1.1 The chemical structure of serrawettin (a) W1 [cyclo(D-3-hydroxydecanoyl-L-seryl)$_2$] (adapted from Matsuyama et al. 1985) and (b) W2 [D-3-hydroxydecanoyl-D-leucyl-L-seryl-L-threonyl-D-phenylalanyl-L-isoleucyl lactone] (adapted from Su et al. 2016).

The diversity in the structure of serrawettin W2 results from variation at the first, second or fifth amino acid positions or the length of the fatty acid chain (C_8 or C_{10}), resulting in the detection of analogues with a molecular weight ranging from 703.3 to 759.3 Da (Matsuyama et al. 1986; Motley

et al. 2016; Su et al. 2016). While the exact chemical composition of serrawettin W3 has yet to be elucidated, the cyclodepsipeptide was found to be composed of a fatty acid (one dodecanoic acid) and five amino acids, including threonine, serine, valine, leucine and isoleucine (Matsuyama et al. 1986). Serrawettins are described as non-ionic biosurfactants as they have no amino acid residues with ionic hydrophilicity (Matsuyama et al. 2011).

1.2.1.2. Stephensiolide Family

A *Serratia* strain that was isolated from the midgut and salivary glands of an *Anopheles stephensi* mosquito was able to produce stephensiolide lipodepsipeptides (A to K) (Ganley et al. 2018). Although stephensiolide mimics the overall structure of serrawettin W2 (as both structures are cyclic pentapeptides), the peptide sequence of the stephensiolides differs. The general chemical structure of stephensiolide includes five amino acids (threonine-serine-serine-valine/isoleucine-isoleucine/valine) attached to a long alkyl chain. The diversity in the structure of stephensiolides exists due to variation in the length of the acyl chain, variation in amino acid residues (presence of either isoleucine or valine at the fourth and fifth amino acid residues) or the presence or absence of a double bond in the fatty acyl chain, resulting in congeners of stephensiolide A to K (Ganley et al. 2018). This results in the molecular masses of the stephensiolides ranging from 599 to 695 Da depending on the congener (A to K).

1.2.2. Glycolipids Produced by *Serratia* species

Glycolipids are a class of low molecular weight biosurfactants, which are comprised of a hydrophilic carbohydrate attached to a hydrophobic aliphatic or hydroxyl-fatty acid (Banat et al. 2010; Shekhar et al. 2015). A number of structurally diverse glycolipid structures have been identified and are produced by a wide range of bacterial and fungal genera. A microorganism can produce homologues of the same glycolipid due to variation in the length and conformation of the fatty acid moiety, while the carbohydrate moiety is comprised of mono-, di-, tri- or tetra-saccharides (de Jesus Cortes-Sanchez et al. 2013; Banat et al. 2014). Previous studies have isolated glycolipids produced by *Serratia* species, including rubiwettin R1, rubiwettin RG1 and rhamnolipids (Matsuyama et al. 1990; Nalini and Parthasarathi 2014). In addition, a number of studies have detected glycolipids such as a sucrose lipid (Pruthi and Cameotra 2000), a glycolipid composed of glucose and palmitic acid (Dusane et al. 2011) and an arabinolipid (Bidlan et al. 2007).

1.2.2.1. Rubiwettin Family

Serratia rubidaea ATCC 27593 is currently the only strain reported to produce rubiwettins and was found to produce both rubiwettin R1 and rubiwettin RG1 (Matsuyama et al. 1990). The general structure (undetermined carbohydrate moiety) and molecular weight of rubiwettin R1 has yet to be

fully elucidated. However, a mixture of linked 3-hydroxy fatty acids comprised of major components, including 3-(3'-hydroxytetradecanoyloxy) decanoate and 3-(3'-hydroxyhexadecanoyloxy) decanoate and minor molecular isomers have been identified and a proposed structure of the fatty acid moiety (**Fig. 1.2a**) was provided by Matsuyama et al. (1990). The general structure of rubiwettin RG1 (**Fig. 1.2b**) was also proposed and consists of β-D-glucopyranosyl 3-(3'-hydroxytetradecanoyloxy) decanoate minor fatty acid isomers (molecular weight of 576.77 Da) (Matsuyama et al. 1990). Therefore, RG1 was found to have a rhamnolipid-like glycolipid structure; however, rhamnose is substituted with a glucose moiety (Matsuyama et al. 1990).

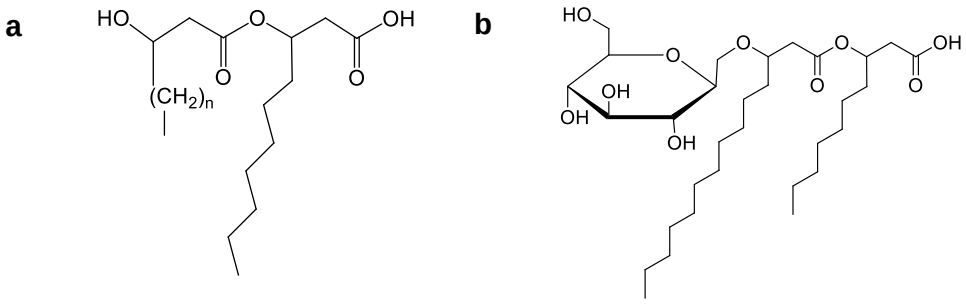

Fig. 1.2 The chemical structure of rubiwettin (a) R1 [3-(3'-hydroxytetradecanoyloxy) decanoate and 3-(3'-hydroxyhexadecanoyloxy) decanoate] and (b) RG1 [β-D-glucopyranosyl 3-(3'-hydroxytetradecanoyloxy) decanoate minor fatty acid isomers] (adapted from Matsuyama et al. 1990).

1.2.2.2. Rhamnolipid Family

Rhamnolipids consist of one (mono-rhamnolipid) or two (di-rhamnolipid) rhamnose sugars bonded to lipid moieties by an O-glycosidic linkage. Although rhamnolipids are primarily produced by *Pseudomonas* species, studies by Nalini and Parthasarathi (2013, 2014) isolated a *S. rubidaea* SNAU02 strain from hydrocarbon contaminated soil that was found to produce this class of glycolipid. Chemical characterisation of the compounds indicated that *S. rubidaea* SNAU02 was able to produce eight rhamnolipid congeners with varying β-hydroxy fatty acid chains ranging from C_8 to C_{16} (Nalini and Parthasarathi 2013, 2014) (**Fig. 1.3**). Among the detected mono- and di-rhamnolipids, the di-rhamnolipid rha-rha-C_{10}-C_8 (β–α rhamnosyl (1 → 2) rhamnosyl-β-hydroxydecanoyl-β-hydroxyoctadecanoic acid) (**Fig. 1.3b**) was found to be the most abundant (Nalini and Parthasarathi 2014). The chemical structure of another major component, a mono-rhamnolipid produced by *S. rubidaea* SNAU02 was also determined, which was rha-C_{10}-C_{10} (rhamnosyl-β-hydroxydecanoyl-β-hydroxydecanoic acid) (**Fig. 1.3a**) (Nalini and Parthasarathi 2014).

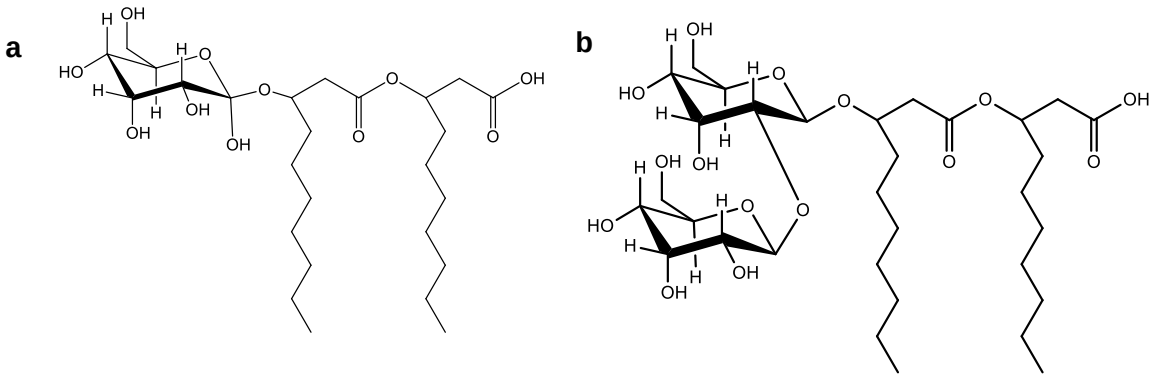

Fig. 1.3 The proposed chemical structures for the (a) mono-rhamnolipid (Rha-C_{10}-C_{10}) and (b) di-rhamnolipid (Rha-Rha C_8-C_{10}) produced by *S. rubidaea* SNAU02 (adapted from Nalini and Parthasarathi 2014).

1.2.3. Prodigiosin

Prodigiosin is a red, linear tripyrrole pigment and is produced by several bacterial species, including *S. marcescens*, *S. plymuthica, S. rubidaea, S. nematodiphila, Hahella chejuensis, Streptomyces variegatus, Zooshikella rubidus, Vibrio psychroerythreus* and *Pseudomonas magnesiorubra*, amongst a few others (Lee et al. 2011; Stankovic et al. 2014; Darshan and Manonmani 2015; Su et al. 2016). Prodigiosin is the primary member of the prodiginine family, which is a group of structural isomers that contain a tripyrrole core with varying alkyl chains (Lee et al. 2011; Darshan and Manonmani 2015). The structure of the red pigment is 2-methyl-3-amyl-6-methoxyprodigiosene (molecular weight of 323.4 Da) and it is comprised of three rings that are typically referred to as pyrrolic ring A, B and C (Yip et al. 2019). The A and B rings are linked in a bipyrrole unit, while the C ring is linked to the A and B rings (methoxy bipyrrole) by a methylene bridge (Yip et al. 2019) (**Fig. 1.4**).

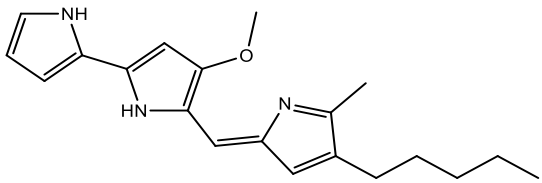

Fig. 1.4 The chemical structure of prodigiosin produced by *S. marcescens* (adapted from Yip et al. 2019).

1.2.4. Glucosamine Derivatives

Glucosamine derivatives are a group of secondary metabolites previously described by Dwivedi et al. (2008). Currently, three glucosamine derivatives (A to C), produced by *S. marcescens* SHHRE645, have been identified and these metabolites were co-produced with serrawettin W1 homologues (Dwivedi et al. 2008). The general structure of glucosamine derivatives involves a core

of *N*-butyl-α-glucopyranosylamide that is acylated with a valine amino acid at the C-1 oxygen. They are thus also referred to as *N*-butylglucosamine ester derivatives. These derivatives are comprised of four residues, including glucose, valine, butyric acid and a saturated or unsaturated β-fatty acid residue (**Fig. 1.5**). Homologues of glucosamine derivatives exist due to the varying length of the fatty acid moiety (including $C_{16:1}$, C_{15}, or C_{14}) attached to the N-terminus of the valine and the presence or absence of double bonds in the β-fatty acid residue, thus resulting in a molecular weight range of 559.4 to 585.4 Da (Dwivedi et al. 2008).

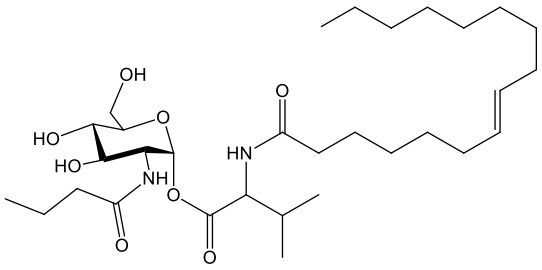

Fig. 1.5 The chemical structure of a glucosamine derivative produced by *S. marcescens* (adapted from Dwivedi et al. 2008).

1.3. Biosynthesis of Secondary Metabolites

The mechanisms involved in the biosynthesis of serrawettin W1, serrawettin W2, stephensiolides and prodigiosin have been identified, while the mechanisms involved in the biosynthesis of serrawettin W3, glucosamine derivatives and glycolipids produced by *Serratia* species have not been fully elucidated. The biosynthesis of lipopeptides produced by *Serratia* species will be discussed first, followed by the biosynthesis of prodigiosin.

The biosynthesis of lipopeptides involves multistep processes mediated by various non-ribosomal peptide synthetase (NRPS) enzymes which catalyse the condensation and selection of amino acid residues to yield various metabolites (including lipopeptides). Investigation into the biosynthesis of serrawettin W1, serrawettin W2 and stephensiolides revealed open reading frames (ORF) namely *swrW*, *swrA* and *sphA* (**Fig. 1.6**), respectively, that displayed high homology with the NRPS family (Marahiel et al. 1997; Li et al. 2005; Ganley et al. 2018). The *swrW* gene (encoding for a unimodular synthetase) is composed of four domains including, condensation, adenylation, thiolation, and thioesterase in functional order (**Fig. 1.6a**), which are commonly found in the NRPS family (Marahiel et al. 1997; Li et al. 2005). The systematic functioning of non-ribosomal peptide synthetases (NRPSs) involved in the biosynthesis of secondary metabolites has been determined and indicates that the precursor molecules (e.g. amino acids) are linked to the phosphopantetheinyl moiety of each thiolation domain in the multimodular enzyme (Matsuyama et al. 2011).

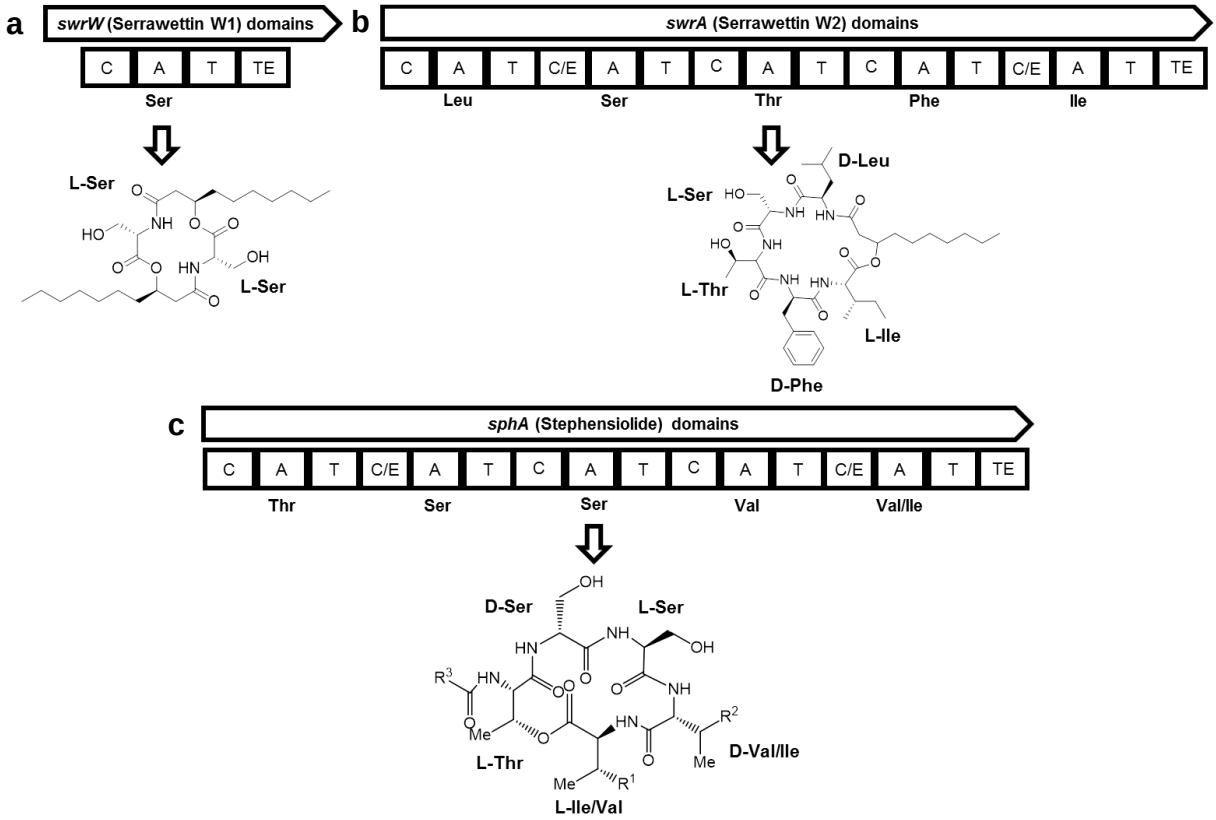

Fig. 1.6 Comparison of the proposed biosynthetic pathways for the biosynthesis of (a) serrawettin W1 encoded by *swrW*, (b) serrawettin W2 encoded by *swrA* and (c) stephensiolide encoded by *sphA* with their respective domain regions [condensation (C), adenylation (A), thiolation (T), and thioesterase (TE)] and general structures produced by each gene cluster (adapted from Ganley et al. 2018).

A previous study by Sunaga et al. (2004) revealed a novel gene, *pswP*, in *S. marcescens* that encodes for 40-phosphopantetheinyl transferase (PPTase). PPTase is the activator of peptidyl carrier protein (PCP) (also known as the thiolation domain in the NRPS family) and was shown to be essential for the biosynthesis of serrawettin W1 (Sunaga et al. 2004). The PPTase is presumed to be involved in the incorporation reaction of L-serine as a molecular component of serrawettin W1 (Sunaga et al. 2004). Therefore, the thiolation domain must be activated by acquiring the phosphopantetheinyl moiety by the action of PPTase for the accurate functioning of serrawettin W1 synthetase (Li et al. 2005). After the activation by PPTase, the adenylation domain is able to adenylate L-serine to an activated form. This activated L-serine will then bind as a thioester to the thiolation domain (that has already been phosphopantetheinylated by PPTase) (Li et al. 2005). The amino group of the L-serine bound to the thiolation domain will react and create an amide linkage with the 3-D-hydroxydecanoyl moiety by detaching from the acyl carrier protein (ACP). This reaction results in the formation of a serratamic acid linked to the thiolation domain (Li et al. 2005). The serratamic acid is transferred to the thioesterase domain and the biosynthesis of a second serratamic acid bound to the free thiolation domain will follow. The two neighbouring serratamic

acids will form an intramolecular linkage which results in the release of a symmetric and circular product, serrawettin W1, from the *swrW* gene region (Li et al. 2005). The serrawettin W2 biosynthetic pathway has a similar mechanism; however, it is encoded by the *swrA* gene (Su et al. 2016).

The biosynthesis of serrawettin W2 was investigated in *S. surfactantfaciens* sp. YD25^T and a hybrid polyketide synthases (PKS)-NRPS gene cluster putatively involved in the biosynthesis of serrawettin W2 was identified (Su et al. 2016). The biosynthetic pathway was determined based on the presence of PKS and NRPS encoding genes. The precursor molecule, a C_{10} fatty acid (FA), is synthesised by the PKS SwrEFG gene cluster and additional undetermined proteins and is released as a fatty acyl-CoA (Su et al. 2016). The NRPS gene cluster encodes the core W2-peptide chain (5-amino acid peptide moiety) and contains five modules (**Fig. 1.6b**) (Su et al. 2016).

Similar to serrawettin W1 and serrawettin W2, the biosynthesis of stephensiolides was investigated in a *Serratia* strain using bioinformatic analysis (sequencing of the *Serratia* sp. genome) and a NRPS gene cluster encoded by the *sphA* gene putatively involved in the biosynthesis of stephensiolides was identified (**Fig. 1.6c**) (Ganley et al. 2018). Further bioinformatics analysis indicated that seven sequenced *S. marcescens* strains contained a homologue with identical predicted domain regions as the *sphA* gene (Ganley et al. 2018). Stephensiolides contain D- and L-amino acids and these lipopeptides are cyclised through a macrolactone ring. Both characteristic properties provide an indication that the peptides are synthesised by NRPSs. Although both serrawettin W2 and stephensiolide are cyclic pentapeptides and are similarly biosynthesised, they are cyclised in a different manner. Serrawettin W2 is cyclised through a 3-hydroxyl group of the fatty acid, while stephensiolides are cyclised through a hydroxyl group of the threonine (Ganley et al. 2018). Therefore, serrawettin W1, serrawettin W2 and stephensiolides are synthesised by various NRPS enzymes.

In contrast, the biosynthesis of prodigiosin has been described in *S. marcescens* ATCC 274 (Sma 274) and *Serratia* sp. ATCC 39006, amongst a few others (Darshan and Manonmani 2015; Yip et al. 2019) and is depicted in **Fig. 1.7**. The biosynthesis of prodigiosin involves a bifurcated pathway which terminates in the enzyme condensation of the individual products from the two precursor pathways, including 4-methoxy-2,2-bipyrrole-5-carboxyaldehyde and 2-methyl-3-n-amyl-pyrrole (MAP) (Darshan and Manonmani 2015; Yip et al. 2019) (**Fig. 1.7**). The pigment (*pig*) gene cluster responsible for prodigiosin biosynthesis is comprised of 14 genes in the Sma 274 strain and encodes for various enzymes in the two pathways. These 14 genes are arranged in the order of *pigA-N*, of which only *pigK* and *pigL* have not been characterised and their function is not yet clarified. The genes *pigB*, *pigD* and *pigE* are responsible for the MAP synthesis, while *pigA, pigF, pigG, pigH, pigI, pigJ, pigM* and *pigN* are responsible for the production of MBC (**Fig. 1.7**). In order

to produce prodigiosin, a terminal condensing enzyme encoded by the *pigC* gene condenses MAP and 4-methoxy-2,2-bipyrrole-5-carboxyaldehyde (**Fig. 1.7**) (Williamson et al. 2006; Yip et al. 2019).

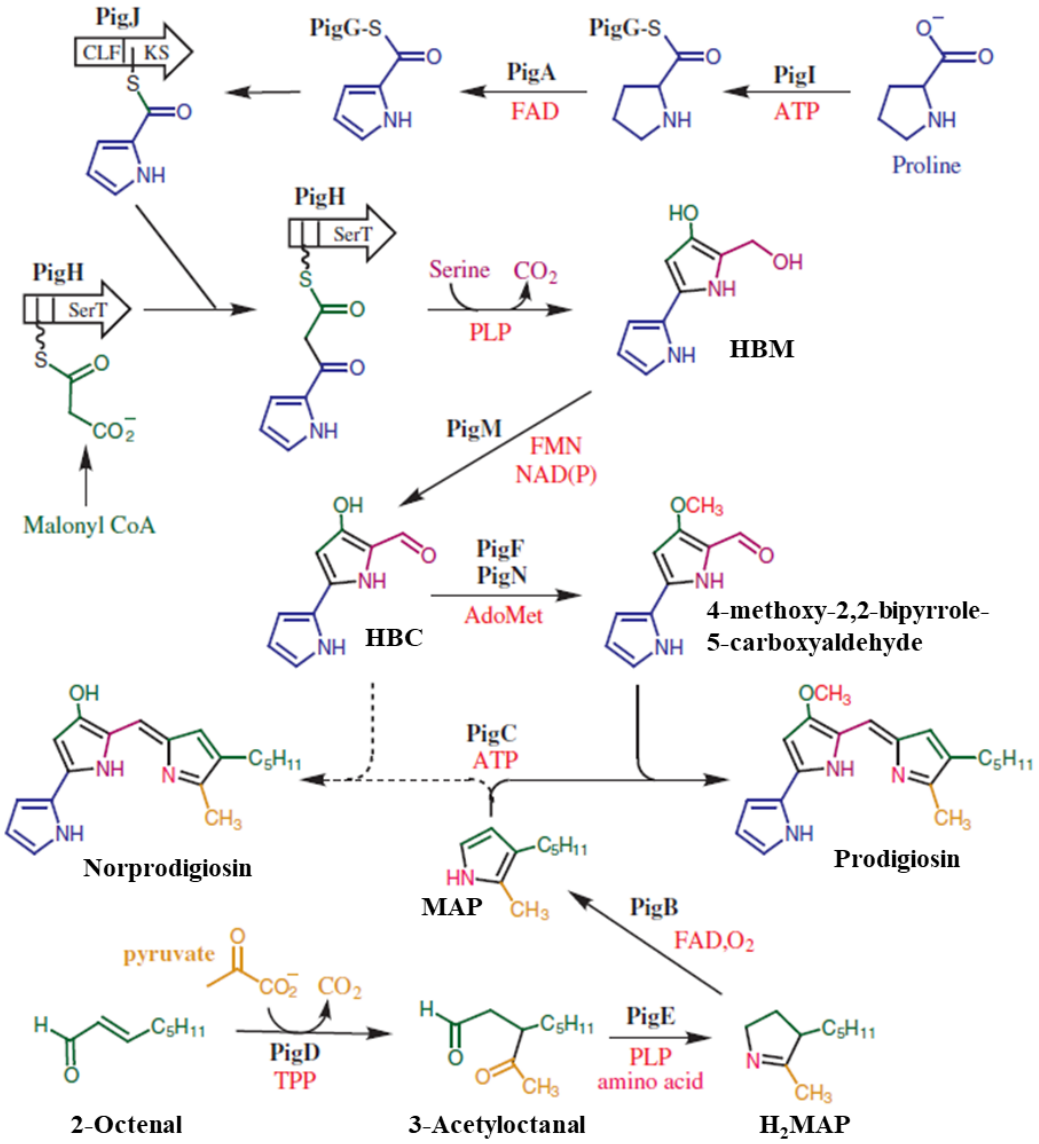

Fig. 1.7 The bifurcated pathway responsible for prodigiosin biosynthesis (adopted from Williamson et al. 2005).

1.4. Physicochemical Characterisation of Biosurfactants Produced by *Serratia* species

In recent years, there has been an increased scientific interest in the isolation of microorganisms that produce biosurfactants with unique physicochemical properties due to their potential application in diverse industries and in bioremediation processes (Fracchia et al. 2012). The amphiphilic nature of biosurfactants allows for their accumulation at the interface between immiscible fluids or between a fluid and a solid, thereby reducing surface (liquid-air) tension and interfacial (liquid-liquid) tension (Varjani and Upasani 2017). The accumulation of these compounds at surfaces or interfaces also decreases the repulsive forces (cohesive forces that hold water molecules together) between two

immiscible phases, such as water and oil (Peele et al. 2016; Varjani and Upasani 2017). This results in the dispersion of one liquid into another leading to the emulsification of the two immiscible liquids (Soberón-Chávez and Maier 2011). The physicochemical properties of biosurfactants thus include their ability to reduce surface tension, form hydrocarbon emulsions (emulsification) and enhance the water solubility of hydrophobic compounds (Desai and Banat 1997).

Surface tension is considered to be the measure of free energy per unit area associated with a surface or interface and is measured using a tensiometer (DuNouy ring method). This is a common screening method to detect the presence of biosurfactant compounds produced by a microorganism (Satpute et al. 2010). Typically, a biosurfactant is considered effective if it can reduce the surface tension between water and air from 72 to 35 mN/m and the interfacial tension between water and n-hexadecane from 40 to 1 mN/m (Soberón-Chávez and Maier 2011). Furthermore, a bacterial strain is considered to be a good biosurfactant producer if it is able to reduce the surface tension of a growth medium by ≥ 20 mN/m compared to distilled water (Walter et al. 2010). Previous studies have identified lipopeptides and glycolipids capable of reducing the surface tension of a growth medium. For example, Dusane et al. (2011) isolated a *S. marcescens* strain that produced a glycolipid that was able to reduce the surface tension of the growth medium from 52.0 to 27 mN/m. Similarly, previously characterised serrawettin W1, serrawettin W2 and serrawettin W3 produced by *S. marcescens* ATCC 13380, NS 25 and NS 45 strains, respectively, were capable of reducing the surface tension of water to 32.2, 33.9 and 28.8 mN/m, respectively (Matsuyama et al. 2011). In addition, Matsuyama et al. (2011) indicated that rubiwettin R1 and rubiwettin RG1 produced by *S. rubidaea* ATCC 27593 reduced the surface tension of water to 25.5 and 25.8 mN/m, respectively.

Biosurfactants are also known to increase the solubility and bioavailability of hydrophobic organic compounds (Mnif and Ghribi 2015). Emulsification activity is thus an indirect method often used to screen for biosurfactant producing microorganisms and the emulsification index can be calculated by measuring the emulsion height divided by the total height of the solution (equal volume of hydrocarbon to cell-free broth culture). Although kerosene is the most commonly used to test for emulsification, previous studies have tested the ability of biosurfactants produced by *Serratia* species to emulsify various hydrocarbons, such as diesel and crude oil (Pruthi and Cameotra 2000; Wei et al. 2004; Ibrahim et al. 2013). For example, Wei et al. (2004) identified a pigmented *S. marcescens* SS-1 strain that was able to emulsify both kerosene (72 %) and diesel (40 %). The amphiphilic nature and structure of these compounds thus confers a diverse range of useful properties, such as emulsification activity, wetting, foaming, dispersion traits, surface activity and the reduction in viscosity of heavy liquids, allowing for their application in many industrial and commercial processes (Satpute et al. 2010; Aparna et al. 2012).

1.5. Industrial Production of Secondary Metabolites by *Serratia* species

Biosurfactants are promising alternatives to synthetic surfactants and have been incorporated into commercialised products, such as Bio Surfactants ACS-Sophor® (sophorolipids) produced by Allied Carbon Solutions Co., Ltd., NatSurFact (rhamnolipids) produced by Logos Technologies, LLC and Yashinomi Vegetable Wash (sophorolipids) produced by Saraya Co. Ltd., amongst others (Geetha et al. 2018). However, the increased global biosurfactant market has resulted in the need for cost-effective, industrial-scale production and purification processes that result in maximum biosurfactant yield (Nitschke and Silva 2018). Biosurfactant production is dependent on the producer strain, physicochemical conditions (temperature, pH, agitation and aeration) and medium composition (carbon source, nitrogen source and salinity). **Table 1.1** indicates various biosurfactant producing *Serratia* species, the type of biosurfactant produced by each strain and the media and culture conditions used for small-scale biosurfactant production (excluding production in bioreactors).

The production of biosurfactants and prodigiosin by *Serratia* species occurs during the late log and early stationary phase of growth (Pruthi and Cameotra 2000; Bidlan et al. 2007; Dusane et al. 2011). It is noteworthy that the production of secondary metabolites, including biosurfactants and prodigiosin, by *Serratia* species is temperature-dependent (Matsuyama et al. 2011; Eckelmann et al. 2018). Matsuyama et al. (1986, 1990) investigated the production of secondary metabolites by *Serratia* species at varying temperatures and found that while the bacterial strains grew well at both 30 °C and 37 °C, serrawettin (W1, W2 and W3), rubiwettin (R1 and RG1) and the pigment (prodigiosin) were produced at 30 °C and were significantly reduced or absent when the bacterial suspension was grown at 37 °C. Numerous studies have subsequently utilised 30 °C as the optimum growth temperature for the production of biosurfactants and prodigiosin by *Serratia* species (Pruthi and Cameotra 2000; Anyanwu et al. 2010; Dusane et al. 2011; Kadouri and Shanks 2013; Su et al. 2016; Almansoory et al. 2017; Yip et al. 2019).

Another physicochemical condition that influences production is oxygen transfer during cell growth. Several factors may contribute to the transfer of oxygen from the gas phase to the aqueous phase within the growth medium, such as agitation speed and aeration, amongst others, thereby affecting cell growth and, ultimately, biosurfactant production (Fakruddin 2012). Various agitation speeds ranging from 100 rpm to 250 rpm have been used during the growth and production of biosurfactants by *Serratia* species (**Table 1.1**). In addition, the media composition, pH values (5 to 9) and cultivation times (24 h to 168 h) similarly influence the quality and quantity of the biosurfactants produced. Almansoory et al. (2017) investigated the effects of varying cultivation times (24 h to 168 h), agitation speeds (100, 125, 150, 180 or 200 rpm) and pH (5 to 9) for the production of biosurfactants by a *Serratia* strain. Results indicated that the optimum cultivation time, agitation speed and pH for maximum biosurfactant production and surface tension reduction was

after 120 h at 200 rpm with the pH of the growth medium at 8.0. However, for the small-scale production of biosurfactants by *Serratia* species an agitation speed of 200 rpm, pH of 7.2 and a cultivation time of 72 h is extensively used (**Table 1.1**). The salt concentration within the growth medium was also hypothesised to influence microbial growth and biosurfactant production by *Serratia* species (Almansoory et al. 2017). Almansoory et al. (2017) further indicated that the growth and production of a biosurfactant by a *S. marcescens* strain was reduced in the absence of salt. The authors additionally tested varying salt concentrations (ranging from 1 % to 5 %), with 1 % recorded as optimum for biosurfactant production.

The production of biosurfactants can also be improved by the presence of different carbon and nitrogen sources, as these factors strongly influence cell growth and the accumulation of metabolic products (Santos et al. 2016). Moreover, research has indicated that the concentration and type of biosurfactant compounds synthesised by the producer strain are influenced by the type of carbon substrate (Rahman and Gakpe 2008; Ndlovu et al. 2017). Water miscible substrates, such as glucose, sucrose, fructose, mannitol and glycerol, and water immiscible substrates, such as mahua oil and olive oil, have been used for biosurfactant production by *Serratia* species (**Table 1.1**; Almansoory et al. 2017). At low nitrogen levels, bacterial growth is also limited, which favours cell metabolism towards the production of secondary metabolites (Santos et al. 2016). Numerous nitrogen sources have subsequently been used for the production of biosurfactants by *Serratia* species, including peptone, yeast extract, tryptone, ammonium sulphate, ammonium nitrate and casamino acids. Of the various carbon and nitrogen sources utilised for the production of biosurfactants by *Serratia* species, the most widely used are glycerol and peptone (**Table 1.1**), respectively. Almansoory et al. (2017) also investigated the effects of different carbon (glycerol, olive oil, glucose, sucrose and fructose) and nitrogen sources (ammonium sulphate, yeast extract, peptone, and combinations of these three nitrogen sources) on lipopeptide production by *S. marcescens* by measuring the biosurfactant yield and the reduction of surface tension. Results indicated that of the five carbon sources used, glycerol resulted in the highest yield of 1.05 g/L and the lowest surface tension, with a value of 30.4 mN/m recorded. Furthermore, the combination of ammonium sulphate and peptone (shown in **Table 1.1**) as nitrogen sources resulted in the highest yield of the biosurfactant compounds (1.33 g/L) and the lowest reduction in surface tension, with a value of 29.9 mN/m recorded. Although biosurfactant production by *Serratia* species is strongly dependent on the producer strain, in summary the most widely used growth conditions and media composition for the small-scale production include an incubation temperature of 30 °C in a medium containing glycerol as a carbon source and peptone as a nitrogen source at a pH of 7.2 with agitation at 200 rpm.

Table 1.1 Culture conditions and media composition for the production of secondary metabolites by *Serratia* spp.

***Serratia* species**	**Strain**	**Metabolite**	**Carbon source**	**Nitrogen source**	**Cultivation time**	**Agitation speed**	**pH**	**Reference**
S. marcescens	ATCC 13880, NS38, 274	Serrawettin W1	Glycerol	Peptone	72 h	n/a	7.2	Matsuyama et al. (1985, 1986)
S. marcescens	SHHRE645	Serratamolide A - F	Glucose	Tryptone and Soytone	120 h	n.s	7.0	Dwivedi et al. (2008)
S. marcescens	H30	Serrawettin W1	Sucrose	Yeast extract	24 h	200 rpm	7.2	Zhang et al. (2010)
S. marcescens	MSRBB2	Serratamolides	Glucose	Peptone and yeast extract	168 h	n.s	n.s	Eckelmann et al. (2018)
S. marcescens	S823	Serratamolide A and G	n.s	Yeast extract	48 h	180 rpm	7.0 – 7.2	Zhu et al. (2018)
S. marcescens	DSM12481	Serrawettin W1	Luria Bertani (LB) media	LB media	24 h	150 rpm; 130 rpm	n.s	Thies et al. (2014); Hage-Hülsmann et al. (2018)
S. marcescens	NS 25	Serrawettin W2	Glycerol	Peptone	72 h	n/a	7.2	Matsuyama et al. (1986, 1992)
S. marcescens	n.s	Serrawettin W2	Glycerol	Ammonium chloride	168 h	135 rpm	7.0	Motley et al. (2016)
S. liquefaciens (*S. marcescens*)	MG1	Serrawettin W2	Glucose	Casamino acids	48 h	n/a	n.s	Lindum et al. (1998)
S. surfactantfaciens	YD25^{T}	Serrawettin W2	Glycerol	Protease peptone	72 h	n.s	7.2	Su et al. (2016)
S. marcescens	NS 45	Serrawettin W3	Glycerol	Peptone	72 h	n/a	7.2	Matsuyama et al. (1986)
S. marcescens	HDB	Lipopeptide	Glycerol*	Ammonium sulphate and peptone*	120 h	100 – 200 rpm	5.0 – 9.0	Almansoory et al. (2017)
S. marcescens	NSK-1	Lipopeptide	Glycerol	Ammonium sulphate	72 h	180 rpm	7.0	Anyanwu et al. (2010)
S. marcescens	n.s	Lipopeptide	n.s	Ammonium nitrate	168 h	n.s	7.2	Ibrahim et al. (2013)
Serratia sp.	n.s	Stephensiolides	LB media	LB media	24 h	250 rpm	7.0	Ganley et al. (2018)
S. marcescens	MTCC 86	Glycolipid (sucrose lipid)	Sucrose	Ammonium sulphate	24 h	200 rpm	7.2	Pruthi and Cameotra (2000)
S. marcescens	n.s	Glycolipid	n.s	Peptic digest of animal tissue and yeast extract	48 h	120 rpm	n.s	Dusane et al. (2011)
S. rubidaea	SNAU02	Rhamnolipid	Mannitol	Yeast extract	72 h	200 rpm	6.97	Nalini and Parthasarathi (2013)
S. rubidaea	SNAU02	Rhamnolipid	Mahua oil	Ammonium nitrate	168 h	n.s	7.0	Nalini and Parthasarathi (2014)
S. rubidaea	ATCC 27593	Rubiwettin R1 and RG1	Glycerol	Peptone	72 h	n/a	7.2	Matsuyama et al. (1990)

n/a – not applicable (agar used); n.s – not specified; * various carbon and nitrogen sources tested.

In addition to the small-scale production of biosurfactants, studies have evaluated the use of bioreactors for the large-scale production of biosurfactants by *Serratia* species. A study by Granada et al. (2018) investigated the effects of dissolved oxygen on the large-scale production of bioactive metabolites, including serratamolide A, prodigiosin and haterumalide NC (a cytotoxic molecule), by *Serratia* sp. ARP5.1 using a 7 L stirred tank bioreactor. The strain was inoculated into 4 L of mineral medium (with glucose as a carbon source) and incubated at 28 °C for 96 h. Additionally, three agitation speeds (150, 300, 450 rpm) and three aeration rates (0.5, 1.0 and 1.5 vvm) were tested for optimal production. It was found that oxygen was a crucial factor for the biosynthesis of these secondary metabolites in a bioreactor, with the best combination of agitation speed and aeration observed at 450 rpm and 1.5 vvm, respectively. It was therefore recommended that dissolved oxygen be included as a parameter for the large-scale production of secondary metabolites by *Serratia* species. In addition, Roldán-Carrillo et al. (2011) utilised a Box-Behnken experimental design to evaluate the effect of nutrient ratios (C/N, C/Mg and C/Fe) on biosurfactant production by a *S. marcescens* strain. The results indicated that a nutrient ratio of C/N = 5, C/Mg = 30 and C/Fe = 26 000 was optimal for biosurfactant production. This media composition was then utilised for large-scale production in a 3 L bioreactor. The large-scale production of the biosurfactant by this strain was conducted in a volume of 1.5 L of the growth medium within the 3 L bioreactor. After 48 h, the biosurfactant was extracted using 2 volumes of ethanol after acid precipitation from the cell-free broth and the crude extract was freeze-dried and weighed. It was thus found that the nutrient ratios optimised by the Box-Behnken experimental design for biosurfactant production by this strain successfully yielded 21.6 g/L of crude extract after 48 h. Although studies have used various methods to recover biosurfactants, further optimisation of the large-scale production process and downstream recovery of biosurfactants produced by *Serratia* species is still required.

1.6. Applications of Secondary Metabolites Produced by *Serratia* species

Biosurfactants have several advantages over chemical surfactants as they exhibit a low toxicity, high biodegradability, can be produced from cost-effective materials and exhibit stability at extreme temperature, pH and salinity (Satpute et al. 2010; Santos et al. 2016). Thus, due to their diverse chemical properties and biological activity, biosurfactants have the potential to replace their chemical counterparts in a number of industries, such as the petroleum, medical, pharmaceutical, food, agriculture, beverage, cosmetics, textiles and mining industries as well as in bioremediation strategies. Furthermore, biosurfactants produced by *Serratia* species have the potential to be applied as antimicrobial compounds, antifouling agents, and antitumor compounds and as emulsifying agents of hydrocarbons.

1.6.1. Medical and Pharmaceutical Industries

1.6.1.1. Seconday Metabolites as Antimicrobial Agents

Microbial secondary metabolites have been identified as a major resource of compounds that exhibit potent antibacterial and antifungal activity, amongst other biological activities (You et al. 2019). Numerous studies have reported on the wide range of biological activity of prodigiosin and certain biosurfactants produced by members of the genus *Serratia*, while one study has indicated that glucosamine derivatives display antibacterial activity (Dwivedi et al. 2008; Soenens and Imperial 2019).

Both lipopeptides (including serrawettin W1, serrawettin W2 and stephensiolides) and glycolipids (rhamnolipid and glucose-palmitic acid glycolipid) produced by *Serratia* species have been reported to display antimicrobial activity (Dwivedi et al. 2008; Dusane et al. 2011; Kadouri and Shanks 2013; Nalini and Parthasarathi 2014; Su et al. 2016; Ganley et al. 2018). Previous studies have reported on the antibacterial, antifungal and anti-mycotic activity of serrawettin W1 (serratamolide A) (Strobel et al. 2005; Kadouri and Shanks 2013; Zhu et al. 2018). Kadouri and Shanks (2013) suggested that *Serratia* spp. could be a potential source for antimicrobials to combat multidrug-resistant opportunistic pathogens, as serrawettin W1 has been shown to exhibit an inhibitory effect towards a broad range of Gram-positive bacteria, including various strains of *Staphylococcus aureus* (S. *aureus*) [including methicillin-resistant S. *aureus* (MRSA)] and *Staphylococcus epidermidis* (*S. epidermidis*) (Kadouri and Shanks 2013). In addition, Zhu et al. (2018) indicated that serrawettin W1 produced by a *S. marcescens* S823 strain displayed antifungal activity against *Candida albicans* (*C. albicans*). Strobel et al. (2005) then showed that serrawettin W1, produced by a *S. marcescens* strain, exhibited anti-mycotic activity against oomycete pathogens, which has potential application in agriculture, especially for crop protection. Similarly, Dwivedi et al. (2008) purified serratamolide homologues (A to F) and glucosamine derivative homologues (A to C) produced by *Serratia* sp. and tested these compounds for antimicrobial activity against *Mycobacterium* species. It was found that all the serratamolide and glucosamine derivative homologues exhibited antibacterial activity against *Mycobacterium diernhoferi* at a minimum inhibitory concentration (MIC) of 0.18 mM.

Su et al. (2016) also investigated the antimicrobial activity of secondary metabolites produced by *S. surfactantfaciens* sp. YD25^{T}. The secondary metabolite was identified as serrawettin W2 and was found to exhibit inhibitory activity against *S. aureus, Pseudomonas aeruginosa* (*P. aeruginosa*) and *Shigella dysenteriae* (*S. dysenteriae*), amongst other bacterial pathogens, at a concentration of 300 µg/mL (Su et al. 2016). The recently discovered stephensiolide F was tested for antibacterial activity and antiprotozoal activity. This lipopeptide was found to exhibit activity against *Bacillus*

subtilis (*B. subtilis*), *Escherichia coli* (*E. coli*) and *Plasmodium falciparum* with half the inhibitory concentration (IC_{50}) determined at 15, 200 and 14 µg/mL, respectively (Ganley et al. 2018).

Additionally, a few studies have shown that glycolipid biosurfactants produced by *S. marcescens* and *S. rubidaea* strains exhibit antifungal and antibacterial activity (Strobel et al. 2005; Dusane et al. 2011; Nalini and Parthasarathi 2014). For example, Dusane et al. (2011) investigated the MIC of a glycolipid produced by a *S. marcescens* strain against *C. albicans, P. aeruginosa* and *Bacillus pumilus* (*B. pumilus*). Results indicated that MIC values of > 25 µg/mL of the glycolipid were required to inhibit the growth of *C. albicans* and *P. aeruginosa*, while > 12.5 µg/mL of the glycolipid was required to inhibit *B. pumilus.* Similarly, a study by Nalini and Parthasarathi (2014) investigated a rhamnolipid produced by *S. rubidaea* SNAU02 and found that the strain exhibited antifungal activity against *Fusarium oxysporum* and *Colletotrichum gloeosporioides* (common plant pathogens).

Research on prodigiosin has received a considerable amount of interest due to the wide range of beneficial antimicrobial properties, including antibacterial, antifungal and antimalarial activity (Yip et al. 2019). A study by Ibrahim et al. (2014) isolated a *S. marcescens* IBRL USM 84 strain from the surface of a marine sponge, *Xestospongia testudinaria*, and investigated the antibacterial properties of the extracted and identified prodigiosin. It was found that prodigiosin displayed activity against MRSA, *S. epidermidis*, *Staphylococcus saprophyticus, Bacillus licheniformis* (*B. licheniformis*), *B. subtilis*, *E. coli* and *Micrococcus* spp., amongst others. Results from the study also indicated that Gram-positive bacterial strains were more susceptible to prodigiosin than the Gram-negative bacterial strains that were tested. Studies have also indicated that prodigiosin inhibits the growth of pathogenic fungal strains, such as *Cryptococcus* spp., *C. albicans* and *Aspergillus niger*, amongst others (Gulani et al. 2012; Shaikh 2016). Hage-Hülsmann et al. (2018) further investigated the synergistic antibiotic effects of prodigiosin and biosurfactants produced by a *S. marcescens* DSM12481 strain against a soil bacterium, *Corynebacterium glutamicum* (*C. glutamicum*). As results indicated that the combination of prodigiosin and serrawettin W1 generated a larger zone of inhibition compared to the individual compounds, employing a combination of biomolecules may be a useful strategy for future antimicrobial formulations.

1.6.1.1.1. Mechanism of Antimicrobial Action of *Serratia* Metabolites

Studies have indicated that serrawettins, glucosamine derivatives and prodigiosin, amongst other metabolites produced by *Serratia*, display antimicrobial activity (Dwivedi et al. 2008; Kadouri and Shanks 2013; Su et al. 2016; Yip et al. 2019). However, the exact mechanism or mode of action of serrawettins and glucosamine derivatives against microbial strains has not been extensively studied. The general mode of action of other members of the lipopeptide class of biosurfactants has

however, been proposed and involves the adhesion of the antimicrobial compound to the microbial membrane due to hydrophobic interactions and electrostatic charges, where they are able to accumulate on the surface of the cell membrane until a threshold concentration has been reached (Fracchia et al. 2015). Thereafter, it is hypothesised that the fatty acid moiety (hydrophobic) of the lipopeptide is inserted into the cell membrane, which results in the disruption or disorganisation of both bacterial and fungal membranes leading to metabolite leakage and ultimately growth inhibition or cell lysis (Banat et al. 2010; Mnif and Ghribi 2015). In addition, biosurfactants may alter the structure of the membrane and disrupt the conformation of membrane bound proteins, leading to changes in membrane functions, such as transport or energy production (Fracchia et al. 2015).

Research has indicated that the mode of action of a biosurfactant is dependent on the type and concentration of the biosurfactant and their structural properties, including hydrophobicity and electrostatic charge (Sapute et al. 2016). A study conducted by Deol et al. (1973) investigated the action of serratamolide (serrawettin W1) produced by a *Serratia* strain on the ion movement in lipid bilayers and biomembranes and found that at a concentration of 10 µg/mL, the serratamolide significantly increased the rate of movement of K^+ and H^+ across the membrane of *S. aureus*. However, no leakage of '260 nm-absorbing products' (such as nucleic acids) was observed at this concentration and thus the serratamolide neither altered membrane permeability nor inhibited cell growth (Deol et al. 1973). It is thus possible that a higher concentration of serrawettins will be required to display significant leakage of 260 nm-absorbing products. Detailed research to elucidate this theory will however, need to be conducted.

Danevčič et al. (2016a) investigated the general mode of action of prodigiosin, produced by *Serratia* species, against *B. subtilis* and found that the metabolite disrupts the cell membrane, interferes with the cytoplasmic membrane function and increases membrane permeability during the exponential phase of bacterial growth. It was also found that this mode of action was dependent on the growth phase of the bacterial cell, as prodigiosin displayed bacteriolytic activity during the exponential growth phase and bacteriostatic activity during the stationary growth phase (Danevčič et al. 2016a). The same research group also found that prodigiosin may interfere with de novo protein and ribosomal ribonucleic acid (rRNA) synthesis and inhibit the production of CO_2 in *E. coli*, providing evidence that the pigment may interfere with cellular respiration (Danevčič et al. 2016b). An additional study by Darshan and Manonmani (2015) indicated that treating *E. coli* and *B. cereus* with prodigiosin resulted in a significant increase in the level of reactive oxygen species, leading to deoxyribonucleic acid (DNA) damage in both bacterial species. The oxidative damage of DNA by prodigiosin may contribute to a programmed cell death-like activity in these bacterial pathogens (You et al. 2019). A follow up study by Suryawanshi et al. (2016) investigated the mode of action of prodigiosin against *S. aureus*. The study indicated that prodigiosin is a hydrophobic stressor that is able to disrupt the plasma membrane and cause leakage of intracellular substances, such as K^+

ions, sugars, amino acids, and proteins from *S. aureus*. Therefore, prodigiosin has multiple mechanisms of action that result in the potent antimicrobial activity observed for this secondary metabolite.

1.6.1.1.2. Development of Antimicrobial Resistance

Literature has reported on the resistance of microorganisms to conventional antibiotics (Robbel and Marahiel 2010). As secondary metabolites produced by *Serratia* spp. are not available for therapeutic use for the treatment of pathogenic infections, limited research has reported on the acquired resistance of microorganisms to serrawettins, prodigiosin or glucosamine derivatives. Although the ability of the target microbial cell to gain resistance to lipopeptides is substantially reduced due to the difficulty of reorganising their cell membranes (Fracchia et al. 2015), a few studies have indicated microbial resistance to conventional lipopeptides (Robbel and Marahiel 2010; Palmer et al. 2011; Hoefler et al. 2012; Lasek-Nesselquist et al. 2019). For example, acquired resistance of microorganisms to a Food and Drug Administration approved cyclic lipopeptide, daptomycin, available for therapeutic use has been reported (Palmer et al. 2011). Daptomycin is produced by *Streptomyces roseosporus* and was released onto the market for treatment of intravenous infections caused by Gram-positive bacteria, such as *S. aureus* [methicillin-susceptible *S. aureus* and MRSA], *Streptococcus* spp. and *Enterococcus* species. The lipopeptide interacts with the bacterial cells via electrostatic charge interactions with the phosphatidylglycerol (PG)-rich (negative charge) region of the bacterial cell membrane. However, a few studies have reported on the development of resistance of *Enterococcus* spp. and *S. aureus* to daptomycin (Bayer et al. 2013; Palmer et al. 2011). This is due to mutations in the *mprF* gene responsible for catalysing the lysinylation of PG (negatively charged) and generating lysylphosphatidylglycerol (Lys-PG) (positively charged). The increased synthesis and translocation (“flipping”) of the Lys-PG from the inner to the outer leaflet of the cell membrane results in an interference with the daptomycin-membrane charge interaction and ultimately results in resistance to daptomycin (Palmer et al. 2011; Bayer et al. 2013).

1.6.1.2. Biofilm Disrupting Activity

A biofilm is described as a community of microorganisms that have colonised a surface and are embedded within an extracellular matrix (Simões et al. 2010). Biofilms are the major cause of biofouling in the medical, food and water industries due to the ability of microorganisms to populate and proliferate on materials used in these environments, such as metals, plastics, rubber and glass (Donlan 2002; Moritz et al. 2010; do Valle Gomes and Nitschke 2012). The occurrence of biofilms in these industries is a serious human health concern as biofilms are known to harbour a variety of potentially pathogenic microorganisms, such as *Klebsiella* spp., *Listeria* spp., *Salmonella* spp., *Staphylococcus* spp., *Pseudomonas* spp., *Legionella* spp., *E. coli*, etc. (Donlan 2002; Moritz et al.

2010; Simões et al. 2010). Strategies aimed at disrupting existing biofilm communities on industrial surfaces are thus essential (Ludensky 2003).

Biosurfactants are considered promising antifouling agents as they have been reported to exhibit antiadhesive and biofilm disruption activity (Banat et al. 2014). McLandsborough et al. (2006) hypothesised that a surfactant is able to penetrate the biofilms extracellular matrix (possibly through the water channels) and adhere to the surface interface, thereby reducing the interfacial tension between the substratum surface and the biofilm. The interactions involved in bacterial adhesion are also reduced, ultimately leading to the removal of biofilms. It was additionally proposed that biosurfactants act as wetting agents, which favours the solubility of the extracellular matrix in an aqueous medium (Nitschke and Silva 2018). Numerous studies have subsequently investigated the biofilm disrupting properties of biosurfactants, such as surfactin and rhamnolipids (Dusane et al. 2010, 2012; do Valle Gomes and Nitschke 2012; Banat et al. 2014; Loiseau et al. 2015; Silva et al. 2017). For example, Dusane et al. (2010) reported that 100 mM of rhamnolipids was able to disrupt a preformed *B. pumilus* biofilm on polystyrene microtiter plates by 93 % (Dusane et al. 2010). Rhamnolipids have also been reported to be more effective at disrupting preformed biofilms of *Yarrowia lipolytica* on glass surfaces in comparison to the synthetic surfactants cetyl-trimethyl ammonium bromide and sodium dodecyl sulphate (Dusane et al. 2012). A study by Loiseau et al. (2015) also demonstrated that 66 µg/mL of surfactin produced by a *B. subtilis* strain successfully eliminated 90 % of a preformed *Legionella pneumophila* biofilm on polystyrene. Furthermore, do Valle Gomes and Nitschke (2012) investigated the biofilm disrupting properties of surfactin produced by *B. subtilis* and rhamnolipids produced by *P. aeruginosa* against individual and mixed culture biofilms of foodborne pathogenic bacteria formed on a polystyrene surface. The study found that after a 2 h exposure to a 0.1 % concentration of surfactin, the preformed pure culture biofilms of *S. aureus* were reduced by 63.7 %, *Listeria monocytogenes* (*L. monocytogenes*) by 95.9 %, *Salmonella* Enteritidis (*S.* Enteritidis) by 35.5 % and the preformed mixed culture biofilm of all three strains was reduced by 58.5 % in comparison to the untreated controls. Following 2 h of exposure to a 0.25 % concentration of rhamnolipids, preformed pure culture biofilms of *S. aureus* was reduced by 58.5 %, *L. monocytogenes* was reduced by 26.5 %, *S.* Enteritidis was reduced by 23.0 %, and the preformed mixed culture biofilm of all three strains was reduced by 24.0 % in comparison to the untreated control.

Although limited research is available on the biofilm disrupting capabilities of lipopeptides produced by *Serratia* species, it is possible that biosurfactants produced by *Serratia* species display similar antifouling properties to other lipopeptides, such as surfactin. As previously indicated, Dusane et al. (2011) investigated the antifouling activity of a glycolipid, composed of palmitic acid esterified to glucose, produced by a *S. marcescens* strain against a biofilm formed on polystyrene microtitre plates. Results indicated that 50 µg/mL of the glycolipid disrupted preformed biofilms of *B. pumilus*

TiO1, *P. aeruginosa* PAO1 and *C. albicans* BH by 55 %, 62 % and 55 %, respectively, on polystyrene microtitre plate surfaces (Dusane et al. 2011).

Prodigiosin has also been reported to display biofilm disrupting activity against *P. aeruginosa* (Kimyon et al. 2016). A study conducted by Kimyon et al. (2016) found that 500 µM of prodigiosin is able to disrupt preformed *P. aeruginosa* PA14 biofilms (reduction of approximately 70 %) through the removal of extracellular DNA (eDNA). Extracellular DNA integrates into the biofilm matrix of various bacterial species, including *P. aeruginosa*, and is able to bind to various biomolecules, as well as increase bacterial adhesion and aggregation strength, thereby acting as a scaffold for the biofilm. The cleavage of eDNA by prodigiosin thus leads to the disintegration of the biofilm matrix and subsequent reduction in bacterial adhesion, aggregation and biofilm formation, thereby disrupting preformed biofilms.

1.6.1.3. Antiadhesive Activity

The initial step in biofilm formation involves microbial adherence to a surface and is influenced by various factors, including the microbial species, hydrophobicity and electrical charge of the surface, environmental conditions and the production of extracellular polymers that aid in the anchoring of microbial cells (Donlan 2002; Nitschke and Silva 2018). In recent years, there has been an increased interest in the application of antimicrobial compounds as coating agents to various materials to prevent biofilm formation (Nitschke and Silva 2018). The adsorption or coating of biosurfactant compounds to the surface of a material modifies the surface hydrophobicity (Nitschke and Silva 2018). Therefore, a reduction in the surface hydrophobicity and subsequent hydrophobic interactions with microbial cells occurs, effectively reducing or preventing microbial adhesion and colonisation (Gudiña et al. 2010; Rufino et al. 2011). Additionally, it has been hypothesised that biosurfactants influence the development of flagella, thus affecting the ability of bacteria to attach to surfaces (Rivardo et al. 2009). The prior absorption of biosurfactant compounds to surfaces can thus be used as a preventative measure to delay the onset or formation of pathogenic biofilms on medical devices and various other surfaces used in the food, medical and water industries (Gudiña et al. 2010; Nitschke and Silva 2018). A number of coating strategies have subsequently been employed to condition the surface of a material with antimicrobial compounds, such as biosurfactants. These coating strategies include simple absorption methods, the incorporation of volatile and non-volatile antimicrobial agents as part of the polymer composition and the immobilisation of antimicrobials, such as lipopeptides and glycolipids, to polymers by ion or covalent linkages, amongst others (Mohorčič et al. 2010; Alves and Pereira 2014; De Zoysa and Sarojini 2017).

Simple absorption of a biosurfactant to the surface of the material involves immersing the desired material into the biosurfactant in solution for a selected time period; thereby allow the compounds to adhere to the surface (Meylheuc et al. 2001). Numerous studies have demonstrated the significant reduction or prevention of microbial adhesion of a solid surface after adsorption of a biosurfactant to the surface (Meylheuc et al. 2001; Rodrigues et al. 2004, 2006; Rivardo et al. 2009; Zeraik and Nitschke 2010; Dusane et al. 2011). A study conducted by Rodrigues et al. (2004) investigated the ability of a biosurfactant produced by a *Lactococcus lactis* 53 strain to inhibit the microbial adhesion of *S. epidermidis, Streptococcus salivarius* (*S. salivarius*) and *S. aureus.* The biosurfactant was absorbed to the surface of silicone rubber and the changes in hydrophobicity and microbial adhesion were investigated. The change in hydrophobicity was characterised using water contact-angle measurements and indicated that the coated silicone rubber surface was more hydrophilic (with a contact angle of 48°) than uncoated silicone rubber (with a contact angle of 109°). The study further investigated the adhesion of microbial cells to the hydrophobic and hydrophilic silicone rubber (with an adsorbed biosurfactant layer) using a parallel-plate flow chamber, and found that the biosurfactant effectively reduced the initial deposition rates of *S. epidermidis, S. salivarius* and *S. aureus* by 90 %. In addition, Rivardo et al. (2009) explored the antiadhesive capability of two lipopeptides produced by *B. subtilis* V9T14 and *B. licheniformis* V19T21 to inhibit biofilm formation of *S. aureus* ATCC 29213 and *E. coli* CFT073 on polystyrene. The biosurfactant produced by the *B. subtilis* V9T14 strain displayed antiadhesive activity against *E. coli* CFT073 by inhibiting 97 % of biofilm formation using a precoating concentration of 2560 µg/mL, while the biosurfactant produced by the *B. licheniformis* V19T21 strain displayed antiadhesive activity against *S. aureus* ATCC 29213 by inhibiting 90 % of biofilm formation using a precoating concentration of 160 to 320 µg/mL (Rivardo et al. 2009).

To date, two studies have investigated the antiadhesive activity of biosurfactants produced by *Serratia* spp. using simple absorption coating methods. Dusane et al. (2011) coated polystyrene microtitre plate and glass surfaces with a glycolipid composed of palmitic acid and glucose produced by a marine *S. marcescens* strain by simple absorption methods and found that it effectively prevented the adhesion of 82 % *C. albicans* BH, 88 % *P. aeruginosa* PAO1 and 94 % *B. pumilus* TiO1 at a 100 µg/mL of biosurfactant (Dusane et al. 2011). A similar study conducted by Motley et al. (2016) investigated the ability of serrawettin W2 produced by a *Serratia* sp. to inhibit the microbial adhesion of *C. albicans* to a 96-microwell plate. This was conducted by incubating the test compound with the inoculum in the wells of the 96-microwell plate and determining the IC_{50} value using a tetrazolium salt (XTT) reduction assay. An IC_{50} value of 7.7 ± 0.7 µM for serrawettin W2 inhibited the biofilm formation of *C. albicans* and it was concluded that the cyclic lipodepsipeptides produced by the *Serratia* sp. may be used to control *C. albicans* infections associated with biofilm modulation. It is thus recognised that when a biosurfactant is absorbed to the

surface of a material, the material becomes more hydrophilic and is thus expected to decrease or prevent microbial attachment (Rodrigues et al. 2004; Gudiña et al. 2010; Zeraik and Nitschke 2010). Although limited research has been conducted on the immobilisation of prodigiosin onto the surface of materials, Kimyon et al. (2016) demonstrated that prodigiosin exhibits biofilm inhibition properties against *P. aeruginosa* (Kimyon et al. 2016). The authors investigated the effects of prodigiosin on non-established biofilms of *P. aeruginosa* PA14 by growing the cultures on either glass or polystyrene in the presence of prodigiosin (100 to 500 µM). As the prodigiosin concentration increased, significant reductions in biofilm formation were observed due to the production of reactive oxygen species when prodigiosin undergoes oxidation.

Another approach to develop biomaterials involves the incorporation of antimicrobial compounds into a material during manufacturing and allows for the slow release of the compound into the surrounding medium (Alves and Pereira 2014; Coad et al. 2015; De Zoysa and Sarojini 2017). A few drawbacks to both the incorporation and adsorption coating methods have however been described, as both methods may lead to reduced activity over an extended period of time and may exhibit potential toxicity due to the rate of release of the compounds, which in turn may lead to the development of resistance if the compound is released at low concentrations (Mohorčič et al. 2010). The covalent immobilisation of antimicrobial compounds onto various surfaces has thus been deemed advantageous in comparison to other strategies as this method prevents peptide leaching, enhances long-term stability, does not significantly reduce antimicrobial activity and increases the duration of antimicrobial efficacy (Alves and Pereira 2014; De Zoysa and Sarojini 2017).

The covalent immobilisation of biosurfactants or antimicrobial peptides to the surface of materials has previously been described (Gabriel et al. 2006; Mohorčič et al. 2010; De Zoysa and Sarojini 2017). Materials such as plastics, metals or ceramics have inert surfaces and can be functionalised by the addition of a silane polymeric layer bearing reactive groups, which enable the covalent binding of antimicrobial compounds to the surface. A study by Mohorčič et al. (2010) successfully demonstrated that a lipopeptide (polymyxin B) can be covalently immobilised to the surface of an indium-tin-oxide glass via silane coating with epoxy groups, with the bioactive material exhibiting activity towards *E. coli*, without the lipopeptide leaching into the environment. Similarly, De Zoysa and Sarojini (2017) covalently immobilised a lipopeptide (battacin) to glass, silicon and titanium surfaces to prevent or reduce surface colonisation by *P. aeruginosa* and *E. coli* cells. The three surfaces were functionalised by silanization followed by the addition of the heterobifunctional cross-linker, succinimidyl-[N-maleimidopropionamido]-poly(ethylene glycol) ester, whereafter the lipopeptide (with an added N-terminal cysteine) covalently attached to the functionalised surfaces. The ability of the battacin-immobilised surfaces to prevent microbial adhesion was subsequently investigated, and a significant reduction (98.6 to 99.9 % reduction) in adhesion of *P. aeruginosa* and

E. coli cells to the surface of all three materials was observed (in comparison to the uncoated control). Lipopeptides therefore have the potential to be utilised as coating agents for the development of biomaterials, which can be utilised in various industries to reduce biofouling.

1.6.2. Other Medical and Pharmaceutical Applications

In addition to antimicrobial activity, Tomas et al. (2005) filed a patent for the use of a serratamolide (serrawettin W1) produced by a *S. marcescens* 2170 strain as a chemotherapeutic agent. The serratamolide was found to reduce the cell viability (induce apoptosis) of various cancer cell lines (Jurkat, Molt-4, NSO, HGT-1, HT-29 and GLC-4S), while displaying no effect on non-malignant cell lines (NIH-3T3, NRK-49F and IEC-18). In addition to serratamolides (serrawettin W1), serrawettin W2 produced by *S. surfactantfaciens* sp. YD25^T was also shown to exhibit anticancer activity by suppressing the growth of cancer cell lines (HeLa and Caco-2 cell lines), while not significantly affecting the viability of non-malignant cells (Vero and HEK293 cell lines) (Su et al. 2016). Based on this research, serrawettins have the potential to be used as anticancer chemotherapeutic agents against leukemia, lymphoma, myeloma, carcinoma, melanoma and sarcoma (Tomas et al. 2005). Similarly, substantial research into prodigiosin has been conducted over the last decade due to its ability to induce apoptosis in cancer cell lines, including acute human T-cell leukemia, promyelocytic leukemia, and human and rat hepatocellular cancer, human breast cancer and TNF-stimulated human cervix carcinoma, while displaying little to no toxicity to normal cell lines at an average inhibitory concentration of 2.1 µM (Darshan and Manonmani 2015).

1.6.3. Bioremediation and Petroleum Industries

Chemically synthesised surfactants have been used for the bioremediation of oil contaminated sites as well as to enhance the recovery of oil from oil reservoirs in the petroleum industry (Banat 1995). However, as synthetic surfactants are not biodegradable and can be toxic to the environment, biosurfactants provide an environmentally friendly alternative and have been shown to exhibit equivalent emulsification properties. In addition to emulsifying hydrocarbons, studies have indicated that biosurfactants produced by *Serratia* species have the potential for application as microbial enhanced oil recovery agents (Pruthi and Cameotra 2000; Ibrahim et al. 2013; Nalini and Parthasarathi 2013). Microbial enhanced oil recovery is considered a tertiary recovery method that could recover the residual oil using microorganisms or their products (biosurfactants) and can be evaluated using a sandpack technique (sand previously saturated with oil in a column) (Pruthi and Cameotra 2000; Amani et al. 2010). A study by Ibrahim et al. (2013) isolated a *S. marcescens* strain that was found to produce a lipopeptide and investigated the effects of the lipopeptide to enhance the recovery of crude oil from a sandpack column. The lipopeptide was able to recover 76 % of the crude oil from the column and was earmarked as a potential enhanced oil recovery agent. In

addition, a sucrose lipid (glycolipid) produced by a *S. marcescens* strain was found to exhibit excellent emulsification activity against a wide range of hydrocarbons and effectively recovered 90 % of residual oil from an oil-saturated sandpack column (Pruthi and Cameotra 2000). Pruthi and Cameotra (2000) further indicated that the glycolipid displayed a strong ability to recover oil from the walls of containers and therefore could possibly be applied in cleaning operations. Similarly, Nalini and Parthasarathi (2013) demonstrated that a concentration of 0.05 % rhamnolipid solution produced by a *S. rubidaea* SNAU02 strain was able to recover 92 % of used engine oil previously absorbed to a sand sample, while the commercially available surfactant (sodium dodecyl sulphate) only removed 60 % of the oil from the contaminated sand sample.

1.7. Project Aims

Antimicrobial resistance is a major threat to global public health and needs to be prioritised (Liu et al. 2016). Although numerous countries worldwide have implemented strategies to reduce the misappropriation of antibiotics [World Health Organisation (WHO) 2018], the situation is exacerbated as pharmaceutical research and development have failed to meet the clinical demand for the discovery of novel antimicrobials. The WHO has thus released a priority list of antibiotic-resistant bacteria to support research and development of effective antimicrobial agents against multidrug-resistant (MDR) microorganisms (WHO 2017). In this regard, secondary metabolites are a well-known source of alternative antimicrobials and investigating these compounds as novel and effective antimicrobial compounds is a priority.

Of interest are the secondary metabolites produced by *Serratia* species as this genus is a relatively unexploited source of bioactive compounds (Strobel et al. 2005; Kadouri and Shanks 2013; Su et al. 2016). *Serratia* species produce secondary metabolites, such as serrawettins, prodigiosin and glucosamine derivatives, that display antibacterial and antifungal activity. Furthermore, serrawettins and prodigiosin have shown promise as antimicrobials against MDR Gram-positive bacteria, such as MRSA. However, limited research exists on the broad-spectrum antibacterial and antifungal activity of the serrawettins and glucosamine derivatives and their effectiveness against clinical Gram-negative bacteria, including MDR and extensive drug-resistant (XDR) bacteria.

Microorganisms are however, rarely found as planktonic cells in the natural environment, but rather aggregate as biofilms on various surfaces in the food, water and health-related industries. It is well-known that biofilms display greater resistance to antimicrobial agents and detergents and there is an urgent need for the discovery of agents that are effective as antimicrobial and antifouling agents that prevent biofilm formation and remove or disrupt established biofilms. While serrawettin W2 has been shown to prevent the formation of a *C. albicans* biofilm (Motley et al. 2017), limited research

has been conducted on the biofilm disrupting or antiadhesive potential of serrawettin W1 and glucosamine derivatives produced by *Serratia* species.

The primary aim of this study was thus to identify environmental *Serratia* species that produce antimicrobial secondary metabolites, elucidate their metabolic profiles and metabolite structures, and apply these bioactive compounds as antifouling and biofilm disrupting agents. This aim was achieved as outlined in the research chapters as follows:

Chapter 2: Broad-spectrum antimicrobial activity of secondary metabolites produced by *Serratia marcescens* strains (published in Microbiological Research):

- Various environmental water samples, including wastewater treatment plant (WWTP) samples, olive oil and wine effluent samples, oil refinery effluent samples, river water samples and rainwater samples, were screened for pigmented and non-pigmented *Serratia* spp. capable of producing biosurfactants by measuring the surface tension reduction (Du Nouy tensiometer) and emulsification (against kerosene, mineral oil and sunflower oil) abilities of the cell free supernatant.
- All biosurfactant producing isolates were identified using *Serratia* genus primers by the polymerase chain reaction (PCR) followed by sequencing and analysis of PCR products.
- The *Serratia* spp. isolates were then screened for the gene (*swrW*) responsible for the biosynthesis of serrawettin W1, while primers were designed to amplify the *swrA* gene, involved in the biosynthesis of serrawettin W2, using PCR analysis.
- The secondary metabolites produced by a pigmented (P1) and two non-pigmented (NP1 and NP2) *S. marcescens* strains were solvent extracted and subjected to ultra-performance liquid chromatography coupled to electrospray ionisation mass spectrometry (UPLC-ESI-MS) to detect and putatively identify the secondary metabolites present in the crude extracts.
- The crude extracts obtained from *S. marcescens* P1, NP1 and NP2 strains were tested for antimicrobial activity against pathogenic and opportunistic bacterial and fungal strains, including MDR and XDR clinical isolates.

Chapter 3: A metabolomics and molecular networking approach to elucidate the structures of the secondary metabolites produced by *Serratia marcescens* strains:

- The *S. marcescens* P1 and NP1 strains were selected for further testing due to the broad-spectrum antimicrobial activity exhibited by these crude extracts.
- Upscaled production and solvent extraction of the P1 and NP1 crude extracts was conducted and both of the extracts were purified using reverse-phase high-performance liquid chromatograph (RP-HPLC).

- All of the fractions collected after the purification of the P1 and NP1 crude extracts by RP-HPLC analysis were subjected to electrospray ionisation mass spectrometry (ESI-MS) and ultra-performance liquid chromatography coupled to tandem mass spectrometry (UPLC-MS^e).
- The UPLC-MS^e data for P1 and NP1 was then subjected to molecular networking using the Global Natural Products Social platform to elucidate the structural similarities between compounds. The combined use of molecular networking and UPLC-MS^e was thus utilised to elucidate the full chemical structure of detected secondary metabolites.
- The collected fractions were subjected to antimicrobial testing against the clinical *E. faecalis* S1 strain using a disc diffusion assay. Five fractions were then selected based on the activity and quantity of each fraction, and were subjected to minimum inhibitory and bactericidal concentration assays.

Chapter 4: Biofilm disruption and antiadhesive activity of secondary metabolites produced by *Serratia marcescens* strains:

- The secondary metabolites produced by *S. marcescens* P1 and NP1 strains were solvent extracted and the P1 and NP1 crude extracts were investigated for their biofilm disruption and antiadhesive activity against single- and dual-species biofilms of *E. faecalis* S1 and *P. aeruginosa* S1 68, using the MBEC Assay® (also known as Calgary Biofilm Device) coupled with the standard plate count method and ethidium monoazide bromide quantitative polymerase chain reaction (EMA-qPCR) analysis.
- Based on the MBEC Assay® results, the P1 and NP1 crude extracts were covalently immobilised onto the surface of the selected polymers, i.e. high-density polyethylene PE300 (HDPE) and polyvinyl chloride (PVC).
- Surface characterisation of the coated and uncoated materials was then conducted to confirm the successful immobilisation of the P1 and NP1 crude extracts, using water contact angle measurements, attenuated total reflectance fourier transform infrared (ATR-FTIR) spectroscopy and scanning electron microscopy (SEM) coupled to backscattered electron imaging-energy dispersive X-ray spectroscopy (BSE-EDX).
- The potential leaching of the compounds immobilised onto the surfaces of the various materials was also determined using UPLC-ESI-MS.
- The coated materials (and uncoated controls) were then exposed to *E. faecalis* S1 or *P. aeruginosa* S1 68 to investigate the antifouling properties of the bioactive materials. This was analysed using standard culture-based techniques, EMA-qPCR and confocal laser scanning microscopy (CLSM) in conjunction with the LIVE/DEAD viability stain to confirm the reduction of microbial adhesion.

1.8. References

Almansoory AF, Hasan HA, Idris M, Abdullah SRS, Anuar N (2017) Biosurfactant production by the hydrocarbon-degrading bacteria (HDB) *Serratia marcescens*: Optimization using central composite design (CCD). J Ind Eng Chem 47:272–280. https://doi.org/10.1016/j.jiec.2016.11.043

Alves D, Pereira OM (2014) Mini-review: Antimicrobial peptides and enzymes as promising candidates to functionalize biomaterial surfaces. Biofouling 30(4):483–499. https://doi.org/10.1080/08927014.2014.889120

Amani H, Sarrafzadeh MH, Haghighi M, Mehrnia MR (2010) Comparative study of biosurfactant producing bacteria in MEOR applications. J Pet Sci Eng 75(1-2):209–214. https://doi.org/10.1016/j.petrol.2010.11.008

Anyanwu CU, Obi SKC, Okolo BN (2010) Production of surface active glycolipid by *Serratia marcescens* NSK-1 isolated from petroleum contaminated soil. Our Nature 8(1):1–11.

Aparna A, Srinikethan G, Smitha H (2012) Production and characterization of biosurfactant produced by a novel *Pseudomonas* sp. 2B. Colloids Surf B Biointerfaces 95:23–29. https://doi.org/10.1016/j.colsurfb.2012.01.043

Banat IM (1995) Biosurfactants production and possible uses in microbial enhanced oil recovery and oil pollution remediation: a review. Bioresour Technol 51(1):1–12. https://doi.org/10.1016/0960-8524(94)00101-6

Banat IM, De Rienzo MAD, Quinn GA (2014) Microbial biofilms: biosurfactants as antibiofilm agents. Appl Microbiol Biotechnol 98(24):9915–9929. https://doi.org/10.1007/s00253-014-6169-6

Banat IM, Franzetti A, Gandolfi I, Bestetti G, Martinotti MG, Fracchia L, Smyth TJ, Marchant R (2010) Microbial biosurfactants production, applications and future potential. Appl Microbiol Biotechnol 87(2):427–444. https://doi.org/10.1007/s00253-010-2589-0

Bar-Ness R, Avrahamy N, Matsuyama T, Rosenberg M (1988) Increased cell surface hydrophobicity of a *Serratia marcescens* NS 38 mutant lacking wetting activity. J Bacteriol 170(9):4361–4364. https://doi.org/10.1128/jb.170.9.4361-4364.1988

Bayer AS, Schneider T, Sahl HG (2013) Mechanisms of daptomycin resistance in *Staphylococcus aureus*: role of the cell membrane and cell wall. An N Y Acad Sci 1277(1):139–158. https://doi.org/10.1111/j.1749-6632.2012.06819.x

Bidlan R, Deepthi N, Rastogi NK, Manonmani HK (2007) Optimized production of biosurfactant by *Serratia marcescens* DT-1P. Res J Microbiol 2:705–716. https://doi.org/10.3923/jm.2007.705.716

Bodour AA, Drees KP, Maier RM (2003) Distribution of biosurfactant-producing bacteria in undisturbed and contaminated arid southwestern soils. Appl Environ Microbiol 69(6):3280–3287. https://doi.org/10.1128/AEM.69.6.3280-3287.2003

Cameotra SS, Makkar RS (2004) Recent applications of biosurfactants as biological and immunological molecules. Curr Opin Microbiol 7(3):262–266. https://doi.org/10.1016/j.mib.2004.04.006

Coad BR, Griesser HJ, Peleg AY, Traven A (2016) Anti-infective surface coatings: design and therapeutic promise against device-associated infections. PLoS Pathog 12(6):e1005598. https://doi.org/10.1371/journal.ppat.1005598

Danevčič T, Vezjak MB, Tabor M, Zorec M, Stopar D (2016b) Prodigiosin induces autolysins in actively grown *Bacillus subtilis* cells. Front Microbiol 7(27):1–10. https://doi.org/10.3389/fmicb.2016.00027

Danevčič T, Vezjak MB, Zorec M, Stopar D (2016a) Prodigiosin - A multifaceted *Escherichia coli* antimicrobial agent. PLoS One 11(9):1–13. https://doi.org/10.1371/journal.pone.0162412

Darshan N, Manonmani HK (2015) Prodigiosin and its potential applications. J Food Sci Technol 52, 5393–5407. https://doi.org/10.1007/s13197-015-1740-4.

de Jesus Cortes-Sanchez A, Hernandez-Sanchez H, Jaramillo-Flores ME (2013) Biological activity of glycolipids produced by microorganisms: new trends and possible therapeutic alternatives. Microbiol Res 168(1):22–32. https://doi.org/10.1016/j.micres.2012.07.002

De Zoysa GH, Sarojini V (2017) Feasibility study exploring the potential of novel battacin lipopeptides as antimicrobial coatings. ACS Appl Mater Interfaces 9(2):1373–1383. https://doi.org/10.1021/acsami.6b15859

Deol BS, Bermingham MA, Still JL, Haydon DA, Gale EF (1973) The action of serratamolide on ion movement in lipid bilayers and biomembranes. Biochim. Biophys. Acta Biomembr. 330(2):192–195. https://doi.org/10.1016/0005-2736(73)90224-1

Desai JD, Banat IM (1997) Microbial production of surfactants and their commercial potential. Microbiol Mol Biol Rev 61(1):47–64.

do Valle Gomes MZ, Nitschke M (2012) Evaluation of rhamnolipid and surfactin to reduce the adhesion and remove biofilms of individual and mixed cultures of food pathogenic bacteria. Food control 25(2):441–447. https://doi.org/10.1016/j.foodcont.2011.11.025

Donlan RM (2002) Biofilms: microbial life on surfaces. Emerg Infect Dis 8(9):881–890. https://doi.org/10.3201/eid0809.020063

Dusane DH, Dam S, Nancharaiah YV, Kumar AR, Venugopalan VP, Zinjarde SS (2012) Disruption of *Yarrowia lipolytica* biofilms by rhamnolipid biosurfactant. Aquat Biosyst 8(17):1-7. https://doi.org/10.1186/2046-9063-8-17

Dusane DH, Nancharaiah YV, Zinjarde SS, Venugopalan VP (2010) Rhamnolipid mediated disruption of marine *Bacillus pumilus* biofilms. Colloids Surf B Biointerfaces 81(1):242–248. https://doi.org/10.1016/j.colsurfb.2010.07.013

Dusane DH, Pawar VS, Nancharaiah YV, Venugopalan VP, Kumar AR, Zinjarde SS (2011) Anti-biofilm potential of a glycolipid surfactant produced by a tropical marine strain of *Serratia marcescens*. Biofouling 27(6):645–654. https://doi.org/10.1080/08927014.2011.594883.

Dwivedi D, Jansen R, Molinari G, Nimtz M, Johri BN, Wray V (2008) Antimycobacterial serratamolides and diacyl peptoglucosamine derivatives from *Serratia* sp. J Nat Prod 71(4):637–641. https://doi.org/10.1021/np7007126

Eckelmann D, Spiteller M, Kusari S (2018) Spatial-temporal profiling of prodiginines and serratamolides produced by endophytic *Serratia marcescens* harbored in *Maytenus serrata*. Sci Rep 8:1–15. https://doi.org/10.1038/s41598-018-23538-5

Escobar-Díaz E, Lopez-Martin EM, Del Cerro MH, Puig-Kroger A, Soto-Cerrato V, Montaner B, Giralt E, García-Marco JA, Perez-Tomas R, García-Pardo A (2005) AT514, a cyclic depsipeptide from *Serratia marcescens*, induces apoptosis of B-chronic lymphocytic leukemia cells: interference with the Akt/NF-κB survival pathway. Leukemia 19(4):572–579. https://doi.org/10.1038/sj.leu.2403679

Fakruddin (2012) Biosurfactant: Production and Application. J Pet Environ Biotechnol 3(4):1–5 https://doi.org/10.4172/2157-7463.1000124

Fiechter A (1992) Biosurfactants: moving towards industrial application. Trends Biotechnol 10:208–217. https://doi.org/10.1016/0167-7799(92)90215-H

Foulds J (1972) Purification and partial characterization of a bacteriocin from *Serratia marcescens*. J Bacteriol 110(3):1001–1009.

Fracchia L, Banat JJ, Cavallo M, Banat IM (2015) Potential therapeutic applications of microbial surface-active compounds. AIMS Bioeng 2(3):144–162. https://doi.org/10.3934/bioeng.2015.3.144

Fracchia L, Cavallo M, Martinotti MG, Banat IM (2012) Biosurfactants and bioemulsifiers biomedical and related applications–present status and future potentials. Biomed Sci, Eng Technol 14:326–335. https://doi.org/10.1002/cbic.201800124

Gabriel M, Nazmi K, Veerman EC, Nieuw Amerongen AV, Zentner A (2006) Preparation of LL-37-grafted titanium surfaces with bactericidal activity. Bioconjugate Chem 17(2):548–550. https://doi.org/10.1021/bc050091v

Ganley J, Carr G, Ioerger T, Sacchettini J, Clardy J, Derbyshire E (2018) Discovery of antimicrobial lipodepsipeptides produced by a *Serratia* sp. within mosquito microbiomes. ChemBioChem 19(15):1590–1594. https://doi.org/10.1002/cbic.201800124

Geetha SJ, Banat IM, Joshi SJ (2018) Biosurfactants: Production and potential applications in microbial enhanced oil recovery (MEOR). Biocatal Agric Biotechnol 14:23–32. https://doi.org/10.1016/j.bcab.2018.01.010

Gerc AJ, Song L, Challis GL, Stanley-Wall NR, Coulthurst SJ (2012) The insect pathogen *Serratia marcescens* Db10 uses a hybrid non-ribosomal peptide synthetase-polyketide synthase to produce the antibiotic althiomycin. PLoS One 7(9):e44673. https://doi.org/10.1371/journal.pone.0044673

Granada SD, Ramírez-Restrepo S, López-Luján L, Peláez-Jaramillo CA, Bedoya-Pérez JC (2018) Screening of a biological control bacterium to fight avocado diseases: From agroecosystem to bioreactor. Biocatal Agric Biotechnol 14:109–115. https://doi.org/10.1016/j.bcab.2018.02.005

Gudiña EJ, Rocha V, Teixeira JA, Rodrigues LR (2010) Antimicrobial and antiadhesive properties of a biosurfactant isolated from *Lactobacillus paracasei* ssp. *paracasei* A20. Lett Appl Microbiol 50(4):419–424. https://doi.org/10.1111/j.1472-765X.2010.02818.x

Gulani C, Bhattacharya S, Das A (2012) Assessment of process parameters influencing the enhanced production of prodigiosin from *Serratia marcescens* and evaluation of its antimicrobial, antioxidant and dyeing potentials. Malays J Microbiol 8(2):116–122. https://doi.org/10.21161/mjm.03612

Hage-Hülsmann J, Grünberger A, Thies S, Santiago-Schübel B, Klein AS, Pietruszka J, Binder D, Hilgers F, Domröse A, Drepper T, Kohlheyer D (2018) Natural biocide cocktails: Combinatorial antibiotic effects of prodigiosin and biosurfactants. PloS One 13(7):e0200940. https://doi.org/10.1371/journal.pone.0200940

Hoefler BC, Gorzelnik KV, Yang JY, Hendricks N, Dorrestein PC, Straight PD (2012) Enzymatic resistance to the lipopeptide surfactin as identified through imaging mass spectrometry of bacterial competition. Proc Natl Acad Sci U S A (PNAS). 109(32):13082–13087. https://doi.org/10.1073/pnas.1205586109

Ibrahim D, Nazari TF, Kassim J, Lim SH (2014) Prodigiosin-an antibacterial red pigment produced by *Serratia marcescens* IBRL USM 84 associated with a marine sponge *Xestospongia testudinaria*. J Appl Pharm Sci 4(10):001–006. https://doi.org/10.7324/JAPS.2014.40101

Ibrahim ML, Ijah UJJ, Manga SB, Bilbis LS, Umar S (2013) Production and partial characterization of biosurfactant produced by crude oil degrading bacteria. Int Biodeterior Biodegradation 81:28–34. https://doi.org/10.1016/j.ibiod.2012.11.012

Kadouri DE, Shanks RM (2013) Identification of a methicillin-resistant *Staphylococcus aureus* inhibitory compound isolated from *Serratia marcescens*. Res Microbiol 164(8):821–826. https://doi.org/10.1016/j.resmic.2013.06.002

Khanna A, Khanna M, Aggarwal A (2013) *Serratia marcescens* – a rare opportunistic nosocomial pathogen and measures to limit its spread in hospitalized patients. J Clin Diagn Res 7(2):243–246. https://doi.org/10.7860/JCDR/2013/5010.2737

Kimyon Ö, Das T, Ibugo AI, Kutty SK, Ho KK, Tebben J, Kumar N, Manefield M (2016) *Serratia* secondary metabolite prodigiosin inhibits *Pseudomonas aeruginosa* biofilm development by producing reactive oxygen species that damage biological molecules. Front Microbiol 7(972), 1–15. https://doi.org/10.3389/fmicb.2016.00972

Lasek-Nesselquist E, Lu J, Schneider R, Ma Z, Russo V, Mishra S, Pata J, McDonough K, Malik M (2019) Insights into the evolution *of Staphylococcus aureus* daptomycin resistance from an in vitro bioreactor model. Front Microbiol 10(345):1–11. https://doi.org/10.3389/fmicb.2019.00345

Lee JS, Kim YS, Park S, Kim J, Kang SJ, Lee MH, Ryu S, Choi JM, Oh TK, Yoon JH (2011) Exceptional production of both prodigiosin and cycloprodigiosin as major metabolic constituents by a novel marine bacterium, *Zooshikella rubidus* S1-1. Appl Environ Microbiol 77(14):4967–4973. https://doi.org/10.1128/AEM.01986-10

Li H, Tanikawa T, Sato Y, Nakagawa Y, Matsuyama T (2005) *Serratia marcescens* gene required for surfactant serrawettin W1 production encodes putative aminolipid synthetase belonging to nonribosomal peptide synthetase family. Microbiol Immunol 49(4):303–310. https://doi.org/10.1111/j.1348-0421.2005.tb03734.x

Lindum PW, Anthoni U, Christophersen C, Eberl L, Molin S, Givskov M (1998) N-Acyl-L-homoserine lactone autoinducers control production of an extracellular lipopeptide biosurfactant required for swarming motility of *Serratia liquefaciens* MG1. J Bacteriol 180(23):6384–6388.

Liu YY, Wang Y, Walsh TR, Yi LX, Zhang R, Spencer J, Doi Y, Tian G, Dong B, Huang X, Yu LF (2016) Emergence of plasmid-mediated colistin resistance mechanism MCR-1 in animals and human beings in China: a microbiological and molecular biological study. Lancet Infect Dis 16(2):161–168. https://doi.org//10.1016/S1473-3099(15)00424-7

Loiseau C, Schlusselhuber M, Bigot R, Bertaux J, Berjeaud JM, Verdon J (2015) Surfactin from *Bacillus subtilis* displays an unexpected anti-*Legionella* activity. Appl Microbiol Biotechnol 99(12):5083–5093. https://doi.org/10.1007/s00253-014-6317-z

Ludensky M (2003) Control and monitoring of biofilms in industrial applications. Int Biodeterior Biodegradation 51(4):255–263. https://doi.org/10.1016/S0964-8305(03)00038-6

Luna M, García S, García O, Trigos Á (2013) Serratin a new metabolite obtained from *Serratia marcescens*, a bacterium isolated from the microflora associated with banana plantations. Nat Prod Res 27(1):49–53. https://doi.org/10.1080/14786419.2011.650638

Marahiel MA, Stachelhaus T, Mootz HD (1997) Modular peptide synthetases involved in nonribosomal peptide synthesis. Chem Rev 97(7):2651–2674. https://doi.org/10.1021/cr960029e

Matsuyama T, Fujita M, Yano I (1985) Wetting agent produced by *Serratia marcescens*. FEMS Microbiol Lett 28(1):125–129. https://doi.org/10.1111/j.1574-6968.1985.tb00777.x

Matsuyama T, Kaneda K, Ishizuka I, Toida T, Yano I (1990) Surface-active novel glycolipid and linked 3-hydroxy fatty acids produced by *Serratia rubidaea*. J Bacteriol 172(6):3015–3022. https://doi.org/10.1128/jb.172.6.3015-3022.1990

Matsuyama T, Kaneda K, Nakagawa Y, Isa K, Hara-Hotta H, Yano I (1992) A novel extracellular cyclic lipopeptide which promotes flagellum-dependent and -independent spreading growth of *Serratia marcescens*. J Bacteriol 174(6):1769–1776. https://doi.org/10.1128/jb.174.6.1769-1776.1992

Matsuyama T, Murakami T, Fujita M, Fujita S, Yano I (1986) Extracellular vesicle formation and biosurfactant production by *Serratia marcescens*. Microbiol 132(4):865–875. https://doi.org/10.1099/00221287-132-4-865

Matsuyama T, Nakagawa Y (1996) Bacterial wetting agents working in colonization of bacteria on surface environments. Colloids Surf B Biointerfaces 7(5-6):207–214. https://doi.org/10.1016/0927-7765(96)01300-8

Matsuyama T, Tanikawa T, Nakagawa Y (2011) Serrawettins and other surfactants produced by *Serratia*. In: Soberón-Chávez G (ed) *Biosurfactants*. Microbiology Monographs, vol 20. Springer, Berlin, Heidelberg, pp. 93–120

McLandsborough L, Rodriguez A, Pérez-Conesa D, Weiss J (2006) Biofilms: at the interface between biophysics and microbiology. Food Biophys 1(2):94–114. https://doi.org/10.1007/s11483-005-9004-x

Meylheuc T, Van Oss CJ, Bellon-Fontaine MN (2001) Adsorption of biosurfactant on solid surfaces and consequences regarding the bioadhesion of *Listeria monocytogenes* LO28. J Appl Microbiol 91(5):822–832. https://doi.org/10.1046/j.1365-2672.2001.01455.x

Mnif I, Ghribi D (2015) Review lipopeptides biosurfactants: mean classes and new insights for industrial, biomedical, and environmental applications. Pept Sci 104(3):129–147. https://doi.org/10.1002/bip.22630

Mohorčič M, Jerman I, Zorko M, Butinar L, Orel B, Jerala R, Friedrich J (2010) Surface with antimicrobial activity obtained through silane coating with covalently bound polymyxin B. J Mater Sci-Mater M 21(10):2775–2782. https://doi.org/10.1007/s10856-010-4136-z

Moritz MM, Flemming HC, Wingender J (2010) Integration of *Pseudomonas aeruginosa* and *Legionella pneumophila* in drinking water biofilms grown on domestic plumbing materials. Int J Hyg Envir Heal 213(3):190–197. https://doi.org/10.1016/j.ijheh.2010.05.003

Motley JL, Stamps BW, Mitchell CA, Thompson AT, Cross J, You J, Powell DR, Stevenson BS, Cichewicz RH (2016) Opportunistic sampling of roadkill as an entry point to accessing natural products assembled by bacteria associated with non-anthropoidal mammalian microbiomes. J Nat Prod 80(3):598–608. https://doi.org/10.1021/acs.jnatprod.6b00772

Mulligan CN, Yong RN, Gibbs BF (2001) Heavy metal removal from sediments by biosurfactants. J Hazard Mater 85(1-2):111–125. https://doi.org/10.1016/S0304-3894(01)00224-2

Nalini S, Parthasarathi R (2013) Biosurfactant production by *Serratia rubidaea* SNAU02 isolated from hydrocarbon contaminated soil and its physico-chemical characterization. Bioresour Technol 147:619–622. https://doi.org/10.1016/j.biortech.2013.08.041

Nalini S, Parthasarathi R (2014) Production and characterization of rhamnolipids produced by *Serratia rubidaea* SNAU02 under solid-state fermentation and its application as biocontrol agent. Bioresour Technol 173:231–238. https://doi.org/10.1016/j.biortech.2014.09.051

Ndlovu T, Khan S, Khan W (2016) Distribution and diversity of biosurfactant-producing bacteria in a wastewater treatment plant. Environ Sci Pollut Res Int 23(10):9993–10004. https://doi.org/10.1007/s11356-016-6249-5

Ndlovu T, Rautenbach M, Vosloo JA, Khan S, Khan W (2017) Characterisation and antimicrobial activity of biosurfactant extracts produced by *Bacillus amyloliquefaciens* and *Pseudomonas aeruginosa* isolated from a wastewater treatment plant. AMB Express 7(108):1–19. https://doi.org/10.1186/s13568-017-0363-8

Nitschke M, Silva SSE (2018) Recent food applications of microbial surfactants. Crit Rev Food Sci Nutr 58(4):631–638. https://doi.org/10.1080/10408398.2016.1208635

Palmer KL, Daniel A, Hardy C, Silverman J, Gilmore MS (2011) Genetic basis for daptomycin resistance in enterococci. Antimicrob Agents Chemother 55(7): 3345–3356. https://doi.org/10.1128/AAC.00207-11

Peele KA, Ch VRT, Kodali VP (2016) Emulsifying activity of a biosurfactant produced by a marine bacterium. 3 Biotech 6(177): 1–6. https://doi.org/10.1007/s13205-016-0494-7

Pruthi V, Cameotra SS (2000) Novel sucrose lipid produced by *Serratia marcescens* and its application in enhanced oil recovery. J Surfactants Deterg 3(4):533–537. https://doi.org/10.1007/s11743-000-0153-9

Rahman PK, Gakpe E (2008) Production, characterisation and applications of biosurfactants-Review. Biotechnol 7:360–370. https://doi.org/10.3923/biotech.2008.360.370

Rivardo F, Turner RJ, Allegrone G, Ceri H, Martinotti MG (2009) Anti-adhesion activity of two biosurfactants produced by *Bacillus* spp. prevents biofilm formation of human bacterial pathogens. Appl Microbiol Biotechnol 83(3):541–553. https://doi.org/10.1007/s00253-009-1987-7

Robbel L, Marahiel MA (2010) Daptomycin, a bacterial lipopeptide synthesized by a nonribosomal machinery. J Biol Chem 285(36):27501–27508. https://doi.org/10.1074/jbc.R110.128181

Rodrigues L, Van der Mei H, Teixeira JA, Oliveira R (2004) Biosurfactant from *Lactococcus lactis* 53 inhibits microbial adhesion on silicone rubber. Appl Microbiol Biotechnol 66(3):306–311. https://doi.org/10.1007/s00253-004-1674-7

Rodrigues LR, Teixeira JA, van der Mei HC, Oliveira R (2006) Physicochemical and functional characterization of a biosurfactant produced by *Lactococcus lactis* 53. Colloids Surf B Biointerfaces 49(1):79–86. https://doi.org/10.1016/j.colsurfb.2006.03.003

Roldán-Carrillo T, Martínez-García X, Zapata-Penasco I, Castorena-Cortés G, Reyes-Avila J, Mayol-Castillo M, Olguín-Lora P (2011) Evaluation of the effect of nutrient ratios on biosurfactant production by *Serratia marcescens* using a Box-Behnken design. Colloids Surf B Biointerfaces 86(2):384–389. https://doi.org/10.1016/j.colsurfb.2011.04.026

Ron EZ, Rosenberg E (2001) Natural roles of biosurfactants: Minireview. Environ Microbiol 3(4):229–236. https://doi.org/10.1046/j.1462-2920.2001.00190.x

Rufino RD, Luna JM, Sarubbo LA, Rodrigues LR, Teixeira JA, Campos-Takaki GM (2011) Antimicrobial and anti-adhesive potential of a biosurfactant Rufisan produced by *Candida lipolytica* UCP 0988. Colloids Surf B Biointerfaces 84(1):1–5. https://doi.org/10.1016/j.colsurfb.2010.10.045

Santos DKF, Rufino RD, Luna JM, Santos VA, Sarubbo LA (2016) Biosurfactants: multifunctional biomolecules of the 21st century. Int J Mol Sci 17(3):1–31. https://doi.org/10.3390/ijms17030401

Satpute SK, Banpurkar AG, Dhakephalkar PK, Banat IM, Chopade BA (2010) Methods for investigating biosurfactants and bioemulsifiers: a review. Crit Rev Biotechnol 30(2):127–144. https://doi.org/10.3109/07388550903427280

Shaikh Z (2016) Biosynthesis of prodigiosin and its applications. IOSR J Pharm Biol Sci 11:1–28. https://doi.org/10.9790/3008-1106050128

Shekhar S, Sundaramanickam A, Balasubramanian T (2015) Biosurfactant producing microbes and their potential applications: a review. Crit Rev Environ Sci Technol (14):1522–1554. https://doi.org/10.1080/10643389.2014.955631

Silva RD, Almeida DG, Rufino RD, Luna JM, Santos VA, Sarubbo LA (2014) Applications of biosurfactants in the petroleum industry and the remediation of oil spills. Int J Mol Sci 15(7):12523–12542. https://doi.org/10.3390/ijms150712523

Silva SS, Carvalho JW, Aires CP, Nitschke M (2017) Disruption of *Staphylococcus aureus* biofilms using rhamnolipid biosurfactants. J Dairy Sci 100(10):7864–7873. https://doi.org/10.3168/jds.2017-13012

Simões M, Simões LC, Vieira MJ (2010) A review of current and emergent biofilm control strategies. LWT-Food Sci Technol 43(4):573–583. https://doi.org/10.1016/j.lwt.2009.12.008

Soberón-Chávez G, Maier RM (2011) Biosurfactants: a general overview. In: Soberón-Chávez G (ed) *Biosurfactants*. Microbiology Monographs, vol 20. Springer, Berlin, Heidelberg, pp 1–11

Soenens A, Imperial J (2019) Biocontrol capabilities of the genus *Serratia*. Phytochem Rev 2019:1–11. https://doi.org/10.1007/s11101-019-09657-5

Srobel G, Li JY, Sugawara F, Koshino H, Harper J, Hess WM (1999) Oocydin A, a chlorinated macrocyclic lactone with potent anti-oomycete activity from *Serratia marcescens*. Microbiol 145(12):3557–3564. https://doi.org/10.1099/00221287-145-12-3557

Stankovic N, Senerovic L, Ilic-Tomic T, Vasiljevic B, Nikodinovic-Runic J (2014) Properties and applications of undecylprodigiosin and other bacterial prodigiosins. Appl Microbiol Biotechnol 98(9):3841–3858. https://doi.org/10.1007/s00253-014-5590-1

Strobel GA, Morrison SL, Cassella M, HMV Corp (2005) Protecting plants from oomycete pathogens by treatment with compositions containing Serratamolide and Oocydin A from *Serratia marcescens*. *Patent number*: 6926892.

Su C, Xiang Z, Liu Y, Zhao X, Sun Y, Li Z, Li L, Chang F, Chen T, Wen X, Zhou Y (2016) Analysis of the genomic sequences and metabolites of *Serratia surfactantfaciens* sp. nov. YD25^T that simultaneously produces prodigiosin and serrawettin W2. BMC Genom 17(865):1–19. https://doi.org/10.1186/s12864-016-3171-7

Sunaga S, Li H, Sato Y, Nakagawa Y, Matsuyama T (2004). Identification and characterization of the *pswP* gene required for the parallel production of prodigiosin and serrawettin W1 in *Serratia marcescens*. Microbiol Immunol 48(10):723–728. https://doi.org/10.1111/j.1348-0421.2004.tb03597.x

Suryawanshi RK, Patil CD, Koli SH, Hallsworth JE, Patil SV (2016) Antimicrobial activity of prodigiosin is attributed to plasma membrane damage. Nat Prod Res 31(5):572–577. https://doi.org/10.1080/14786419.2016.1195380

Thies S, Santiago-Schübel B, Kovačić F, Rosenau F, Hausmann R, Jaeger KE (2014) Heterologous production of the lipopeptide biosurfactant serrawettin W1 in *Escherichia coli*. J Biotechnol 181:27–30. https://doi.org/10.1016/j.jbiotec.2014.03.037

Tomas RP, Ramoneda BM, Lledo EG, Pedemonte MM, Casas MV (2005) Use of cyclic depsipeptide as a chemotherapeutic agent against cancer. *Patent Number: EP1553080*.

Varjani SJ, Upasani VN (2017) Critical review on biosurfactant analysis, purification and characterization using rhamnolipid as a model biosurfactant. Bioresour Technol 232:389–397. https://doi.org/10.1016/j.biortech.2017.02.047

Walter V, Syldatk C, Hausmann R (2010) Screening concepts for the isolation of biosurfactant producing microorganisms. In: Sen R. (ed) *Biosurfactants*. Advances in Experimental Medicine and Biology, vol 672. Springer, New York, NY, pp 1–13

Wasserman HH, Keggi JJ, McKeon JE (1961) Serratamolide, a metabolic product of *Serratia*. J Am Chem Soc 83(19):4107–4108. https://doi.org/10.1021/ja01480a046

Wei YH, Lai HC, Chen SY, Yeh MS, Chang JS (2004) Biosurfactant production by *Serratia marcescens* SS-1 and its isogenic strain SMΔR defective in SpnR, a quorum-sensing LuxR family protein. Biotechnol Lett 26(10):799–802. https://doi.org/10.1023/B:BILE.0000025881.95596.23

WHO (2017) Prioritization of pathogens to guide discovery, research and development of new antibiotics for drug resistant bacterial infections, including tuberculosis. Geneva: World Health Organization. Available at: https://apps.who.int/iris/handle/10665/311820

WHO (2018) Monitoring global progress on addressing antimicrobial resistance: analysis report of the second round of results of AMR country self-assessment survey 2018. Geneva: World Health Organization. Available at: https://apps.who.int/iris/bitstream/handle/10665/273128/9789241514422-eng.pdf

Wilf NM, Salmond GP (2012) The stationary phase sigma factor, RpoS, regulates the production of a carbapenem antibiotic, a bioactive prodigiosin and virulence in the enterobacterial pathogen *Serratia* sp. ATCC 39006. Microbiol 158(3):648–658. https://doi.org/10.1099/mic.0.055780-0

Williamson NR, Fineran PC, Leeper FJ, Salmond GP (2006) The biosynthesis and regulation of bacterial prodiginines. Nat Rev Microbiol 4(12):887–899. https://doi.org/10.1038/nrmicro1531

Williamson NR, Simonsen HT, Ahmed RA, Goldet G, Slater H, Woodley L, Leeper FJ, Salmond, GP (2005) Biosynthesis of the red antibiotic, prodigiosin, in *Serratia*: identification of a novel 2-methyl-3-

n-amyl-pyrrole (MAP) assembly pathway, definition of the terminal condensing enzyme, and implications for undecylprodigiosin biosynthesis in *Streptomyces*. Mol Microbiol 56(4):971–989.

Yip CH, Yarkoni O, Ajioka J, Wan KL, Nathan S (2019) Recent advancements in high-level synthesis of the promising clinical drug, prodigiosin. Appl Microbiol Biotechnol 103(4):1667–1680. https://doi.org/10.1007/s00253-018-09611-z

You Z, Zhang S, Liu X, Zhang J, Wang Y, Peng Y, Wu W (2019) Insights into the anti-infective properties of prodiginines. Appl Microbiol Biotechnol 103(7):2873–2887. https://doi.org/10.1007/s00253-019-09641-1

Zeraik AE, Nitschke M (2010) Biosurfactants as agents to reduce adhesion of pathogenic bacteria to polystyrene surfaces: effect of temperature and hydrophobicity. Curr Microbiol 61(6):554–559. https://doi.org/10.1007/s00284-010-9652-z

Zhang L, Sun JA, Hao Y, Zhu J, Chu J, Wei D, Shen Y (2010) Microbial production of 2, 3-butanediol by a surfactant (serrawettin)-deficient mutant of *Serratia marcescens* H30. J Ind Microbiol Biotechnol 37(8):857–862. https://doi.org/10.1007/s10295-010-0733-6

Zhang X, Xu D, Zhu C, Lundaa T, Scherr KE (2012) Isolation and identification of biosurfactant producing and crude oil degrading *Pseudomonas aeruginosa* strains. Chem Eng J 209:138–146. https://doi.org/10.1016/j.cej.2012.07.110

Zhu L, Pang C, Chen L, Zhu X (2018) Antibacterial activity of a novel depsipeptide and prodigiosine of *Serratia marcescens* S823. Nat Prod Chem Res 6(2):1–7. https://doi.org/10.4172/2329-6836.1000312

Chapter 2:

Published in Microbiological Research (2019),

Volume 229: pages 1-10

(This chapter is compiled in the format of Microbiological Research and UK spelling is employed)

Broad-spectrum antimicrobial activity of secondary metabolites produced by *Serratia marcescens* strains

Tanya Clements[a], Thando Ndlovu[a] and Wesaal Khan[a*]

[a]Department of Microbiology, Faculty of Science, Stellenbosch University, Private Bag X1, Stellenbosch, 7602, South Africa

*Corresponding Author: Wesaal Khan; Phone: +27 21 808 5804; E-mail: wesaal@sun.ac.za

Abstract

The genus *Serratia* is a predominantly unexplored source of antimicrobial secondary metabolites. The aim of the current study was thus to isolate and evaluate the antimicrobial properties of biosurfactants produced by *Serratia* species. Forty-nine (*n* = 34 pigmented; *n* = 15 non-pigmented) biosurfactant producing *Serratia* strains were isolated from environmental sources and selected isolates (*n* = 11 pigmented; *n* = 11 non-pigmented) were identified as *Serratia marcescens* (*S. marcescens*) using molecular typing. The *swrW* gene (serrawettin W1 synthetase) was detected in all the screened pigmented strains and one non-pigmented strain and primers were designed for the detection of the *swrA* gene (non-ribosomal serrawettin W2 synthetase), which was detected in nine non-pigmented strains. Crude extracts obtained from *S. marcescens* P1, NP1 and NP2 were chemically characterised using ultra-performance liquid chromatography coupled to electrospray ionisation mass spectrometry (UPLC-ESI-MS), which revealed that P1 produced serrawettin W1 homologues and prodigiosin, while NP1 produced serrawettin W1 homologues and glucosamine derivative A. In contrast, serrawettin W2 analogues were predominantly identified in the crude extract obtained from *S. marcescens* NP2. Both P1 and NP1 crude extracts displayed broad-spectrum antimicrobial activity against clinical, food and environmental pathogens, such as multidrug-resistant (MDR) *Pseudomonas aeruginosa,* methicillin-resistant *Staphylococcus aureus* and *Cryptococcus neoformans*. In contrast, the NP2 crude extract displayed antibacterial activity against a limited range of pathogenic and opportunistic pathogens. The serrawettin W1 homologues, in combination with prodigiosin and glucosamine derivatives, produced by pigmented and non-pigmented *S. marcescens* strains, could thus potentially be employed as broad-spectrum therapeutic agents against MDR bacterial and fungal pathogens.

Keywords: *Serratia marcescens*; serrawettin W1; serrawettin W2; secondary metabolites; antimicrobial activity

2.1. Introduction

The rapid spread and emergence of multidrug- (MDR) and extensive drug-resistant (XDR) bacteria and fungi is considered one of the major threats to global public health in the 21st century (Colombo et al., 2017; McCarthy et al., 2017). This has resulted in organisations, such as the World Health Organisation (WHO) and the Centres for Disease Control and Prevention (CDC), implementing vital strategies to combat the misappropriation of current antibiotic therapies and prioritise the research and development of alternative antimicrobial compounds (CDC, 2013; WHO, 2015). In this regard, several bacterial species have been reported to produce bioactive secondary metabolites, which are considered promising alternatives to antibiotics (Bérdy, 2005). Moreover, *Serratia* spp. represent a relatively unexploited source of valuable secondary metabolites with potential activity against MDR and XDR pathogens.

The *Serratia* genus consists of 18 species that have been isolated from various environmental sources, such as water and marine environments, contaminated soil, plants, animals or hospitalised patients (Grimont and Grimont, 2006; Su et al., 2016). The ubiquitous nature of this genus is due to the synthesis of numerous extracellular products, including exoenzymes, nucleases and secondary metabolites that aid in the adaption of *Serratia* to harsh environmental conditions (Harris et al., 2004). One such secondary metabolite includes a non-diffusible red pigment, identified as prodigiosin. Prodigiosin is produced by certain strains of *Serratia marcescens* (*S. marcescens*), *Serratia rubidaea* (*S. rubidaea*) and *Serratia surfactantfaciens* (*S. surfactantfaciens*), amongst others (Grimont and Grimont, 2006; Su et al., 2016) and displays antibacterial, antifungal, antiprotozoal, antitumor and immunosuppressant activities (Stankovic et al., 2014). *Serratia* spp. are capable of synthesising additional bioactive secondary metabolites, such as biosurfactants (serrawettins, stephensiolides, rubiwettins and rhamnolipids), althiomycin and bacteriocins (Clements et al., 2019a).

Two species within the *Serratia* genus, namely *S. marcescens* and *S. surfactantfaciens*, have been reported to produce the lipopeptide biosurfactant class known as serrawettins (Matsuyama et al., 1985, 1990; Lindum et al., 1998; Su et al., 2016). Three molecular species of serrawettins have been identified thus far, including serrawettin W1 (also known as serratamolide A), serrawettin W2 and serrawettin W3 (Matsuyama et al., 1985). The general structure of serrawettin W1 includes a symmetric dilactone structure composed of two L-serine amino acids linked to two β-hydroxy fatty acids (comprised of 3-hydroxydecanoic acids) (Eckelmann et al., 2018). Numerous homologues of serrawettin W1 (serratamolide A) have also been detected, namely serratamolide B to G, which differ based on the variation in the length of the fatty acid chain (C_8 to C_{14}) and the presence of a double bond (Dwivedi et al., 2008; Zhu et al., 2018). The open reading frame (ORF) responsible for

the biosynthesis of serrawettin W1 and homologues of this compound was identified as *swrW* and encodes for serrawettin W1 synthetase (Li et al., 2005; Thies et al., 2014).

The general structure of serrawettin W2 includes five amino acids (D-leucine/isoleucine-L-serine-L-threonine-D-phenylalanine-L-isoleucine/leucine) linked to a β-hydroxy fatty acid moiety (Matsuyama et al., 1992; Motley et al., 2016). Analogues of serrawettin W2 have been detected and differ based on the variation at the first, fourth or fifth amino acid positions or the length of the fatty acid chain (C_8 or C_{10}) (Motley et al., 2016; Su et al., 2016). The open reading frame (ORF) responsible for the biosynthesis of serrawettin W2, and analogues of this compound, was identified as *swrA*, encoding for non-ribosomal serrawettin W2 synthetase (Su et al., 2016). While the full chemical composition of serrawettin W3 has yet to be determined, the cyclodepsipeptide was found to be composed of a fatty acid (one dodecanoic acid) and five amino acids, including threonine, serine, valine, leucine and isoleucine (Matsuyama et al., 1986; Matsuyama et al., 2011).

The most prominent properties displayed by serrawettin W1 and W2 include emulsification activity, surface activity, antitumor activity, antibacterial activity and antifungal activity (Clements et al., 2019a). Kadouri and Shanks (2013) investigated the antimicrobial activity of serrawettin W1, produced by a *S. marcescens* strain, and found that this compound exhibited activity against primarily Gram-positive bacteria, such as *Staphylococcus aureus* (*S. aureus*) [including methicillin-resistant *S. aureus* (MRSA)]. Similarly, serrawettin W2 has been shown to exhibit activity against Gram-positive bacteria, such as *S. aureus* and *Micrococcus* spp., whilst also exhibiting activity against a few Gram-negative bacteria, such as *Pseudomonas* and *Shigella* spp. (Su et al., 2016). Thus, while studies have indicated that serrawettins are effective against several Gram-positive bacteria, limited research has been conducted on the broad-spectrum antibacterial and antifungal activity of the serrawettins and their effectiveness against MDR and XDR Gram-negative bacteria. Accordingly, the primary aim of this study was to screen various environmental sources for *Serratia* isolates capable of biosurfactant production. A second aim was to chemically characterise the crude extracts produced by selected *Serratia* strains and assess the broad-spectrum antimicrobial activity of the extracts against pathogenic and opportunistic bacterial and fungal strains, including MDR and XDR clinical isolates. To the best of the author's knowledge, this is one of the first studies investigating the broad-spectrum antimicrobial potential of chemically characterised crude lipopeptide extracts obtained from *Serratia* spp. and exploring the activity of these compounds against MDR and XDR Gram-negative bacteria and fungi.

2.2. Materials and Methods

2.2.1. Sampling Sites

Various environmental sources were selected as the sampling sites for this study, including three municipal wastewater treatment plants (WWTPs) with samples collected from the influent point, aeration tanks, settling tanks and effluent points (*n* = 12). In addition, olive oil (*n* = 4) and wine (*n* = 4) effluent samples were collected at the points following the washing or crushing of olives and two wine grapes varietals, respectively. Samples (*n* = 7) were also collected from the inlet point, four different compartments of a bioreactor, sludge from one of the bioreactor compartments and an outlet point of an oil refinery treatment plant. Three river water samples (Plankenbrug River, Eerste River and Krom River) were collected within the Stellenbosch area and a sample of harvested rainwater was collected from a first flush diverter attached to the rooftop at Welgevallen experimental farm. Thus, 31 samples were collected in 1 L sterile schott bottles and samples were processed within 6 h of collection.

2.2.2. Isolation of Biosurfactant Producing *Serratia* species

In order to isolate *Serratia* spp. from each environmental sample, a serial dilution (10^{-1} to 10^{-4}) in 0.85% saline was prepared. Thereafter, 100 µL of the undiluted and each dilution was spread plated onto Caprylate-Thallous (CT) agar (Grimont and Grimont, 2006) in duplicate. The plates were incubated at 30ºC for 24 to 48 h. Following incubation, morphologically distinct colonies were selected and re-streaked onto nutrient agar (NA) (Merck, Biolab Diagnostic, South Africa) to obtain pure cultures. The isolates obtained were assigned a code identifier, which denoted the pigmentation of the isolate [P – pigmented (red); NP – non-pigmented] and each isolate was numbered.

2.2.3. Growth Conditions and Media Composition for Biosurfactant Production

Purified pigmented and non-pigmented isolates were inoculated into 5 mL Peptone Glycerol (PG, pH 7.2 ± 0.2) broth composed of 5 g Bactopeptone (Merck) and 10 mL glycerol (Promega, Wisconsin, United States) in 1 L distilled water (Matsuyama et al., 1985). For the oil spreading method, the test tube broth cultures were incubated aerobically on a test tube rotator (MRCLAB, London, UK) at 30ºC for 48 to 96 h. For emulsification, surface tension and antimicrobial analysis, a seed culture of each biosurfactant producing strain was prepared by inoculation of a single colony into 5 mL of Luria Bertani (LB) broth (Merck) which was incubated at 30ºC for 18 to 24 h. Each seed culture was subsequently inoculated into a 500 mL baffled flask containing 100 mL PG broth, which was incubated on an orbital shaker (MRCLAB) at 30ºC for 120 h at 120 rpm. After incubation, the broth culture was centrifuged at 10 000 rpm for 20 min at 4°C to obtain the cell free supernatant.

2.2.4. Screening for Biosurfactant Production: Oil Spreading Method

The oil spreading method was used to screen the cell free supernatant obtained from the broth cultures of single bacterial colonies (*n* = 596) for the presence of biosurfactants as previously described by Youssef et al. (2004). Briefly, approximately 40 mL of distilled water was added to a 90 mm petri dish. Thereafter, 10 µL of mineral oil was added to the surface of the distilled water to form a thin layer of oil. Ten microlitres of cell free supernatant was placed in the centre of the petri dish containing the distilled water and an oil layer. The presence of a biosurfactant in the cell free supernatant was indicated by the displacement of the oil layer and formation of a clear zone. The oil spreading analysis for all samples was conducted in duplicate. The bacterial isolates that were able to produce a biosurfactant based on the results obtained from the oil spreading method were further subjected to physico-chemical characterisation.

2.2.5. Physico-Chemical Characterisation

2.2.5.1. Emulsification Capacity Assays

Based on the results obtained from the oil spreading method, the cell free supernatant from selected biosurfactant producing strains (*n* = 22) were subjected to emulsification capacity assays, as outlined by Ndlovu et al. (2016). The emulsification index (E_{24}) of the cell free supernatant obtained from each bacterial isolate was determined by adding 2 mL of the supernatant to an equal volume of diesel, kerosene, sunflower or mineral oil. Thereafter, the solution was vortexed for approximately 5 min. For all samples, the emulsification capacity assays were conducted in duplicate. The solution was left at room temperature for 24 h and the E_{24} for each substrate was measured and calculated using **Equation 2.1**:

$$\text{Emulsification index } (E_{24})\% = \frac{\text{Height of the emulsion layer}}{\text{Total height of the solution}} \times 10 \quad \text{[2.1]}$$

2.2.5.2. Surface Tension Measurements

The surface tension of the cell free supernatant was measured using a Du Nouy ring tensiometer, as previously outlined by Youssef et al. (2004). The surface tension of the biosurfactant compounds present in the cell free supernatant of each bacterial isolate was measured at room temperature. Prior to surface tension measurements of each cell free supernatant sample and sterile PG broth, calibration was performed using distilled water to ensure validity of the measurements. All samples were measured in triplicate and an average value was recorded as the surface tension of the sample.

2.2.6. Molecular Identification of Biosurfactant Producing *Serratia* spp.

The extraction of genomic deoxyribonucleic acid (DNA) was performed for the identification of the biosurfactant producing bacterial strains (*n* = 22) using the High Pure Polymerase Chain Reaction (PCR) Template Preparation Kit (Roche Diagnostics, Risch-Rotkreuz, Switzerland) as per the manufacturer's instructions. Deoxyribonucleic acid samples were stored at -20ºC until utilised for PCR analysis.

The biosurfactant producing isolates (*n* = 22) were subjected to PCR amplification of the *pfs* gene using *Serratia* specific primers Fpfs1 (5' CCGGCATCGGCAAAGTCT 3') and Rpfs2 (5' ATCTGGCCCGGCTCGTAGCC 3') (Zhu et al., 2008). The *pfs* gene encodes for an S-adenosylhomocysteine nucleosidase enzyme and is involved in quorum-sensing within *Serratia* spp. (Zhu et al., 2008). The reaction mixture consisted of 1X Green GoTaq® Flexi buffer (Promega), 2.0 mM $MgCl_2$ (Promega), 0.1 mM of each dNTP (Thermo Fisher Scientific, Waltham, Massachusetts, United States), 0.3 µM of each primer, 1.5 U of GoTaq® G2 DNA polymerase (Promega) and 2 µL of template DNA, which was made up to a final volume of 25 µL using sterile nuclease-free water. Amplification was performed using the T100™ thermal cycler (Bio-Rad Laboratories, Netherlands) and the PCR cycling parameters consisted of initial denaturation at 94°C for 5 min followed by 30 cycles of 94°C for 45 s, 55°C for 30 s, and 72°C for 15 s, and then a single final extension step of 72°C for 5 min. Sterile nuclease free water was used as a negative control, while genomic DNA extracted from *S. marcescens* American Type Culture Collection (ATCC) 13880 was used as a positive control.

The 193 bp PCR products were electrophoresed on a 1.0% agarose gel stained with ethidium bromide (0.5 µg/mL) in 1X tris/acetate/ethylenediaminetetraacetic acid (TAE) buffer and were visualised through UV illumination, with the images captured using the MiniBIS Pro (Bio-Imaging Systems, California, USA). All the PCR products (*n* = 22) were purified using the Wizard® SV Gel and PCR Clean-Up System (Promega) as per manufacturer's instructions and were sequenced in accordance with the BigDye Terminator Version 3.1 Sequencing Kit (Applied Biosystems, USA) at the Central Analytical Facility (CAF), Stellenbosch University (Stellenbosch, South Africa). Chromatograms for each sequence were examined using the Finch TV Version 1.4.0 software and were identified using the National Centre for Biotechnological Information (NCBI) Basic Local Alignment Search Tool (BLAST) (https://blast.ncbi.nlm.nih.gov).

2.2.7. Detection of Genes Encoding for the Biosynthesis of Serrawettins

A primer set was designed for the detection of the *swrA* gene that encodes for non-ribosomal serrawettin W2 synthetase. The two available gene sequences for *swrA* were obtained from the

Genbank (http://www3.ncbi.nlm.nih.gov) database (Accession numbers: JX667980.1; AF039572.1) and were aligned using CLC Main Workbench 7.6.2 software (CLC Bio, Aarhus, Denmark) to obtain the consensus sequence. Consensus regions were used to design specific primers using the IDT PrimerQuest Tool software (https://eu.idtdna.com/PrimerQuest/Home/Index). The primers were further analysed in IDT OligoAnalyzer 3.1 (https://eu.idtdna.com/calc/analyzer) and BLAST (https://blast.ncbi.nlm.nih.gov/Blast.cgi) to ensure the primer sequences are able to detect the available genes.

Hereafter, the DNA extracted from all biosurfactant producing isolates (*n* = 22) was subjected to PCR amplification using primers to detect the *swrW* and *swrA* genes (**Table 2.1**), known to be involved in the biosynthesis of serrawettin W1 and serrawettin W2, respectively. The primer sequences and cycling parameters used to amplify each target gene are indicated in **Table 2.1**. For both the *swrW* and *swrA* genes, the reaction mixture consisted of 1X Green GoTaq® Flexi buffer (Promega), 2 mM $MgCl_2$ (Promega), 0.1 mM dNTP mix (Thermo Scientific), 0.1 µM of each primer, 1.5 U of GoTaq® G2 DNA Polymerase (Promega) and 2.5 µL of template DNA. All reaction mixtures were made up to a final volume of 25 µL with sterile nuclease-free water. The PCRs were performed using a T100™ thermal cycler (Bio-Rad Laboratories), with the cycling parameters outlined in **Table 2.1**.

Table 2.1 The primer sequences and PCR cycling parameters used for the detection of genes encoding for the biosynthesis of serrawettin W1 and W2.

Lipopeptide (gene name)	Primer name	Primer (5' – 3')	Cycling parameter	Size (Bp)	Reference
Serrawettin W1 (*swrW*)	SW2-F3 SW2-R3	GCGACAAAAGCAATGACAAA GTCGGCGTATTGTTCCAACT	94°C for 5 min; 30 cycles: 94°C for 45 s; 55°C for 45 s; 72°C for 3 min; 72°C for 10 min.	915 to 975 bp	Apao et al. (2012)
Serrawettin W2 (*swrA*)	SRA-F SRA-R	ACTTCAGCAGCCAGGAATAC GGACGAATAAGGGACGAGTTT		398 bp	This study

The DNA extracted from *S. marcescens* ATCC 13880 (*swrW* gene) and a sequence verified gene of *swrA* were used as positive controls in the PCR assays, while sterile nuclease free water was used as a negative control. After PCR amplification, representative PCR products for the *swrW* and *swrA* genes were purified, concentrated and sent for sequencing as outlined in section 2.2.6.

2.2.8. Extraction and Partial Purification of Biosurfactant Compounds

Based on the physico-chemical properties and molecular analysis, two pigmented (P1 and P4) and five non-pigmented strains (NP1 – NP5) were selected for preliminary antimicrobial testing (using the methodology outlined in section 2.2.10; results not shown). Thereafter, the P1, NP1 and NP2 strains were selected for further chemical characterisation and broad-spectrum antimicrobial testing, as the crude extracts obtained from P1 and NP1 strains (containing the gene encoding for serrawettin W1) displayed the highest antimicrobial activity for the pigmented and non-pigmented strains analysed, respectively, while the NP2 strain displayed the second highest antimicrobial activity for the non-pigmented strains (containing the serrawettin W2 gene). Therefore, the *S. marcescens* P1, NP1 and NP2 strains were selected for biosurfactant production, purification and partial chemical characterisation as previously outlined by Ndlovu et al. (2017). Briefly, the cell free supernatants of P1, NP1 and NP2 obtained in section 2.2.3 were lyophilised and dissolved in 70% (*v/v*) acetonitrile (Romil, Darmstadt, Germany). The acetonitrile soluble fraction was transferred into a sterile McCartney bottle and lyophilised. This step was repeated three times to further purify the biosurfactant compounds. The weighed extracts were utilised for chemical characterisation and were stored at -20ºC until used for antimicrobial analysis.

2.2.9. Ultra-Performance Liquid Chromatography Coupled to Mass Spectrometry

The compounds present in the crude extracts produced by *S. marcescens* P1, NP1 and NP2 were analysed by the Liquid chromatography-mass spectrometry (LC-MS) unit at the CAF (Stellenbosch University). A Waters Quadrupole Time-of-Flight Synapt G2 (Waters Corporation, Miliford, USA) mass spectrometer was utilised for the electrospray ionisation mass spectrometry (ESI-MS) for direct mass analysis and was coupled to an Acquity ultra-performance liquid chromatography (UPLC) for the UPLC-ESI-MS analysis.

Briefly, 3 µL of the acetonitrile soluble extract obtained from P1, NP1 and NP2 strains were injected and separated on an UPLC C18 reverse-phase analytical column (Acquity UPLC® HSS T3, 1.8 µm particle size, 2.1 x 150 mm, Waters corporation, Dublin, Ireland) at a flow rate of 0.300 mL/min using a 0.1% formic acid (A) to acetonitrile (B) gradient (60% A from 0 to 0.5 min for loading, gradient was from 40 to 95% B from 0.5 to 11 min and then 95 to 40% B from 15 to 18 min) (Ndlovu et al., 2017). The analytes were subjected to a capillary voltage of 3 kV, cone voltage of 15 V and a source temperature of 120°C. Data acquisition in the positive mode was performed by MS scanning a second analyser through the *m/z* range of 200-3000 daltons. The UPLC-ESI-MS profiles of the crude extracts were then compared to literature for the partial characterisation of the compounds produced by the selected strains. The data obtained was analysed using the Masslynx software version 4.1 (Waters Corporation).

2.2.10. Antimicrobial and Haemolytic Activity of the Crude Extracts

The crude extracts produced by the *S. marcescens* P1, NP1 and NP2 strains were subjected to broad-spectrum antimicrobial testing. The lyophilised P1, NP1 and NP2 crude extracts obtained in section 2.2.8 were dissolved in 15% (*v/v*) methanol (Sigma Aldrich, United States) to obtain a 1.00 mg/mL (extract) concentration for antimicrobial disc susceptibility testing.

The antimicrobial activity of the crude extracts produced by the three strains were tested against various actively growing microorganisms available in the Water Resource Laboratory Culture Collection, including ATCC, environmental, and clinical bacterial and fungal strains. In addition, fungal strains isolated from surface water (Benadé et al., 2016) and clinical samples were obtained from the Environmental Biotechnology laboratory in the Department of Microbiology. All test microorganisms were inoculated into Mueller Hinton Broth (MHB, Merck) and were incubated at 37ºC for 18 to 24 h, with the exception of *Legionella* spp., *Enterococcus* spp. and *Listeria* spp. Following incubation, 100 µL of the bacterial suspension was spread plated onto Mueller Hinton agar (MHA, Merck) to create a microbial lawn. The *Legionella* spp. isolates were grown in Lennox broth [10 g/L Tryptone (Biolab, Merck), 5 g/L Yeast Extract (Biolab, Merck), 5 g/L sodium chloride (NaCl; Saarchem, Durban, South Africa)] supplemented with *Legionella* Buffered Charcoal Yeast Extract (BCYE) growth supplement [*N*-(2-acetamido)-2-aminoethanesulfonic acid buffer/potassium hydroxide (10.0 g/L), ferric pyrophosphate (0.25 g/L), alpha-ketoglutarate (1.0 g/L) and *L*-cysteine HCl (0.4 g/L) (Oxoid, Basingstoke, United Kingdom)] and were incubated for 48 h at 30°C. Following incubation, 100 µL of each *Legionella* suspension was spread plated onto BCYE agar (Oxoid) supplemented with *Legionella* BCYE growth supplement (Oxoid) to create a bacterial lawn. The *Enterococcus* and *Listeria* isolates were grown in Tryptone Soy Broth (Merck) supplemented with 6 g/L yeast extract (Merck) ($TSBYE_{0.6\%}$) and were incubated at 37ºC for 18 to 24 h. Following incubation, 100 µL of each *Enterococcus* and *Listeria* suspension was spread plated onto Tryptone Soy agar (Merck) supplemented with 6 g/L yeast extract (Merck) ($TSAYE_{0.6\%}$) to create a bacterial lawn.

For all the isolates, 6 mm filter paper discs (Oxoid) were placed onto the respective lawns using a sterile needle and 50 µL of each crude extract (1.00 mg/mL) was pipetted directly onto the filter paper in order to create an antimicrobial disc. A negative control of 50 µL of 15% (*v/v*) methanol was included for each test strain. All tests were performed in triplicate. The MHA and $TSAYE_{0.6\%}$ plates were incubated for 24 to 48 h at 37°C, while the BCYE plates were incubated for 48 h at 30°C. Thereafter, the diameter of the zone of inhibition around the inoculated paper disc was measured (Ndlovu et al., 2017). The average of the triplicates and standard deviation of each crude extract was determined against the selected test microorganism.

The haemolytic activity of each crude extract was also assessed as described by Das et al. (2008). The P1, NP1 and NP2 crude extracts (20 µL of 1.00 mg/mL crude extract concentration) were spot plated onto sheep blood agar (Selecta-Media, Johannesburg, South Africa) plates in duplicate. In addition, a surfactin standard (20 µL of 1.00 mg/mL; Sigma Aldrich) was included as a positive control and 15% methanol was included as a negative control. The plates were incubated for 24 h at 30°C and were analysed for the zone of haemolysis following overnight incubation.

2.3. Results

2.3.1. Screening of *Serratia* spp. for Biosurfactant Production

All the presumptive *Serratia* strains (*n* = 569) isolated from the various environmental samples were screened using the oil spreading method (preliminary screening for biosurfactant production), with oil displacement observed for 49 isolates (*n* = 34 pigmented; *n* = 15 non-pigmented; 8.6%). Of the 49 presumptive *Serratia* isolates capable of biosurfactant production, 85.7% were isolated from the WWTP samples, 12.2% were isolated from the river (Eerste River and Krom River) water samples and 2.1% were isolated from the oil refinery samples. However, no biosurfactant producing strains were isolated from the Plankenbrug River water sample, wine or olive oil effluent samples and the first flush diverter rainwater sample.

2.3.2. Physico-Chemical Characterisation

Based on the zone diameter of the dispersed oil (oil spreading method), 11 pigmented and 11 non-pigmented presumptive *Serratia* isolates were selected and analysed for their ability to emulsify diesel, kerosene, sunflower oil and mineral oil. The emulsification indices obtained for the cell free supernatant of the 22 isolates are indicated in **Table 2.2**. The overall E_{24} for the pigmented *Serratia* isolates (P1 to P11) ranged from 0 to 63.7%, 0 to 58.9%, 0 to 16.3% and 0 to 59.3% with mineral oil, kerosene, diesel and sunflower oil as substrates, respectively. Similarly, the overall E_{24} for the non-pigmented *Serratia* isolates (NP1 to NP11) ranged from 0 to 56.7%, 0 to 46.5%, 0 to 59.3% and 0 to 61.5% with mineral oil, kerosene, diesel and sunflower oil as substrates, respectively. Twenty (91%) of the 22 presumptive *Serratia* isolates screened for biosurfactant production using the emulsification capacity assay were thus able to emulsify at least one hydrocarbon analysed in this study (**Table 2.2**).

The 22 presumptive *Serratia* isolates (*n* = 11 pigmented; *n* = 11 non-pigmented) were then tested for their ability to reduce the surface tension of sterile PG broth (**Table 2.2**). The highest reduction in surface tension for pigmented isolates was from 61.7 ± 0.5 mN/m to 32.0 ± 0.0 mN/m (P2, P4, P7, P8 and P9), while the highest reduction in surface tension for the non-pigmented isolates was from 61.7 ± 0.5 mN/m to 29.7 ± 0.0 mN/m (NP4 and NP6) (**Table 2.2**). Based on the results obtained, the

22 (100%) presumptive *Serratia* isolates screened for biosurfactant production using the Du Nouy ring tensiometer were able to reduce the surface tension of the growth medium by ≥ 26.0 ± 0.0 mN/m.

Table 2.2 Genus specific sequence identification and emulsification indices of representative *Serratia* isolates producing surface-active compounds.

Isolate number	Organism (Genebank accession no.)	% ID	Source	Surface tension (mN/m)	Emulsification indices (%)			
					MO	K	D	SO
P1	*S. marcescens* (CP005927.1)	100	OS	32.7 ± 0.3	34.1	24.6	14.8	3.7
P2	*S. marcescens* (CP016032.1)	100	WWTP	32.0 ± 0.0	20.3	14.7	0.0	0.0
P3	*S. marcescens* (CP018927.1)	100	WWTP	35.7 ± 0.3	63.7	21.0	0.0	23.1
P4	*S. marcescens* (CP016032.1)	99	WWTP	32.0 ± 0.0	7.3	58.9	3.8	59.3
P5	*S. marcescens* (CP013046.2)	100	WWTP	33.0 ± 0.3	23.6	30.8	1.8	14.3
P6	*S. marcescens* (CP018927.1)	100	WWTP	32.7 ± 0.3	0.0	0.0	0.0	33.3
P7	*S. marcescens* (CP018927.1)	100	WWTP	32.0 ± 0.0	0.0	0.0	0.0	0.0
P8	*S. marcescens* (CP021984.1)	100	WWTP	32.0 ± 0.0	24.1	27.6	16.3	0.0
P9	*S. marcescens* (CP005927.1)	100	WWTP	32.0 ± 0.0	32.3	21.4	1.9	0.0
P10	*S. marcescens* (CP021984.1)	98	WWTP	33.3 ± 0.0	30.9	16.7	5.6	35.7
P11	*S. marcescens* (CP013046.2)	100	WWTP	33.8 ± 0.0	16.2	3.9	1.9	29.6
NP1	*S. marcescens* (CP021984.1)	100	KR	32.9 ± 0.0	56.7	24.1	48.2	53.9
NP2	*S. marcescens* (CP018917.1)	100	WWTP	30.2 ± 0.0	3.7	16.7	52.7	37.7
NP3	*S. marcescens* (CP018923.1)	100	KR	30.2 ± 0.0	1.9	25.9	37.0	40.7
NP4	*S. marcescens* (CP018928.1)	100	KR	29.7 ± 0.0	14.8	44.4	59.3	61.5
NP5	*S. marcescens* (CP018929.1)	100	WWTP	30.2 ± 0.0	16.1	46.5	42.1	55.6
NP6	*S. marcescens* (CP018930.1)	100	WWTP	29.7 ± 0.0	0.0	14.8	21.6	7.7
NP7	*S. marcescens* (CP018929.1)	100	WWTP	30.9 ± 0.3	14.0	0.0	0.0	0.0
NP8	*S. marcescens* (CP018930.1)	100	WWTP	30.6 ± 0.0	3.9	5.6	5.7	53.6
NP9	*S. marcescens* (LT575490.1)	100	WWTP	30.3 ± 0.3	25.9	0.0	0.0	46.3
NP10	*S. marcescens* (CP012639.1)	100	ER	32.9 ± 0.0	7.7	21.4	1.9	0.0
NP11	*S. marcescens* (HG738868.1)	100	ER	30.9 ± 0.5	0.0	0.0	0.0	0.0

ID – Identity, OS – Oil sludge from an oil refinery bioreactor, WWTP - municipal wastewater treatment plant, KR – Krom River, ER – Eerste River, MO – Mineral oil, K – Kerosene, D – Diesel and SO – Sunflower oil.

2.3.3. Molecular Characterisation of the Biosurfactant Producing Bacteria

Sequencing of the *pfs* PCR product (193 bp) and BLAST analysis identified the 22 bacterial isolates (screened for emulsification and surface tension properties) as *S. marcescens* strains (**Table 2.2**).

All the identified *S. marcescens* strains (*n* = 22) were further screened for the presence of the *swrW* and *swrA* genes encoding for the biosynthesis of serrawettin W1 and serrawettin W2, respectively. Results indicated that the pigmented strains isolated in this study primarily contained the *swrW* gene encoding for serrawettin W1 synthetase (*n* = 11), while 82% (*n* = 9) of the non-pigmented strains contained the *swrA* gene encoding for non-ribosomal serrawettin W2 synthetase (**Appendix A Table A1**). One non-pigmented isolate (*S. marcescens* NP1) contained the *swrW* gene encoding for serrawettin W1. Furthermore, *S. marcescens* NP10 did not contain the *swrW* or *swrA* genes, while none of the *S. marcescens* strains (*n* = 22) contained both the *swrW* and *swrA* genes.

2.3.4. Ultra-Performance Liquid Chromatography Coupled to Mass Spectrometry

Based on the physico-chemical properties, molecular analysis, and preliminary antimicrobial testing (results not shown), three *S. marcescens* strains (P1, NP1 and NP2) were selected for the production and extraction of biosurfactant crude extracts. Following solvent extraction, the crude extracts were subjected to chemical characterisation utilising UPLC coupled to ESI-MS analysis for identification of potential antimicrobial compounds present in the crude extracts.

2.3.4.1. P1 crude extract

The positive mode ESI-MS analysis of the crude extract obtained from the *S. marcescens* P1 strain revealed a cluster of *m/z* peaks with a difference of approximately 2, 26 or 28 atomic mass units (amu) in their molecular ion species, revealing four groups of homologues. The spectra in positive mode revealed the main groups of molecular ions at *m/z* 487.30, 515.33, 541.35 and 543.37 $[M+H]^+$ (**Table 2.3**; **Appendix A Fig. A1 a1-5**), which corresponded to the protonated singly charged species. Their corresponding sodium adducts were also detected at *m/z* 509.27, 537.31, 563.33 and 565.35 $[M+Na]^+$ (**Table 2.3**). Additionally, the detected molecular ions at *m/z* 487.30, 515.33, 541.35 and 543.37 $[M+H]^+$ corresponded to serratamolide E, A, B and C, respectively (**Table 2.3**), as previously reported by Dwivedi et al. (2008). The protonated singly charged specie was observed at *m/z* 324.21 $[M+H]^+$ (**Appendix A Fig. A1 a5**) and corresponded to the *m/z* of prodigiosin as previously reported by Eckelmann et al. (2018).

The UPLC-MS analysis revealed five significant peaks between 5 and 10 min (**Appendix A Fig. A2**). The five peak clusters observed corresponded to prodigiosin [retention time (Rt) 5.11 min], serratamolide E (Rt 5.74 min), serratamolide A (Rt 7.14 and 7.36 min), serratamolide B (Rt 8.21 and 8.49 min) and serratamolide C (Rt 8.74 and 9.00 min) (Dwivedi et al., 2008; Thies et al., 2014) (**Table 2.3**). The main peak observed at 7.36 min corresponded to serratamolide A, based on the M_r 514.33 corresponding to the detected protonated molecule (*m/z* 515.33) and sodiated molecule (*m/z* 537.31) (Dwivedi et al., 2008), as indicated in **Table 2.3**.

Table 2.3 Summary of the compounds identified in the crude extracts obtained from *S. marcescens* P1 and NP1 strains, detected using high-resolution mass spectrometry (UPLC-ESI-MS analysis) (< 10 ppm).

Compound	UPLC Rt (min)	UPLC Rt (min)	Proposed fatty acid chain length	Monoisotopic mass (M_r)	Theoretical/ Detected Protonated specie (*m/z*)		Theoretical/ Detected Sodiated specie (*m/z*)	
	P1 crude extract	NP1 crude extract			P1 crude extract	NP1 crude extract	P1 crude extract	NP1 crude extract
Prodigiosin	5.11	N/D	-	323.1998	324.2077 324.2065	N/D	N/D	N/D
Serratamolide A (Serrawettin W1)	7.14 7.36	7.14 7.36	C_{10}+C_{10}	514.3254	515.3333 515.3325	515.3333 515.3325	537.3152 537.3103	537.3152 537.3204
Serratamolide B	8.21 8.49	8.21 8.49	C_{10}+$C_{12:1}$	540.3411	541.3490 541.3463	541.3490 541.3463	563.3309 563.3271	563.3309 563.3271
Serratamolide C	8.74 9.00	8.74 9.00	C_{10}+C_{12}	542.3567	543.3646 543.3700	543.3646 543.3598	565.3465 565.3500	565.3465 565.3500
Serratamolide E	5.74	5.74	C_{8}+C_{10}	486.2941	487.3020 487.3048	487.3020 487.3048	509.2839 509.2740	509.2839 509.2740
Glucosamine derivative A	N/D	9.54	-	584.4073	N/D	585.4116 585.4073	N/D	607.3935 607.3953

N/D – not detected

2.3.4.2. NP1 crude extract

Similar to the crude extract obtained from *S. marcescens* P1, the positive mode ESI-MS analysis of the crude extract obtained from *S. marcescens* NP1 revealed a cluster of *m/z* peaks with a difference of 2, 26, or 28 amu in their molecular ion species, revealing four groups of homologues. The spectra in the positive mode revealed the main groups of molecular ions at *m/z* 487.30, 515.33, 541.35 and 543.36 $[M+H]^+$ (**Table 2.3**; **Appendix A Fig. A1 b1-5**) which corresponded to the protonated singly charged species. Their corresponding sodium adducts were also detected at *m/z* 509.27, 537.32, 563.33 and 565.35 $[M+Na]^+$ (**Table 2.3**). The detected molecular ions at *m/z* 487.30, 515.33, 541.35 and 543.36 corresponded to serratamolide E, A, B and C, respectively (**Table 2.3**), as previously reported by Dwivedi et al. (2008). However, *m/z* 585.41 $[M+H]^+$ and *m/z* 607.40 $[M+Na]^+$ were also detected and corresponded to a protonated and sodiated singly charged glucosamine derivative A (Dwivedi et al., 2008).

The UPLC-MS analysis revealed five significant peaks between 5 and 10 min (**Appendix A Fig. A3**). The peaks eluted corresponded to serratamolide E (Rt 5.74 min), serratamolide A (Rt 7.14 and 7.36 min), serratamolide B (Rt 8.21 and 8.49 min) and serratamolide C (Rt 8.74 and 9.00 min), as reported in literature (Dwivedi et al., 2008; Thies et al., 2014) (**Table 2.3**). However, a peak was observed at a retention time of 9.54 min that corresponded to a glucosamine derivative A (Dwivedi et al., 2008), while prodigiosin was not detected. The main peak observed at 7.36 min corresponded to serratamolide A, based on the M_r 514.33 corresponding to the detected protonated molecule (*m/z* 515.33) and sodiated molecule (*m/z* 537.32), as indicated in **Table 2.3**.

2.3.4.3. NP2 crude extract

The positive mode ESI-MS analysis of the crude extract obtained from the *S. marcescens* NP2 strain revealed a cluster of *m/z* peaks with a difference of approximately 14 and 16 amu in their molecular ion species, revealing five groups of homologues. The spectra in positive mode revealed the main groups of molecular ions at *m/z* 690.41, 704.42, 718.44, 732.45 and 748.46 $[M+H]^+$ (**Table 2.4**; **Appendix A Fig. A4**) which corresponded to the protonated singly charged species.

Table 2.4 Summary of the analogues identified in the crude extract obtained from the *S. marcescens* NP2 strain, detected using high-resolution mass spectrometry (UPLC-ESI-MS analysis) (< 10 ppm).

Compound name	Literature name of compound	UPLC Rt (min)	Proposed analogue structure (Literature)	Monoisotopic mass (M_r)	Theoretical/ Detected Protonated specie (*m/z*)	Theoretical/ Detected Sodiated specie (*m/z*)
Serrawettin W2 E	Unidentified	6.34	-	N/A	N/A 690.4106	N/A 712.3941
Serrawettin W2 D	Serrawettin W6	6.88	C_{10}OH-Ile/Leu-Ser-Thr-Tyr-Ile/Leu	747.4418	748.4497 748.4564	770.4316 770.4290
Serrawettin W2 C	Serrawettin W5; sw-1	6.80 7.02	C_8OH-Ile/Leu-Ser-Thr-Phe-Ile/Leu C_{10}OH-Abu/Aib-Ser-Thr-Phe-Ile/Leu	703.4156	704.4235 704.4213	726.4054 726.4014
Serrawettin W2 B	sw-2; Serrawettin W4	7.81	C_{10}OH-Val-Ser-Thr-Phe-Ile/Leu C_{10}OH-Ile/Leu-Ser-Thr-Phe-Val	717.4313	718.4392 718.4441	740.4211 740.4263
Serrawettin W2 A	Serrawettin W2; sw-3; sw-4; sw-5	8.22 8.46	C_{10}OH-Leu/Ile-Ser-Thr-Phe-Ile/Leu	731.4469	732.4548 732.4514	754.4367 754.4413

N/A – Not applicable

Their corresponding sodium adducts were also detected at *m/z* 712.39, 726.41, 740.43, 754.44 and 770.43 $[M+Na]^+$ (**Table 2.4**). The detected molecular ions were denoted serrawettin W2 C (*m/z* 704.42), serrawettin W2 B (*m/z* 718.44), serrawettin W2 A (*m/z* 732.45) and serrawettin W2 D (*m/z* 748.46) (**Table 2.4**). Therefore, serrawettin W2 A (*m/z* 732.45), serrawettin W2 C (*m/z* 704.42) and serrawettin W2 D (*m/z* 748.46) corresponded to serrawettin W2, serrawettin W5 and serrawettin W6, respectively, as previously reported by Motley et al. (2016), while serrawettin W2 B (*m/z* 718.44) corresponded to an analogue, referred to as sw-2 or serrawettin W4 (Motley et al., 2016; Su et al., 2016). Lastly, a molecular ion species was detected at *m/z* 690.41 $[M+H]^+$; however, it did not correspond to the *m/z* of any previously reported analogues of serrawettin W2.

The UPLC-MS analysis revealed five significant peaks between 5 and 10 min (**Appendix A Fig. A5**). The peaks eluted corresponded to serrawettin W2 D (Rt 6.88 min), serrawettin W2 C (Rt 6.80 and 7.02 min), serrawettin W2 B (Rt 7.81 min) and serrawettin W2 A (Rt 8.22 and 8.46 min) as reported in literature (Motley et al., 2016; Su et al., 2016). In contrast, the peak detected at a retention time of 6.34 min did not correspond to a serrawettin W2 analogue previously reported in literature. The main peak observed at 8.46 min corresponded to serrawettin W2, based on the M_r 731.45 corresponding to the detected protonated molecule (*m/z* 732.45) and sodiated molecule (*m/z* 754.44) (Su et al., 2016), as indicated in **Table 2.4**.

2.3.5. Antimicrobial and Haemolytic Activity of the Crude Extracts

The chemically characterised crude extracts produced by *S. marcescens* P1, NP1 and NP2 were subjected to antimicrobial assays against a broad range of bacterial and fungal strains (**Table 2.5**). The crude extract produced by the pigmented *S. marcescens* P1 strain (oil refinery isolate) displayed activity against 63.6% (*n* = 7) of the Gram-negative bacteria tested in the current study (**Table 2.5**). The Gram-negative bacterial strains that were the most susceptible were *P. aeruginosa* S1 68 (environmental strain) and PA3 (clinical strain) with inhibition zones of 18.0 ± 1.0 mm recorded, respectively, while the clinical *A. baumannii* AB3 strain was the least susceptible with an inhibition zone of 9.7 ± 0.6 mm. The P1 crude extract also displayed activity against 90% (*n* = 9) of the Gram-positive bacteria tested in the current study (**Table 2.5**). The *L. monocytogenes* G1 food isolate was the most susceptible with an inhibition zone of 24.7 ± 0.6 mm recorded, while the least susceptible strain was *B. cereus* ATCC 10876 with an inhibition zone of 12.3 ± 0.6 mm. Lastly, the P1 crude extract displayed activity against 100% (*n* = 6) of the *C. albicans* and *C. neoformans* strains tested. The most susceptible fungal strain was *C. albicans* ATCC 66027 with an inhibition zone of 25.0 ± 0.0 mm recorded, while the least susceptible was the environmental *C. neoformans* CAB831 strain with an inhibition zone of 12.0 ± 0.0 mm.

Table 2.5 Activity of the biosurfactant extracts (1.00 mg/mL) against a panel of Gram-negative and Gram-positive bacterial and fungal isolates as determined by agar disc diffusion method.

***S. marcescens* strain number**		**P1**	**NP1**	**NP2**
Test microorganism	**Source**	**Antimicrobial zone of inhibition (mm; mean ± standard deviation)**		
Gram-negative bacteria				
Escherichia coli (ATCC 13706)	ATCC	17.0 ± 1.0	0.0	0.0
Enterohaemorrhagic E. coli (O157:H7)	ATCC	0.0	0.0	0.0
Legionella longbeachae (ATCC 33462)	ATCC	0.0	0.0	12.0 ± 0.0
Legionella pneumophila (ATCC 33152)	ATCC	12.7 ± 0.6	13.7 ± 0.6	0.0
Pseudomonas aeruginosa (ATCC 27853)	ATCC	15.0 ± 1.0	14.7 ± 1.2	0.0
P. aeruginosa (S1 68)	Environmental	18.0 ± 1.0	15.0 ± 1.7	0.0
**P. aeruginosa* (PA3)	Clinical	18.0 ± 1.0	11.0 ± 1.0	11.0 ± 1.0
Klebsiella pneumoniae (ATCC 10031)	ATCC	0.0	0.0	0.0
**K. pneumoniae* KP3	Clinical	0.0	0.0	0.0
Acinetobacter baumannii (ATCC 19606)	ATCC	12.3 ± 0.6	12.3 ± 0.6	10.0 ± 1.0
***A. baumannii* (AB3)	Clinical	9.7 ± 0.6	0.0	14.0 ± 1.0
Gram-positive bacteria				
Bacillus cereus (ATCC 10876)	ATCC	12.3 ± 0.6	10.3 ± 0.6	0.0
B. cereus (S1 77)	Environmental	18.3 ± 0.6	15.7 ± 0.6	12.7 ± 0.6
Bacillus sp. (S8 38)	Environmental	0.0	0.0	8.7 ± 0.6
Enterococcus faecalis (ATCC 7080)	ATCC	15.0 ± 0.0	12.7 ± 0.6	0.0
E. faecalis (S1)	Clinical	18.0 ± 0.0	16.7 ± 0.6	0.0
Listeria monocytogenes (ATCC 13932)	ATCC	20.7 ± 0.6	21.0 ± 1.0	0.0
L. monocytogenes (G1)	Food	24.7 ± 0.6	0.0	17.7 ± 1.5
Staphylococcus aureus (ATCC 25923)	ATCC	14.0 ± 0.0	19.0 ± 0.6	0.0
Staphylococcus equorum (SP2)	Environmental	22.3 ± 0.6	0.0	0.0
Methicillin-resistant *S. aureus* (MRSA) (Xen 30)	Clinical	19.3 ± 0.6	14.0 ± 0.0	0.0
Fungal strains				
Candida albicans (ATCC 66027)	ATCC	25.0 ± 0.0	15.0 ± 0.0	0.0
C. albicans (CAB8911)	Clinical	12.3 ± 0.6	11.3 ± 1.5	0.0
C. albicans (CAB1085)	Environmental	14.3 ± 0.6	12.6 ± 1.5	0.0
Cryptococcus neoformans (CAB831)	Environmental	12.0 ± 0.0	12.0 ± 0.6	0.0
C. neoformans (CAB1055)	Clinical	12.6 ± 1.2	11.3 ± 0.5	7.7 ± 0.6
C. neoformans (CAB844)	Environmental	13.0 ± 1.7	15.0 ± 1.7	0.0

*MDR strain, **XDR strain

The crude extract produced by the non-pigmented *S. marcescens* NP1 strain (Krom River isolate) displayed activity against 45.5% (*n* = 5) of the Gram-negative bacteria tested in the current study (**Table 2.5**). The most susceptible Gram-negative bacterial strain was *P. aeruginosa* S1 68 with an inhibition zone of 15.0 ± 1.7 mm, while the least susceptible strain was *P. aeruginosa* PA3 with an inhibition zone of 11.0 ± 1.0 mm. The NP1 crude extract also displayed activity against 70% (*n* = 7) of the Gram-positive bacteria tested in the current study (**Table 2.5**). The most susceptible Gram-positive bacterial strain was *L. monocytogenes* ATCC 13932 with an inhibition zone of 21.0 ± 1.0 mm recorded, while the least susceptible strain was *B. cereus* ATCC 10876 with an inhibition zone of 10.3 ± 0.6 mm. Lastly, the NP1 crude extract displayed activity against 100% (*n* = 6) of the *C. albicans* and *C. neoformans* strains tested. The most susceptible fungal strains were *C. albicans* ATCC 66027 and *C. neoformans* CAB844 (environmental strain) with inhibition zones of 15.0 ± 0.0 mm and 15.0 ± 1.7 mm recorded, respectively. The clinical *C. albicans* CAB8911 and *C. neoformans* CAB1055 strains were the least susceptible with inhibition zones of 11.3 ± 1.5 mm and 11.3 ± 0.5 mm recorded, respectively.

The crude extract produced by the non-pigmented *S. marcescens* NP2 strain (WWTP isolate) displayed activity against 36.4% (*n* = 4) of the Gram-negative bacteria tested in the current study (**Table 2.5**). *Acinetobacter baumannii* AB3 was the most susceptible Gram-negative bacterial strain with an inhibition zone of 14.0 ± 1.0 mm recorded, while the least susceptible strain was *A. baumannii* ATCC 19606 with an inhibition zone of 10.0 ± 1.0 mm. Similarly, the NP2 crude extract displayed activity against 30% (*n* = 3) of the Gram-positive bacteria tested (**Table 2.5**). The most susceptible strain was *L. monocytogenes* G1 with an inhibition zone of 17.7 ± 1.5 mm, while the least susceptible was the environmental *Bacillus* sp. S8 38 strain with an inhibition zone of 8.7 ± 0.6 mm. Lastly, the NP2 crude extract only displayed activity against one (16.7%) of the fungal strains (*C. neoformans* CAB1055), with an inhibition zone of 7.7 ± 0.6 mm recorded.

In addition to antimicrobial activity, the P1, NP1 and NP2 crude extracts were tested for haemolytic activity on sheep blood agar. The crude extracts were found to be γ-haemolytic on sheep blood agar, indicating that the extracts did not lyse the red blood cells in comparison to the positive control, surfactin (Sigma-Aldrich), which displayed prominent β-haemolytic (clear lysis zone) activity.

2.4. Discussion

Based on the physico-chemical and molecular analysis, one pigmented (P1; isolated from oil refinery effluent) and two non-pigmented [NP1 (isolated from the Krom River) and NP2 (isolated from a WWTP sample)] *S. marcescens* strains were selected for UPLC-ESI-MS analysis to identify potential antimicrobial compounds present in the crude extracts. The major peak detected in both *S. marcescens* P1 and NP1 crude extracts corresponded to serrawettin W1 (serratamolide A;

m/z 515.33 $[M+H]^+$), while homologues of serratamolide A (namely, serratamolide B, C and E) were also detected. The chemical characterisation of the compounds produced by the *S. marcescens* P1 and NP1 strains thus correspond to the molecular analysis, where the *swrW* gene that encodes for serrawettin W1 synthetase (serratamolides) was detected in both strains. The detected serratamolides are comprised of a cyclic peptide moiety of two serine amino acids and are linked to two β-hydroxy fatty acids that vary in chain length, thus resulting in various homologues (Eckelmann et al., 2018). Thies et al. (2014) identified various serrawettin W1 homologues, including serratamolide C, D, E and F as well as two novel homologues (*m/z* of 557 and 571), in a crude extract obtained from a pigmented *S. marcescens* DSM12481 strain, while Dwivedi et al. (2008) found that a pigmented *Serratia* sp. strain SHHRE645 produced serratamolide A, B, C, D and F homologues. In the current study, *S. marcescens* P1 was also found to produce prodigiosin and previous studies have similarly isolated *S. marcescens* strains that are capable of co-producing prodigiosin and serratamolide homologues (serrawettin W1) (Eckelmann et al., 2018; Hage-Hülsmann et al., 2018). As expected, the non-pigmented strain did not produce prodigiosin; however, the NP1 strain produced another secondary metabolite referred to as glucosamine derivative A. This corresponds to literature, where Dwivedi et al. (2008) reported on the co-production of serratamolides with glucosamine derivatives by a pigmented *Serratia* sp. strain SHHRE645 previously isolated from the rhizosphere of wheat.

In contrast, the major peak detected in the *S. marcescens* NP2 crude extract corresponded to serrawettin W2 (*m/z* 732.45 $[M+H]^+$), while analogues of this compound were also detected. The detected serrawettin W2 is comprised of a cyclic peptide moiety of five amino acids (D-leucine/isoleucine-L-serine-L-threonine-D-phenylalanine-L-isoleucine/leucine) linked to a β-hydroxy fatty acid moiety of varying chain length (Matsuyama et al., 1992). However, further chemical characterisation is required to determine the exact amino acid composition of each analogue and confirm the identity of the potential novel analogue of serrawettin W2 with a molecular ion detected at *m/z* 690.41 $[M+H]^+$. The chemical characterisation of the compounds within the NP2 crude extract also corresponded to the molecular analysis, where the *swrA* gene that encodes for non-ribosomal serrawettin W2 synthetase was detected. Moreover, as the chemical characterisation of the crude extract indicated that serrawettin W2 and analogues of this lipopeptide were produced, the primers designed in this study successfully provided an indication of the biosurfactant produced by the *Serratia* strain. *Serratia* spp. capable of producing serrawettin W2 and analogues of this lipopeptide have been isolated by various research groups (Motley et al., 2016; Su et al., 2016; Heise et al., 2019). A study by Heise et al. (2019) isolated and identified a *S. marcescens* strain from the gut of a burying beetle, *Nicrophorus vespilloides* and discovered that the *S. marcescens* strain was able to produce serrawettin W2 (*m/z* 732.45 $[M+H]^+$). Similarly, Su et al. (2016) isolated a pigmented

S. surfactantfaciens YD25^T strain from rhizosphere soil and found that the strain produced various serrawettin W2 analogues, including *m/z* 704.3, 718.3, 732.2 and 746.4 $[M+H]^+$, amongst others.

The antimicrobial activity of the crude extracts obtained from the three *S. marcescens* strains was subsequently assessed against pathogenic and opportunistic bacterial and fungal strains (including MDR and XDR clinical isolates), using disc diffusion assays. The P1 and NP1 crude extracts were both effective against a broader range of Gram-positive bacteria (90% and 70%, respectively) in comparison to Gram-negative bacteria (64% and 45%, respectively), while both crude extracts displayed activity against all fungal strains tested. These results correlate to previous research where it was indicated that serrawettin W1 (serratamolide) exhibits antimicrobial activity towards Gram-positive bacteria, such as MRSA strains (Kadouri and Shanks, 2013) and fungal strains, such as *C. albicans* (Zhu et al., 2018). However limited research on the activity of serrawettin W1 (and its homologues) against Gram-negative bacteria has been reported. In contrast, in the current study, the NP2 crude extract was effective against 36% of the Gram-negative bacteria and 30% of the Gram-positive bacteria analysed, and a low antifungal activity was recorded (17%). Thus, in comparison to the P1 and NP1 crude extracts, a narrow-spectrum of antimicrobial activity was observed for the secondary metabolites produced by the *S. marcescens* NP2 strain. Literature has however, indicated that serrawettin W2 displays antimicrobial activity against Gram-positive and Gram-negative bacteria, such as *S. aureus, P. aeruginosa, Micrococcus luteus* and *S. dysenteriae*, amongst others (Su et al., 2016). A study by Motley et al. (2016) also reported that serrawettin W2 analogues displayed antifungal activity against *C. albicans*.

Moreover, despite the fact that serrawettin W1 and serrawettin W2 were discovered more than 30 years ago (Wasserman et al., 1962; Matsuyama et al., 1986), limited information is currently available on the antimicrobial mode of action of these compounds. It is however, well-known that the primary target of lipopeptides is the cell membrane (Schlusselhuber et al., 2018). The proposed general mode of action is driven by the interaction of the peptide moiety of the lipopeptide with the polar head groups of the phospholipids. Thereafter, the hydrophobic moiety of the lipopeptide (fatty acids) is incorporated into the hydrophilic moiety (lipopolysaccharides) of the cell membrane (Jenssen, 2006; Schlusselhuber et al., 2018). A few studies have also revealed that the length of the fatty acid chain affects the antimicrobial potency of the lipopeptide due to the changes in the hydrophobic interaction of the lipopeptide with the cell membrane (Malina and Shai, 2005; Chu-Kung et al., 2010; Schlusselhuber et al., 2018). As the P1 and NP1 crude extracts were comprised of four serratamolide homologues with two fatty acid chains of varying lengths (C_8 to C_{12}) per homologue, the combination of the lipopeptides with varying lengths could provide an explanation for the broad-spectrum activity observed for these crude extracts against both bacteria and fungi. In contrast, the NP2 crude extract was comprised of serrawettin W2 analogues with one C_{10} fatty acid

chain (with the exception of one analogue that has a C_8 fatty acid chain) attached to a peptide moiety, which could elucidate the reduced antimicrobial activity.

As indicated, an additional secondary metabolite, prodigiosin, was detected in the P1 crude extract and has been reported to display antimicrobial activity against *S. aureus, B. subtilis* and *Streptococcus pyogenes*, amongst others (Darshan and Manonmani, 2015). Danevčič et al. (2016) investigated the mode of action of prodigiosin and found that this compound interacts with the cytoplasmic membrane and increases the membrane permeability in *B. subtilis*, as well as uncouples proton transport and disrupts energy generation, ultimately leading to cell lysis and death. Hage-Hülsmann et al. (2018) further found that prodigiosin and serrawettin W1, produced by a *S. marcescens* DSM12481 strain, displayed greater antimicrobial activity in combination against a soil bacterium, *C. glutamicum,* compared to the individual activity of these two compounds. Moreover, the NP1 crude extract was found to contain a secondary metabolite known as glucosamine derivative A, which could have contributed to the observed antibacterial and antifungal activity. Although limited information is available on the antifungal activity of glucosamine derivatives produced by *Serratia* spp., Dwivedi et al. (2008) has indicated that all compounds, including serratamolides A to F, open ring-serratamolides B and D and glucosamine derivatives A to C, produced by a pigmented *Serratia* sp. SHHRE645 strain, exhibited antimycobacterial activities. Based on the results obtained in the current study, many of the water- and foodborne pathogens and opportunistic pathogens selected as test organisms, e.g. *L. monocytogenes*, *S. aureus*, *Bacillus* spp. virulent *E. coli*, *Enterococcus* spp., *Legionella* spp. and *Pseudomonas* spp. (Sharma et al., 2003; Mayrhofer et al., 2004; Moritz et al., 2010; Clements et al., 2019b), were susceptible to the metabolites present in the P1 and NP1 crude extracts. Moreover, MDR and XDR bacteria frequently associated with hospital-acquired infections, such as *A. baumannii*, *P. aeruginosa*, *Enterococcus* spp. and MRSA (Khan et al., 2015; Khan et al., 2017), as well as fungal opportunistic pathogens, such as *C. albicans* and *C. neoformans* were also inhibited by the P1 and NP1 crude extracts. It is thus hypothesised that the broad-spectrum antimicrobial activity observed for the P1 and NP1 crude extracts was due to the synergistic effect of serratamolide homologues and prodigiosin (P1) and the glucosamine derivative A (NP1), which effectively inhibited the proliferation of these water- and foodborne opportunistic pathogens and clinical strains. In comparison, a narrow or limited activity against the test strains was observed for the NP2 crude extract, where serrawettin W2 analogues only were identified.

Previous studies have however, indicated that serratamolides exhibit cytotoxic and haemolytic activity (Shanks et al., 2012; Petersen et al., 2017). A study by Shanks et al. (2012) investigated the haemolytic and cytotoxic activity of purified serratamolide A and found that the lipopeptide haemolysed sheep and murine red blood cells and was cytotoxic to human airway and corneal limbal epithelial cells *in vitro*. Furthermore, Su et al. (2016) demonstrated that serrawettin W2

exhibits cytotoxicity to cancer cell lines (such as Hela cells), while reduced activity towards non-malignant cell lines (such as Vero cells) was recorded. Results obtained in the current study however, indicated that at a concentration of 1.00 mg/mL, the P1, NP1 and NP2 crude extracts did not display haemolytic activity on sheep blood agar. While further analysis of the purified compounds and crude extracts' cytotoxicity and haemolytic activity against human red blood cells is required, the secondary metabolites produced by *S. marcescens* P1, NP1 and NP2 strains may still have the potential to be applied as broad- or narrow-spectrum antimicrobial agents.

2.5. Conclusions

The crude extracts obtained from *S. marcescens* P1 and NP1 exhibited broad-spectrum antibacterial and antifungal activity against MDR *P. aeruginosa,* MRSA and clinical *C. neoformans*, amongst others. Although the mode of action of serrawettins has not yet been fully elucidated, secondary metabolites produced by specifically *S. marcescens* strains P1 and NP1 have thus emerged as promising candidates for the treatment of infections caused by Gram-negative and Gram-positive pathogens and opportunistic pathogens as well as fungal pathogens of clinical and industrial significance. In comparison, whilst displaying activity against MDR *P. aeruginosa* and XDR *A. baumannii*, the crude extract obtained from *S. marcescens* NP2 exhibited a narrow-spectrum antimicrobial activity.

It is also important to note that limited information on the acquired resistance of pathogens and opportunistic pathogens to these secondary metabolites has been recorded. This implies that these bioactive compounds could serve as promising antibacterial and antifungal agents for therapeutic application. It is however, recommended that the crude extracts be further purified to elucidate the detailed structure of each homologue of serrawettin W1 and analogue of serrawettin W2. It is further recommended that the biofilm disruption and antiadhesive potential of the extracts against bacterial and fungal strains be investigated for application as antifouling agents in the food, water and medical industries.

Acknowledgements

This work was supported by the Water Research Commission (Grant number K5/2728//3) and the National Research Foundation of South Africa (Grant number: 113849). Opinions expressed and conclusions arrived at, are those of the authors and are not necessarily to be attributed to the National Research Foundation. The authors also wish to thank the Department of Chemistry at Stellenbosch University and Mrs Peta Steyn for the use of the Du Nouy tensiometer.

Compliance with ethical standards

Conflict of interest: The authors declare that they have no competing interests.

Ethical approval: This article does not contain any studies with human participants or animals.

2.6. References

Apao, M.M.N., Teves, F.G., Madamba, M.R.S.B., 2012. Sequence analysis of putative *swrW* gene required for surfactant serrawettin W1 production from *Serratia marcescens*. Afr. J. Biotechnol. 11, 12040-12044. https://doi.org/10.5897/AJB12.1213.

Benadé, E., Stone, W., Mouton, M., Postma, F., Wilsenach, J., Botha, A., 2016. Binary interactions of antagonistic bacteria with *Candida albicans* under aerobic and anaerobic conditions. Microb. Ecol. 71, 645-659. https://doi.org/10.1007/s00248-015-0706-4.

Bérdy, J., 2005. Bioactive microbial metabolites. J. Antibiotics. 58(1), 1. https://doi.org/10.1038/ja.2005.1.

Centres for Disease Control and Prevention (CDC), 2013. Antibiotic resistance threats in the United States, 2013. https://www.cdc.gov/drugresistance/pdf/ar-threats-2013-508.pdf (accessed at 11 March 2019).

Chu-Kung, A.F., Nguyen, R., Bozzelli, K.N., Tirrell, M., 2010. Chain length dependence of antimicrobial peptide–fatty acid conjugate activity. J. Colloid Interface Sci. 345(2), 160-167. https://doi.org/10.1016/j.jcis.2009.11.057.

Clements, T., Ndlovu, T., Khan, S., Khan, W., 2019a. Biosurfactants produced by *Serratia* species: Classification, biosynthesis, production and application. Appl. Microbiol. Biotechnol. 103, 589-602. https://doi.org/10.1007/s00253-018-9520-5.

Clements, T., Reyneke, B., Strauss, A., Khan, W., 2019b. Persistence of Viable Bacteria in Solar Pasteurised Harvested Rainwater. Water Air Soil Poll. 230(6), 130. https://doi.org/10.1007/s11270-019-4184-z.

Colombo, A.L., Júnior, J.N., Guinea, J., 2017. Emerging multidrug-resistant *Candida* species. Curr. Opin. Infect. Dis. 30, 528-538. https://doi.org/10.1097/QCO.0000000000000411.

Danevčič, T., Borić Vezjak, M., Tabor, M., Zorec, M., Stopar, D., 2016. Prodigiosin induces autolysins in actively grown *Bacillus subtilis* cells. Front. Microbiol. 7, 27. https://doi.org/10.3389/fmicb.2016.00027.

Darshan, N., Manonmani, H.K., 2015. Prodigiosin and its potential applications. J. Food Sci. Technol. 52, 5393-5407. https://doi.org/10.1007/s13197-015-1740-4.

Das, P., Mukherjee, S., Sen, R., 2008. Antimicrobial potential of a lipopeptide biosurfactant derived from a marine *Bacillus circulans*. J. Appl. Microbiol. 104(6), 1675-1684. https://doi.org/10.1111/j.1365-2672.2007.03701.x.

Dwivedi, D., Jansen, R., Molinari, G., Nimtz, M., Johri, B.N., Wray, V., 2008. Antimycobacterial serratamolides and diacyl peptoglucosamine derivatives from *Serratia* sp. J. Nat. Prod. 71, 637-641. https://doi.org/10.1021/np7007126.

Eckelmann, D., Spiteller, M., Kusari, S., 2018. Spatial-temporal profiling of prodiginines and serratamolides produced by endophytic *Serratia marcescens* harbored in *Maytenus serrata*. Sci. Rep. 8, 5283. https://doi.org/10.1038/s41598-018-23538-5.

Grimont, F., Grimont, P.A., 2006. The genus *Serratia*, in: The prokaryotes. Springer, New York, pp. 219-244.

Hage-Hülsmann, J., Grünberger, A., Thies, S., Santiago-Schübel, B., Klein, A.S., Pietruszka, J., Binder, D., Hilgers, F., Domröse, A., Drepper, T., Kohlheyer, D., 2018. Natural biocide cocktails: Combinatorial antibiotic effects of prodigiosin and biosurfactants. PloS One. 13, p.e0200940. https://doi.org/10.1371/journal.pone.0200940.

Harris, A.K., Williamson, N.R., Slater, H., Cox, A., Abbasi, S., Foulds, I., Simonsen, H.T., Leeper, F.J., Salmond, G.P., 2004. The *Serratia* gene cluster encoding biosynthesis of the red antibiotic, prodigiosin, shows species-and strain-dependent genome context variation. Microbiol. 150, 3547-3560. https://doi.org/10.1099/mic.0.27222-0.

Heise, P., Liu, Y., Degenkolb, T., Vogel, H., Schäberle, T.F., Vilcinskas, A., 2019. Antibiotic-producing beneficial bacteria in the gut of the burying beetle *Nicrophorus vespilloides*. Front. Microbiol. 10, 1178. https://doi.org/10.3389/fmicb.2019.01178.

Jenssen, H., Hamill, P., Hancock, R.E., 2006. Peptide antimicrobial agents. Clin. Microbiol. Rev. 19(3), 491-511. https://doi.org/10.1128/CMR.00056-05.

Kadouri, D.E., Shanks, R.M., 2013. Identification of a methicillin-resistant *Staphylococcus aureus* inhibitory compound isolated from *Serratia marcescens*. Res. Microbiol. 164, 821-826. https://doi.org/10.1016/j.resmic.2013.06.002.

Khan, H.A., Ahmad, A., Mehboob, R., 2015. Nosocomial infections and their control strategies. Asian Pac. J. Trop. Biomed. 5(7), 509-514. https://doi.org/10.1016/j.apjtb.2015.05.001.

Khan, H.A., Baig, F.K., Mehboob, R., 2017. Nosocomial infections: Epidemiology, prevention, control and surveillance. Asian Pac. J. Trop. Biomed. 7(5), 478-482. https://doi.org/10.1016/j.apjtb.2017.01.019

Li, H., Tanikawa, T., Sato, Y., Nakagawa, Y., Matsuyama, T., 2005. *Serratia marcescens* gene required for surfactant serrawettin W1 production encodes putative aminolipid synthetase belonging

to nonribosomal peptide synthetase family. Microbiol. Immunol. 49, 303-310. https://doi.org/10.1111/j.1348-0421.2005.tb03734.x.

Lindum, P.W., Anthoni, U., Christophersen, C., Eberl, L., Molin, S., Givskov, M., 1998. N-Acyl-L-homoserine lactone autoinducers control production of an extracellular lipopeptide biosurfactant required for swarming motility of *Serratia liquefaciens* MG1. J. Bacteriol. 180, 6384-6388.

Malina, A., Shai, Y., 2005. Conjugation of fatty acids with different lengths modulates the antibacterial and antifungal activity of a cationic biologically inactive peptide. Biochem. J. 390(3), 695-702. https://doi.org/10.1042/BJ20050520.

Matsuyama, T., Fujita, M., Yano, I., 1985. Wetting agent produced by *Serratia marcescens*. FEMS Microbiol. Lett. 28, 125-129. https://doi.org/10.1111/j.1574-6968.1985.tb00777.x

Matsuyama, T., Murakami, T., Fujita, M., Fujita, S., Yano, I., 1986. Extracellular vesicle formation and biosurfactant production by *Serratia marcescens*. Microbiol. 132, 865-875. https://doi.org/10.1099/00221287-132-4-865.

Matsuyama, T., Kaneda, K., Ishizuka, I., Toida, T., Yano, I., 1990. Surface-active novel glycolipid and linked 3-hydroxy fatty acids produced by *Serratia rubidaea*. J. Bacteriol. 172, 3015-3022. https://doi.org/10.1128/jb.172.6.3015-3022.1990.

Matsuyama, T., Kaneda, K., Nakagawa, Y., Isa, K., Hara-Hotta, H., Yano, I., 1992. A novel extracellular cyclic lipopeptide which promotes flagellum-dependent and-independent spreading growth of *Serratia marcescens*. J. Bacteriol. 174, 1769-1776. https://doi.org/10.1128/jb.174.6.1769-1776.1992.

Matsuyama, T., Tanikawa, T., Nakagawa, Y., 2011. Serrawettins and other surfactants produced by *Serratia*, in: Soberón-Chávez G. (Eds.), Biosurfactants. Springer, Berlin, Heidelberg, pp. 93-120. https://doi.org/10.1007/978-3-642-14490-5_4.

Mayrhofer, S., Paulsen, P., Smulders, F.J., Hilbert, F., 2004. Antimicrobial resistance profile of five major food-borne pathogens isolated from beef, pork and poultry. Int. J. Food Microbiol. 97, 23-29. https://doi.org/10.1016/j.ijfoodmicro.2004.04.006.

McCarthy, M.W., Kontoyiannis, D.P., Cornely, O.A., Perfect, J.R., Walsh, T.J., 2017. Novel agents and drug targets to meet the challenges of resistant fungi. J. Infect. Dis. 216(S3), S474-S483. https://doi.org/10.1093/infdis/jix130.

Moritz, M.M., Flemming, H.C., Wingender, J., 2010. Integration of *Pseudomonas aeruginosa* and *Legionella pneumophila* in drinking water biofilms grown on domestic plumbing materials. Int. J. Hyg. Environ. Health. 213(3), 190-197. https://doi.org/10.1016/j.ijheh.2010.05.003.

Motley, J.L., Stamps, B.W., Mitchell, C.A., Thompson, A.T., Cross, J., You, J., Powell, D.R., Stevenson, B.S., Cichewicz, R.H., 2016. Opportunistic sampling of roadkill as an entry point to accessing natural products assembled by bacteria associated with non-anthropoidal mammalian microbiomes. J. Nat. Prod. 80, 598-608. https://doi.org/10.1021/acs.jnatprod.6b00772.

Ndlovu, T., Khan, S., Khan, W., 2016. Distribution and diversity of biosurfactant-producing bacteria in a wastewater treatment plant. Environ. Sci. Pollut. Res. 23, 9993-10004. https://doi.org/10.1007/s11356-016-6249-5.

Ndlovu, T., Rautenbach, M., Vosloo, J.A., Khan, S., Khan, W., 2017. Characterisation and antimicrobial activity of biosurfactant extracts produced by *Bacillus amyloliquefaciens* and *Pseudomonas aeruginosa* isolated from a wastewater treatment plant. AMB Express, 7(1): 108. https://doi.org/10.1186/s13568-017-0363-8.

Petersen, L.M., LaCourse, K., Schöner, T.A., Bode, H., Tisa, L.S., 2017. Inactivation of the major hemolysin gene influences expression of the nonribosomal peptide synthetase gene *swrA* in the insect pathogen *Serratia* sp. strain SCBI. J. Bacteriol. 199, e00333-17. https://doi.org/10.1128/JB.00333-17.

Schlusselhuber, M., Godard, J., Sebban, M., Bernay, B., Garon, D., Seguin, V., Oulyadi, H., Desmasures, N., 2018. Characterization of Milkisin, a novel lipopeptide with antimicrobial properties produced by *Pseudomonas* sp. UCMA 17988 isolated from bovine raw milk. Front. Microbiol. 9. https://doi.org/10.3389/fmicb.2018.01030.

Shanks, R.M., Stella, N.A., Lahr, R.M., Wang, S., Veverka, T.I., Kowalski, R.P., Liu, X., 2012. Serratamolide is a hemolytic factor produced by *Serratia marcescens*. PLoS One. 7, e36398. https://doi.org/10.1371/journal.pone.0036398.

Sharma, S., Sachdeva, P., Virdi, J.S., 2003. Emerging water-borne pathogens. Appl. Microbiol. Biotechnol. 61, 424-428. https://doi.org/10.1007/s00253-003-1302-y.

Stankovic, N., Senerovic, L., Ilic-Tomic, T., Vasiljevic, B., Nikodinovic-Runic, J., 2014. Properties and applications of undecylprodigiosin and other bacterial prodigiosins. Appl. Microbiol. Biotechnol. 98, 3841-3858. https://doi.org/10.1007/s00253-014-5590-1.

Su, C., Xiang, Z., Liu, Y., Zhao, X., Sun, Y., Li, Z., Li, L., Chang, F., Chen, T., Wen, X., Zhou, Y., 2016. Analysis of the genomic sequences and metabolites of *Serratia surfactantfaciens* sp. nov. YD25^T that simultaneously produces prodigiosin and serrawettin W2. BMC Genom. 17, 865. https://doi.org/10.1186/s12864-016-3171-7.

Thies, S., Santiago-Schübel, B., Kovačić, F., Rosenau, F., Hausmann, R., Jaeger, K.E., 2014. Heterologous production of the lipopeptide biosurfactant serrawettin W1 in *Escherichia coli*. J. Biotechnol. 181, 27-30. https://doi.org/10.1016/j.jbiotec.2014.03.037.

Wasserman, H.H., Keggi, J.J., McKeon, J.E., 1962. The Structure of Serratamolide[1-3]. J. Am. Chem. Soc. 84(15), 2978-2982. https://doi.org/10.1021/ja00874a028.

World Health Organization (WHO), 2015. Global action plan on antimicrobial resistance. https://www.who.int/medicines/publications/WHO-PPL-Short_Summary_25Feb-ET_NM_WHO.pdf (accessed 11 March 2019).

Youssef, N.H., Duncan, K.E., Nagle, D.P., Savage, K.N., Knapp, R.M., McInerney, M.J., 2004. Comparison of methods to detect biosurfactant production by diverse microorganisms. J. Microbiol. Methods. 56, 339-347. https://doi.org/10.1016/j.mimet.2003.11.001.

Zhu, H., Sun, S.J., Dang, H.Y., 2008. PCR detection of *Serratia* spp. using primers targeting *pfs* and *luxS* genes involved in AI-2-dependent quorum sensing. Curr. Microbiol. 57, 326-330. https://doi.org/10.1007/s00284-008-9197-6.

Zhu, L., Pang, C., Chen, L., Zhu, X., 2018. Antibacterial activity of a novel depsipeptide and prodigiosine of *Serratia marcescens* S823. Nat. Prod. Chem. Res. 6, 312.

Chapter 3:

(This chapter is compiled in the format of Frontiers in Chemistry and UK spelling is employed)

A metabolomics and molecular networking approach to elucidate the structures of the secondary metabolites produced by *Serratia marcescens* strains

Tanya Clements [1], Marina Rautenbach [2], Thando Ndlovu [1], Sehaam Khan [3] and Wesaal Khan [1]*

[1] Department of Microbiology, Faculty of Science, Stellenbosch University, Private Bag X1, Stellenbosch, 7602, South Africa

[2] Department of Biochemistry, Faculty of Science, Stellenbosch University, Private Bag X1, Stellenbosch, 7602, South Africa

[3] Faculty of Health Sciences, University of Johannesburg, PO Box 17011, Doornfontein, 2028, South Africa.

*Corresponding Author: Wesaal Khan; Phone: +27 21 808 5804; E-mail: wesaal@sun.ac.za

Abstract

This study aimed to elucidate the metabolic profiles and chemical structures of the secondary metabolites produced by pigmented (P1) and non-pigmented (NP1) *Serratia marcescens* (*S. marcescens*) strains. Additionally, the inhibitory potential of the selected compounds against a clinical *Enterococcus faecalis* (*E. faecalis*) S1 strain was assessed. An integrated approach that combines reverse-phase high-performance liquid chromatography (RP-HPLC), electrospray ionisation mass spectrometry, ultra-performance liquid chromatography coupled to tandem mass spectrometry (UPLC-MS^e) and molecular networking (using the Global Natural Products Social molecular network platform) was utilised. A molecular network of the metabolites produced by the P1 and NP1 strains was generated using the UPLC-MS^e data and revealed four major clusters, including two known families [serratiochelin and prodigiosin (P1)] that corresponded to spectral library databases and two unknown families. The molecular network then guided the elucidation of the unknown metabolites in combination with the UPLC-MS^e fragmentation patterns. Similar metabolic profiles were observed between the P1 and NP1 strains, where the structures of 18 compounds were elucidated for the P1 strain (including 6 serratamolides, 10 glucosamine derivatives, prodigiosin and serratiochelin A) and the structures of 15 compounds were elucidated for the NP1 strain (including 8 serratamolides, 6 glucosamine derivatives and serratiochelin A). The serratamolide homologues were comprised of a peptide moiety of two L-serine residues (cyclic or open-ring) linked to two fatty acid chains (lengths of C_{10}, C_{12} or $C_{12:1}$ chains). Moreover, the putative structure of a novel open-ring serratamolide homologue was described. The glucosamine derivative homologues (i.e *N*-butylglucosamine ester derivatives) consisted of four residues, including glucose/hexose, valine, a fatty acid chain (lengths of C_{13} to C_{17} and varying from saturated to unsaturated) and butyric acid. The putative structures of seven novel glucosamine derivative homologues and one glucosamine derivative congener (containing an oxo-hexanoic acid residue instead of a butyric acid residue) were described. Moreover, seven fractions collected during RP-HPLC, with major molecular ions corresponding to prodigiosin, serratamolides (A, B and C), and glucosamine derivatives (A, C and E), displayed antimicrobial activity against the clinical *E. faecalis* S1 strain using the disc diffusion assay. The minimum inhibitory and bactericidal concentration assays however, revealed that prodigiosin exhibited the greatest antimicrobial potency, followed by glucosamine derivative A and then the serratamolides (A, B and C). These results provide crucial insight into the secondary metabolic prolife of pigmented and non-pigmented *S. marcescens* strains and confirms that *S. marcescens* strains are a promising natural source of novel antimicrobial metabolites.

Keywords: Serratamolide; glucosamine derivative; *Serratia*; molecular network; UPLC-MS^e; antimicrobial

3.1. Introduction

Serratia are facultatively anaerobic, Gram-negative rods that are classified into the Enterobacteriaceae family (Grimont and Grimont 2015). The type species of this genus, *Serratia marcescens* (*S. marcescens*), is widely known to produce a distinctive red pigment referred to as prodigiosin (Su et al. 2016). *Serratia plymuthica* (*S. plymuthica*), *Serratia rubidaea* (*S. rubidaea*) and *Serratia nematodiphila* (*S. nematodiphila*) have also been reported to synthesise this pigment, while non-pigmented strains of these species have been identified (Su et al. 2016). In recent years, pigmented and non-pigmented *Serratia* species have been recognised as a potential source of novel and structurally diverse bioactive secondary metabolites (Soenens and Imperial 2019). These bioactive metabolites include the pigment prodigiosin as well as biosurfactants (lipopeptides and glycolipids), glucosamine derivatives, oocydin A, siderophores, bacteriocins, carbapenem, althiomycin and serratin, amongst others (Clements et al. 2019a; Khilyas et al. 2019). Prodigiosin and serrawettins are two of the more extensively studied secondary metabolites due to their diverse biological activity and application as antitumor, antibacterial and antifungal agents (Stankovic et al. 2014; Eckelmann et al. 2018; Clements et al. 2019a).

Prodigiosin is a red, tripyrrole pigment (family of prodiginines) that is produced by several bacterial genera, such as *Serratia, Hahella, Streptomyces, Zooshikella, Vibrio* and *Pseudomonas,* amongst others (Darshan and Manonmani 2015). Prodigiosin has a general structure of 2-methyl-3-pentyl-6-methoxyprodiginine and is composed of three rings referred to as pyrrolic ring A, B and C (Hage-Hülsmann et al. 2018; Yip et al. 2019). Research has indicated that it is synthesised via a bifurcated pathway encoded in a pigment (*pig*) gene cluster comprised of 14 genes (*pigABCDEFGHIJKLMN*) (Williamson et al. 2006). In contrast, serrawettins are non-ribosomally synthesised cyclodepsipeptides solely produced by several members of the *Serratia* genus. Serrawettins are classified as lipopeptides as they are composed of a hydrophilic peptide moiety and a hydrophobic fatty acid moiety. Three unique structures of serrawettins were initially identified, including serrawettin W1 (also referred to as serratamolide A), serrawettin W2 and serrawettin W3 (Wasserman et al. 1961; Matsuyama et al. 1985, 1986, 1992), while various analogues and homologues of serrawettin W1 and W2 have since been described (Dwivedi et al. 2008; Motley et al. 2016; Su et al. 2016). Serratamolide A and homologues of this lipopeptide (including serratamolide B to G) are comprised of a cyclic peptide moiety of two L-serine amino acids linked to two β-hydroxy fatty acid moieties that may vary in length (C_8 to C_{14}) of the fatty acyl chain and may be saturated or unsaturated (Dwivedi et al. 2008). In comparison, serrawettin W2 and W3 are comprised of five amino acids linked to one β-hydroxy fatty acid (Matsuyama et al. 1986, 1992).

Glucosamine derivatives (also referred to as *N*-butylglucosamine ester derivatives) are non-ribosomally synthesised diacylated peptoglucosamine derivatives (Dwivedi et al. 2008; Khilyas et al. 2019) produced by *Serratia* species. They have not been extensively studied and to date only Dwivedi et al. (2008) characterised glucosamine derivatives produced by a pigmented *S. marcescens* SHHRE645 strain. The identified glucosamine derivative homologues (A to C) were comprised of four residues, including glucose, valine, butyric acid and a saturated or unsaturated β-fatty acid residue of varying length. It was observed that the glucosamine derivatives were co-produced with serratamolide homologues. Although extensive research into the biological properties of glucosamine derivative homologues (A to C) is still required, Dwivedi et al. (2008) reported on the anti-mycobacterial activity observed for each homologue.

To date, several analytical methods have been utilised to elucidate the detailed structures and composition of secondary metabolites produced by *Serratia* species, including mass spectrometry (MS), liquid chromatography (LC), gas chromatography and nuclear magnetic resonance (NMR) (Dwivedi et al. 2008; Thies et al. 2014; Eckelmann et al. 2018). Chromatography methods are commonly coupled with mass spectroscopy for the reliable separation and identification of bioactive compounds (Fu et al. 2019). Moreover, tandem MS analysis allows for the detection and structural characterisation of a broad range of compounds and distinguishes between closely related forms of the same compound produced by a bacterial strain (Knolhoff et al. 2015). For example, a study by Eckelmann et al. (2018) unravelled the secondary metabolic profile of a pigmented *S. marcescens* strain MSRBB2 using high performance liquid chromatography (HPLC) linked to high resolution mass spectrometry (HRMS) and $HRMS^n$ analysis. The characteristic fragmentation patterns produced by $HRMS^n$ analysis allowed for the identification and elucidation of 33 compounds, including 7 prodiginines and 26 serratamolides (Eckelmann et al. 2018).

Recently, a novel approach has been developed to analyse large data sets from tandem MS spectra of natural product extracts. This approach involves the Global Natural Products Social Molecular Network (GNPS) platform (http://gnps.ucsd.edu) as an open-access tool that employs a computational algorithm to compare the degree of similarity between tandem MS spectra and generates a molecular network comprised of clusters of structurally related metabolites. Thus, a visual representation of the structural relationships between natural compounds within crude extracts is generated, where a node within the network represents a compound and the relatedness between two compounds (nodes) is referred to as an edge. Moreover, GNPS allows for the comparison of the tandem MS spectra to the publicly available spectral library for rapid identification of known compounds (Wang et al. 2016; Philippus et al. 2018).

Here, we present an integrated approach to identify and structurally elucidate the naturally produced complex of secondary metabolites of a pigmented (P1) and non-pigmented (NP1)

S. marcescens strain using reverse-phase high performance liquid chromatography (RP-HPLC), electrospray ionisation mass spectrometry (ESI-MS), ultra-performance liquid chromatography coupled to tandem mass spectrometry (UPLC-MS^e) and molecular networking (using the GNPS molecular network platform) analysis. In addition, the susceptibility of a clinical *Enterococcus faecalis* (*E. faecalis*) strain to fractions collected during RP-HPLC analysis was evaluated using disc diffusion assays (all fractions) and broth microdilution assays to determine the minimum inhibitory concentration (MIC) and minimum bactericidal concentration (MBC) of selected fractions.

3.2. Materials and Methods

3.2.1. Bacterial Strains

A previous study by Clements et al. (2019b; chapter two) outlined the isolation of the P1 and NP1 *S. marcescens* strains from an oil refinery effluent sample and a river water sample, respectively as well as the molecular identification of the strains. The two *S. marcescens* strains were streaked from the glycerol stocks onto Nutrient agar (Merck, Johannesburg, South Africa) and were incubated at 30°C for 18 to 24 h. The clinical *E. faecalis* S1 strain, used for the disc diffusion and MIC assays, was streaked from the glycerol stock onto tryptone soy agar (Biolab, Merck, Johannesburg, South Africa) supplemented with 6 g/L yeast extract (Biolab, Merck, Johannesburg, South Africa) ($TSAYE_{0.6\%}$) and was incubated at 37°C for 18 to 24 h.

3.2.2. Production and Extraction of Secondary Metabolites

The production and partial purification of secondary metabolites was performed as described by Clements et al. (2019b; chapter two), with slight modifications to the scale of production (increased volume) and the peptone powder (Biolab, Merck, Johannesburg, South Africa) utilised. Briefly, seed cultures were grown overnight by inoculating the *S. marcescens* P1 and NP1 strains into 10 mL Luria Bertani broth (Biolab, Merck, South Africa) in triplicate and incubating on a test tube rotator (MRCLAB, London, United Kingdom) at 30°C. Each seed culture was subsequently inoculated into a 2 L baffled flask containing 500 mL Peptone Glycerol (PG, pH 7.2 ± 0.2) broth [composed of 5 g peptone powder and 10 mL glycerol (Promega, Wisconsin, United States) in 1 L distilled water] in triplicate, which was incubated on an orbital shaker (MRCLAB, London, United Kingdom) at 30°C for 120 h at 120 rpm. Following a 5 day incubation period, the P1 and NP1 broth cultures were centrifuged at 10 000 rpm for 20 min at 4°C to obtain the cell free supernatant. The cell free supernatants were lyophilised and dissolved in 70% HPLC-grade acetonitrile (Romil, Darmstadt, Germany) in analytical quality water (milliQ water) (*v/v*). The acetonitrile soluble fraction was transferred into a sterile McCartney bottle and lyophilised. This step was repeated thrice to

further purify the crude extracts. The triplicate crude extracts were then pooled, lyophilised, analytically weighed and stored at -20°C until further use.

3.2.3. Purification and Detection of Secondary Metabolites

The P1 and NP1 crude extracts were subjected to RP-HPLC (Finnigan Survey UV-VIS Plus detector, Thermo-Scientific, Waltham, MA, USA) analysis in order to obtain purified fractions. The lyophilised P1 and NP1 crude extracts were dissolved in 40% acetonitrile in milliQ water (*v/v*) to a concentration of 10.00 mg/mL and were injected into a Discovery BIO Wide Pore C_{18} HPLC column (10 µm, 250 × 10 mm; Sigma-Aldrich, St. Louis, USA). Liquid chromatography was conducted with milliQ water containing 0.1% trifluoroacetic acid (TFA; *v/v*; Sigma-Aldrich, St. Louis, USA) as solution A and acetonitrile containing 0.1% TFA (*v/v*) as solution B. An isocratic flow at 40% B from 0 to 2 min for sample loading was followed by a linear gradient from 40 to 95% B from 2 to 36 min. The column was washed for 2 min with 95% B and then regenerated with a reversed gradient from 95 to 40% B from 38 to 45 min. Chromatographic peaks were detected by measuring the absorbance at 230 and 254 nm.

The fractions collected from the RP-HPLC were analysed using a Waters Synapt G2 high resolution mass spectrometer (Waters Corporation, Milford, USA). For direct mass analysis, 3 µL of the sample [250 µg/mL; dissolved in 50% acetonitrile in milliQ water (*v/v*)] was injected into a Z spray ionisation source at a flow rate of 0.3 mL/min. The analytes were subjected to a capillary voltage of 2.5 kV, cone voltage of 15 V, a source temperature of 120°C, desolvation gas (N_2) flow of 650 L/h and desolvation temperature at 275°C. Data acquisition in the positive mode was performed by MS scanning a second analyser through the *m/z* range of 300 to 1500 in centroid mode. The high resolution mass calibration was done with sodium formate and in analysis single point lock spray using leucine enkephalin (*m/z* = 556.2771). The ESI-MS data was processed using MassLynx software version 4.1 (Waters Corporation, Milford, USA). The accurate masses and molecular formula of the detected compounds were used to search online databases, such as Norine (https://bioinfo.lifl.fr/norine/) and PubChem (https://pubchem.ncbi.nlm.nih.gov/), of known natural products and an extensive literature search was conducted for the putative identification of the metabolites.

3.2.4. Ultra-performance Liquid Chromatography Tandem Mass Spectrometry Analysis

In order to elucidate the structure of the detected compounds, all fractions were subjected to ultra-performance liquid chromatography coupled to tandem mass spectrometry (UPLC-MS/MS) analysis at the LCMS unit at the Central Analytical Facility (CAF, Stellenbosch University). The RP-HPLC purified fractions obtained from the P1 and NP1 crude extracts were prepared in 70%

acetonitrile in milliQ water (*v/v*) to a concentration of 250 µg/mL and were subjected to the Waters Synapt G2 high resolution mass spectrometer linked to an Acquity UPLC™ for UPLC-MS analysis. Three microlitres of each fraction (1.00 mg/mL) was separated on an UPLC C_{18} reverse-phase analytical column (Acquity UPLC® HSS T3, 1.8 µm particle size, 2.1 x 150 mm, Waters Corporation, Dublin, Ireland). The UPLC-MS was conducted with milliQ water containing 0.1% (*v/v*) formic acid as solution A and acetonitrile containing 0.1% (*v/v*) formic acid as solution B. The gradient was developed at a flow rate of 0.300 mL/min as follows: 60% A from 0 to 0.5 min for loading, linear gradient from 20 to 80% (B) from 0.5 to 14 min and 0 to 100% (B) from 14 to 15 min. The instrument settings were as described for the direct mass analysis.

High resolution collisionally induced dissociation (CID) analysis was conducted in the MS^e mode (MS/MS) during the UPLC-MS analysis and was monitored on a second MS channel. The CID was conducted at a collision energy gradient of 20 to 70 eV at 1 s MS/MS scan time. Data was collected in the second mass analyser (MS2) through *m/z* range of 40 to 1500 in centroid mode. The rest of the instrument settings were as described above. The UPLC-MS^e data was processed using MassLynx software version 4.1 (Waters Corporation).

3.2.5. Molecular Networking Analysis

The Waters RAW files for the P1 and NP1 fractions obtained after UPLC-MS^e analysis were converted into an Analysis Base File (ABF) format using Reifycs Analysis Base File Converter before data processing. Ion chromatogram extraction, alignment and peak deconvolution of the ABF converted files was then conducted using MS-DIAL software version 4.24. The aligned results were exported as a mascot generic format (mgf) file for P1 and NP1 (Tsugawa et al. 2015). Thereafter, the mgf files for the two strains were uploaded to the GNPS platform (http://gnps.ucsd.edu) and a molecular network was created using the workflow published by Wang et al. (2016). Briefly, the data was filtered by removing all MS/MS fragment ions within +/- 17 Da of the precursor *m/z*. The MS/MS spectra were window filtered by selecting only the top 6 fragment ions in the +/- 50 Da window throughout the spectrum. The precursor ion mass tolerance was set to 0.03 Da and a MS/MS fragment ion tolerance of 0.02 Da. A network was then created where edges were filtered to have a cosine score above 0.6 and more than 10 matched peaks. Further, edges between two nodes were kept in the network only if each of the nodes appeared in each other's respective top 10 most similar nodes. Finally, the maximum size of a molecular family was set to 100, and the lowest scoring edges were removed from the molecular families until the molecular family size was below this threshold. The spectra in the network were then searched against GNPS' spectral libraries. The library spectra were filtered in the same manner as the input data. All matches retained between network spectra and library spectra were required to have a score above 0.7 and at least 6 matched peaks (Wang et al. 2016). The output of the molecular

network was visualised using Cytoscape version 3.8.0. The nodes (compounds) originating from media and solvent controls (acetonitrile) were excluded from the original network in order to visualise the secondary metabolites derived from the P1 and NP1 strains.

3.2.6. Antimicrobial Susceptibility Testing

3.2.6.1. Disc Diffusion Assay

The lyophilised fraction stocks (obtained after RP-HPLC) were dissolved in 100% dimethyl sulfoxide (DMSO; Sigma-Aldrich, St. Louis, USA) and diluted in milliQ water to 3.00 mg/mL. The fractions were then subjected to antimicrobial testing using a standard disc diffusion assay as described by Das et al. (2008) and Ndlovu et al. (2017). Briefly, the *E. faecalis* S1 test strain was inoculated into 5 mL of tryptone soy broth (Biolab, Merck, Johannesburg, South Africa) supplemented with 6 g/L yeast extract ($TSBYE_{0.6\%}$) and was incubated at 37°C for 18 to 24 h. Following incubation, 100 µL of the *E. faecalis* S1 suspension was spread plated onto $TSAYE_{0.6\%}$ to create a microbial lawn. Thereafter, 6 mm filter paper discs (Oxoid, Basingstoke, UK) were placed onto the microbial lawn using a sterile needle and 50 µL of each fraction [3.00 mg/mL in 15% (*v/v*) DMSO] was pipetted directly onto the filter paper (in triplicate) in order to create an antimicrobial disc. A negative control of 50 µL of 15% (*v/v*) DMSO was included and the plates were incubated for 24 h at 37°C.

3.2.6.2. Minimum inhibitory and bactericidal concentration

Fractions were selected for further antimicrobial testing based on the results of the disc diffusion assay and the quantity of each fraction remaining. The fraction stocks were prepared in 100% DMSO and diluted to a concentration range of 1.50 to 6.00 mg/mL using milliQ water. The selected fractions were subjected to antimicrobial testing using a broth microdilution susceptibility assay as outlined by the European Committee on Antimicrobial Susceptibility Testing (EUCAST, 2018) and Magalhães and Nitschke et al. (2013). Briefly, *E. faecalis* S1 was inoculated into 5 mL of $TSBYE_{0.6\%}$ and was incubated at 37°C for 18 to 24 h. Following overnight incubation, the culture was diluted to an optical density (OD) of approximately 0.08 at 625 nm [~10^7 colony forming units (CFU)/mL]. One hundred microlitres of each fraction was dispensed into the respective wells of a Greiner CELLSTAR® 96-well culture plate (Merck, Johannesburg, South Africa) containing 100 µL of sterile $TSBYE_{0.6\%}$ (final concentration of 0.75 to 3.00 mg/mL in 15% DMSO). All the wells of the microtiter plate were inoculated with 10 µL of the bacterial inoculum (final concentration of ~10^5 CFU/mL). Sterile broth, 15% DMSO and the OD adjusted inoculum were included in the assay as positive controls, while sterile broth with 15% DMSO was included as a negative control. All the tests were performed in triplicate and the microtiter plate was incubated for 18 to 24 h at 37°C.

Following incubation, the absorbance was measured using a microtiter plate reader. The MIC was assigned as the lowest concentration of the respective compounds that reduced bacterial numbers by ≥ 90% (Yasir et al. 2019). The MBC was determined as previously described by Das et al. (2008). Briefly, after the MIC determination, the wells that showed ≥ 90% inhibition of growth were identified and 20 µL of each well was spot plated onto $TSAYE_{0.6\%}$. The lowest concentration showing no revival of the test culture was recorded as the MBC.

3.3. Results

3.3.1. Purification and Identification of Secondary Metabolites

Reverse-phase high performance liquid chromatography was used to fractionate the secondary metabolites within the P1 and NP1 crude extracts. The RP-HPLC analysis of the P1 and NP1 crude extracts revealed *n* = 11 absorption peaks in the P1 crude extract and *n* = 8 absorption peaks in the NP1 crude extract, between 8 and 35 min. All the collected fractions were then subjected to ESI-MS analysis to detect potential metabolites produced by each strain. As a result, a combined total of 21 compounds, produced by the P1 and/or NP1 strains, were detected [arranged according to the retention time (Rt), **Appendix B Table B1**]. The positive mode ESI-MS analysis of each collected fraction obtained from the P1 crude extract revealed a profile with major molecular ions at *m/z* 430.1609, 324.2073, 515.3331, 557.3804, 541.3485, 543.3644, 571.3931 and 559.3953. The ESI-MS analysis of the NP1 crude extract revealed a similar profile with the major molecular ions of *m/z* 430.1609, 515.3331, 557.3804, 541.3485, 543.3644, 559.4953 and 585.4117. The corresponding sodium and potassium adducts of the compounds from the P1 and NP1 fractions were also detected (**Appendix B Table B1**).

It should be noted that several compounds co-eluted with the major compounds (higher molecular ion signal), including minor compounds with *m/z* 573.4136 and 627.4192 $[M+H]^+$ that co-eluted with a compound with *m/z* 571.3931 $[M+H]^+$ at 31.8 min in the P1 crude extract. In addition, for the P1 crude extract, a minor compound at *m/z* 559.3600 also co-eluted with a compound at *m/z* 324.2073 $[M+H]^+$ in 20.9 min peak, while a minor compound at *m/z* 575.3902 co-eluted with one at *m/z* 515.3331 $[M+H]^+$ in the 22.0 min peak. Minor compounds with *m/z* 545.3787, 585.3738 and 587.3908 $[M+H]^+$ were detected in the NP1 crude extract and co-eluted with a compound at *m/z* 541.3485 $[M+H]^+$ at 24.6 min. For both the P1 and NP1 crude extracts, a minor compound at *m/z* 561.3749 $[M+H]^+$ was detected and co-eluted with a compound at *m/z* 515.3331 $[M+H]^+$ in the 22.0 min peak. Similarly, a minor compound at *m/z* 589.4056 $[M+H]^+$ co-eluted with one at *m/z* 543.3644 $[M+H]^+$ in a broad peak at 26.4 to 26.5 min in the P1 and NP1 crude extracts, respectively. Finally, a minor compound at *m/z* 583.3947 $[M+H]^+$ co-eluted with a compound at *m/z* 585.4117 $[M+H]^+$ in the 29.7 min peak for both the P1 and NP1 crude extracts. Due to the co-

elution of presumptive known (*n* = 12) and unknown (*n* = 9) compounds (**Appendix B Table B1**) detected in the P1 and/or NP1 crude extracts, UPLC-MS^e coupled with molecular networking analysis was used to cluster structurally similar compounds and elucidate the putative structures of the unknown compounds and facilitate the confirmation of the known structures.

3.3.2. Molecular Networking Analysis

The fractions obtained after RP-HPLC of the secondary metabolites extracted from the P1 and NP1 strains were subjected to UPLC-MS^e analysis and the raw MS^e data was used to generate a molecular network. Analysis of the molecular network revealed four clusters (**Fig 3.1**), including families of serratiochelin (comprised of 5 nodes) and prodigiosin (comprised of 2 nodes) that were identified using the GNPS and MS-DIAL libraries, respectively, and two unidentified F1 (comprised of 15 nodes) and F2 (comprised of 22 nodes) families that did not correspond to compounds within the GNPS and MS-DIAL libraries. In general, the majority of the metabolites (nodes) clustered in the F1, F2 and serratiochelin families and were detected in both P1 and NP1 strains; however, only the P1 strain produced compounds in the prodigiosin cluster. The entire network was formed by 55 nodes, including 11 individual nodes.

3.3.3. UPLC-MS^e Analysis

Following molecular networking, the structural elucidation of the four distinct metabolite clusters produced by the *S. marcescens* P1 and NP1 strains was conducted by analysing the fragmentation profiles of the UPLC-MS^e data. A summary of the UPLC-MS^e data for the metabolites produced by the P1 and NP1 strains is presented in **Tables 3.1** and **3.2** and **Appendix B Fig. B22 – B23**, and the structures of the known metabolites and putative structures of the unknown compounds produced by the P1 and NP1 strains are depicted in **Fig. 3.2** and **3.3** and **Appendix B Fig. B1 – B21**. The fragmentation profiles and structural elucidation of the detected compounds will be discussed according to each metabolite family (cluster).

3.3.3.1. Structural Elucidation of Serratiochelin A

The serratiochelin cluster (**Fig. 3.1**) revealed a node with *m/z* 430.1609 $[C_{21}H_{23}N_3O_7 + H]^+$ (calculated 430.1614) corresponding to the peak observed at 3.76 min in the UPLC-MS^e data for the P1 and NP1 strains (**Table 3.1**; **Appendix B Fig. B1**). The fragmentation pattern of the *m/z* 430.1609 molecular ion that was observed, using UPLC-MS^e, revealed four major fragments.

A major fragmentation ion at *m/z* 137.0234 corresponded to the 2,3-dihydroxybenzaldehyde fragment of the *m/z* 430.1609 molecular ion, while the corresponding fragment of *m/z* 294.1455 was also observed. In addition, the removal of 2,3-dihydroxybenzamide from the *m/z* 430.1609 ion

resulted in the major fragment at *m/z* 277.1194. The loss of 2,3-dihydroxybenzoyl nitrile from the *m/z* 430.1609 molecular ion resulted in a remaining fragment at *m/z* 194.0804. A few other minor fragments were detected and corresponded to the serratiochelin A structure reported by Seyedsayamdost et al. (2012). Thus, the compound identity of the $[M+H]^+$ ion at *m/z* 430.1609 was confirmed as serratiochelin A (also referred to as serranticin) based on the characteristic fragmentation pattern and elementary composition (Kuo et al. 2010; Seyedsayamdost et al. 2012).

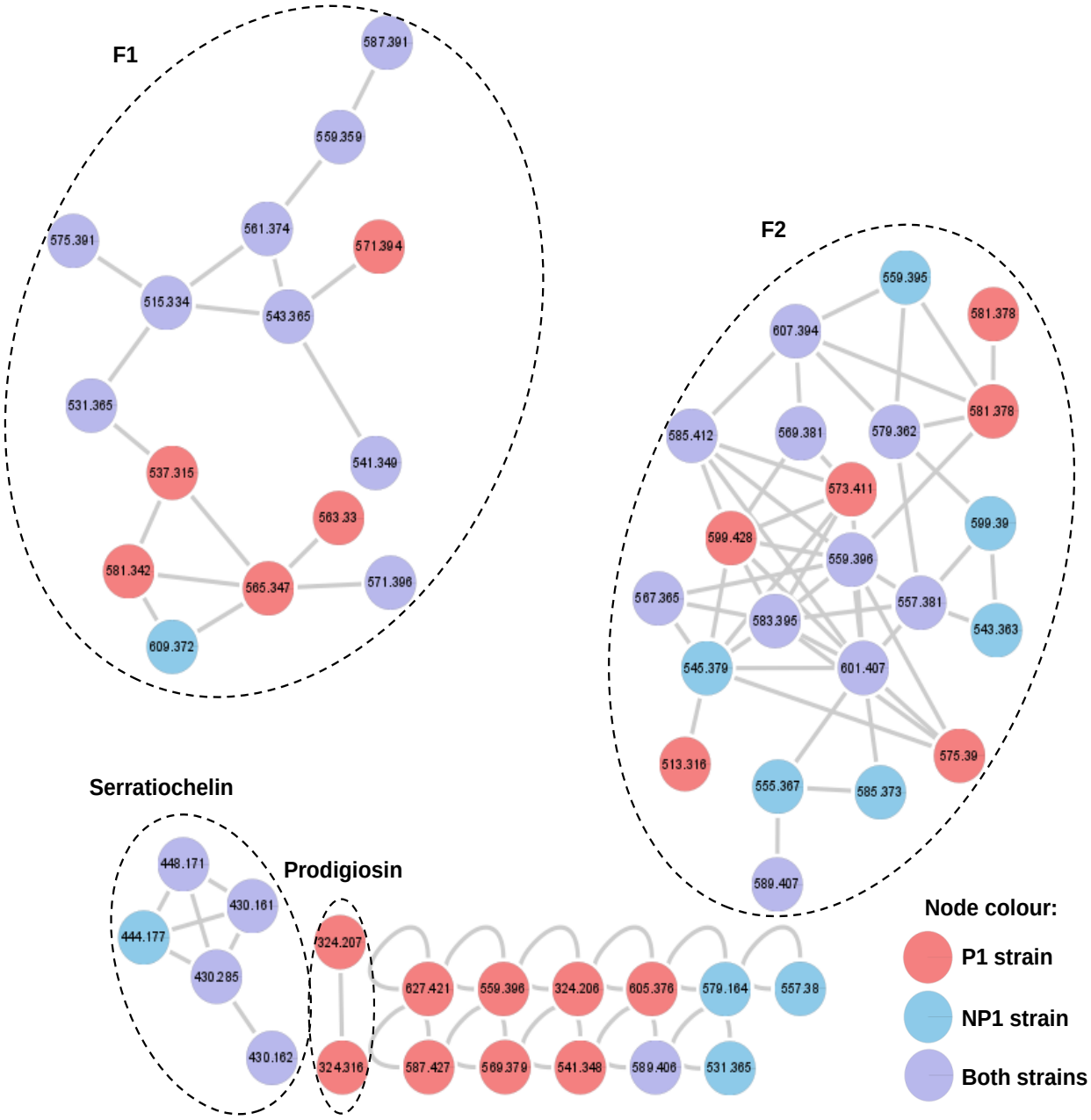

Fig. 3.1 Molecular network of the secondary metabolites produced by the *S. marcescens* P1 and NP1 strains generated using the UPLC-MS^e data. Nodes are labeled with the corresponding *m/z* values (detected in the positive mode) and respective strain colours are indicated in the node colour key. The four clusters are labeled with either the corresponding compound family name

detected using GNPS or MS-DIAL library search, or F1 and F2 corresponding to metabolite clusters that were not identified using the library searches.

3.3.3.2. Structural Elucidation of Prodigiosin

The prodigiosin cluster (**Fig. 3.1**) revealed a node with *m/z* 324.2073 $[C_{20}H_{25}N_3O + H]^+$ (calculated 324.2076) corresponding to the peak observed at 8.48 min in the UPLC-MS^e data for the P1 strain (**Table 3.1**; **Appendix B Fig. B2**). The fragmentation pattern of the *m/z* 324.2073 compound that was observed using UPLC-MS^e analysis revealed four major fragments. The fragment with a *m/z* 309.1836 $[M+H]^+$ corresponded to the demethylation [removal of a methyl (CH_4) group] of *m/z* 324.2073 $[M+H]^+$, while the removal of a butane (C_4H_{10}) group from the *m/z* 324.2073 compound resulted in a remaining fragment of *m/z* 266.1296. The major fragment ion *m/z* 252.1140 corresponded to the removal of pentane (C_5H_{12}) from the compound at *m/z* 324.2073 ($[M+H]^+$). The removal of methanol (CH_4O) from the *m/z* 324.2073 compound resulted in a fragment with *m/z* 292.1797. A few other minor fragments were detected and corresponded to the prodigiosin structure described by Lee et al. (2011). Thus, the compound identity at *m/z* 324.2073 was confirmed as prodigiosin based on the characteristic fragmentation pattern and molecular formula (Su et al. 2016).

3.3.3.3. Structural Elucidation of Serratamolide Homologues

The molecular network of the F1 cluster and corresponding structures for the known and novel compounds in the F1 cluster are presented in **Fig. 3.2**. The F1 cluster (**Fig. 3.2A**) revealed a node with *m/z* 515.3331 $[C_{26}H_{46}N_2O_8 + H]^+$ (calculated 515.3332) corresponding to the peak observed at 11.49 min in the UPLC-MS^e data for the P1 and NP1 strains. The fragmentation pattern of the *m/z* 515.3331 compound that was observed using UPLC-MS^e analysis revealed four major fragments (**Table 3.1**; **Appendix B Fig. B3**). The fragment with a *m/z* 497.3239 corresponded to a product of dehydration (removal of H_2O). A major fragment at *m/z* 258.1679 was then observed, representing a dehydrated L-serine group coupled to a saturated D-3-hydroxydecanoic acid (C_{10}). In addition, the dehydration and hydration products of the *m/z* 258.1679 fragment were detected at *m/z* 240.1595 and 276.1823, respectively. The compound with *m/z* 515.3331 was thus comprised of two L-serine residues (cyclic peptide moiety) coupled to two saturated D-3-hydroxydecanoic acids (C_{10}) (**Fig. 3.2B**) confirming the identity of the compound as serratamolide A (Dwivedi et al. 2008).

Table 3.1 Summary of the serratamolide homologues, prodigiosin and serratiochelin A detected in the crude extracts obtained from *S. marcescens* P1 and NP1 that were identified using UPLC-MS[e] analysis.

Crude extract	UPLC Rt (min)	Compound identity	Proposed fatty acid chain lengths	[d]Molecular formula	*m/z* $[M+H]^+$	[a]Experimental M_r	[b]Theoretical M_r	[c]Mass error (Δ_{ppm})	Major UPLC-MS[e] fragments
P1 NP1	3.76	Serranticin/ Serratiochelin A	N/A	$C_{21}H_{23}N_3O_7$	430.1609	429.1530	429.1536	1.49	137, 158, 194, 211, 233, 250, 277, 294
P1	8.48	Prodigiosin	N/A	$C_{20}H_{25}N_3O$	324.2073	323.1994	323.1998	1.36	161, 182, 207, 224, 238, 252, 266, 294, 309
P1 NP1	11.20	Open-ring Serratamolide B	C_{10}+$C_{12:1}$	$C_{28}H_{51}N_2O_9$	559.3600	558.3522	558.3516	-1.03	258, 266, 276, 284, 302, 541
P1 NP1	11.28	Open-ring serratamolide C	C_{10}+C_{12}	$C_{28}H_{53}N_2O_9$	561.3749	560.3671	560.3673	0.89	240, 258, 268, 276, 286, 304, 543
P1 NP1	11.49	Serratamolide A/ Serrawettin W1	C_{10}+C_{10}	$C_{26}H_{46}N_2O_8$	515.3331	514.3252	514.3254	0.47	212, 240, 258, 276, 469, 487, 497
NP1	12.46	*Open-ring serratamolide 585	$C_{12:1}$+$C_{12:1}$	$C_{30}H_{53}N_2O_9$	585.3738	584.3660	584.3673	2.26	238, 266, 284, 302, 567
P1 NP1	12.77	Serratamolide B	C_{10}+$C_{12:1}$	$C_{28}H_{48}N_2O_8$	541.3485	540.3404	540.3411	0.55	212, 240, 258, 266, 276, 284, 302, 513, 523
P1 NP1	13.06	Serratamolide C	C_{10}+C_{12}	$C_{28}H_{50}N_2O_8$	543.3644	542.3565	542.3567	0.44	212, 240, 258, 268, 276, 286, 304, 515, 525
NP1	13.76	Open-ring serratamolide 587	C_{12}+$C_{12:1}$	$C_{30}H_{55}N_2O_9$	587.3908	586.3830	586.3829	-0.13	240, 258, 266, 268, 284, 286, 304, 569
P1 NP1	14.02	Serratamolide 571	C_{12}+C_{12}	$C_{30}H_{54}N_2O_8$	571.3931	570.3852	570.3880	4.98	222, 240, 268, 286, 304, 525, 553

[a]Experimental monoisotopic M_r of compound was calculated using the Time-of-Flight (TOF) transform function in the MassLynx 4.1 software package.
[b]Theoretical monoisotopic M_r of compound was calculated using ChemDraw Ultra 12.0 software package.
[c]Mass error in ppm = $\left(\frac{\text{Theoretical } M_r - \text{Experimental } M_r}{\text{Theoretical } M_r}\right) \times 10^6$
[d]Theoretical molecular formula of compound was calculated using ChemDraw Ultra 12.0 software package and experimental molecular formula was confirmed using the MassLynx 4.1 software package.
N/A – not applicable.
*Novel serratamolide homologue.

Other F1 nodes (**Fig. 3.2A**) at *m/z* 541.3485 $[C_{28}H_{48}N_2O_8 + H]^+$ (calculated 541.3488), 543.3644 $[C_{28}H_{50}N_2O_8 + H]^+$ (calculated 543.3645), 561.3749 $[C_{28}H_{53}N_2O_9 + H]^+$ (calculated 561.3754), 559.3600 $[C_{28}H_{51}N_2O_9 + H]^+$ (calculated 559.3594) and 571.3931 $[C_{30}H_{54}N_2O_8 + H]^+$ (calculated 571.3958) exhibited similar fragmentation profiles to serratamolide A (serrawettin W1) and corresponded to peaks observed in the UPLC-MS^e data for the P1 and NP1 strains (**Table 3.1**; **Appendix B Fig. B4 – B8 & B22**). In addition, the F1 cluster (**Fig. 3.2A**) revealed a node with *m/z* 587.3908 $[C_{30}H_{55}N_2O_9 + H]^+$ (calculated 587.3907) corresponding to the peak observed at 13.76 min in the UPLC-MS^e data for the NP1 strain (**Table 3.1**; **Appendix B Fig. B9**). The *m/z* 585.3738 $[C_{30}H_{53}N_2O_9 + H]^+$ (calculated 585.3751) compound did not cluster in the molecular network; however, it was detected at 12.46 min in the UPLC-MS^e data for the NP1 strain (**Table 3.1**; **Appendix B Fig. B10**). For the compounds at *m/z* 541.3485, 543.3644, 561.3749, 559.3600, 571.3931, 585.3738 and 587.3908; fragment ions due to dehydration (removal of H_2O, or H, OH) at *m/z* 523.3371, 525.3543, 543.3660, 541.3496, 553.3831, 567.3681 and 569.3787, respectively, were observed. Similar to serratamolide A, the compounds at *m/z* 541.3485, 543.3644, 559.3600 and 561.3749 had a major fragment with *m/z* 258.1679, representing a dehydrated L-serine group coupled to a saturated D-3-hydroxydecanoic acid (C_{10}). In addition, the dehydration and hydration products of the *m/z* 258.1679 fragment were detected at *m/z* 240.1595 and 276.1823, respectively. The compounds with *m/z* 543.3644, 561.3749, 571.3931 and 587.3908 had a major fragment of *m/z* 286.2025 $[M+H]^+$, respectively, that correspond to the dehydrated L-serine residue linked to a saturated D-3-hydroxydodecanoic acid (C_{12}). The compounds with *m/z* 541.3485, 559.3600, 585.3738 and 587.3908 all shared a major fragment at *m/z* 284.1850 that corresponded to the dehydrated L-serine residue linked to an unsaturated D-3-hydroxydodecanoic acid ($C_{12:1}$).

The compound with *m/z* 571.3931 $[M+H]^+$ was comprised of two L-serine residues (cyclic peptide moiety) linked to two saturated D-3-hydroxydodecanoic acids (C_{12}), which corresponded to a serratamolide homologue reported by Eckelmann et al. (2018) (**Fig. 3.2B**). In contrast, the compounds with *m/z* 541.3485 and 543.3644 were comprised of two L-serine residues (cyclic peptide moiety) coupled to a D-3-hydroxydecanoic acid (C_{10}) and a D-3-hydroxydodecanoic acid (C_{12}) (**Fig. 3.2B**). The compound with *m/z* 543.3644 thus corresponded to the previously described serratamolide C (Dwivedi et al. 2008). However, the compound *m/z* 541.3485 $[M+H]^+$ had a double bond in the D-3-hydroxydodecanoic acid ($C_{12:1}$) residue (**Fig. 3.2B**) confirming the structure as serratamolide B (Dwivedi et al. 2008). The double bond position was putatively placed at the C_5 position (from the C=O group) of the fatty acid chain, as this corresponded to the position previously reported in literature (Eckelmann et al. 2018).

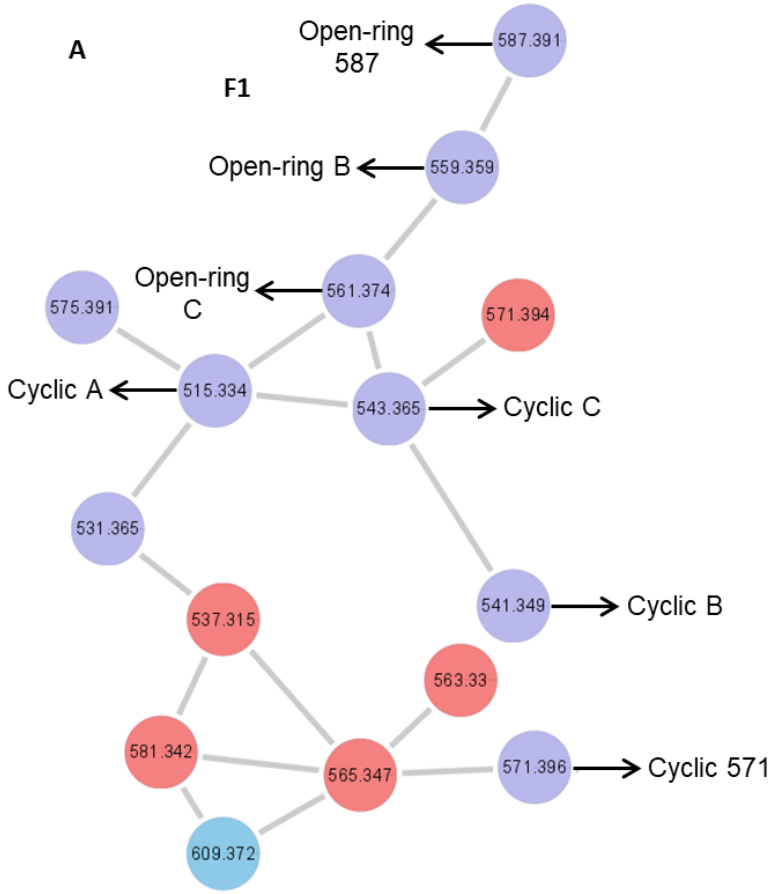

B

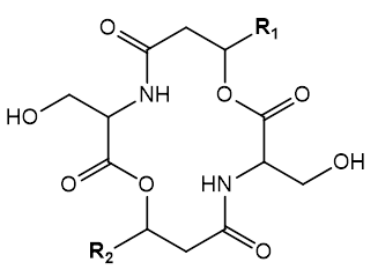

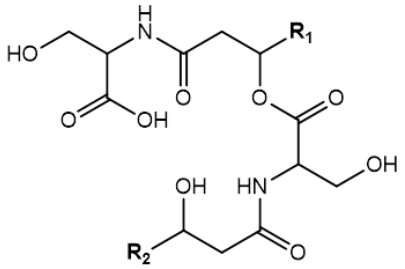

Type	Serratamolide ([M+H]$^+$)	R_1	R_2
Cyclic	A (*m/z* 515)	$-(CH_2)_6CH_3$	$-(CH_2)_6CH_3$
Cyclic	B (*m/z* 541)	$-CH_2CH{=}CH(CH_2)_5CH_3$	$-(CH_2)_6CH_3$
Cyclic	C (*m/z* 543)	$-(CH_2)_8CH_3$	$-(CH_2)_6CH_3$
Cyclic	Serratamolide (*m/z* 571)	$-(CH_2)_8CH_3$	$-(CH_2)_8CH_3$
Open-ring	B (*m/z* 559)	$-CH_2CH{=}CH(CH_2)_5CH_3$	$-(CH_2)_6CH_3$
Open-ring	C (*m/z* 561)	$-(CH_2)_8CH_3$	$-(CH_2)_6CH_3$
Open-ring	*Serratamolide (*m/z* 585)	$-CH_2CH{=}CH(CH_2)_5CH_3$	$-CH_2CH{=}CH(CH_2)_5CH_3$
Open-ring	Serratamolide (*m/z* 587)	$-CH_2CH{=}CH(CH_2)_5CH_3$	$-(CH_2)_8CH_3$

Fig. 3.2 The (**A**) molecular network of cluster F1 (magnified) labelled with the corresponding serratamolide homologues detected in the P1 and NP1 crude extracts and (**B**) structures of the detected cyclic and open-ring serratamolide homologues elucidated using UPLC-MS^e analysis. Red nodes = metabolites produced by the P1 strain; Blue node = metabolites produced by the NP1 strain; Purple nodes = metabolites produced by both P1 and NP1 strains. *Serratamolide homologue not present in the molecular network.

The compounds with *m/z* 559.3600 and 561.3749 had identical fatty acid chain lengths as serratamolide B and C, respectively; however, the addition of a hydroxyl group, based on the experimental molecular formula (elemental composition) predicted using the MassLynx 4.1 software package, in the compound suggested that both lipopeptides were open-ring structures and corresponded to the fragmentation pattern of the previously described open-ring serratamolides C and B (Eckelmann et al. 2018) (**Fig. 3.2B**). Similarly, the compound with *m/z* 587.3908 was comprised of one L-serine residue coupled to one saturated D-3-hydroxydodecanoic acid (C_{12}) and one L-serine residue coupled to one unsaturated D-3-hydroxydodecanoic acid ($C_{12:1}$). However, the addition of a hydroxyl group [based on the experimental molecular formula (elemental composition)] in the compound suggested that the lipopeptide was an open-ring structure and corresponded to the fragmentation pattern previously described by Eckelmann et al. (2018) (**Fig. 3.2B**). Finally, the compound with *m/z* 585.3738 was comprised of two L-serine residues coupled to two unsaturated D-3-hydroxydodecanoic acids ($C_{12:1}$). Similar to the previously described open-ring structures, the addition of a hydroxyl group [based on the experimental molecular formula (elemental composition)] in the compound suggested that the lipopeptide was an open-ring structure; however, this compound has not previously been reported in literature or databases (Norine and PubChem) (**Fig. 3.2B**). The described serratamolides were thus comprised of four residues, including a peptide moiety of two L-serine residues (cyclic or open-ring) attached to two fatty acid residues (varying in length and presence or absence of double bonds).

The F1 nodes with *m/z* 537.3147, 563.3290, 565.3455, 581.3405 and 609.3735 were found in the UPLC-MS^e data and corresponds to the sodiated adducts of the compounds with *m/z* 515.3331, 541.3485, 543.3644, 559.3600 and 587.3908, respectively (**Appendix B Table B1**). In contrast, no structures were established for the F1 nodes with *m/z* 531.365 and 575.391.

3.3.3.4. Structural Elucidation of Glucosamine Derivatives

The molecular network of the F2 cluster and corresponding structures for the known and novel compounds in the F2 cluster are presented in **Fig. 3.3**. The F2 cluster (**Fig. 3.3A**) revealed nodes with *m/z* 585.4117 $[C_{31}H_{56}N_2O_8 + H]^+$ (calculated 585.4115) and 559.3953 $[C_{29}H_{54}N_2O_8 + H]^+$ (calculated 559.3958) corresponding to the peaks observed in the UPLC-MS^e data for the P1 and NP1 strains, while *m/z* 573.4136 $[C_{30}H_{57}N_2O_8 + H]^+$ (calculated 573.4115) corresponded to a peak observed in the UPLC-MS^e data for the P1 strain (**Table 3.2**; **Appendix B Fig. B11 – B13**). A major fragment at *m/z* 232.1163 $[M+H]^+$ was observed in the fragmentation profile of each of these three compounds, corresponding to a glucose residue linked to butyric acid. Further dehydration products of the *m/z* 232.1163 fragment were observed at *m/z* 214.1069 and 196.0971 that indicated the presence of hydroxyl groups. The compound with *m/z* 585.4117 had a second major

fragment of *m/z* 354.2999 $[M+H]^+$, which corresponded to a valine residue linked to an unsaturated $C_{16:1}$ fatty acid chain. The compounds with *m/z* 573.4136 and 559.3953 had a second major fragment at *m/z* 342.2991 and 328.2819, respectively, which corresponded to a valine residue linked to a saturated C_{15} and C_{14} fatty acid chain, respectively. For all three compounds, the two major fragments were linked together via an anomeric C-O bond between the glucose and valine amino acid residues. Therefore, the compound *m/z* 585.4117 was proposed to be comprised of a glucose residue linked to butyric acid, which was in turn was coupled to a valine residue linked to an unsaturated $C_{16:1}$ fatty acid chain correlating to a previously described compound, glucosamine derivative A (Dwivedi et al. 2008) (**Fig. 3.3B**). The double bond within the fatty acyl chain of glucosamine derivative A was assumed to be a *cis* double bond corresponding to the structure previously described in literature (Dwivedi et al. 2008). The compound with *m/z* 573.4136 was also proposed to comprise of a glucose residue linked to a butyric acid, coupled to a valine residue linked to a saturated C_{15} fatty acid chain, thus correlating with the structure of glucosamine derivative B as described by Dwivedi et al. (2008) (**Fig. 3.3B**). Finally, the last compound in the group had an *m/z* 559.3953 and structure similar to the other two glucosamine derivatives. The compound with *m/z* 559.3953 was also proposed to be comprised of a glucose residue linked to butyric acid, a valine residue linked to a saturated C_{14} fatty acid chain and thus the structure correlated to the glucosamine derivative C (Dwivedi et al. 2008) (**Fig. 3.3B**). Overall, it is proposed that this compound group is comprised of four residues, namely glucose, valine, butyric acid and a saturated or unsaturated β-fatty acid residue of varying length (C_{14} to C_{16}).

Other F2 nodes (**Fig. 3.3A**) at *m/z* 557.3804 $[C_{29}H_{52}N_2O_8 + H]^+$ (calculated 557.3802), 583.3947 $[C_{31}H_{55}N_2O_8 + H]^+$ (calculated 583.3958) and 589.4056 $[C_{30}H_{57}N_2O_9 + H]^+$ (calculated 589.4064) had similar fragmentation profiles to glucosamine derivative A to C and corresponded to peaks observed in the UPLC-MS^e data for P1 and NP1 strains (**Table 3.2**; **Appendix B Fig. B14 – B16**). In addition, F2 nodes at *m/z* 575.3902 $[C_{29}H_{55}N_2O_9 + H]^+$ (calculated 575.3907), 587.4268 $[C_{31}H_{58}N_2O_8 + H]^+$ (calculated 587.4271) and 599.4265 $[C_{32}H_{58}N_2O_8 + H]^+$ (calculated 599.4271) also had similar profiles to glucosamine derivative A to C and corresponded to peaks observed in the UPLC-MS^e data for the P1 strain, while another node at *m/z* 545.3787 $[C_{28}H_{53}N_2O_8 + H]^+$ (calculated 545.3802) corresponded to peaks observed in the UPLC-MS^e data for the NP1 strain (**Table 3.2**; **Appendix B Fig. B17 – B20 & B23**). The cleavage of all seven compounds at the anomeric C-O bond resulted in two major fragments for each compound. Similar to the previously described glucosamine derivative A to C, each compound had a major fragment of *m/z* 232.1177 corresponding to the glucose/hexose residue linked to butyric acid, and dehydration products of the *m/z* 232.1163 fragment were observed at *m/z* 214.1069 and 196.0971. The compounds with *m/z* 545.3787 and 587.4268 had a second major fragment of *m/z* 314.2716 and 356.3164, which corresponded to a valine residue linked to a saturated C_{13} and C_{16} fatty acid chain, respectively.

Table 3.2 Summary of the glucosamine derivative homologues detected in the crude extracts obtained from *S. marcescens* P1 and NP1 that were identified using UPLC-MS[e].

Crude extract	UPLC Rt (min)	Proposed compound identity	Fatty acid chain length	[d]Molecular formula	*m/z* $[M+H]^+$	[a]Experimental M_r	[b]Theoretical M_r	[c]Mass error (Δ_{ppm})	Major UPLC-MS[e] fragments
P1	11.44	*Glucosamine derivative D	C_{14}	$C_{29}H_{55}N_2O_9$	575.3902	574.3828	574.3829	1.11	196, 214, 232, 254, 326, 344, 366
P1 NP1	11.98	*Glucosamine derivative E	$C_{14:1}$	$C_{29}H_{52}N_2O_8$	557.3804	556.3722	556.3724	-0.31	196, 214, 232, 326, 348
NP1	12.67	*Glucosamine derivative F	C_{13}	$C_{28}H_{53}N_2O_8$	545.3787	544.3719	544.3724	3.01	196, 214, 232, 314, 336
P1 NP1	12.94	*Glucosamine derivative G	C_{15}	$C_{30}H_{57}N_2O_9$	589.4056	588.3985	588.3986	1.60	196, 214, 232, 254, 340, 358, 380
P1 NP1	12.95	Glucosamine derivative C	C_{14}	$C_{29}H_{54}N_2O_8$	559.3953	558.3877	558.3880	1.15	196, 214, 232, 254, 328, 350
P1 NP1	13.14	*Glucosamine derivative H	$C_{16:2}$	$C_{31}H_{55}N_2O_8$	583.3947	582.3868	582.3880	2.13	196, 214, 232, 254, 352, 374
P1 NP1	13.50	Glucosamine derivative A	$C_{16:1}$	$C_{31}H_{56}N_2O_8$	585.4117	584.4035	584.4037	-0.10	196, 214, 232, 254, 354, 376
P1	15.69	Glucosamine derivative B	C_{15}	$C_{30}H_{57}N_2O_8$	573.4136	572.4034	572.4037	-3.42	196, 214, 232, 254, 342, 364
P1	16.01	*Glucosamine derivative I	$C_{17:1}$	$C_{32}H_{58}N_2O_8$	599.4265	598.4203	598.4193	1.24	196, 214, 232, 254, 368, 390
P1	16.28	*Glucosamine derivative J	$C_{16:1}$	$C_{33}H_{59}N_2O_9$	627.4192	626.4114	626.4142	4.69	238, 256, 274, 296, 354, 376
P1	16.50	*Glucosamine derivative K	C_{16}	$C_{31}H_{58}N_2O_8$	587.4268	586.4187	586.4193	0.55	196, 214, 232, 254, 356, 378

[a]Experimental monoisotopic M_r of compound was calculated using the TOF transform function in the MassLynx 4.1 software package.
[b]Theoretical monoisotopic M_r of compound was calculated using ChemDraw Ultra 12.0 software package.
[c]Mass error in parts per million (ppm) = $\left(\frac{\text{Theoretical } M_r - \text{Experimental } M_r}{\text{Theoretical } M_r}\right) \times 10^6$
[d]Theoretical molecular formula of compound was calculated using ChemDraw Ultra 12.0 software package and experimental molecular formula was confirmed using the MassLynx 4.1 software package.
*Novel glucosamine derivative homologues.

In addition, the compounds with *m/z* 557.3804, 583.3947 and 599.4265 had a second major fragment of *m/z* 326.2669, 352.2823 and 368.3160 which corresponded to a valine residue linked to an unsaturated $C_{14:1}$, $C_{16:2}$ and $C_{17:1}$ fatty acid chain, respectively. Finally, the compounds with *m/z* 575.3902 and 589.4056 had a major fragment of *m/z* 344.2798 and 358.2958, which corresponded to a valine residue linked to a saturated C_{14} and C_{15} fatty acid chain with an additional hydroxyl group in the fatty acid residue. The presence of the hydroxyl group within the fatty acid moiety was further confirmed, as the loss of a hydroxyl group was observed within the fragmentation profile for both *m/z* 344.2798 and 358.2958 fragments, including *m/z* 326.2694 and 340.2863, respectively. In addition, the experimental molecular formula (elemental composition) predicted by the MassLynx 4.1 software package provided further indication of the addition of the hydroxyl group for both the compounds at *m/z* 575.3902 and 589.4056 (**Table 3.2**).

Typically, MS analysis is used in conjunction with other analytical methods, such as NMR, to determine the position of double bonds and hydroxyl groups within a structure (Eckelmann et al. 2018). However, the majority of the glucosamine derivative compounds were obtained in low quantities and could thus not be subjected to NMR analysis. A *cis* configuration was thus proposed for the double bonds in the fatty acid chain of the various unknown compounds, as the geometric isomerism of a double bond is typically a *cis* configuration in natural fatty acids (Kobelnik et al. 2018). Therefore, we propose that the compounds at *m/z* 557.3804, 583.3947 and 599.4265 $[M+H]^+$ were comprised of a glucose residue linked to butyric acid, coupled to a valine residue linked to an unsaturated $C_{14:1}$, $C_{16:2}$, $C_{17:1}$ fatty acid chain, respectively (**Fig. 3.3B**). The compounds with *m/z* 545.3787 and 587.4268 were proposed to be comprised of a glucose residue linked to a butyric acid, coupled to a valine residue linked to a saturated C_{13} and C_{16} fatty acid chain, respectively (**Fig. 3.3B**). Finally, the compounds with *m/z* 575.3902 and 589.4056 were also proposed to be comprised of a glucose residue linked to butyric acid, coupled to a valine residue linked to a saturated C_{14} and C_{15} fatty acid chain, respectively; however, the fatty acid chain had an additional hydroxyl group (**Fig. 3.3B**). Overall, this compound group, correlating to the previous group, were proposed to be comprised of four residues, including glucose, valine, butyric acid and a fatty acid chain (**Fig. 3.3B**). Following an extensive literature and database search (Norine and PubChem), the identified structures and fragmentation patterns did not correspond to previously identified glucosamine derivatives (*N*-butylglucosamine ester derivatives), and are hypothesised to be novel glucosamine derivatives homologues. The F2 nodes with *m/z* 607.3924, 581.3781, 579.3623 and 567.3618 were found in the UPLC-MS^e data and corresponded to the sodiated adducts of the compounds with *m/z* 585.4117, 559.3953, 557.3804 and 545.3787, respectively (**Appendix B Table B1**). No structures were elucidated for the F2 nodes with *m/z* 513.316, 543.363, 555.367, 569.381 and 601.407.

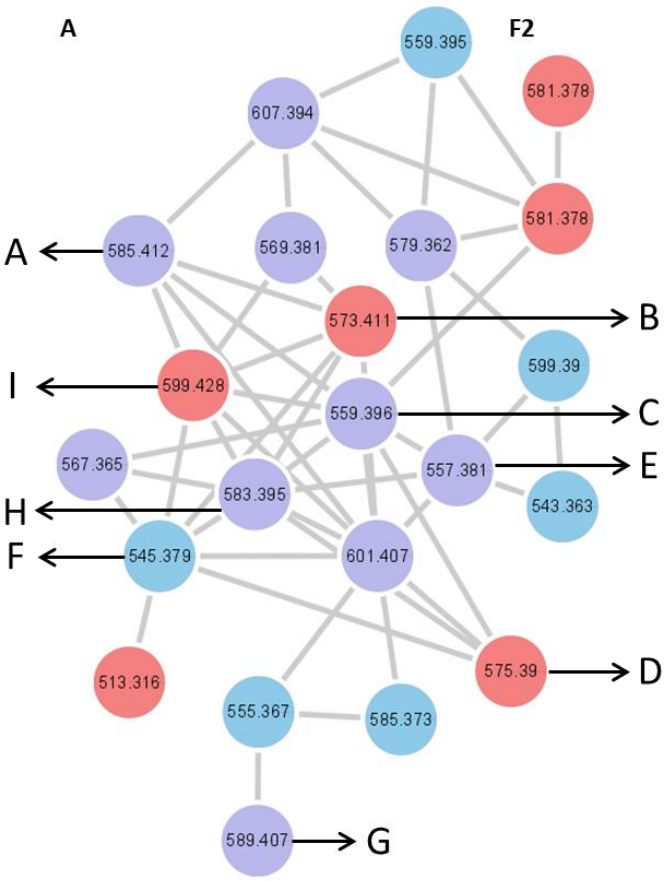

B

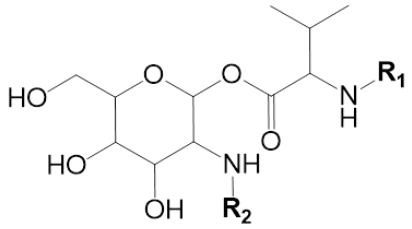

Glucosamine derivative ([M+H]$^+$)	R_1	R_2
A (*m/z* 585)	-CO-CH_2CH_2…CH_2-CH=CH-CH_2…$^{16}CH_3$	-CO-$(CH_2)_2CH_3$
B (*m/z* 573)	-CO-$(CH_2)_{13}$-CH_3	-CO-$(CH_2)_2CH_3$
C (*m/z* 559)	-CO-$(CH_2)_{12}$-CH_3	-CO-$(CH_2)_2CH_3$
D (*m/z* 575)	-CO-CH_2CH_2…CH(OH)-CH_2-CH_2…$^{14}CH_3$	-CO-$(CH_2)_2CH_3$
E (*m/z* 557)	-CO-CH_2CH_2…CH_2-CH=CH-CH_2…$^{14}CH_3$	-CO-$(CH_2)_2CH_3$
F (*m/z* 545)	-CO-$(CH_2)_{11}$-CH_3	-CO-$(CH_2)_2CH_3$
G (*m/z* 589)	-CO-CH_2CH_2…CH(OH)-CH_2-CH_2…$^{15}CH_3$	-CO-$(CH_2)_2CH_3$
H (*m/z* 583)	-CO-CH_2CH_2…CH_2-CH=CH-CH_2-CH=CH-CH_2…$^{16}CH_3$	-CO-$(CH_2)_2CH_3$
I (*m/z* 599)	-CO-CH_2CH_2…CH_2-CH=CH-CH_2…$^{17}CH_3$	-CO-$(CH_2)_2CH_3$
*J (*m/z* 627)	-CO-CH_2CH_2…CH_2-CH=CH-CH_2…$^{16}CH_3$	-CO-CH_2-CO-CH_2-CH_3
*K (*m/z* 587)	-CO-$(CH_2)_{14}CH_3$	-CO-$(CH_2)_2CH_3$

Fig. 3.3 The (**A**) molecular network of cluster F1 (magnified) labelled with the corresponding glucosamine derivative homologues detected in the P1 and NP1 crude extracts and (**B**) the structures of the detected cyclic and open-ring glucosamine derivative homologues identified using UPLC-MS^e analysis. Red nodes = metabolites produced by the P1 strain; Blue nodes = metabolites produced by the NP1 strain; Purple nodes = metabolites produced by both P1 and NP1 strains. *Glucosamine derivatives not present in the molecular network.

In contrast, to the above mentioned glucosamine derivatives, an individual node (**Fig. 3.1**) with *m/z* 627.4192 $[C_{33}H_{59}N_2O_9 + H]^+$ (calculated 627.4220) exhibited a unique fragmentation profile and corresponded to a peak at 16.28 min observed in the UPLC-MS^e data for the P1 strain (**Table 3.2; Appendix B Fig. B21**). The fragmentation profile was unique as the *m/z* 627.4192 compound did not have a major fragment of *m/z* 232.1163 (corresponding to the glucose/hexose residue linked to butyric acid) that was common in all of the previously described glucosamine derivatives. Instead, a major fragment at *m/z* 274.1287 was observed, which suggested a modification in the fragment corresponding to the glucose and butyric acid moiety. The major fragment at *m/z* 274.1287 potentially corresponded to a glucose/hexose residue linked to an oxo-hexanoic acid (rather than a butyric acid), and a dehydration product of the *m/z* 274.1287 fragment was observed at *m/z* 256.1174. Furthermore, a second major fragment of *m/z* 354.3016 was observed, which corresponded to an unsaturated $C_{16:1}$ fatty acid chain. In comparison to the glucosamine derivative A (*m/z* 585.4117) which also had an unsaturated $C_{16:1}$ fatty acid chain, this glucosamine derivative had an additional C_2H_3O based on the experimental molecular formula (elemental composition) predicted using the MassLynx 4.1 software package, which corresponded to the difference between butyric acid ($C_4H_8O_2$) and oxo-hexanoic acid ($C_6H_{10}O_3$). Moreover, *S. marcescens* strains are capable of producing oxo-hexanoic acid for the biosynthesis of *N*-(3-oxo-hexanoyl)-homoserine lactone (Okano et al. 2012), and it is thus feasible that oxo-hexanoic acid was incorporated into the glucosamine derivative instead of butyric acid. In addition, the compound at *m/z* 627.4192 did not cluster with the glucosamine derivatives in the molecular network; rather, the compound formed an individual cluster and this further suggests the reduced relatedness of this compound to the glucosamine derivatives. Although NMR is required to confirm the structure, the putative structure of the compound at *m/z* 627.4192 was proposed to consist of glucose, oxo-hexanoic acid, valine and an unsaturated $C_{16:1}$ fatty acid chain, which is distinctive from that of the previously described glucosamine derivatives.

3.3.4. Antimicrobial Activity

The bioactivity of the secondary metabolites produced by the P1 and NP1 strains was then investigated using disc diffusion, MIC and MBC assays. All of the fractions collected during RP-HPLC analysis were subjected to antimicrobial testing using a disc diffusion assay against *E. faecalis* S1. It was found that *E. faecalis* S1 was susceptible (diameter range of 9.3 ± 2.1 to 19.3 ± 1.5 mm) to the fractions with the major molecular ions of *m/z* 515.3331, 541.3485, 543.3644, 557.3804, 559.3953 and 585.4117 (for both P1 and NP1), and the fraction with *m/z* 324.2073 collected from P1 crude extract (results not shown). Thereafter, the MIC and MBC assays were performed using five fractions (selected based on activity and quantity available), including fractions

with the major molecular ions of *m/z* 324.2073, 515.3331, 541.3485, 543.3644 and 585.4117. A summary of the MIC and MBC assay results are outlined in **Table 3.3**.

Table 3.3 Minimum inhibition and bactericidal concentrations of selected fractions against the clinical *E. faecalis* S1 stain.

Major molecular ion $[M+H]^+$	Proposed identification (fatty acid chain length)	MIC (mg/mL)	MBC (mg/mL)
515.3331	Serratamolide A (C_{10}+C_{10})	3	> 3
541.3485	Serratamolide B (C_{10}+$C_{12:1}$)	3	> 3
543.3644	Serratamolide C (C_{10}+C_{12})	3	> 3
585.4117	Glucosamine derivative A ($C_{16:1}$)	0.75	3
324.2073	Prodigiosin	< 0.75	1.5

It was observed that all three serratamolides (A to C) (identified as outlined in section 3.3.3.3) exhibited identical activity against *E. faecalis* S1 with a MIC of 3 mg/mL and MBC of > 3 mg/mL. In comparison, glucosamine derivative A (identified as outlined in section 3.3.3.4) was found to have a lower MIC and MBC of 0.75 mg/mL and 3 mg/mL, respectively. Overall, however, the lowest MIC and MBC against *E. faecalis* S1 was observed for prodigiosin (identified as outlined in section 3.3.3.2), at < 0.75 and 1.5 mg/mL, respectively (**Table 3.3**).

3.4. Discussion

3.4.1. UPLC-MS^e and Molecular Networking Analysis

A combination of RP-HPLC, ESI-MS and UPLC-MS^e analysis, with MS-based molecular networking, was used to unravel the metabolic profiles of environmental pigmented and non-pigmented *S. marcescens* strains with the aim of identifying bioactive compounds. This work reports on the identification of four molecular families of secondary metabolites associated with *Serratia* species, including prodigiosin, serratiochelin A, serratamolide homologues and glucosamine derivative homologues. The structures of prodigiosin and serratiochelin A have previously been elucidated, where prodigiosin was described as a tripyrrole red pigment with an alkyl substituent (Lee et al. 2011) and serratiochelin A was described as a low-molecular weight siderophore with high affinity for iron (Khilyas et al. 2019). Moreover, based on their characteristic fragmentation patterns, as observed in the UPLC-MS^e data, eight serratamolides (including the putative structure of a novel open-ring serratamolide homologue) and 11 glucosamine derivatives (including the putative structures of eight novel glucosamine derivative congeners) were identified in this study and their structures were elucidated.

It is well-known that certain bacteria naturally produce various lipopeptide congeners which vary in fatty acid chain length, fatty acyl saturation or in the amino acids residues of the peptide moiety (Das et al. 2008). This was similarly observed in the current study as the identified serratamolides, comprised of two L-serine residues linked to two fatty acyl residues, varied in the length (C_{10} to C_{12}) and the presence or absence of double bonds (saturated or mono-unsaturated) in the fatty acyl chains and cyclisation (open-ring or cyclic) of the peptide moiety. During UPLC-MS^e analysis, the elution (Rt) of the serratamolide homologues was, as expected, dependent on the length of the β-hydroxy fatty acid chains of the compound, as the serratamolides with shorter saturated fatty acid moieties [such as serratamolide A (C_{10}+C_{10})] eluted from the column before the serratamolides with longer saturated fatty acid moieties [such as serratamolide 571 (C_{12}+C_{12})]. This elution profile is based on basic reverse-phase chromatography principles, where more hydrophobic (longer fatty acid chain) compounds have increased adhesion strength to the stationary phase and will thus elute at a later retention time from the column (Ndlovu et al. 2017; Takashima et al. 2018). It was also observed that the elution (Rt) of the serratamolide homologues was dependent on the saturation or unsaturation of the fatty acid moieties, as the mono-unsaturated serratamolide B (C_{10}+$C_{12:1}$) eluted from the column before the corresponding saturated serratamolide C (C_{10}+C_{12}) with the same fatty acyl chain lengths and peptide moieties. Previous research has indicated that the presence and position of a double bond within the fatty acyl chain influences the elution (Rt) of a compound (Takashima et al. 2018) and the retention time of a mono-unsaturated fatty acid is reduced to that of the equivalent saturated fatty acid with two carbon units. A *cis* double bond causes a kink in the chain and reduces the actual molecular length by nearly two carbon units, thereby resulting in the elution of a $C_{18:1}$ fatty acid just after a C_{16} fatty acid (Plattner et al. 1977; Takashima et al. 2018). It has also been reported that an open-chain lipopeptide is retained in the column for a shorter time period than the corresponding cyclic lipopeptide due to the increased polarity of the compound (due to the addition of the OH group) (Qiu et al. 2019), which clarifies for example, why the cyclic serratamolide C (C_{10}+C_{12}) eluted from the column after the open-chain serratamolide 561 (C_{10}+C_{12}) with the same fatty acid chain length.

The glucosamine derivative congeners detected in this study, were proposed to be comprised of glucose, valine, butyric acid (or oxo-hexanoic acid for novel derivative at *m/z* 627.4192) and a saturated or unsaturated β-fatty acid residue that varied in the length (C_{13} to C_{17}) and the presence or absence of a hydroxyl group. During UPLC-MS^e analysis, it was observed that the elution (Rt) of the glucosamine derivative homologues was also dependent on the length of the fatty acid moiety, as the glucosamine derivatives with shorter saturated fatty acid moieties (such as glucosamine derivative C with a C_{14} fatty acyl chain) eluted from the column before the glucosamine derivatives with longer saturated fatty acid moieties (such as the novel glucosamine derivative K homologue with a C_{16} fatty acyl chain). This is similar to what was observed for the serratamolides, where more

hydrophobic (longer fatty acid chain) compounds eluted at a later retention time from the C_{18} matrix (Ndlovu et al. 2017; Takashima et al. 2018). It was also observed that the elution (Rt) of the glucosamine derivative homologues was dependent on the presence of one or more double bonds within the fatty acyl chain, as the novel poly-unsaturated (two double bonds) glucosamine derivative H homologue ($C_{16:2}$) eluted before the corresponding mono-unsaturated (one double bond) glucosamine derivative A ($C_{16:1}$). Moreover, both unsaturated glucosamine derivatives A and H eluted before the corresponding saturated novel glucosamine derivative K homologue (C_{16}) with the same valine, butyric acid and glucose residues, as well as the same fatty acyl chain length. Furthermore, it was observed that the glucosamine derivatives with an additional hydroxyl group within the fatty acid moieties were retained in the column for a shorter time period than the corresponding glucosamine derivative without a hydroxyl group, due to the increased polarity of the compound. For instance, the glucosamine derivative C ($C_{29}H_{54}N_2O_8$) with a C_{14} fatty acyl chain eluted from the column after the corresponding novel glucosamine derivative D homologue ($C_{29}H_{55}N_2O_9$) with a C_{14} fatty acyl chain that has an additional hydroxyl group. Overall, it was observed that the glucosamine derivative homologues and serratamolide homologues separated as expected according to hydrophobicity (fatty acyl chain length) and chain saturation.

3.4.2. Secondary Metabolic Profile of the *S. marcescens* P1 and NP1 strains

Clements et al. (2019b; chapter two) previously identified the secondary metabolites produced by the P1 and NP1 strains using UPLC-ESI-MS analysis, which proposed that the P1 strain produced prodigiosin and serratamolides (A, B, C and E), while the NP1 strain produced glucosamine derivative A and serratamolides (A, B, C and E). The use of RP-HPLC and UPLC-MS^e analysis in the current study revealed that the P1 strain produced four metabolic classes, including prodigiosin, serratiochelin A, serratamolide homologues and glucosamine derivative homologues, while NP1 produced three metabolic classes, including serratiochelin A, serratamolide homologues and glucosamine derivative homologues. The combination of RP-HPLC and UPLC-MS^e analysis was thus an effective and vital approach to identify the minor metabolic constituents and fully elucidate the microbial metabolic profile of the environmental *Serratia* strains.

Genetically, secondary metabolites are synthesised by a number of gene clusters that can be identified using a bioinformatics approach (Romano et al. 2018). Certain gene clusters involved in secondary metabolism [such as non-ribosomal peptide synthetase (NRPS) gene clusters] may not be expressed under laboratory conditions and may be considered as ‘silent’ gene clusters (Bode et al. 2002). Minor alterations in the cultivation conditions of a particular strain may however, trigger the expression of the ‘silent’ gene clusters and may allow for the discovery of novel small molecules (Bode et al. 2002). This phenomenon is known as the “one strain many compounds” (OSMAC) approach, which indicates that a single strain can produce various metabolites when grown under

different media composition and cultivation conditions, leading to the activation of the 'silent' metabolic pathways within the genome of the microbial strain (Bode et al. 2002; Romano et al. 2018). When comparing the culture conditions of Clements et al. (2019b; chapter two) to the culture conditions employed in the current study, an increased production scale (from 100 mL to 1500 mL) in baffled flasks, as well as the change in media components (from bactopeptone to peptone powder) was applied. Thus, while the combination of RP-HPLC and UPLC-MS^e analysis may have aided in the detection of the minor metabolites; it is also probable that the altered culture conditions and media composition employed, may have activated 'silent' NRPS clusters (such as the glucosamine derivatives in the P1 strain and the serratiochelin in both strains), thereby increasing the metabolic constituents produced by both the pigmented and non-pigmented *S. marcescens* strains.

Although genome mining of the P1 and NP1 strains was not within the scope of this study, Khilyas et al. (2019) sequenced the genome of a pigmented *S. marcescens* SM6 strain and used the antiSMASH 5.0 prediction tool to identify biosynthetic gene clusters involved in secondary metabolism within the strain. The authors identified five biosynthetic gene clusters involved in secondary metabolite production, including gene clusters responsible for the production of two siderophores (serratiochelin and chrysobactin), a thiopeptide, a serratamolide and a glucosamine derivative (Khilyas et al. 2019). It is possible that the P1 and NP1 strains possess similar NRPS gene clusters as both strains were able to produce serratiochelin, serratamolides and glucosamine derivatives. In addition, the bifurcated biosynthetic pathway responsible for the production of prodigiosin was additionally activated in the P1 strain (Lee et al. 2011). Following an extensive literature search, and to the best of the author's knowledge, this is the first report of the co-production of all four secondary metabolic classes (including prodigiosin, serratiochelin A, serratamolides and glucosamine derivatives) by a *Serratia* strain.

3.4.3. Antimicrobial Activity

Results from this study indicated that prodigiosin, serratamolide homologues (A to C) and glucosamine derivative homologues (A and C), as well as the novel glucosamine derivative E homologue exhibited activity against a clinical Gram-positive bacterial strain. The MIC and MBC assays further revealed that serratamolide A, B and C exhibited identical activity against *E. faecalis* S1, suggesting that the presence of a double bond or the increased length of one of the two fatty acid chains from C_{10} to C_{12} exhibited no additional antimicrobial potency against the Gram-positive strain. In comparison, glucosamine derivative A was found to exhibit a lower MIC and MBC in comparison to the serratamolides. This indicates that *E. faecalis* S1 was more susceptible to the glucosamine derivative A than the serratamolides. Overall, however, *E. faecalis* S1 was found to be

the most susceptible to prodigiosin, as a lower MIC and MBC was obtained against the clinical strain in comparison to glucosamine derivative A and the serratamolides.

The potent activity of prodigiosin corresponds to previous research that similarly recorded activity of this pigmented compound against Gram-positive bacteria such as *Staphylococcus aureus* (*S. aureus*) and *Bacillus subtilis* (*B. subtilis*) (Darshan and Manonmani 2015). It has also been suggested that prodigiosin is a hydrophobic stressor that disrupts the cell membrane and results in the leakage of intracellular products, such as K^+ ions, amino acids, sugars and proteins (Suryawanshi et al. 2016). Furthermore, prodigiosin may interfere with cellular respiration and protein and ribosomal ribonucleic acid synthesis (Danevčič et al. 2016a, 2016b). Serratamolide A has similarly been reported to display activity towards Gram-positive bacteria, such as *S. aureus* strains (Kadouri and Shanks 2013). It has additionally been reported that serratamolide A (serrawettin W1) increased the rate of movement of K^+ and H^+ across the membrane of *S. aureus* at a concentration of 10 µg/mL, while no leakage of '260 nm-absorbing products' (such as nucleic acids), membrane permeability or cell growth inhibition was observed at this concentration (Deol et al. 1973). Currently, one study has reported on the antimicrobial activity of glucosamine derivative homologues (A to C) toward *Mycobacterium diernhoferi*; however, little is known about the mechanism of action of these metabolites (Dwivedi et al. 2008). Moreover, Hage-Hülsmann et al. (2018) described the enhanced antimicrobial activity of serrawettin W1 (serratamolide A) and prodigiosin in combination, in comparison to the individual bioactive metabolites, against *Corynebacterium glutamicum*. The authors hypothesised that the co-production of serrawettin W1 and prodigiosin may provide a competitive advantage to the producing strain due to the increased bioactive potency, whilst also aiding in the colonisation and biofilm development of the producing strain by inhibiting or delaying the growth of competing microorganisms. Thus, whilst extensive research is required to investigate the ecological role of co-producing prodigiosin, serratamolides and glucosamine derivatives; the combined production of these bioactive metabolites by *S. marcescens* may provide a competitive advantage to the producing strain (Darshan and Manonmani 2015; Hage-Hülsmann et al. 2018). Moreover, as indicated in chapter two (Clements et al. 2019b), the metabolites in the P1 strain may exhibit a higher antimicrobial effect in comparison to the metabolites in the NP1 strain, as the secondary metabolites in the P1 crude extract were effective against 81% of the test microbial organisms, in comparison to the 67% antimicrobial efficacy recorded for the NP1 strain.

3.5. Conclusions

The use of chromatographic fractionation, ESI-MS, UPLC-MS^e and molecular networking analysis allowed for the separation, identification and elucidation of 21 secondary metabolites (combined total for P1 and NP1 strains), including serratamolide homologues, glucosamine derivative

homologues, prodigiosin (P1) and serratiochelin A. Moreover, the putative structure of an open-ring serratamolide homologue and putative structures of eight novel glucosamine derivative congeners were elucidated. The structural relatedness of the novel open-ring serratamolide and glucosamine derivative congeners to the known serratamolides and glucosamine derivatives, respectively, was revealed using molecular networking and fragmentation patterns of the UPLC-MS^{e} data. This approach thus proved vital for metabolite identification and characterisation. The identified metabolic families exhibited structural diversity and well-ordered chromatographic behaviours due to structural modifications of fatty acid chain lengths, open-ring or cyclic structures and the degree of saturation (saturated or mono-unsaturated) of the fatty acid chain. Moreover, seven fractions collected during RP-HPLC, with major molecular ions corresponding to prodigiosin, serratamolides (A, B and C), and glucosamine derivatives (A, C and E), displayed antimicrobial activity against the clinical *E. faecalis* S1 strain using the disc diffusion assay. However, the MIC and MBC assays revealed that prodigiosin exhibited the greatest antimicrobial potency in comparison to serratamolide A, B and C, and glucosamine derivative A. This study thus highlights the importance of *Serratia* species as a source of novel antimicrobial compounds for potential therapeutic application. It is recommended that future research investigate the mode of action and synergism of the bioactive secondary metabolites produced by these two *S. marcescens* strains. In addition, the use of whole genome sequencing of the P1 and NP1 strains and subsequent genome mining of NRPS gene clusters is a promising future endeavour to identify additional secondary metabolites not actively being produced under typical cultivation conditions.

Acknowledgements

This work was financially supported by the Water Research Commission under (grant number K5/2728//3) and the National Research Foundation of South Africa (grant number: 113849). Opinions expressed and conclusions arrived at, are those of the authors and are not necessarily to be attributed to the National Research Foundation. The authors wish to thank Dr. Anton Du Preez van Staden at Stellenbosch University for assistance with the RP-HPLC analysis to purify the crude extracts. The authors also thank Dr. Marietjie Stander from the LCMS Central Analytical Facility, Stellenbosch University, for assistance with the tandem-mass spectrometric protocol used in this study.

3.6. References

Bode, H.B., Bethe, B., Höfs, R., and Zeeck, A. (2002). Big effects from small changes: possible ways to explore nature's chemical diversity. ChemBioChem 3:7, 619–627. https://doi.org/10.1002/1439-7633(20020703)3:7<619::AID-CBIC619>3.0.CO;2-9

Clements, T., Ndlovu, T., Khan, S., and Khan, W. (2019a). Biosurfactants produced by *Serratia* species: Classification, biosynthesis, production and application. Appl. Microbiol. Biotechnol. 103, 589–602. https://doi.org/10.1007/s00253-018-9520-5

Clements, T., Ndlovu, T., and Khan, W. (2019b). Broad-spectrum antimicrobial activity of secondary metabolites produced by *Serratia marcescens* strains. Microbiol. Res. 229:126329, 1–10. https://doi.org/10.1016/j.micres.2019.126329

Danevčič, T., Vezjak, M.B., Tabor, M., Zorec, M., and Stopar, D. (2016b). Prodigiosin induces autolysins in actively grown *Bacillus subtilis* cells. Front. Microbiol. 7:27, 1–10. https://doi.org/10.3389/fmicb.2016.00027

Danevčič, T., Vezjak, M.B., Zorec, M., and Stopar, D. (2016a). Prodigiosin - A multifaceted *Escherichia coli* antimicrobial agent. PLoS One 11:9, 1–13. https://doi.org/10.1371/journal.pone.0162412

Darshan, N., and Manonmani, H.K. (2015). Prodigiosin and its potential applications. J. Food Sci. Technol. 52, 5393–5407. https://doi.org/10.1007/s13197-015-1740-4

Das, P., Mukherjee, S., and Sen, R. (2008). Antimicrobial potential of a lipopeptide biosurfactant derived from a marine *Bacillus circulans*. J. Appl. Microbiol. 104:6, 1675–1684. doi:10.1111/j.1365-2672.2007.03701.x

Deol, B.S., Bermingham, M.A., Still, J.L., Haydon, D.A., and Gale, E.F. (1973). The action of serratamolide on ion movement in lipid bilayers and biomembranes. Biochim. Biophys. Acta Biomembr. 330:2, 192–195. https://doi.org/10.1016/0005-2736(73)90224-1

Dwivedi, D., Jansen, R., Molinari, G., Nimtz, M., Johri, B.N., and Wray, V. (2008). Antimycobacterial serratamolides and diacyl peptoglucosamine derivatives from *Serratia* sp. J. Nat. Prod. 71:4, 637–641. https://doi.org/10.1021/np7007126

Eckelmann, D., Spiteller, M., and Kusari, S. (2018). Spatial-temporal profiling of prodiginines and serratamolides produced by endophytic *Serratia marcescens* harbored in *Maytenus serrata*. Sci. Rep. 8, 1–15. https://doi.org/10.1038/s41598-018-23538-5

EUCAST (2018). Breakpoint tables for interpretation of MICs and zone diameters. http://www.eucast.org/fileadmin/src/media/PDFs/EUCAST_files/Breakpoint_tables/v_8.0_Breakpoint_Tables.pdf. Accessed 10 July 2020.

Fu, Y., Luo, J., Qin, J., and Yang, M. (2019). Screening techniques for the identification of bioactive compounds in natural products. J. Pharm. Biomed. Anal. 168, 189–200. https://doi.org/10.1016/j.jpba.2019.02.027

Grimont, F., and Grimont, P.A. (2015). *Serratia*. Bergey's Manual of Systematics of Archaea and Bacteria, pp.1–22.

Hage-Hülsmann, J., Grünberger, A., Thies, S., Santiago-Schübel, B., Klein, A.S., Pietruszka, J., Binder, D., Hilgers, F., Domröse, A., Drepper, T., and Kohlheyer, D. (2018). Natural biocide cocktails: Combinatorial antibiotic effects of prodigiosin and biosurfactants. PloS One 13:7, e0200940. https://doi.org/10.1371/journal.pone.0200940

Kadouri, D.E., and Shanks, R.M. (2013). Identification of a methicillin-resistant *Staphylococcus aureus* inhibitory compound isolated from *Serratia marcescens*. Res. Microbiol. 164:8, 821–826. https://doi.org/10.1016/j.resmic.2013.06.002

Khilyas, I.V., Tursunov, K.A., Shirshikova, T.V., Kamaletdinova, L.K., Matrosova, L.E., Desai, P.T., McClelland, M., and Bogomolnaya, L.M. (2019). Genome Sequence of Pigmented Siderophore-Producing Strain *Serratia marcescens* SM6. Microbiol. Resour. Announc. 8:18, e00247–19. https://doi.org/10.1128/MRA.00247-19

Knolhoff, A.M., Zheng, J., McFarland, M.A., Luo, Y., Callahan, J.H., Brown, E.W., and Croley, T.R. (2015). Identification and structural characterization of naturally-occurring broad-spectrum cyclic antibiotics isolated from *Paenibacillus*. J. Am. Soc. Mass Spectr. 26:10, 1768–1779. https://doi.org/10.1021/jasms.8b04889

Kobelnik, M., Fontanari, G.G., Ribeiro, C.A., and Crespi, M.S. (2018). Evaluation of thermal behavior and chromatographic characterization of oil extracted from seed of *Pittosporum undulatum*. J. Therm. Anal. Calorim. 131:1, 371–378. https://doi.org/10.1007/s10973-017-6763-9

Kuo, Y.H., Liang, T.W., Liu, K.C., Hsu, Y.W., Hsu, H.C., and Wang, S.L. (2011). Isolation and identification of a novel antioxidant with antitumour activity from *Serratia ureilytica* using squid pen as fermentation substrate. Mar. Biotechnol. 13:3, 451–461. https://doi.org/10.1007/s10126-010-9316-9

Lee, J.S., Kim, Y.S., Park, S., Kim, J., Kang, S.J., Lee, M.H., Ryu, S., Choi, J.M., Oh, T.K., and Yoon, J.H. (2011). Exceptional production of both prodigiosin and cycloprodigiosin as major metabolic constituents by a novel marine bacterium, *Zooshikella rubidus* S1-1. Appl. Environ. Microbiol. 77:14, 4967–4973. https://doi.org/10.1128/AEM.01986-10

Magalhães, L., and Nitschke, M., (2013). Antimicrobial activity of rhamnolipids against *Listeria monocytogenes* and their synergistic interaction with nisin. Food Control 29:1, 138–142.

Matsuyama, T., Fujita, M., and Yano, I. (1985). Wetting agent produced by *Serratia marcescens*. FEMS Microbiol. Lett. 28:1, 125–129. https://doi.org/10.1111/j.1574-6968.1985.tb00777.x

Matsuyama, T., Kaneda, K., Nakagawa, Y., Isa, K., Hara-Hotta, H., and Yano, I. (1992). A novel extracellular cyclic lipopeptide which promotes flagellum-dependent and -independent spreading

growth of *Serratia marcescens*. J. Bacteriol. 174:6, 1769–1776. https://doi.org/10.1128/jb.174.6.1769-1776.1992

Matsuyama, T., Murakami, T., Fujita, M., Fujita, S., and Yano, I. (1986). Extracellular vesicle formation and biosurfactant production by *Serratia marcescens*. Microbiol. 132:4, 865–875. https://doi.org/10.1099/00221287-132-4-865

Motley, J.L., Stamps, B.W., Mitchell, C.A., Thompson, A.T., Cross, J., You, J., Powell, D.R., Stevenson, B.S., and Cichewicz, R.H. (2016). Opportunistic sampling of roadkill as an entry point to accessing natural products assembled by bacteria associated with non-anthropoidal mammalian microbiomes. J. Nat. Prod. 80, 598–608. https://doi.org/10.1021/acs.jnatprod.6b00772

Ndlovu, T., Rautenbach, M., Vosloo, J.A., Khan, S., and Khan, W. (2017). Characterisation and antimicrobial activity of biosurfactant extracts produced by *Bacillus amyloliquefaciens* and *Pseudomonas aeruginosa* isolated from a wastewater treatment plant. AMB Express 7:108, 1–19. https://doi.org/10.1186/s13568-017-0363-8

Okano, C., Arai, M., Nasuno, E., Iimura, K.I., Morohoshi, T., Ikeda, T., and Kato, N. (2012). β-Cyclodextrin Interaction with N-Hexanoyl Homoserine Lactone as Quorum Sensing Signal Produced in Gram-Negative Bacteria. Trans. Mat. Res. Soc. Japan 37:2, 315–318. https://doi.org/10.14723/tmrsj.37.315

Philippus, A.C., Zatelli, G.A., Wanke, T., Barros, M.G.D.A., Kami, S.A., Lhullier, C., Armstrong, L., Sandjo, L.P., and Falkenberg, M. (2018). Molecular networking prospection and characterization of terpenoids and C 15-acetogenins in Brazilian seaweed extracts. RSC Adv. 8:52, 29654–29661. https://doi.org/10.1039/C8RA02802H

Plattner, R.D., Spencer, G.F., and Kleiman, R. (1977). Triglyceride separation by reverse phase high performance liquid chromatography. J. Am. Oil Chem.' Soc. 54:11, 511–515. https://doi.org/10.1007/BF02909070

Qiu, S., Avula, B., Guan, S., Ravu, R.R., Wang, M., Zhao, J., Khan, I.A., Hinchee, M., and Li, X.C. (2019). Identification of fusaricidins from the antifungal microbial strain *Paenibacillus* sp. MS2379 using ultra-high performance liquid chromatography coupled to quadrupole time-of-flight mass spectrometry. J. Chromatogr. A 1586, 91–100. https://doi.org/10.1016/j.chroma.2018.12.007

Romano, S., Jackson, S.A., Patry, S., and Dobson, A.D. (2018). Extending the “one strain many compounds” (OSMAC) principle to marine microorganisms. Mar. Drugs 16:7, 244. https://doi.org/10.3390/md16070244

Seyedsayamdost, M.R., Cleto, S., Carr, G., Vlamakis, H., João Vieira, M., Kolter, R., and Clardy, J. (2012). Mixing and matching siderophore clusters: structure and biosynthesis of serratiochelins from *Serratia* sp. V4. J. Am. Chem. Soc. 134:33, 13550–13553. https://doi.org/10.1021/ja304941d

Soenens, A., and Imperial, J. (2019). Biocontrol capabilities of the genus *Serratia*. Phytochem. Rev. 2019:1–11. https://doi.org/10.1007/s11101-019-09657-5

Stankovic, N., Senerovic, L., Ilic-Tomic, T., Vasiljevic, B., and Nikodinovic-Runic, J. (2014). Properties and applications of undecylprodigiosin and other bacterial prodigiosins. Appl. Microbiol. Biotechnol. 98, 3841–3858. https://doi.org/10.1007/s00253-014-5590-1.

Su, C., Xiang, Z., Liu, Y., Zhao, X., Sun, Y., Li, Z., Li, L., Chang, F., Chen, T., Wen, X., and Zhou, Y. (2016). Analysis of the genomic sequences and metabolites of *Serratia surfactantfaciens* sp. nov. YD25^T that simultaneously produces prodigiosin and serrawettin W2. BMC Genom. 17:865, 1–19. https://doi.org/10.1186/s12864-016-3171-7

Suryawanshi, R.K., Patil, C.D., Koli, S.H., Hallsworth, J.E., and Patil, S.V. (2016). Antimicrobial activity of prodigiosin is attributed to plasma membrane damage. Nat. Prod. Res. 31:5, 572–577. https://doi.org/10.1080/14786419.2016.1195380

Takashima, S., Toyoshi, K., and Shimozawa, N. (2018). Analyses of the fatty acid separation principle using liquid chromatography-mass spectrometry. Med. Mass Spectrom. 2, 1–13. https://doi.org/10.24508/mms.2018.06.002

Thies, S., Santiago-Schübel, B., Kovačić, F., Rosenau, F., Hausmann, R., and Jaeger, K.E. (2014). Heterologous production of the lipopeptide biosurfactant serrawettin W1 in *Escherichia coli*. J. Biotechnol. 181, 27–30. https://doi.org/10.1016/j.jbiotec.2014.03.037

Tsugawa, H., Cajka, T., Kind, T., Ma, Y., Higgins, B., Ikeda, K., Kanazawa, M., VanderGheynst, J., Fiehn, O., and Arita, M. (2015). MS-DIAL: data-independent MS/MS deconvolution for comprehensive metabolome analysis. Nat. Methods 12:6, 523–526. http://dx.doi.org.ez.sun.ac.za/10.1038/NMETH.3393

Wang, M., Carver, J.J., Phelan, V.V., Sanchez, L.M., Garg, N., Peng, Y., Nguyen, D.D., Watrous, J., Kapono, C.A., Luzzatto-Knaan, T., and Porto, C. (2016). Sharing and community curation of mass spectrometry data with Global Natural Products Social Molecular Networking. Nat. Biotechnol. 34:8, 828–837. https://doi.org/10.1038/nbt.3597

Wasserman, H.H., Keggi, J.J., and McKeon, J.E. (1961). Serratamolide, a metabolic product of *Serratia*. J. Am. Chem. Soc. 83:19, 4107–4108. https://doi.org/10.1021/ja01480a046

Williamson, N.R., Fineran, P.C., Leeper, F.J., and Salmond, G.P. (2006). The biosynthesis and regulation of bacterial prodiginines. Nat. Rev. Microbiol. 4:12, 887–899. https://doi.org/10.1038/nrmicro1531

Yasir, M., Dutta, D., and Willcox, M.D. (2019). Comparative mode of action of the antimicrobial peptide melimine and its derivative Mel4 against *Pseudomonas aeruginosa*. Sci. Rep. 9:1, 1–12. https://doi.org/10.1038/s41598-019-42440-2

Yip, C.H., Yarkoni, O., Ajioka, J., Wan, K.L., and Nathan, S. (2019). Recent advancements in high-level synthesis of the promising clinical drug, prodigiosin. Appl. Microbiol. Biotechnol. 103:4, 1667–1680. https://doi.org/10.1007/s00253-018-09611-z

Chapter 4:

(Sections of this chapter are included in the South African Patent Application No. 2020/05912; UK spelling is employed)

Biofilm disruption and antiadhesive activity of secondary metabolites produced by *Serratia marcescens* strains

Tanya Clements[a], Thando Ndlovu[a], Nusrat Begum[b] and Wesaal Khan[a*]

[a] Department of Microbiology, Faculty of Science, Stellenbosch University, Private Bag X1, Stellenbosch, 7602, South Africa

[b] Department of Chemistry and Polymer Science, Faculty of Science, Stellenbosch University, Private Bag X1, Stellenbosch, 7602, South Africa

*Corresponding Author: Wesaal Khan; Phone: +27 21 808 5804; E-mail: wesaal@sun.ac.za

Abstract

The antifouling potential of secondary metabolites produced by a pigmented (P1) and a non-pigmented (NP1) *Serratia marcescens* (*S. marcescens*) strain was investigated. The P1 and NP1 crude extracts, comprised of serratamolide and glucosamine derivative homologues (as well as prodigiosin in the P1 crude extract), were tested against single- and dual-species *Pseudomonas aeruginosa* (*P. aeruginosa*) S1 68 and *Enterococcus faecalis* (*E. faecalis*) S1 biofilms to determine the minimum biofilm eradication concentration (MBEC) using the MBEC Assay®. Results indicated a significant reduction (≥ 2 logs) in plate counts and gene copies [ethidium monoazide bromide quantitative polymerase chain reaction (EMA-qPCR)] of the single-species *P. aeruginosa* S1 68 and *E. faecalis* S1 biofilms after exposure to the P1 and NP1 crude extract, with the exception of the single-species *P. aeruginosa* S1 68 biofilm where a one log reduction was observed (based on gene copies) after exposure to the NP1 crude extract. The P1 and NP1 extracts significantly reduced the dual-species *P. aeruginosa* and *E. faecalis* biofilm based on plate counts and gene copies; however, a 10- and 5-fold increase in the concentration of P1 and NP1 was required to reduce *E. faecalis* by ≥ 2 logs in comparison to the single-species *E. faecalis* biofilm. Moreover, pre-adsorption of 50 mg/mL of the P1 and NP1 crude extracts to the pegs of the MBEC Assay® reduced the adhesion of mono-cultures of *P. aeruginosa* S1 68 and *E. faecalis* S1 by ≥ 93% based on plate counts and ≥ 80% based on gene copies. In co-culture, reductions in *E. faecalis* S1 adhesion to the P1 and NP1 coated pegs were comparable to the results recorded for the mono-culture experiments, while a ≤ 80% reduction in *P. aeruginosa* S1 68 was obtained. Surface characterisation methods, including water contact angle measurements, attenuated total reflectance Fourier transform infrared spectroscopy and scanning electron microscope coupled to backscattered electron imaging-energy dispersive x-ray spectroscopy, then confirmed the successful immobilisation of serratamolides and glucosamine derivatives (detected in P1 and NP1 crude extracts) onto the surface of high-density polyethylene PE300 (HDPE) and polyvinyl chloride (PVC). The P1 and NP1 coated HDPE effectively reduced the adhesion of *P. aeruginosa* S1 68 cells by ≥ 87% based on plate counts and ≥ 64% based on gene copies, while the adhesion of *E. faecalis* S1 was reduced by ≥ 96% based on plate counts and ≥ 87% based on gene copies. In contrast, while the P1 and NP1 coated PVC effectively reduced the adhesion of *P. aeruginosa* S1 68 cells by ≥ 81% based on plate counts and ≥ 99% based on gene copies, minor reductions in adhesion were observed for *E. faecalis* S1. The P1 and NP1 crude extracts thus have the potential to be used as biodetergents for controlling *P. aeruginosa* and *E. faecalis* biofilms in industrial settings and can be applied as a preventative strategy to delay the onset of biofilm formation on polymeric materials.

Keynotes: Serratamolide; glucosamine derivative; prodigiosin; biofilm disruption; antiadhesive; surface immobilisation

4.1. Introduction

Biofilms are a complex aggregation of single- or multi-species microbial communities that are able to proliferate on biotic and abiotic surfaces commonly utilised within the water, food and medical industries (Donlan 2002; Kiran et al. 2010; do Valle Gomes and Nitschke 2012). Microbial contamination within these environments can pose a serious human health risk, as biofilms are known to harbour opportunistic and pathogenic microorganisms (Banerjee et al. 2011; Abdallah et al. 2014). In particular, *Pseudomonas aeruginosa* (*P. aeruginosa*), *Klebsiella pneumoniae* (*K. pneumoniae*), *Staphylococcus aureus* (*S. aureus*), *Listeria monocytogenes* (*L. monocytogenes*) and *Enterococcus faecalis* (*E. faecalis*), are often detected in contaminated water sources, food processing units and as part of a biofilm community on medical equipment, devices and implants (Wingender and Flemming 2011; Abdallah et al. 2014; Lee et al. 2017; Meier et al. 2018). Several strategies such as the use of chlorine based disinfectants, peracetic acid and quaternary ammonium compounds, amongst others, are thus being implemented to reduce the formation of biofilms and disrupt existing biofilm communities (Simões et al. 2010). However, research has indicated that the biofilm extracellular polymeric substance (EPS) matrix provides a protective barrier that delays or prevents conventional disinfectants from reaching the target microbial cells within the biofilm, contributing to inefficient biofilm control and eradication. Moreover, microorganisms within biofilms may possess inherent resistance mechanisms or may acquire resistance to antimicrobial or disinfectant products through genetic exchange or mutations, further contributing to the persistence of biofilm communities (Simões et al. 2010). The discovery of potent antifouling agents capable of removing microbial biofilms and reducing the adhesion of microbial cells to solid surfaces is thus a priority (Ludensky 2003).

Biosurfactants are a diverse group of bioactive amphiphilic compounds produced by bacteria, yeast and filamentous fungi during secondary metabolism (Janek et al. 2012). Numerous biosurfactants exhibit antibacterial, antifungal and antiviral activities, which make them valuable for application in several fields (such as the water, medical and food industries) (Gudiña et al. 2010). Investigations into the antifouling properties of biosurfactants have also gained momentum over the last 20 years (Meylheuc et al. 2001; Rivardo et al. 2009; Dusane et al. 2010, 2012; Sambanthamoorthy et al. 2014), with studies indicating that biosurfactants may be more effective at disrupting existing biofilms than traditional inhibitory agents (Epstein et al. 2011; Banat et al. 2014). Glycolipids and lipopeptides, produced by bacterial genera such as *Bacillus* spp., *Paenibacillus* spp., *Pseudomonas* spp. and *Lactobacillus* spp., amongst others, are the two main classes of biosurfactant compounds that have been reported to display biofilm disrupting and antiadhesive activity (Banat et al. 2014). While these biosurfactant classes are also produced by *Serratia* spp., they have not been extensively investigated as a natural source of antifouling agents.

Various *Serratia* species produce serrawettins, which form part of the lipopeptide class of biosurfactants, and are comprised of a hydrophilic peptide moiety attached to a hydrophobic fatty acid moiety (Thies et al. 2014; Clements et al. 2019a). Three structurally distinct molecular species of serrawettins have been identified, including serrawettin W1, serrawettin W2 and serrawettin W3 (Matsuyama et al. 1985). Serrawettin W1 (also referred to as serratamolide A) has been extensively investigated and is a cyclic peptide of two serine amino acids linked to two fatty acid chains (Thies et al. 2014). Homologues of serrawettin W1 (serratamolide B to F) exist due to the varying fatty acid chain length, open-ring structures and the presence or absence of double bonds (Eckelmann et al. 2018). Since their discovery, several studies have indicated that serrawettins exhibit bioactivity against bacteria, fungi, nematodes and cancer cells (Tomas et al. 2005; Pradel et al. 2007; Dwivedi et al. 2008; Kadouri and Shanks 2013; Su et al. 2016; Zhu et al. 2018). Dusane et al. (2011) was the first to report on the antifouling properties of a glycolipid composed of palmitic acid esterified to glucose, produced by a *Serratia marcescens* (*S. marcescens*) strain. A glycolipid concentration of 50 µg/mL resulted in preformed biofilm reductions of up to 55% for *Candida albicans* (*C. albicans*), 62% for *P. aeruginosa* and 55% for *Bacillus pumilus,* when grown in a polystyrene microtiter plate (Dusane et al. 2011). Thereafter, Motley et al. (2016) investigated the ability of serrawettin W2, produced by a *Serratia* strain, to inhibit biofilm formation by *C. albicans*. The *C. albicans* strain was incubated with the biosurfactant for 48 h in the wells of a 96-well polystyrene microtiter plate, with results indicating that half the inhibitory concentration (IC_{50}) of 7.7 ± 0.7 µM for serrawettin W2 inhibited biofilm formation (Motley et al. 2016).

Previous studies have indicated that the coating of biosurfactants to a solid substratum can modify its surface hydrophobicity, thereby reducing the adhesion of microorganisms to the material and ultimately results in a reduction of biofilm formation (do Valle Gomes and Nitschke 2012). One of the most common coating techniques involves simple adsorption of an antimicrobial compound to the surface of the material (Meylheuc et al. 2001, 2006; Pirog et al. 2014; Shubina et al. 2015). Moreover, the encapsulation or incorporation of an antimicrobial substance within a material has also been described (Verma et al. 2019). However, several limitations to these methods exist, including the loss of antifouling potency over time, potential toxicity or the development of antimicrobial resistance due to a low concentration of the compound being released (Alves and Pereira 2014; De Zoysa and Sarojini 2017; Verma et al. 2019). Alternative coating strategies are thus required for industrial application and the immobilisation of antimicrobials (including biosurfactants) to polymers using covalent linkages is advantageous as this method prevents leaching, enhances long-term stability and increases the duration of antimicrobial efficacy (Alves and Pereira 2014; De Zoysa and Sarojini 2017). Antimicrobial materials that prevent or significantly reduce microbial adhesion by covalently immobilising a lipopeptide to the surface of a material have thus been developed (Mohorčič et al. 2010; De Zoysa and Sarojini 2017). For example, De Zoysa

and Sarojini (2017) covalently immobilised a lipopeptide (battacin) to glass, silicon, and titanium surfaces, and found that the battacin-immobilised surfaces prevented microbial adhesion of *P. aeruginosa* and *Escherichia coli* cells (98.6 to 99.9% reduction of adhesion) to all three surfaces.

Considering the relevance of developing lipopeptide-coated surfaces with antifouling activity for industrial application, the search for secondary metabolites produced by *Serratia* spp. that display biofilm disruption and antiadhesive activity is of interest. As outlined in chapter three, the *S. marcescens* P1 and NP1 strains produce various bioactive secondary metabolites, including serratamolide homologues in combination with glucosamine derivative homologues in the P1 and NP1 crude extracts, while prodigiosin (red pigment) was detected in the P1 crude extract. Moreover, both P1 and NP1 crude extracts were found to exhibit broad-spectrum antimicrobial activity (Clements et al. 2019b; chapter two). The primary aim of the current study was thus to explore the potential biofilm disrupting and antiadhesive activity of the P1 and NP1 crude extracts against single- and dual-species biofilms of *E. faecalis* S1 and *P. aeruginosa* S1 68, using the MBEC Assay®. A secondary aim was to use these metabolites to develop a non-leaching biomaterial by covalently immobilising serratamolide and glucosamine derivative homologues detected in the P1 and NP1 crude extracts, to discs of high-density polyethylene PE300 (HDPE) and polyvinyl chloride (PVC) and investigate the antifouling potency of the biomaterials against mono-cultures of *E. faecalis* S1 and *P. aeruginosa* S1 68.

4.2. Materials and Methods

4.2.1. Bacterial Strains

The biosurfactant producing *S. marcescens* P1 (pigmented) and NP1 (non-pigmented) strains used in this study were previously isolated from oil refinery effluent and river water samples, respectively (Clements et al. 2019b; chapter two). The test microorganisms used for the antifouling assays included *P. aeruginosa* S1 68 [environmental strain isolated from rainwater (Clements et al. 2019c)] and *E. faecalis* S1 (clinical isolate). *Pseudomonas aeruginosa* S1 68 was streaked from the glycerol stocks onto Nutrient agar (Merck, South Africa), while *E. faecalis* S1 was streaked onto Tryptone Soy agar (Biolab, Merck, South Africa) supplemented with 6 g/L yeast extract (Biolab, Merck, South Africa) ($TSAYE_{0.6\%}$) and both strains were incubated at 37 °C for 18 to 24 h.

4.2.2. Production and Partial Purification of Secondary Metabolites

The crude extracts of *S. marcescens* P1 and NP1 were produced, extracted and partially purified as described in chapter three. Briefly, the *S. marcescens* P1 and NP1 strains were inoculated into 10 mL Luria Bertani broth (Biolab, Merck, South Africa) and incubated aerobically on a test tube rotator (MRCLAB, London, United Kingdom) at 30 °C for 18 to 24 h. Each seed culture was subsequently

inoculated into a 2 000 mL baffled flask containing 500 mL Peptone Glycerol (pH 7.2 ± 0.2) broth [composed of 5 g Peptone powder (Biolab, Merck, South Africa) and 10 mL glycerol (Promega, Wisconsin, United States) in 1 L distilled water] in triplicate, which was incubated on an orbital shaker (MRCLAB, London, UK) at 30 °C for 120 h at 120 rpm. The broth culture was then centrifuged at 10 000 rpm for 20 min at 4 °C to obtain the cell free supernatant. The cell free supernatants were lyophilised and dissolved in 70% (*v/v*) acetonitrile (Romil, Darmstadt, Germany). The acetonitrile soluble fraction was transferred into a sterile McCartney bottle and lyophilised. This step was repeated thrice to further purify the crude extracts. The lyophilised extracts were analytically weighed to determine the mass of each extract and subsequently stored at -20 °C.

4.2.3. Biofilm Disruption (MBEC Assay®)

The minimum biofilm eradication concentration (MBEC) of each crude extract against preformed single- and dual-species biofilms was determined using the MBEC Assay® (P&G, Innovotech, Edmonton, AB, Canada), as per the manufacturer's instructions with minor modifications. The MBEC Assay® is composed of a 96-well microtiter plate and a lid containing 96 pegs that fit into each well of the microtiter plate. It is on the pegs of the lid that the biofilm will develop. The test microorganisms were first inoculated into 5 mL Mueller Hinton Broth (MHB, Merck, South Africa) (*P. aeruginosa* S1 68) or Tryptone Soy Broth (Biolab, Merck, South Africa) supplemented with 6 g/L yeast extract ($TSBYE_{0.6\%}$) (*E. faecalis* S1) and incubated at 37 °C for 18 to 24 h. For single-species biofilms, the MBEC Assay® lid was placed into a microtiter plate containing 150 µL of the cell suspension of each test microorganism adjusted to an optical density at 625 nm (OD_{625}) of 0.08 to 0.13 [~10^7 to 10^9 colony forming units (CFU)/mL]. A trial was first conducted to determine the appropriate ratio of each test strain in $TSBYE_{0.6\%}$ to be added to the MBEC Assay® to form dual-species biofilms. Based on the results obtained (results not shown) the lid was placed into a new Nunc® Microwell™ 96-well tissue culture microtiter plate (Merck, South Africa) containing 75 µL of the *P. aeruginosa* S1 68 [OD_{625} = 0.08 (~10^7 CFU/mL)] suspended in $TSBYE_{0.6\%}$ and 75 µL *E. faecalis* S1 [OD_{625} = 0.13 (~10^9 CFU/mL)] suspended in $TSBYE_{0.6\%}$. For each single- or dual-species biofilm assay, sterile broth was included as a negative control, while sterile broth with the respective test organism(s) was included as a positive control. The MBEC Assay® was assembled and incubated on an orbital shaker at 120 rpm for 18 to 24 h at 37 °C.

Following incubation, the MBEC Assay® lid was rinsed with sterile saline (0.85% NaCl) and transferred to a challenge plate containing P1 or NP1 crude extract. The single- and dual- species biofilms were exposed to 6.25 to 50 mg/mL [prepared in 15% methanol (Sigma-Aldrich, St. Louis, USA)] of P1 or NP1 crude extracts, with the exception of the single-species *E. faecalis* S1 biofilm that was exposed to 1.25 to 10 mg/mL of the P1 or NP1 crude extracts. The single- and dual-species biofilms were exposed to the various concentrations of the crude extracts (in triplicate) for

2 h at 37 °C. After exposure, the MBEC Assay® lid was transferred to a recovery plate containing 200 µL of sterile organism specific media containing universal neutraliser recovery media (as per manufacturer's instructions). Thereafter, the plate was sonicated in an ultrasonic cleaner (Branson model 5510) (containing a dry stainless steel insert tray) for 30 min to dislodge the remaining biofilm, which was quantified as described in section 4.2.5. The log reduction of the preformed biofilm cells disrupted by P1 and NP1 crude extracts was determined.

4.2.4. Antiadhesive Activity (MBEC Assay®)

The antiadhesive activity of the P1 and NP1 crude extracts against pure and co-culture cell suspensions of *P. aeruginosa* S1 68 and *E. faecalis* S1 was also conducted using the MBEC Assay®. In order to coat the pegs of the MBEC Assay® lid, the protocol described by Rivardo et al. (2009) was utilised. Briefly, the MBEC Assay® lid was transferred to a Nunc™ Nunclon™ 96-well tissue culture microtiter plate containing 200 µL of P1 or NP1 crude extracts (in triplicate) at varying concentrations of 6.25 to 50 mg/mL [prepared in 15% methanol]. Negative controls of 200 µL sterile broth and 15% methanol were included in each assay, in triplicate (uncoated pegs). The MBEC Assay® was assembled and incubated at 4 °C for 24 h. After 24 h, the lid was removed and allowed to dry in a sterile environment for 10 min. For mono-culture cell suspensions, the lid was placed into a microtiter plate containing 150 µL of the test microorganism [OD_{625} = 0.08 to 0.13 (~10^7 to 10^9 CFU/mL)]. In contrast, for co-culture cell suspensions, a trial was conducted to determine the appropriate ratio of each test microorganism in $TSBYE_{0.6\%}$ to be added to each well of the MBEC Assay® (results not shown). Thus, the MBEC Assay® lid was placed into a new microtiter plate containing an equal volume of *P. aeruginosa* S1 68 and *E. faecalis* S1 [75 µL of each strain suspended to an OD_{625} = 0.1 (~10^8 CFU/mL)] broth cultures. The lid was then removed after 1 h of exposure to the test microorganism(s) at 37 °C and was rinsed in sterile saline (0.85% NaCl) to remove non-adherent cells, as described by Sambanthamoorthy et al. (2014). Thereafter, the lid was transferred to a new microtiter plate containing 200 µL of sterile organism specific media containing universal neutraliser recovery media (as per manufacturer's instructions). The plate was sonicated in an ultrasonic cleaner for 30 min to dislodge the attached cells and were quantified as described in section 4.2.5. The percentage of bacterial cells inhibited from adhering to the pre-coated surface was determined as indicated in Eq.1.

$$\%\ Microbial\ inhibition = \left[1 - \left(\frac{A_c}{A_0}\right)\right] \times 100 \quad \text{[Eq. 4.1]}$$

where A_c represents the CFU/mL or gene copies/mL of the well at a crude extract concentration *c*, and A_0 represents the CFU/mL or gene copies/mL of the control well.

4.2.5. Quantification of Biofilm Disruption and Antiadhesive Activity

4.2.5.1. Culture-based Analysis

The cell suspensions recovered after sonication (sections 4.2.3 and 4.2.4) were quantified by using a standard culture-based technique. Briefly, 20 µL of each suspension (in triplicate) was used for serial dilutions (10^{-1} to 10^{-6}) in 180 µL sterile saline in a 96-well microtiter plate. For single-species biofilms, the dilutions (as well as 20 µL of the respective undiluted sample) were spot plated onto Nutrient agar (single-species biofilm of *P. aeruginosa* S1 68) or $TSAYE_{0.6\%}$ (single-species biofilm of *E. faecalis* S1). For the dual-species biofilms, the dilutions were spot plated onto Slanetz and Bartley agar (Oxoid, Hampshire, England) for *E. faecalis* S1 and Cetrimide agar (Merck, South Africa) for *P. aeruginosa* S1 68 quantification, respectively. The plates were incubated at 37 °C for 18 to 24 h. Thereafter, the bacterial colonies were enumerated and the bacterial counts were recorded as an average of the triplicate ± standard deviation.

4.2.5.2. Ethidium Monoazide Bromide (EMA) Treatment and Deoxyribonucleic acid (DNA) Extraction

Following the culture-based quantification, the remaining triplicate cell suspensions for each crude extract concentration was pooled to yield a total volume of 480 µL, which was then subjected to ethidium monoazide bromide (EMA) treatment, DNA extraction and quantitative PCR (qPCR) [also known as ethidium monoazide bromide quantitative PCR (EMA-qPCR)].

The viability dye, EMA, was obtained from Biotium (Hayward, CA, USA) and was dissolved in 20% dimethyl sulfoxide (DMSO; Sigma-Aldrich, St. Louis, USA) to obtain a 5 mg/mL stock solution (Reyneke et al. 2016). The EMA treatment of the remaining recovered cell suspensions were conducted as previously described by Reyneke et al. (2016) and Delgado-Viscogliosi et al. (2009). Briefly, 480 µL of the remaining cell suspension was exposed to 6 µM of EMA, followed by an incubation period of 10 min in the dark on ice. The samples were then subjected to a 15 min halogen light (500 W; Eurolux, South Africa) exposure at an exposure distance of 20 cm, in order to crosslink the dye to extracellular DNA or the DNA from membrane compromised cells. The EMA-treated samples were washed with an equal volume of sterile saline (0.85% NaCl) and were centrifuged at 13 000 rpm for 5 min. The supernatant was discarded after centrifugation and the resulting pellet was re-suspended in 750 µL lysis solution from the Quick-DNA™ Fecal/Soil Microbe Miniprep Kit (Zymo Research, Irvine, CA, USA) and the DNA extractions were completed according to the manufacturer's instructions. In addition, genomic DNA was extracted from the American Type Culture Collection (ATCC) microorganisms, *E. faecalis* ATCC 7080 and *P. aeruginosa* ATCC 27853 using the Quick-DNA™ Fecal/Soil Microbe Miniprep Kit.

4.2.5.3. Quantitative PCR

The EMA-treated samples from the single- and dual-species *P. aeruginosa* S1 68 and *E. faecalis* S1 biofilm assays (biofilm disruption and antiadhesive activity) were subjected to qPCR using the primers and cycling parameters outlined in **Table 4.1**. The qPCR was performed on a LightCycler® 96 (Roche Applied Science, Mannheim, Germany) using the FastStart Essential DNA Green Master Mix (Roche Applied Science, Mannheim, Germany). The reaction mixture (20 µL) consisted of 1X FastStart Essential DNA Green Master Mix, 0.2 µM of each primer (both *Pseudomonas* spp. and *Enterococcus* spp.) (**Table 4.1**) and 5 µL template DNA.

Table 4.1 The cycling parameters used for conventional and quantitative PCR for the respective test microorganisms.

Microorganism	*Pseudomonas* spp.	*Enterococcus* spp.
Primer name and sequence (5' to 3')	PS1: ATGAACAACGTTCTGAAATTC PS2: CTGCGGCTGGCTTTTTCCAG	ECST784F: AGAAATTCCAAACGAACTTG ENC854R: CAGTGCTCTACCTCCATCATT
Cycling parameters for conventional PCR	5 min at 95 °C; 50 cycles of 94 °C for 30 s, 58 °C for 30 s, 72 °C for 30 s; 72 °C for 10 min	5 min at 95 °C; 50 cycles of 95 °C for 15 s, 60 °C for 1 min, 72 °C for 20 s; 72 °C for 10 min
Cycling parameters for qPCR	10 min at 95 °C; 50 cycles of 94 °C for 30 s, 58 °C for 30 s, 72 °C for 30 s	10 min at 95 °C; 50 cycles of 95 °C for 15 s, **60 °C for 1 min
Gene (bp)	*oprI* (249)	23S rRNA (75)
Reference	Bergmark et al. (2012)	Frahm and Obst (2003)

**Combined annealing and elongation step

Melt curve analysis was included during the SYBR green real-time PCR assay in order to verify the specificity of the primer set by increasing the temperature from 65 to 97 °C at a rate of 0.2 °C/s with continuous fluorescent signal acquisition at 5 readings/ °C. To generate a standard curve for the quantification of *Pseudomonas* and *Enterococcus*, conventional PCR was performed on the extracted positive control (*E. faecalis* ATCC 7080 and *P. aeruginosa* ATCC 27853) DNA. Conventional PCR was performed using the primers and cycling parameters, as outlined in **Table 4.1**, using the T100™ Thermal Cycler (Bio-Rad Laboratories, Hercules, CA, USA). Each PCR mixture was performed in a final volume of 25 µL using a standard PCR mixture consisting of 1X Green GoTaq® Flexi buffer (Promega), 2.0 mM $MgCl_2$ (Promega, Wisconsin, US), 0.1 mM dNTP mix (Thermo Fisher Scientific, Waltham, Massachusetts, United States), 1.5 U of GoTaq® Flexi

DNA polymerase (Promega, Wisconsin, US), 0.2 µM (*Pseudomonas* spp.) or 0.5 µM (*Enterococcus* spp.) of each primer (**Table 4.1**) and 2 µL of template DNA. Sterile water was used as a negative control, while genomic DNA extracted from the ATCC strains was used as a positive control. The products of the conventional PCR amplification were analysed by gel electrophoresis using 1.5% agarose, containing 0.5 µg/mL ethidium bromide in a 1X tris/acetate/ethylenediaminetetraacetic acid (TAE) buffer. The PCR products were cleaned and concentrated using the Wizard® SV Gel and PCR Clean-up System (Promega, Wisconsin, US) as per manufacturer's instructions.

A standard curve was prepared by using the clean and concentrated conventional PCR products. Briefly, the DNA concentration of each cleaned-up PCR product of the ATCC strains was determined using a NanoDrop® ND-1000 (Nanodrop Technologies Inc.). The DNA concentration and gene product size was then used to dilute the DNA to a final concentration of 10^9 gene copies/µL as previously described by Dobrowsky et al. (2016). Serial 10-fold dilutions of the PCR products were then prepared in order to generate a standard curve, with a concentration of 1.00×10^9 gene copies/µL for the dilution with the highest copy number and a concentration of 1.00×10^0 gene copies/µL for the dilution with the lowest copy number. The lower limit of detection (LLOD) for all qPCR assays was determined as the lowest number of genome copies consistently detected for each organism.

4.2.6. Coating of Polymers with P1 and NP1 Crude Extracts

4.2.6.1. Modification of Antimicrobial Compounds

The crude extracts obtained from *S. marcescens* P1 and NP1 (as outlined in section 4.2.2) were utilised for coating experiments onto high-density polyethylene PE300 (HDPE) (Maizey, South Africa) and unplasticised polyvinyl chloride (PVC) (Maizey, South Africa) discs of 20 mm x 10 mm, 1.5 mm thick. Prior to the coating of the two materials (HDPE and PVC), the P1 and NP1 crude extracts [comprised of serratamolide and glucosamine derivative homologues (and prodigiosin in the P1 crude extract)] were subjected to chemical modification in order to ensure that the compounds would covalently attach to the materials. It is important to note that prodigiosin was not modified or attached to the silanized materials, due to the absence of reactive functional groups within the prodigiosin structure. The P1 and NP1 crude extracts were modified as illustrated in **Scheme 4.1**.

Briefly, P1 or NP1 crude extracts (350 mg, 0.714 mmol), pyridine (282.47 mg, 3.571 mmol; Merck, South Africa) and dry ethanol (50 mL; Merck, South Africa) were added into a round bottom flask (100 mL) equipped with a magnetic stirrer and chilled. Following solubilisation of the respective compounds, nitrogen gas was bubbled into the solution. Thionyl chloride ($SOCl_2$) (424.8 mg, 3.571 mmol, 97% purity, Merck, South Africa) was slowly added drop-wise into the mixture and the

reaction was continuously stirred for 20 to 24 h at ambient temperature under a nitrogen blanket. Subsequently, the excess solvent was removed under reduced pressure using a Buchi Rotavapor R-114 (Buchi Labortechnik AG, Switzerland) and the residue was washed three times with dichloromethane (DCM, Merck, South Africa). Following the washing step, the mixture (composed of the modified compounds) was placed in a 40 °C oven for approximately 4 h to dry. All modified compounds were sealed in inert vials and stored at -20 °C until required. In order to confirm the successful substitution of the hydroxyl groups (-OH) with chlorine groups (-Cl) in the structures of the secondary metabolites, approximately 200 µg of the dry chemically modified P1 and NP1 crude extracts and 200 µg of dry unmodified crude extracts were subjected to attenuated total reflectance Fourier transform infrared (ATR-FTIR) spectroscopy (as indicated in section 4.2.7.2). The remaining dry modified extracts were weighed and used for the coating experiments as described in section 4.2.6.2.

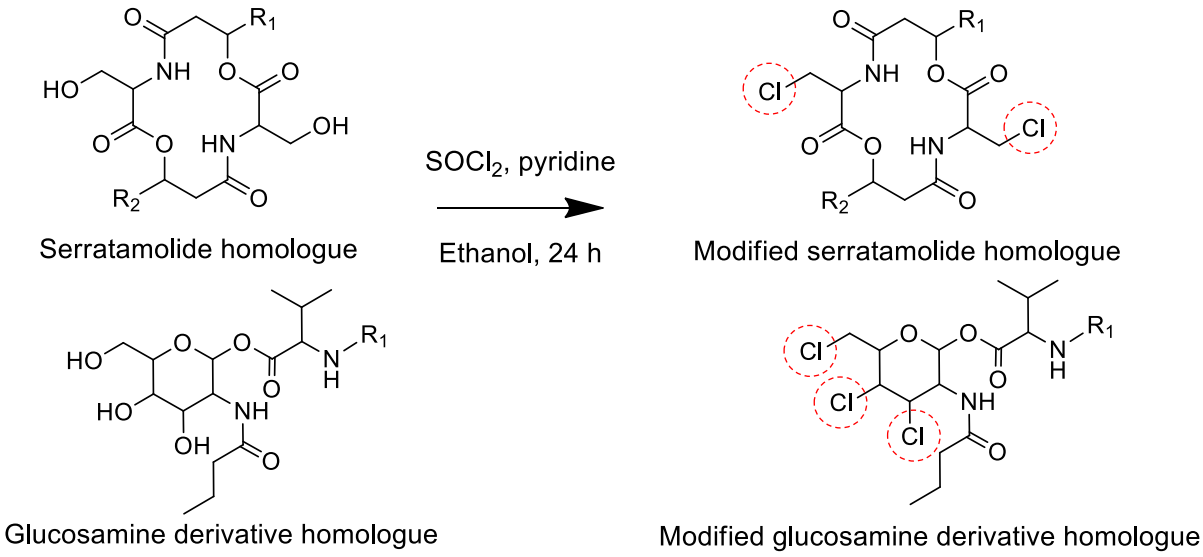

Scheme 4.1 Synthesis of modified serratamolides and glucosamine derivative homologues present in the P1 and NP1 crude extracts. The R_1 and R_2 groups on the serratamolides and glucosamine derivative homologue structures indicate the fatty acyl moieties and these chains may vary in length and saturation (saturated, mono-unsaturated or poly-unsaturated) (as described in chapter three).

4.2.6.2. Immobilisation of Modified Compounds onto the Polymers

The modified crude extracts (P1 and NP1) were utilised for the coating of the HDPE and PVC surfaces, as illustrated in **Scheme 4.2**. The immobilisation procedure of the above crude extracts was adapted and modified as previously described by De Zoysa and Sarojini (2017). Prior to the coating steps, all surfaces were washed with acetone and sterile Milli-Q water and dried at room temperature. The coating was conducted in duplicate. Briefly, the HDPE and PVC discs were immersed in a test tube containing 4 mL piranha solution [50% hydrogen peroxide (H_2O_2, 30% *v/v* in

water; Merck, South Africa) and 50% concentrated sulphuric acid (H_2SO_4, 95-97%; Merck, South Africa)], for 30 min on a rotary wheel at 37 °C (**Scheme 4.2**). After treatment, the materials were rinsed in Milli-Q water and ethanol and dried under nitrogen gas. The piranha-treated materials were then silanized in 3% of 3-triethoxysilylpropan-1-amine (99%, APTES, Sigma-Aldrich, St. Louis, USA) in dry ethanol (4 mL in a test tube; Merck, South Africa) for 48 h on a rotary wheel at 37 °C. The APTES treated materials were sequentially washed in Milli-Q water and ethanol, soaked in ethanol for 10 min and sonicated for 10 min. The soaked surfaces were rinsed in ethanol to remove the non-attached APTES and were dried under a stream of nitrogen gas and placed in a desiccator for 10 min to stabilise the APTES monolayer. Thereafter, the APTES-coated surfaces were immersed in 4 mL of the modified compounds at 5 mg/mL (in duplicate for each material) in dry ethanol, in a test tube and were placed on a rotary wheel at 37 °C for 24 h. The coated surfaces were again washed in Milli-Q and ethanol and dried under nitrogen gas. The coated and control (uncoated and APTES silanized) materials were stored at -20 °C until further analysis.

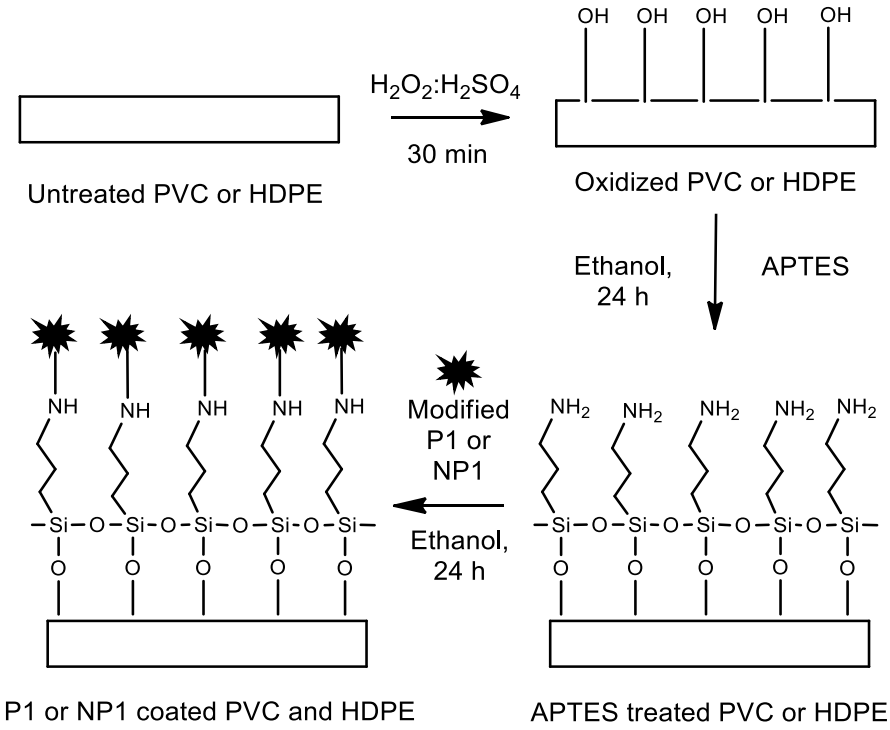

Scheme 4.2 Schematic synthetic pathway employed for the selective immobilisation of compounds onto surfaces of HDPE and PVC.

4.2.7. Surface Characterisation

4.2.7.1. Water Contact Angle Measurements

In order to confirm the successful immobilisation of the respective crude extracts onto the materials, the contact angle of water on the APTES coated, P1 and NP1 crude extract coated and uncoated

materials (PVC and HDPE), was measured using a KSV Cam 100 Goniometer (Biolin Scientific, Manchester, UK) using Attension Theta analysis software (Biolin Scientific Manchester, UK) as previously described by De Zoysa and Sarojini (2017). Briefly, a water droplet (1.0 µL) was placed onto the surface of the APTES coated, crude extract coated and uncoated materials and was left to equilibrate for 10 s. The contact angle was measured using the planar charged coupled display (CCD) camera of the Goniometer. This was repeated at five different regions of the material and the contact angles are reported as an average and its standard deviation.

4.2.7.2. Attenuated Total Reflectance Fourier Transform Infrared (ATR-FTIR) Spectroscopy

Prior to covalent immobilisation, the compounds in the P1 and NP1 crude extracts were modified (as indicated in section 4.2.6.1) and ATR-FTIR spectroscopy was utilised to confirm the successful modification. In addition, surface characterisation of the coated and uncoated materials was monitored using Thermo Scientific Nicolet iS10 ATR-FTIR spectrometer. The spectrometer is fitted with a diamond disc and Zinc Selenide lenses whose measurements were taken at spectral resolution of 4 cm^{-1} with infrared range between 500 and 4 000 cm^{-1}. The spectral data were obtained after 32 background scans followed by a total of 64 scans per sample. The ATR-FTIR analysis was used to confirm the presence of functional groups and compare the spectra of uncoated (PVC and HDPE), APTES coated and crude extract coated materials. The data was acquired using Omnic software and processed in Origin version 9.0.

4.2.7.3. Scanning Electron Microscope (SEM) Coupled to Backscattered Electron Imaging-energy Dispersive X-ray Spectroscopy (BSE-EDX)

The surface morphology of the crude extract coated (also referred to as immobilised) and uncoated materials (PVC and HDPE) were analysed using a MIRA3 TESCAN scanning electron microscope (SEM) after carbon sputter coating at the Centre for Imaging and Analysis, Electron Microscopy Unit (University of Cape Town). For the acquisition of the image, a voltage of 7 kV and a probe current of 150 pA was employed. For the determination of the surface morphology of the materials, the SEM-I mg-studio software version 1.1.0 was used, which operates using the National Instruments LVRunTime Engine. Energy dispersive X-ray (EDX) spectroscopy was used in conjunction with FEI NovaNano SEM to confirm the immobilisation of the respective crude extracts onto the materials (PVC and HDPE).

4.2.8. Stability of the Immobilised Compounds onto the Polymers

The stability of the compounds immobilised onto the materials (PVC and HDPE) was analysed, by placing the crude extract coated material into 250 mL Erlenmeyer flask containing 100 mL Milli-Q water. The Erlenmeyer flasks were incubated on an orbital shaker at 120 rpm at ambient

temperature and 15 mL of the suspension was collected after 24 h of incubation. The suspensions were lyophilised and dissolved in 15% acetonitrile to obtain a concentration of 1.00 mg/mL. The samples were then subjected to ultra-performance liquid chromatography coupled to electrospray ionisation mass spectrometry (UPLC-ESI-MS) at the Mass Spectrometry unit of the Central Analytical Facilities (CAF) at Stellenbosch University, as previously outlined in Clements et al. (2019b; chapter two).

4.2.9. Antifouling Activity of the Crude Extract-immobilised Polymers

The antifouling activity of the materials coated with crude extracts were analysed as described by De Zoysa and Sarojini (2017) with minor modifications. Briefly, seed cultures of *P. aeruginosa* S1 68 or *E. faecalis* S1 were prepared in 5 mL of $TSBYE_{0.6\%}$ and were incubated for 18 to 24 h at 37 °C. The seed cultures were diluted in 250 mL of $TSBYE_{0.6\%}$ to an OD_{625} = 0.08 to 0.13 (~10^7 to 10^9 CFU/mL) and 5 mL of the respective diluted seed culture was aliquoted into test tubes. Subsequently, the coated and uncoated materials were placed into the test tubes containing the diluted seed culture and the test tubes were incubated at 37 °C for 18 to 24 h on a test tube rotator. The analysis was conducted in duplicate. Uncoated materials were placed into 5 mL of sterile $TSBYE_{0.6\%}$ and were included as negative controls, while uncoated materials placed in a test tube containing 5 mL of each diluted seed culture of the respective microorganisms served as positive controls. After 24 h, the materials were removed from the test tubes and were rinsed with sterile saline (0.85% NaCl) to remove non-adherent microbial cells. The materials were then transferred to 3 mL sterile saline (0.85% NaCl) in a test tube and were sonicated for 5 min to recover the microbial cells that were able to attach to the surface of the coated and control (uncoated) materials. The resulting cell suspensions were centrifuged at 10 000 rpm for 10 min to concentrate the microbial cells and the pellet was resuspended in 1 mL of saline (0.85% NaCl). The cell suspensions were serially diluted from 10^0 to 10^6 and 100 µL was spread plated onto $TSAYE_{0.6\%}$ plates in triplicate. The plates were then incubated at 37 °C for 24 h and the CFU/mL was determined. In addition, EMA treatments and DNA extractions were conducted on 500 µL of each of the remaining cell suspensions, as outlined in section 4.2.5.2. Thereafter, the DNA samples were subjected to qPCR analysis as outlined in section 4.2.5.3 (for the *P. aeruginosa* S1 68 and *E. faecalis* S1) to quantify the intact cells capable of adhering to the surface of the crude extract coated and control materials.

4.2.10. Confocal Laser Scanning Microscopy (CLSM)

In order to visually confirm the reduction in microbial adhesion of *E. faecalis* S1 and *P. aeruginosa* S1 68, each of the coated and control materials were stained with 3.35 µM SYTO-9 and 20 µM propidium iodide (LIVE/DEAD Viability Kit, Invitrogen, Leiden, the Netherlands) as per the manufacturer's instructions. Following staining, the uncoated and coated materials were examined

for the viability of microbial cells using a Carl Zeiss LSM780 CLSM (Carl Zeiss, Germany) at the Fluorescence Microscopy Unit of the CAF (Stellenbosch University). Images were processed using ZEN 2012 imaging software (Carl Zeiss) with respect to quality (live/dead ratio) as outlined in Abdulkareem et al. (2015). All samples were sequentially scanned, frame-by-frame, first at 488 nm and then at 561 nm.

4.3. Results

4.3.1. Biofilm Disrupting Activity (MBEC Assay®)

Standard plate count methods and EMA-qPCR analysis was used to evaluate the potential of the P1 and NP1 crude extracts to disrupt preformed single- and dual-species biofilms of *P. aeruginosa* S1 68 (concentration range of 6.25 to 50 mg/mL) and *E. faecalis* S1 (concentration range of 1.25 to 10 mg/mL for single-species and 6.25 to 50 mg/mL for dual-species). Using a standard curve, *P. aeruginosa* and *E. faecalis* gene copy numbers from intact cells were quantified in the untreated and corresponding crude extract treated biofilms and are represented as *oprI* gene copies per mL and 23S rRNA gene copies per mL, respectively. The qPCR efficiency and linear regression coefficient (R^2) values for all of the MBEC Assays® were within the recommended range and are indicated in **Appendix C Table C1**.

4.3.1.1. Single-species Biofilm Disruption

The results of the plate counts and EMA-qPCR analysis of the untreated (control) and P1 and NP1 crude extract treated *P. aeruginosa* S1 68 biofilms are illustrated in **Fig. 4.1A** and **C**. For the untreated *P. aeruginosa* S1 68 biofilm samples, an average of 6.50×10^5 CFU/mL was obtained using culture-based analysis (**Fig. 4.1A**). Similar log reductions were then observed when the preformed *P. aeruginosa* S1 68 biofilms were treated with the P1 crude extract at 6.25 and 12.5 mg/mL, with average plate counts of 3.33×10^3 CFU/mL (2.29 log reduction) and 2.33×10^3 CFU/mL (2.44 log reduction) recorded, respectively (**Fig. 4.1A**). A significant log reduction of 4.59 was then obtained at 25 mg/mL of the P1 crude extract, with the *P. aeruginosa* S1 68 plate counts reduced to below the detection limit (BDL, < 1 CFU/mL) at 50 mg/mL. For the NP1 crude extract, average *P. aeruginosa* S1 68 plate counts of 5.17×10^4 CFU/mL (1.10 log reduction) and 5.83×10^4 CFU/mL (1.05 log reduction) were recorded at 6.25 and 12.5 mg/mL, respectively, with a significant log reduction of 2.59 (average of 1.67×10^3 CFU/mL) recorded at 25 mg/mL (**Fig. 4.1A**). Although the *P. aeruginosa* S1 68 plate counts were not reduced to BDL at a NP1 crude extract concentration of 50 mg/mL, a significant reduction of 3.53 logs was recorded (average of 1.92×10^2 CFU/mL) (**Fig. 4.1A**).

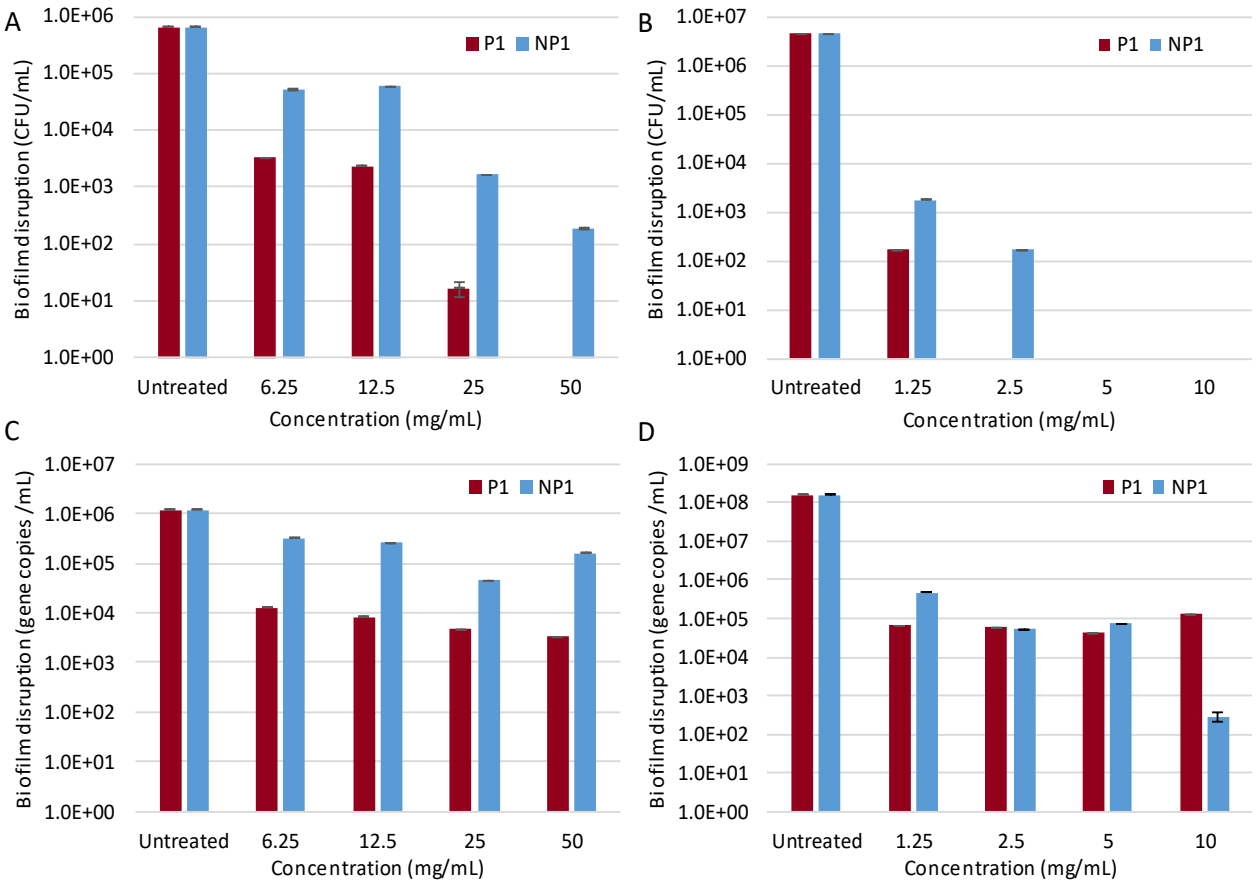

Fig. 4.1 The disruption of preformed single-species biofilms (biofilm disruption activity) treated with varying concentrations (1.25 to 50 mg/mL) of P1 (red) or NP1 (blue) crude extracts against (**A**) *P. aeruginosa* S1 68 and (**B**) *E. faecalis* S1 determined using standard plate count methods, and (**C**) *P. aeruginosa* S1 68 and (**D**) *E. faecalis* S1 determined using EMA-qPCR analysis.

For the untreated *P. aeruginosa* S1 68 biofilm samples, an average of 1.21×10^6 gene copies/mL was obtained using EMA-qPCR analysis (**Fig. 4.1C**). Similar log reductions were observed when the preformed *P. aeruginosa* S1 68 biofilms were treated with 6.25 and 12.5 mg/mL of the P1 crude extract, with average gene copy numbers of 1.26×10^4 gene copies/mL (1.98 log reduction) and 8.28×10^3 gene copies/mL (2.16 log reduction) recorded, respectively (**Fig. 4.1C**). A log reduction of 2.41 (4.66×10^3 gene copies/mL) was then obtained at 25 mg/mL of the P1 crude extract, with the *P. aeruginosa* S1 68 gene copy numbers reduced to 3.30×10^3 gene copies/mL (2.56 log reduction) at 50 mg/mL. A similar trend in gene copy number reduction was observed when the preformed *P. aeruginosa* S1 68 biofilms were treated with NP1 crude extract, with average gene copy numbers of 3.25×10^5 gene copies/mL (0.57 log reduction) and 2.64×10^5 gene copies/mL (0.66 log reduction) recorded at 6.25 and 12.5 mg/mL, respectively (**Fig. 4.1C**). However, a log reduction of 1.42 (4.56×10^4 gene copies/mL) was obtained at 25 mg/mL of the NP1 crude extract, while an average of 1.59×10^5 gene copies/mL (0.88 log reduction) was recorded for the preformed *P. aeruginosa* S1 68 biofilms treated with the 50 mg/mL of the NP1 crude extract (**Fig. 4.1C**).

The results of the plate counts and EMA-qPCR analysis of the untreated (control) and P1 and NP1 crude extract treated *E. faecalis* S1 biofilms are illustrated in **Fig. 4.1B** and **D**. For the untreated *E. faecalis* S1 biofilm samples, an average of 4.59×10^6 CFU/mL was obtained using culture-based analysis (**Fig. 4.1B**). A significant log reduction of 4.44 (average of 1.67×10^2 CFU/mL) was obtained at 1.25 mg/mL of the P1 crude extract, with the *E. faecalis* S1 plate counts reduced to BDL (< 1 CFU/mL) at 2.5, 5 and 10 mg/mL (**Fig. 4.1B**). A similar trend in *E. faecalis* S1 plate counts was observed for the NP1 crude extract, with average counts of 1.75×10^3 CFU/mL (3.42 log reduction) and 1.67×10^2 CFU/mL (4.44 log reduction) recorded at 1.25 and 2.5 mg/mL, respectively, with the *E. faecalis* S1 plate counts reduced to BDL (< 1 CFU/mL) at 5 and 10 mg/mL (**Fig. 4.1B**).

For the untreated *E. faecalis* S1 biofilm samples, an average of 1.57×10^8 gene copies/mL was obtained using EMA-qPCR analysis (**Fig. 4.1D**). Significant reductions ranging between 3.38 and 3.56 logs were observed when the preformed *E. faecalis* S1 biofilms were treated with 1.25, 2.5 and 5 mg/mL of the P1 crude extract, with average gene copy numbers of 6.48×10^4 gene copies/mL, 5.74×10^4 gene copies/mL and 4.29×10^4 gene copies/mL recorded, respectively. A reduction of 3.08 logs (average of 1.30×10^5 gene copies/mL) was observed in the samples treated with 10 mg/mL P1 crude extract (**Fig. 4.1D**). Log reductions of 2.53 (4.68×10^5 gene copies/mL), 3.46 (5.40×10^4 gene copies/mL) and 3.33 (7.27×10^4 gene copies/mL) were then observed when the preformed *E. faecalis* S1 biofilms were treated with NP1 crude extract concentrations of 1.25, 2.5 and 5 mg/mL, respectively. A significant reduction of 5.74 logs (average of 2.88×10^2 gene copies/mL) was however, observed in the samples treated with 10 mg/mL NP1 crude extract (**Fig. 4.1D**).

4.3.1.2. Dual-species Biofilm Disruption

The results of the plate counts and EMA-qPCR analysis of the untreated (control) and P1 crude extract treated preformed *P. aeruginosa* S1 68 and *E. faecalis* S1 biofilms (dual-species) are illustrated in **Fig. 4.2A** and **C**, respectively. For the untreated dual-species biofilm sample, an average of 3.33×10^7 CFU/mL and 6.17×10^6 CFU/mL was obtained for *P. aeruginosa* S1 68 and *E. faecalis* S1 using culture-based analysis, respectively (**Fig. 4.2A**). For *P. aeruginosa* S1 68, average plate counts of 1.45×10^4 CFU/mL (3.36 log reduction) and 5 CFU/mL (6.82 log reduction) were recorded when the dual-species biofilm was treated with 6.25 and 12.5 mg/mL of the P1 crude extract, respectively, while *P. aeruginosa* S1 68 plate counts were reduced to BDL (< 1 CFU/mL) at a concentration of 25 and 50 mg/mL of the P1 crude extract (**Fig. 4.2A**). A similar trend was observed for the *E. faecalis* S1 plate counts, with a significant log reduction of 5.04 (average of 5.67×10^1 CFU/mL) recorded when the dual-species biofilm was treated with 6.25 mg/mL of the P1 crude extract, with *E. faecalis* S1 plate counts reduced to BDL (< 1 CFU/mL) at a concentration of 12.5, 25 and 50 mg/mL of the P1 crude extract (**Fig. 4.2A**).

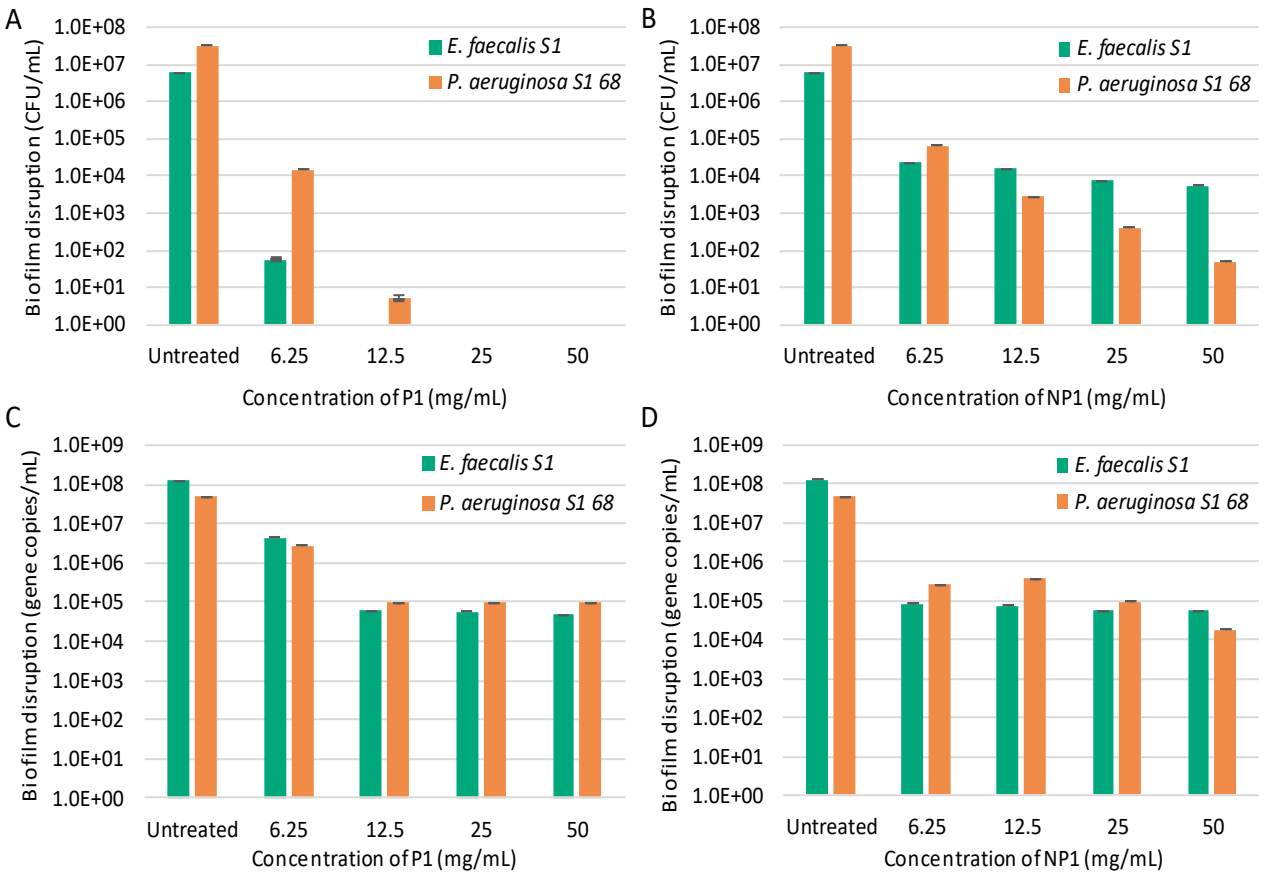

Fig. 4.2 The disruption of preformed dual-species biofilms (biofilm disruption activity) of *E. faecalis* S1 (green) and *P. aeruginosa* S1 68 (orange) treated with varying concentrations (6.25 to 50 mg/mL) of (**A**) P1 and (**B**) NP1 crude extracts determined using standard plate count methods (CFU/mL), and (**C**) P1 and (**D**) NP1 determined using EMA-qPCR (gene copies/mL) analysis.

For the untreated dual-species biofilm samples, an average of 4.86×10^7 gene copies/mL and 1.26×10^8 gene copies/mL was obtained for *P. aeruginosa* S1 68 and *E. faecalis* S1 using EMA-qPCR analysis, respectively (**Fig. 4.2C**). For *P. aeruginosa* S1 68, a reduction of 1.25 logs was obtained when the dual-species biofilm was treated with 6.25 mg/mL of the P1 crude extract, with an average of 2.72×10^6 gene copies/mL recorded. Similar reductions ranging between 2.70 and 2.71 logs were then observed for *P. aeruginosa* S1 68 when the dual-species biofilm was treated with 12.5, 25 and 50 mg/mL of the P1 crude extract, with 9.67×10^4 gene copies/mL, 9.79×10^4 gene copies/mL and 9.54×10^4 gene copies/mL recorded, respectively (**Fig. 4.2C**). A similar trend was observed for *E. faecalis* S1, as a reduction of 1.46 logs (average of 4.38×10^6 gene copies/mL) was obtained when the dual-species biofilm was treated with 6.25 mg/mL of the P1 crude extract. Similar log reductions ranging from 3.33 to 3.43 logs were then observed for *E. faecalis* S1 when the dual-species biofilm was treated with 12.5, 25 and 50 mg/mL of the P1 crude extract, with 5.88×10^4 gene copies/mL, 5.53×10^4 gene copies/mL and 4.64×10^4 gene copies/mL recorded, respectively (**Fig. 4.2C**).

The results of the plate counts and EMA-qPCR analysis of the untreated (control) and NP1 crude extract treated *P. aeruginosa* S1 68 and *E. faecalis* S1 biofilms (dual-species) are illustrated in **Fig. 4.2B** and **D**. For the untreated dual-species biofilm sample, an average of 3.33×10^7 CFU/mL and 6.17×10^6 CFU/mL was obtained for *P. aeruginosa* S1 68 and *E. faecalis* S1 using culture-based analysis, respectively (**Fig. 4.2B**). For *P. aeruginosa* S1 68, a reduction of 2.70 logs was obtained when the dual-species biofilm was treated with 6.25 mg/mL of the NP1 crude extract, with an average of 6.58×10^4 CFU/mL recorded. Significant reductions of 4.08, 4.91 and 5.82 logs were then obtained for *P. aeruginosa* S1 68 when the dual-species biofilm was treated with 12.5, 25 and 50 mg/mL of the NP1 crude extract, with average plate counts of 2.75×10^3 CFU/mL, 4.08×10^2 CFU/mL and 5.00×10^1 CFU/mL recorded, respectively (**Fig. 4.2B**). For *E. faecalis* S1, reductions of 2.42 and 2.58 logs were then observed when the dual-species biofilm was treated with 6.25 and 12.5 mg/mL of the NP1 crude extract, with average plate counts of 2.33×10^4 CFU/mL and 1.63×10^4 CFU/mL recorded, respectively (**Fig. 4.2B**). A significant reduction of 2.90 logs (7.75×10^3 CFU/mL) was obtained for *E. faecalis* S1 when the dual-species biofilm was treated with 25 mg/mL of the NP1 crude extract, with the *E. faecalis* S1 plate counts reduced to 5.42×10^3 CFU/mL (3.06 log reduction) at 50 mg/mL (**Fig. 4.2B**).

The results of the EMA-qPCR analysis of the untreated (control) and NP1 crude extract treated *P. aeruginosa* S1 68 and *E. faecalis* S1 biofilms (dual-species) are illustrated in **Fig. 4.2D**. For the untreated dual-species biofilm samples, an average of 4.86×10^7 gene copies/mL and 1.26×10^8 gene copies/mL was obtained for *P. aeruginosa* S1 68 and *E. faecalis* S1 using EMA-qPCR analysis, respectively (**Fig. 4.2D**). For *P. aeruginosa* S1 68, similar reductions of between 2.11 and 2.71 logs were then observed when the dual-species biofilm was treated with 6.25, 12.5 and 25 mg/mL of the NP1 crude extract, with average gene copies of 2.58×10^5 gene copies/mL, 3.76×10^5 gene copies/mL and 9.37×10^4 gene copies/mL recorded, respectively (**Fig. 4.2D**). A significant reduction of 3.42 logs was observed for *P. aeruginosa* S1 68 when the dual-species biofilm was treated with 50 mg/mL of the NP1 crude extract, with 1.76×10^4 gene copies/mL recorded (**Fig. 4.2D**). Significant reductions ranging between 3.17 and 3.36 logs were then observed for *E. faecalis* S1 biofilms when the dual-species biofilm was treated with 6.25, 12.5, 25 and 50 mg/mL of NP1 crude extract, with average gene copy numbers of 8.49×10^4 gene copies/mL, 7.58×10^4 gene copies/mL, 5.63×10^4 gene copies/mL and 5.51×10^4 gene copies/mL recorded, respectively (**Fig. 4.2D**).

4.3.2. Antiadhesive Activity (MBEC Assay®)

Standard culture-based and EMA-qPCR analysis was also used to evaluate the potential of the P1 and NP1 crude extracts to reduce the adhesion of a mono- and co-culture suspension of

P. aeruginosa and *E. faecalis* (extract concentration range of 6.25 to 50 mg/mL) to the pre-coated surface of the pegs of the MBEC Assay®.

4.3.2.1. Mono-culture Antiadhesive Experiments

Following exposure to the uncoated pegs of the MBEC Assay® (control) and the pegs coated with the P1 and NP1 crude extracts, the *P. aeruginosa* S1 68 cells that were capable of adhering to the surface of the pegs (biofilm suspension) were enumerated using plate counts and EMA-qPCR analysis as presented in **Fig. 4.3A** and **C**, respectively. For the uncoated pegs, an average of 1.49 × 10^5 CFU/mL of *P. aeruginosa* S1 68 was enumerated in the biofilm suspension using culture-based analysis (**Fig. 4.3A**). Similar inhibition percentages ranging from 87.9% to 89.0% were observed for the pegs pre-coated with 6.25, 12.5 and 25 mg/mL of the P1 crude extract, with *P. aeruginosa* S1 68 plate counts of 1.80 × 10^4 CFU/mL (6.25 and 12.5 mg/mL) and 1.63 × 10^4 CFU/mL enumerated in the biofilm suspensions, respectively. A significant inhibition of 94.4% was then observed for the pegs pre-coated with 50 mg/mL of the P1 crude extract, with an average *P. aeruginosa* S1 68 plate count of 8.33 × 10^3 CFU/mL recorded (**Fig. 4.3A**). Pre-coating the pegs with 6.25 mg/mL of NP1 crude extract resulted in an 81.7% inhibition of *P. aeruginosa* S1 68 cells adhering to the coated surface, with an average of 2.73 × 10^4 CFU/mL enumerated in the biofilm suspension (**Fig. 4.3A**). Similar inhibition percentages ranging from 90.6% to 93.1% were then observed for pegs pre-coated with 12.5, 25 and 50 mg/mL of the NP1 crude extract, with average *P. aeruginosa* S1 68 plate counts of 1.38 × 10^4 CFU/mL, 1.40 × 10^4 CFU/mL and 1.03 × 10^4 CFU/mL enumerated in the biofilm suspensions, respectively (**Fig. 4.3A**).

For the uncoated pegs, an average of 3.39 × 10^5 gene copies/mL of *P. aeruginosa* S1 68 was enumerated in the biofilm suspension using EMA-qPCR analysis (**Fig. 4.3C**). Pre-coating the pegs with 6.25 mg/mL of P1 crude extract resulted in a 41.6% inhibition of *P. aeruginosa* S1 68 cells adhering to the coated surface, with an average of 1.98 × 10^5 CFU/mL enumerated in the biofilm suspension (**Fig. 4.3C**). Similar inhibition percentages of 80.4% and 78.5% were then observed for pegs pre-coated with 12.5 and 25 mg/mL of the P1 crude extract, with 6.64 × 10^4 gene copies/mL and 7.30 × 10^4 gene copies/mL enumerated in the *P. aeruginosa* S1 68 biofilm suspension, respectively. An 89.5% inhibition (3.57 × 10^4 gene copies/mL) of adhesion of *P. aeruginosa* S1 68 cells was then observed at 50 mg/mL (**Fig. 4.3C**). Pre-coating the pegs with 6.25 mg/mL of NP1 crude extract resulted in the highest recorded inhibition of *P. aeruginosa* S1 68 cells adhering to the coated surface, with an average of 4.83 × 10^3 gene copies/mL (98.9%) enumerated in the biofilm suspension (**Fig. 4.3A**). However, for pegs pre-coated with 12.5, 25 and 50 mg/mL of the NP1 crude extract, inhibition percentages of 80.5%, 80.4% and 85.4% were observed, with *P. aeruginosa* S1 68 gene copy numbers of 6.62 × 10^4 gene copies/mL, 6.64 × 10^4 gene copies/mL and 4.96 × 10^4 gene copies/mL enumerated in the biofilm suspensions, respectively (**Fig. 4.3C**).

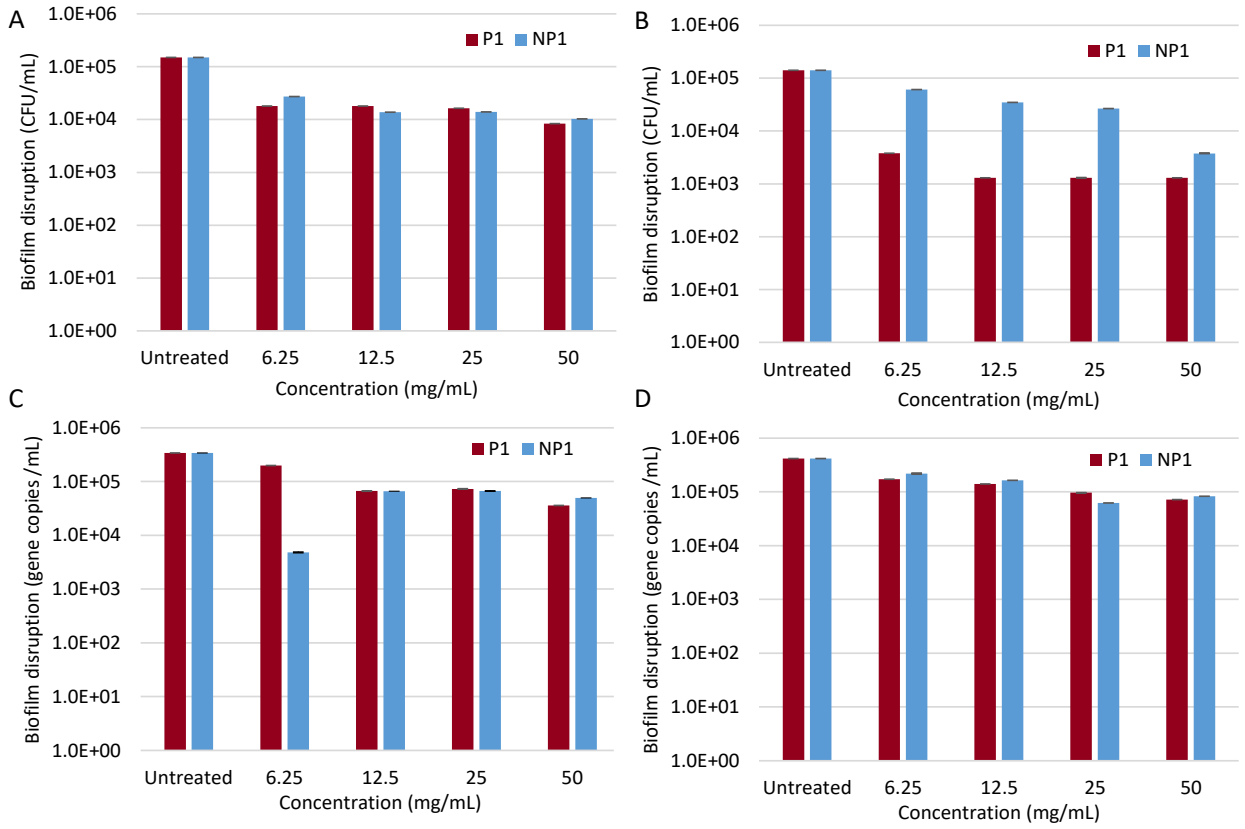

Fig. 4.3 The adherence of mono-culture bacterial test strains (antiadhesive activity) to surface of the pegs of the MBEC Assay® lid with and without an absorbed P1 (red) or NP1 (blue) crude extract layer (6.25 to 50 mg/mL) against (**A**) *P. aeruginosa* S1 68 and (**B**) *E. faecalis* S1 determined using standard plate count methods, and (**C**) *P. aeruginosa* S1 68 and (**D**) *E. faecalis* S1 determined using EMA-qPCR.

Following exposure to the uncoated pegs of the MBEC Assay® (control) and the pegs coated with the P1 and NP1 crude extracts, the *E. faecalis* S1 cells that were capable of adhering to the surface of the pegs (biofilm suspension) were enumerated using plate counts and EMA-qPCR analysis, as presented in **Fig. 4.3B and D**, respectively. For the uncoated pegs, an average of 1.40×10^5 CFU/mL of *E. faecalis* S1 was enumerated in the biofilm suspension using culture-based analysis. Pre-coating the pegs with 6.25 mg/mL of P1 crude extract resulted in a 97.3% inhibition of *E. faecalis* S1 cells adhering to the coated surface, with an average of 3.80×10^3 CFU/mL enumerated in the biofilm suspension (**Fig. 4.3B**). Identical inhibition percentages were then observed for pegs pre-coated with 12.5, 25 and 50 mg/mL of the P1 crude extract, with *E. faecalis* S1 plate counts of 1.30×10^3 CFU/mL (99.1% inhibition) enumerated in the biofilm suspensions at all three concentrations (**Fig. 4.3B**). However, pre-coating the pegs with 6.25, 12.5, 25 and 50 mg/mL of the NP1 crude extract resulted in a systematic decrease in the adhesion of *E. faecalis* S1 cells to the coated surface, with average plate counts of 6.07×10^4 CFU/mL (56.7% inhibition),

3.47 × 10^4 CFU/mL (75.2% inhibition), 2.67 × 10^4 CFU/mL (81.0% inhibition) and 3.75 × 10^3 CFU/mL (97.3% inhibition) enumerated in the biofilm suspension, respectively (**Fig. 4.3B**).

For the uncoated pegs, an average of 4.15 × 10^5 gene copies/mL of *E. faecalis* S1 was enumerated in the biofilm suspension using EMA-qPCR analysis (**Fig. 4.3D**). Pre-coating the pegs with 6.25, 12.5, 25 and 50 mg/mL of the P1 crude extract resulted in a gradual decrease in the adhesion of *E. faecalis* S1 cells to the coated surface, with average gene copy numbers of 1.72 × 10^5 gene copies/mL (58.6% inhibition), 1.40 × 10^5 gene copies/mL (66.2% inhibition), 9.64 × 10^4 (76.8% inhibition) and 7.18 × 10^4 gene copies/mL (82.7% inhibition) enumerated in the biofilm suspension, respectively (**Fig. 4.3D**). For the pegs pre-coated with 6.25, 12.5 and 25 mg/mL of the NP1 crude extract, a gradual decrease of *E. faecalis* S1 cells adhering to the coated surface was also recorded, with an average of 2.18 × 10^5 gene copies/mL (47.3% inhibition), 1.63 × 10^5 gene copies/mL (60.7% inhibition), 6.23 × 10^4 gene copies/mL (85.0% inhibition) enumerated in the biofilm suspension, respectively (**Fig. 4.3D**). Pre-coating the pegs with 50 mg/mL of NP1 crude extract resulted in an 80.0% inhibition of *E. faecalis* S1 cells adhering to the coated surface, with an average of 8.28 × 10^4 gene copies/mL enumerated in the biofilm suspension (**Fig. 4.3D**).

4.3.2.2. Co-culture Antiadhesive Experiments

Following exposure to the uncoated pegs of the MBEC Assay® (control) and the pegs coated with the P1 crude extract, the *P. aeruginosa* S1 68 and *E. faecalis* S1 cells (co-culture) that were capable of adhering to the surface of the pegs (biofilm suspension) were enumerated using plate counts and EMA-qPCR analysis, as presented in **Fig 4.4A** and **C**, respectively. For the uncoated pegs, an average of 1.95 × 10^4 CFU/mL and 4.58 × 10^4 CFU/mL was enumerated for *P. aeruginosa* S1 68 and *E. faecalis* S1, respectively, in the biofilm suspension using culture-based analysis (**Fig. 4.4A**). For *P. aeruginosa* S1 68, low percentage inhibitions ranging between 29.9 and 48.7% were observed for the pegs pre-coated with 6.25, 12.5, 25 and 50 mg/mL of the P1 crude extract, with average *P. aeruginosa* S1 68 plate counts of 1.30 × 10^4 CFU/mL, 1.37 × 10^4 CFU/mL, 1.00 × 10^4 CFU/mL and 1.05 × 10^4 CFU/mL enumerated in the dual-species biofilm suspension, respectively (**Fig. 4.4A**). In contrast, pre-coating the pegs with 6.25 mg/mL of the P1 crude extract resulted in an 80.4% inhibition of *E. faecalis* S1 cells to the coated surface, with an average of 9.00 × 10^3 CFU/mL enumerated in the biofilm suspension. Similar inhibition percentages ranging from 96.4 to 97.5% were then observed for pegs pre-coated with 12.5, 25 and 50 mg/mL of the P1 crude extract, with average *E. faecalis* S1 plate counts of 1.67 × 10^3 CFU/mL, 1.17 × 10^3 CFU/mL and 1.63 × 10^3 CFU/mL enumerated in the dual-species biofilm suspensions, respectively (**Fig. 4.4A**).

For the uncoated pegs, averages of 9.29 × 10^5 gene copies/mL and 1.22 × 10^7 gene copies/mL were recorded for *P. aeruginosa* S1 68 and *E. faecalis* S1, respectively, in the biofilm suspension

using EMA-qPCR analysis (**Fig. 4.4C**). Pre-coating the pegs with 6.25 and 12.5 mg/mL of the P1 crude extract resulted in a 72.6% and 54.4% inhibition of *P. aeruginosa* S1 68 cells to the coated surface, with average gene copy numbers of 2.54 × 10^5 gene copies/mL and 4.23 × 10^5 copies/mL enumerated in the biofilm suspensions, respectively (**Fig. 4.4C**). An identical inhibition percentage of 71.1% was then observed for pegs pre-coated with 25 and 50 mg/mL of the P1 crude extract, with *P. aeruginosa* S1 68 gene copy numbers of 2.68 × 10^5 CFU/mL and 2.69 × 10^5 CFU/mL enumerated in the dual-species biofilm suspensions, respectively (**Fig. 4.4C**). Pre-coating the pegs with 6.25, 12.5, 25 and 50 mg/mL of the P1 crude extract resulted in fluctuating inhibition percentages ranging from 88.2% to 94.9%, with average *E. faecalis* S1 gene copy numbers of 6.14 × 10^5 gene copies/mL, 1.44 × 10^6 gene copies/mL, 9.63 × 10^5 gene copies/mL and 1.22 × 10^6 gene copies/mL enumerated in the biofilm suspensions, respectively (**Fig. 4.4C**).

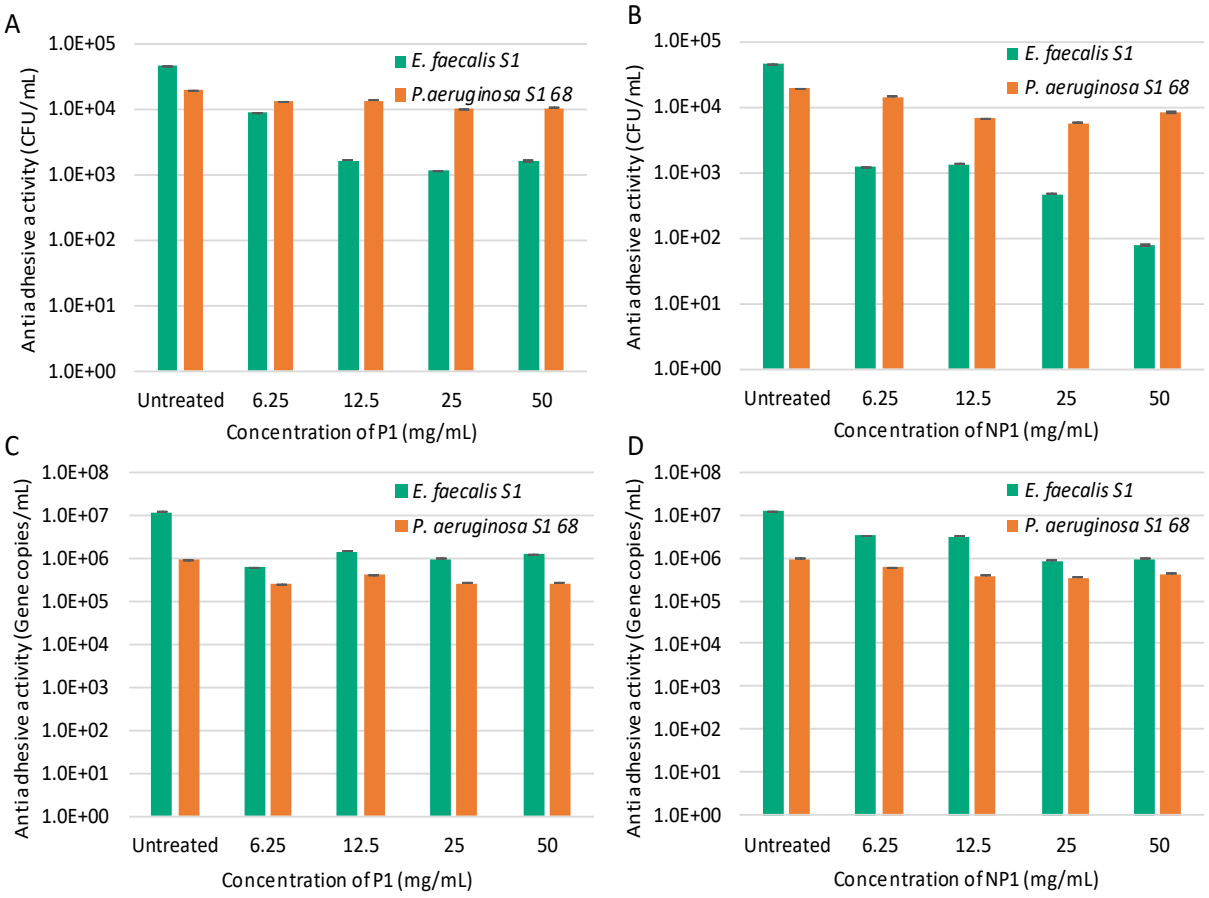

Fig. 4.4 The adherence of a co-culture cell suspension (antiadhesive activity) of *E. faecalis* S1 (green) and *P. aeruginosa* S1 68 (orange) to pegs of the MBEC Assay® lid treated with varying concentrations (6.25 to 50 mg/mL) of (**A**) P1 or (**B**) NP1 crude extracts determined using standard plate count methods (CFU/mL), and (**C**) P1 and (**D**) NP1 determined using EMA-qPCR (gene copies/mL) analysis.

Following exposure to the uncoated pegs of the MBEC Assay® (control) and the pegs coated with the NP1 crude extract, the *P. aeruginosa* S1 68 and *E. faecalis* S1 cells (co-culture) that were capable of adhering to the surface of the pegs (biofilm suspension) were enumerated using plate counts and EMA-qPCR analysis, as presented in **Fig 4.4B** and **D**, respectively. For the uncoated pegs, an average of 1.95×10^4 CFU/mL and 4.58×10^4 CFU/mL was enumerated for *P. aeruginosa* S1 68 and *E. faecalis* S1, respectively, in the biofilm suspension using culture-based analysis (**Fig. 4.4B**). Pre-coating the pegs with 6.25, 12.5 and 25 mg/mL of the NP1 crude extract resulted in a gradual decrease of *P. aeruginosa* S1 68 cells adhering to the coated surface, with an average of 1.43×10^4 CFU/mL (26.5% inhibition), 6.67×10^3 CFU/mL (65.8% inhibition), 5.67×10^3 CFU/mL (70.9% inhibition) enumerated in the dual-species biofilm suspension, respectively (**Fig. 4.4B**). However, pre-coating the pegs with 50 mg/mL of NP1 crude extract resulted in a 57.3% inhibition of *P. aeruginosa* S1 68 cells adhering to the coated surface, with an average of 8.33×10^3 CFU/mL enumerated in the dual-species biofilm suspension (**Fig. 4.4B**). In contrast, pre-coating the pegs with 6.25 and 12.5 mg/mL of the NP1 crude extract resulted in similar inhibition percentages of 97.3% and 97.1% of *E. faecalis* S1 cells adhering to the coated surface, with an average of 1.23×10^3 CFU/mL and 1.33×10^3 CFU/mL enumerated in the dual-species biofilm suspension, respectively (**Fig. 4.4B**). Significant inhibition percentages of 99.0% and 99.8% were then observed for pegs pre-coated with 25 and 50 mg/mL of the NP1 crude extract, with *E. faecalis* S1 plate counts of 4.67×10^2 CFU/mL and 7.67×10^1 CFU/mL enumerated in the dual-species biofilm suspensions, respectively (**Fig. 4.4B**).

For the uncoated pegs, averages of 9.29×10^5 gene copies/mL and 1.22×10^7 gene copies/mL were enumerated for *P. aeruginosa* S1 68 and *E. faecalis* S1, respectively, in the biofilm suspension using EMA-qPCR analysis (**Fig. 4.4D**). Pre-coating the pegs with 6.25, 12.5 and 25 mg/mL of the NP1 crude extract resulted in a systematic decrease of *P. aeruginosa* S1 68 cells adhering to the coated surface, with an average of 6.00×10^5 gene copies/mL (35.4 % inhibition), 3.83×10^5 gene copies/mL (58.8% inhibition), 3.51×10^5 gene copies/mL (62.2% inhibition) enumerated in the dual-species biofilm suspension, respectively (**Fig. 4.4D**). However, pre-coating the pegs with 50 mg/mL of NP1 crude extract resulted in a 55.1% inhibition of *P. aeruginosa* S1 68 cells adhering to the coated surface, with an average of 4.17×10^5 gene copies/mL enumerated in the dual-species biofilm suspension (**Fig. 4.4D**). Pre-coating the pegs with 6.25 and 12.5 mg/mL of the NP1 crude extract then resulted in similar inhibition percentages of 73.3% and 74.0% of *E. faecalis* S1 cells adhering to the coated surface, with an average of 3.24×10^6 gene copies/mL and 3.16×10^6 gene copies/mL enumerated in the biofilm suspension, respectively (**Fig. 4.4D**). Significant inhibition percentages of 93.0% and 92.3% were then observed for pegs pre-coated with 25 and 50 mg/mL of the NP1 crude extract, with *E. faecalis* S1 gene copy numbers of 8.46×10^5 gene copies/mL and 9.41×10^5 gene copies/mL enumerated in the biofilm suspensions, respectively (**Fig. 4.4D**).

4.3.3. Coating of Polymers with P1 and NP1 Crude Extracts

4.3.3.1. Water Contact Angle Measurements

The change in surface hydrophobicity can be determined using water contact angle measurements. A change in the contact angle of water on a surface following each step of the surface modification thus indicates the change in hydrophobicity of the polymer after modification. The water contact angles of the untreated (not coated), APTES treated and crude extract immobilised polymers are summarised in **Table 4.2**.

Water contact angles of 85.8° ± 1.6 and 86.4° ± 3.5 were recorded for the uncoated HDPE and PVC, respectively. This provides an indication that the uncoated polymer materials (HDPE and PVC) have a hydrophobic surface. After silanization with APTES, the water contact angle decreased to 43.9° ± 9.0 (HDPE) and 47.4° ± 1.3 (PVC) (**Table 4.2**). The silanization of the surfaces with APTES indicates a more hydrophilic surface (change in wettability) on both HDPE and PVC.

A significant reduction in the water contact angle of the P1 crude extract immobilised surfaces from 43.9° ± 9.0 (APTES treated) to 19.3° ± 3.9 (HDPE) and 47.4° ± 1.3 (APTES treated) to 28.8° ± 3.7 (PVC) was then observed (**Table 4.2**). Similarly, a significant decrease in the water contact angle was observed following the immobilisation of the NP1 crude extract to the APTES-coated surface, i.e. from 43.9° ± 9.0 to 22.2° ± 3.6 (HDPE) and 47.4° ± 1.3 to 25.1° ± 1.5 (PVC). Therefore, both HDPE and PVC became less hydrophobic following the immobilisation of serratamolide and glucosamine derivative homologues present in the P1 and NP1 crude extracts.

Table 4.2 Water contact angle measurements for various uncoated and crude extract immobilised surfaces of HDPE and PVC.

Sample name	Water contact angle (°)	
	HDPE	PVC
Uncoated	85.8 ± 1.6	86.4 ± 3.5
APTES	43.9 ± 9.0	47.4 ± 1.3
P1	19.3 ± 3.9	28.8 ± 3.7
NP1	22.2 ± 3.6	25.1 ± 1.5

4.3.3.2. Attenuated Total Reflectance Fourier Transform Infrared (ATR-FTIR) Spectroscopy

Prior to covalent immobilisation, the compounds in the P1 and NP1 crude extracts were modified (as indicated in section 4.2.6.1), and ATR-FTIR spectroscopy was used to confirm the successful modification of the extracts (results not shown). In order to confirm the successful immobilisation of

serratamolides and glucosamine derivatives to the polymers, ATR-FTIR spectroscopy was utilised to detect the functional groups present on the surface of the untreated (not coated), APTES coated and crude extract coated polymers. The untreated HDPE and PVC will be discussed first, followed by the APTES treated polymers and P1 and NP1 crude extract immobilised polymers.

The ATR-FTIR spectra obtained for the untreated and APTES treated materials of HDPE and PVC are indicated in **Fig. 4.5A** and **B**. Two distinct absorbance peaks were observed between 2 950 and 2 850 cm^{-1} for the untreated HDPE, signifying the presence of both –CH stretching and -CH_2- groups (**Fig. 4.5A**). In addition, a C-H bending band of –CH_2 groups is observed at 1 470–1 460 cm^{-1}, while a rocking vibration of CH_2 is observed at 730–700 cm^{-1} for untreated HDPE. The untreated PVC had similar characteristic absorbance peak of the polymer backbone due to –CH_2 groups. The peaks between 2 950 cm^{-1} - 2 850 cm^{-1} signifying –CH bond stretching in –CH_2 groups, 2 911 cm^{-1} and 2 822 cm^{-1} were assigned to –CH_2 asymmetric stretching (**Fig. 4.5B**). The bands at 1 426 cm^{-1} on the untreated PVC spectra are due to CH_2–Cl bending vibration mode, while the peak observed at approximately 1 340 cm^{-1} on the untreated PVC spectra was assigned to –CH_2 and CH_3 groups deformation. In addition, the peak observed at 1 251 cm^{-1} on the untreated PVC spectra corresponded to the Cl–CH rocking mode, while the peaks at 970 cm^{-1} and 612 cm^{-1} are attributed to bond C–Cl trans and cis wagging mode, respectively.

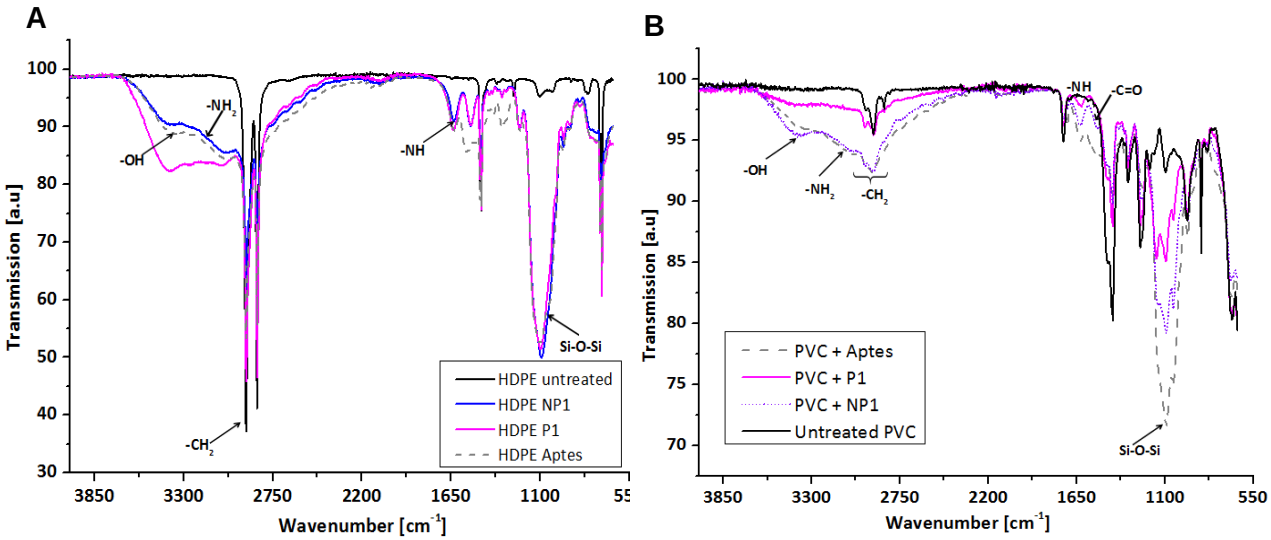

Fig. 4.5 ATR-FTIR spectra of the (**A**) untreated HDPE, APTES treated, and P1 and NP1 crude extract coated HDPE spectra and the (**B**) untreated PVC, APTES treated, and P1 and NP1 crude extract coated PVC.

Following the silanization of APTES to the surface of the piranha treated HDPE and PVC (**Fig. 4.5A** and **B**), a distinct absorbance peak was observed within the spectral region of 3 200–2 900 cm^{-1} due the terminal primary amine (-NH_2). The broader peak in the range 3 300–3 800 cm^{-1} is due to -

OH in silica APTES. For both HDPE and PVC, the 1 660 cm^{-1} peak was assigned to the -NH of the primary amine groups. Furthermore, a major absorbance peak was observed for the APTES treated HDPE and PVC samples between 1 160–1 050 cm^{-1}, which is caused by stretching mode of the Si-O-Si functional group. The detection of the functional groups (NH_2, CH_2 and Si-O-Si) on the surface of the material provides an indication that the APTES is covalently attached to the oxidised (-OH groups obtained during the piranha treatment) surface of the HDPE and PVC (**Fig. 4.5A** and **B**).

Following the coating of the HDPE with the NP1 crude extract, the ATR-FTIR spectra had a broad peak observed between 3 700–2 800 cm^{-1}, while the spectra for the P1 crude extract coated HDPE remained relatively the same as the ATPES treated HDPE. The absorbance peak of approximately 3 370 cm^{-1} was an indication of the hydroxyl group (-OH) stretching detected in both P1 and NP1 treated HDPE spectra (**Fig. 4.5A**). A broad peak was also observed at 1 650 cm^{-1} in the P1 and NP1 treated HDPE spectra, which corresponds to the stretching of the amine group (-NH). In addition, the absorption peak at approximately 1 545 cm^{-1} was an indication of the -C=O group of the ester stretch observed on the P1 and NP1 treated HDPE spectra (**Fig. 4.5A**). The hydroxyl, amine and carbonyl groups detected in the P1 and NP1 treated HDPE spectra corresponded to functional groups of the serratamolide and glucosamine derivatives homologues. No major changes were observed for the peaks at 1 160–1 050 cm^{-1} (caused by stretching mode of -Si-O-Si) for P1 and NP1 coated HDPE indicating successful immobilisation of the crude extracts on the APTES (**Fig. 4.5A**).

For the immobilisation of serratamolides and glucosamine derivatives in the P1 and NP1 crude extracts onto PVC, the ATR-FTIR spectra revealed a broad absorbance peak between 3 700–2 800 cm^{-1}. The absorbance peak of approximately 3 370 cm^{-1} was an indication of the hydroxyl group (-OH) stretching detected in both P1 and NP1 treated PVC spectra (**Fig. 4.5B**). In addition, an absorption peak was observed at 1 650 cm^{-1} indicating the stretching of the amine group (-NH) in both of the P1 and NP1 treated PVC spectra. An absorbance peak at approximately 1 545 cm^{-1} also served as an indication of the -C=O group of the ester stretch observed on the P1 and NP1 treated PVC spectra. The hydroxyl, amine and carbonyl groups detected in the P1 and NP1 spectra corresponded to functional groups of the serratamolide and glucosamine derivatives homologues. The characteristic peak observed at 1 160–1 050 cm^{-1} (caused by stretching mode of Si-O-Si) for HDPE and PVC, indicates the stability of APTES and its retention upon further surface immobilisation (**Fig. 4.5B**).

4.3.3.3. Scanning Electron Microscope (SEM) Coupled to Backscattered Electron Imaging-Energy Dispersive X-ray Spectroscopy (BSE-EDX)

Scanning electron microscopy (SEM) coupled to backscattered electron imaging-energy dispersive X-ray spectroscopy (BSE-EDX) was used to evaluate the surface morphology and the elemental composition changes between the uncoated and crude extract immobilised HDPE and PVC. The SEM micrographs obtained for the uncoated and coated materials are illustrated in **Fig. 4.6**. A relatively smooth and uniform morphology was observed for the untreated HDPE sample (**Fig. 4.6A**) and the APTES treated HDPE (**Fig. 4.6B**). A rougher surface topology was then observed for the P1 and NP1 coated HDPE samples, suggesting that the HDPE surface had been exposed to surface modification (**Fig. 4.6C** and **D**). A uniform rough surface was observed for the untreated PVC samples (**Fig. 4.6E**) and APTES treated (**Fig. 4.6F**) samples. Immobilisation of these samples with P1 and NP1 crude extracts resulted in an appearance of a rougher PVC surface morphology in comparison to the uncoated and APTES coated PVC surfaces. This suggests that the PVC surface had been successfully modified (**Fig. 4.6G** and **H**).

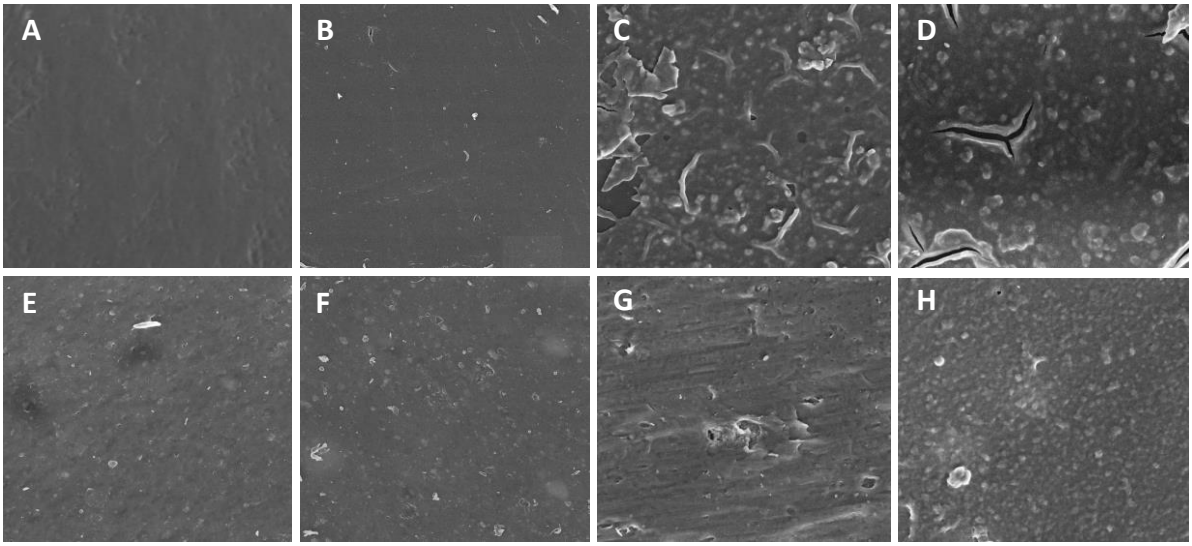

Fig. 4.6 Scanning electron microscope micrographs (10 000 × magnification) of the (**A**) uncoated HDPE and the HDPE treated with (**B**) APTES, (**C**) P1 crude extract and (**D**) NP1 crude extract as well as the (**E**) uncoated PVC and the PVC treated with (**F**) APTES, (**G**) P1 crude extract and (**H**) NP1 crude extract.

The results obtained from the BSE-EDX analysis for the uncoated and coated materials are presented in **Table 4.3**. Although various elements were detected on the uncoated and coated materials, carbon (C), oxygen (O), silica (Si) and nitrogen (N) were the main focus as they are present in APTES, serratamolide homologues and glucosamine derivative homologues. It was found that C (97.9%) and O (2%) were present on the surface of the uncoated HDPE. After

silanization, Si (0.01%) was detected on the surface of the APTES silanized HDPE. A decrease in O to 0.7% (1.3 decrease) was observed in comparison to the uncoated control, which not only indicates the reduction of surface OH, but also surface modification with APTES. The detection of Si further confirms the attachment of APTES onto the piranha treated (-OH) HDPE. A significant decrease in the element weight percentage of the C was then observed on the P1 and NP1 immobilised HDPE surfaces, from 97.9% (uncoated HDPE) to 85.3% (12.6% decrease on the P1 immobilised surface) and 74.7% (23.2% decrease on the NP1 immobilised surface), respectively (**Table 4.3**).

In comparison, an increase in the element weight percentage of O was observed, from 2.0% (uncoated HDPE) to 13.7% (11.7% increase on the P1 immobilised surface) and 23.1% (21.1% increase on the NP1 immobilised surface), respectively. This is attributed to C=O bond in the amide linkage of the extracts. In addition, an increase in the element weight percentage of Si from 0% (uncoated HDPE) to 0.6% and 1.5% on the P1 and NP1 immobilised HDPE, respectively, was observed (**Table 4.3**). However, N was not detected in any of the HDPE samples tested. This could possibly be due to the lower abundance of N relative to the other elements. The overall change in the elemental weight percentage of C, O and Si on the surface of HDPE provided an indication that the compounds within the P1 and NP1 extracts were chemically immobilised.

Table 4.3 Backscattered Electron Imaging-energy Dispersive X-ray Spectroscopy analysis of the elemental composition of uncoated and crude extract coated HDPE and PVC.

Element	HDPE (% composition)				PVC (% composition)			
	Before Coating	APTES	P1	NP1	Before Coating	APTES	P1	NP1
Carbon	97.9	97.9	85.3	74.7	62.1	65.5	51.9	48.0
Calcium	0.04	0	0	0	1.2	1.0	1.3	1.2
Chlorine	0.1	0.08	0.1	0	29.6	27.2	35.1	33.3
Nitrogen	0	0	0	0	0.7	0.8	0.9	0
Oxygen	2.0	0.7	13.7	23.1	5.3	4.4	8.7	15.4
Sulphur	0	0	0.3	0.8	0	0	0.6	0.4
Silica	0	0.01	0.6	1.5	0.1	0.1	0.4	0.6
Titanium	0	0	0	0	1.0	1.0	1.3	1.1

The BSE-EDX analysis indicated that C (62.1%), O (5.3%), N (0.7%) and Si (0.1%) were present on the surface of uncoated PVC. Following silanization of PVC with APTES, an increase in the elemental weight percentage of C to 65.5% (3.4% increase) and N to 0.8% (0.1% increase) was observed, while Si remained the same and O decreased to 4.4% (0.9% decrease) in comparison to the uncoated control. The increased C and detection of Si provided an indication that APTES had

covalently attached to the -OH groups of the piranha treated PVC, as these elements are present within the APTES structure. A decrease in the element weight percentage of the C was then observed, from 62.1% (uncoated PVC) to 51.9% (10.2% decrease) on the P1 immobilised surface and 48.0% (14.1% decrease) on the NP1 immobilised surface (**Table 4.3**). As previously stipulated with HPDE surfaces, an increase in the element weight percentage of O was observed, from 5.3% (uncoated PVC) to 8.7% (3.4% increase) on the P1 immobilised surface and 15.4% (10.1% increase) on the NP1 immobilised surface. In addition, an increase in the element weight percentage of Si was observed, from 0.1% (uncoated PVC) to 0.4% (0.3% increase) and 0.6% (0.5% increase) on the P1 and NP1 immobilised PVC, respectively (**Table 4.3**). Following immobilisation with NP1 to the PVC surface however, a decrease in the element weight percentage of N from 0.7% to 0% was observed, while an increase in the element weight percentage of N from 0.7% (uncoated PVC) to 0.9% on the P1 immobilised PVC was observed. The overall change in the elemental weight percentage of C, O and Si on the surface of PVC provided additional evidence of covalent attachment of the compounds within the P1 and NP1 extracts.

4.3.4. Stability of the Compounds Immobilised onto the Polymers

The stability of the immobilised compounds in the P1 and NP1 crude extracts on the surface materials (PVC and HDPE) was analysed by placing the coated material into Milli-Q water for 24 h. The suspension collected after exposure was freeze-dried and UPLC-ESI-MS analysis was conducted on the recovered freeze-dried samples as described by Clements et al. (2019b; chapter two). The UPLC-ESI-MS analysis revealed that no compounds were detected in the freeze-dried samples obtained after 24 h of incubation for all crude extracts (P1 and NP1) coated materials. This provided an indication that no leaching of compounds occurred and the compounds on HDPE and PVC were thus stable for a minimum of 24 h in Milli-Q water at ambient temperature.

4.3.5. Antifouling Activity of Crude Extract-immobilised Polymers

Standard culture-based methods and EMA-qPCR analysis were used to evaluate the potential of the compounds (P1 and NP1 crude extracts) immobilised onto HDPE and PVC to prevent biofilm formation by *E. faecalis* S1 and *P. aeruginosa* S1 68 (**Fig. 4.7**). The qPCR efficiency and linear regression coefficient (R^2) values for all of the MBEC Assays® were within the recommended range and are indicated in **Appendix C Table C1**.

For the uncoated HDPE, an average of 1.46×10^6 CFU/mL *E. faecalis* S1 cells was enumerated in the biofilm suspension (obtained after sonication) using culture-based analysis (**Fig. 4.7A**). For the P1 and NP1 crude extracts immobilised onto HDPE, culture-based analysis of the *E. faecalis* S1 cells in the biofilm suspension indicated that 1.86×10^4 (98.7% inhibition) and 5.20×10^4 (96.4%

inhibition) CFU/mL were recorded, respectively. Similarly, EMA-qPCR indicated that *E. faecalis* S1 was detected at 1.25×10^6 gene copies/mL in the biofilm suspension obtained from the uncoated HDPE (**Fig. 4.7C**). For the P1 and NP1 crude extracts immobilised onto HDPE, EMA-qPCR analysis of the *E. faecalis* S1 cells in the biofilm suspension indicated that 1.59×10^5 (87.2% inhibition) and 1.12×10^5 (91.0% inhibition) gene copies/mL were recorded, respectively.

The ability of the P1 and NP1 crude extract coated onto PVC to prevent adhesion of *E. faecalis* S1 is presented in **Fig. 4.7B** and **D**. For the uncoated PVC, an average of 1.79×10^5 CFU/mL *E. faecalis* S1 cells was enumerated in the biofilm suspension (obtained after sonication) using culture-based analysis (**Fig. 4.7B**). For the P1 and NP1 crude extracts immobilised onto PVC, culture-based analysis of the *E. faecalis* S1 cells in the biofilm suspension indicated that 4.88×10^4 (72.7% inhibition) and 4.15×10^4 (76.8% inhibition) CFU/mL were recorded, respectively. For the uncoated PVC, an average of 1.54×10^5 gene copies/mL was enumerated in the biofilm suspension using EMA-qPCR analysis (**Fig. 4.7D**). For the P1 and NP1 crude extracts immobilised onto PVC, EMA-qPCR analysis of the *E. faecalis* S1 cells in the biofilm suspension then indicated that 1.13×10^5 (26.6% inhibition) and 1.41×10^5 (8.8% inhibition) gene copies/mL were recorded, respectively.

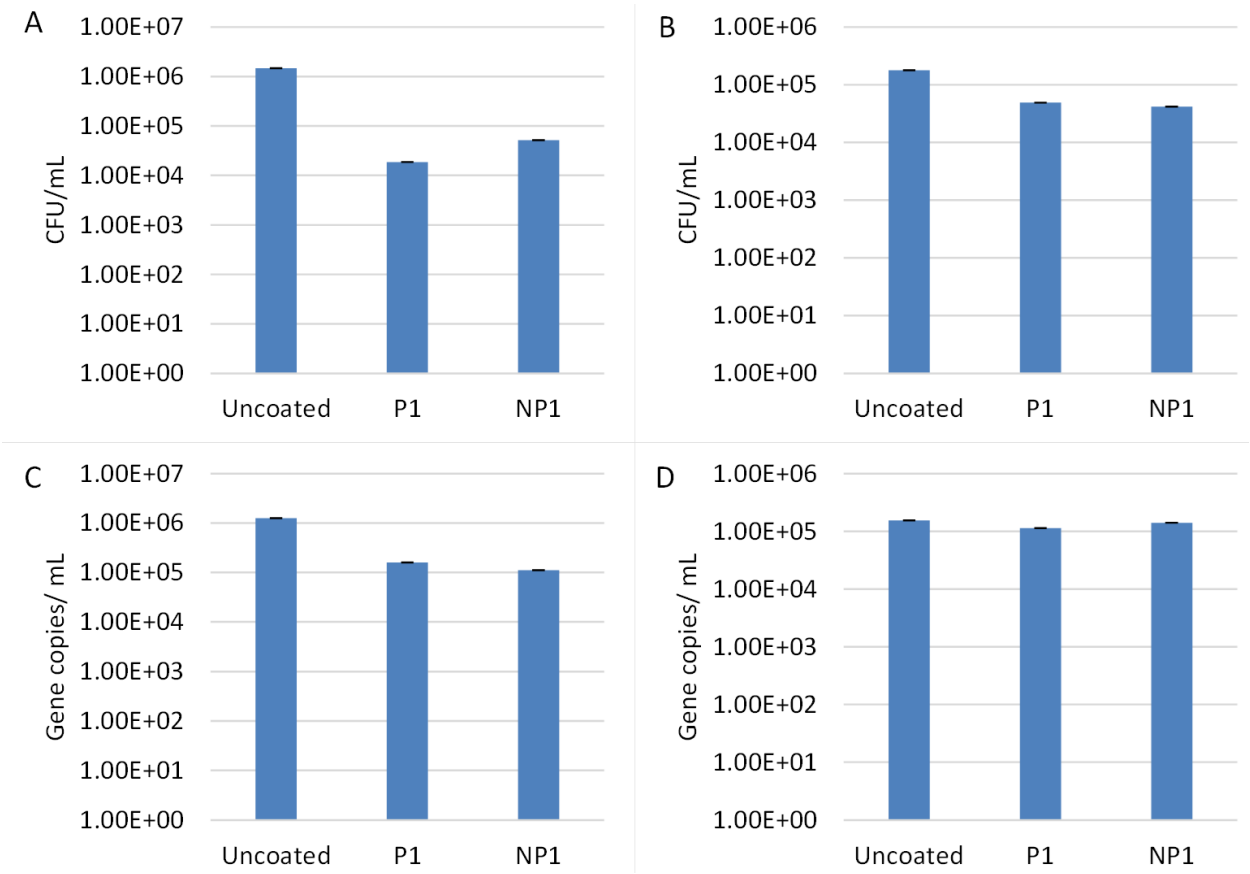

Fig. 4.7 Colony forming units and gene copies/mL of the *E. faecalis* S1 that were attached to uncoated and crude extract (P1 and NP1) immobilised materials analysed using plate counts [culture-based analysis; (**A**) HDPE and (**B**) PVC] and EMA-qPCR analysis [(**C**) HDPE and (**D**) PVC].

Additionally, the ability of the P1 and NP1 crude extracts immobilised onto HDPE and PVC to prevent *E. faecalis* S1 biofilm formation was visualised using the LIVE/DEAD cell viability assay coupled to CLSM (**Fig. 4.8**). The LIVE/DEAD viability assay provides discrimination between viable and non-viable cells, as SYTO-9 is able to stain live cells green, while propidium iodide is able to stain dead or membrane compromised cells red. After 20 h of exposure, *E. faecalis* S1 cells were able to colonise and form a biofilm on the uncoated HDPE and PVC surfaces (**Fig. 4.8A** and **D**). A reduction in viable biofilm cells was then observed on the surface of the HDPE and PVC immobilised with P1 (**Fig. 4.8B** and **E**) and NP1 (**Fig. 4.8C** and **F**), while an increase in the number of dead cells was also apparent on all coated materials.

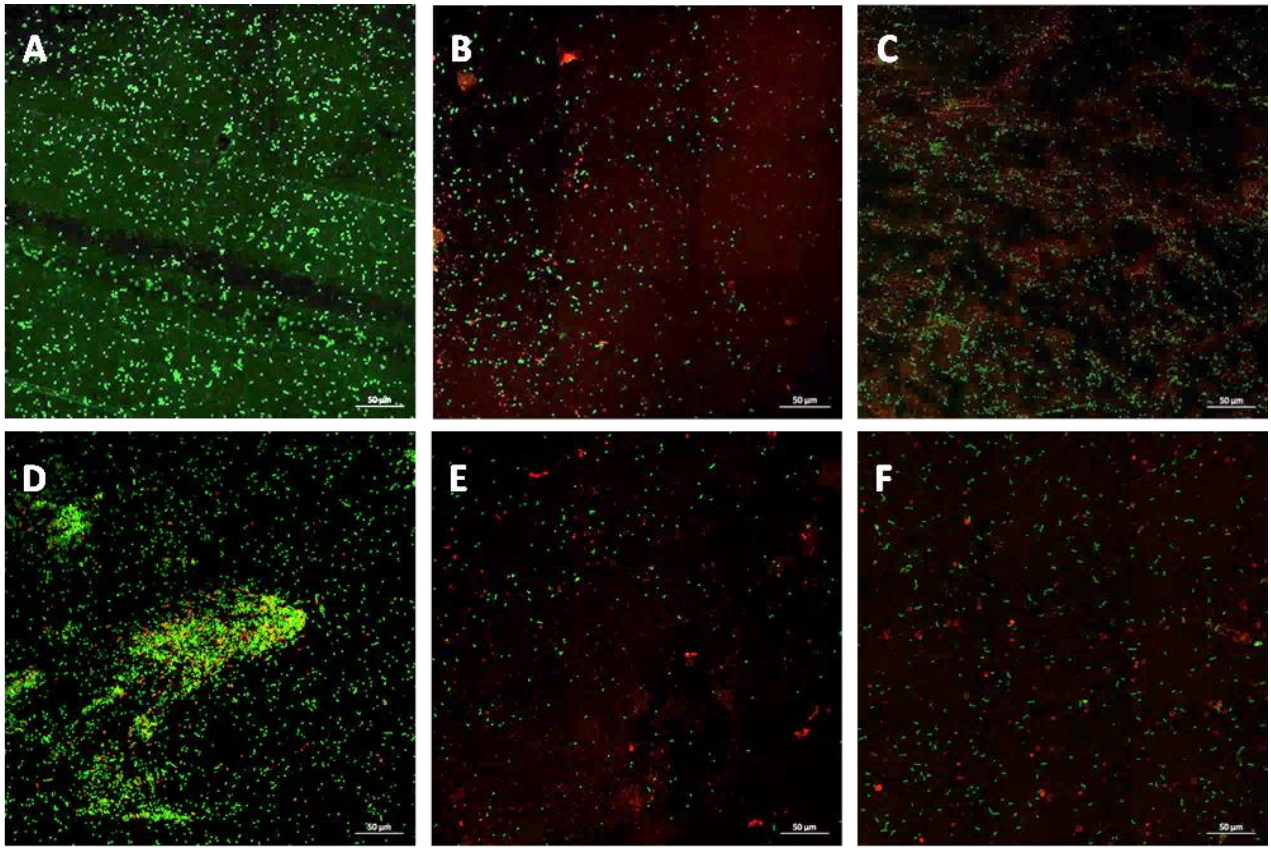

Fig. 4.8 Representative CLSM images (measured at a magnification of 50 µm) of live (green) and dead (red) *E. faecalis* S1 cells adhering onto uncoated (**A**) HDPE and (**D**) PVC; HDPE immobilised with (**B**) P1 and (**C**) NP1 crude extracts; and PVC immobilised with (**E**) P1 and (**F**) NP1 crude extracts.

Standard culture-based methods and EMA-qPCR analysis were also used to evaluate the antifouling properties of the P1 and NP1 crude extracts immobilised onto HDPE and PVC against *P. aeruginosa* S1 68 (**Fig. 4.9**). For the uncoated HDPE, an average of 3.86×10^7 CFU/mL *P. aeruginosa* S1 68 cells was enumerated in the biofilm suspension (obtained after sonication) using culture-based analysis (**Fig. 4.9A**). For the P1 and NP1 crude extracts immobilised onto

HDPE, culture-based analysis of the *P. aeruginosa* S1 68 cells in the biofilm suspension indicated that 4.90 × 10^6 (87.3% inhibition) and 4.78 × 10^6 (87.6% inhibition) CFU/mL were recorded, respectively. The EMA-qPCR analysis then indicated that *P. aeruginosa* S1 68 was detected at 1.01 × 10^6 gene copies/mL in the biofilm suspension (obtained after sonication) from the uncoated HDPE (**Fig. 4.9C**). For the P1 and NP1 crude extracts immobilised onto HDPE, EMA-qPCR analysis of the *P. aeruginosa* S1 68 cells in the biofilm suspension indicated that 2.83 × 10^5 (72.1% inhibition) and 3.62 × 10^5 (64.3% inhibition) gene copies/mL were recorded, respectively.

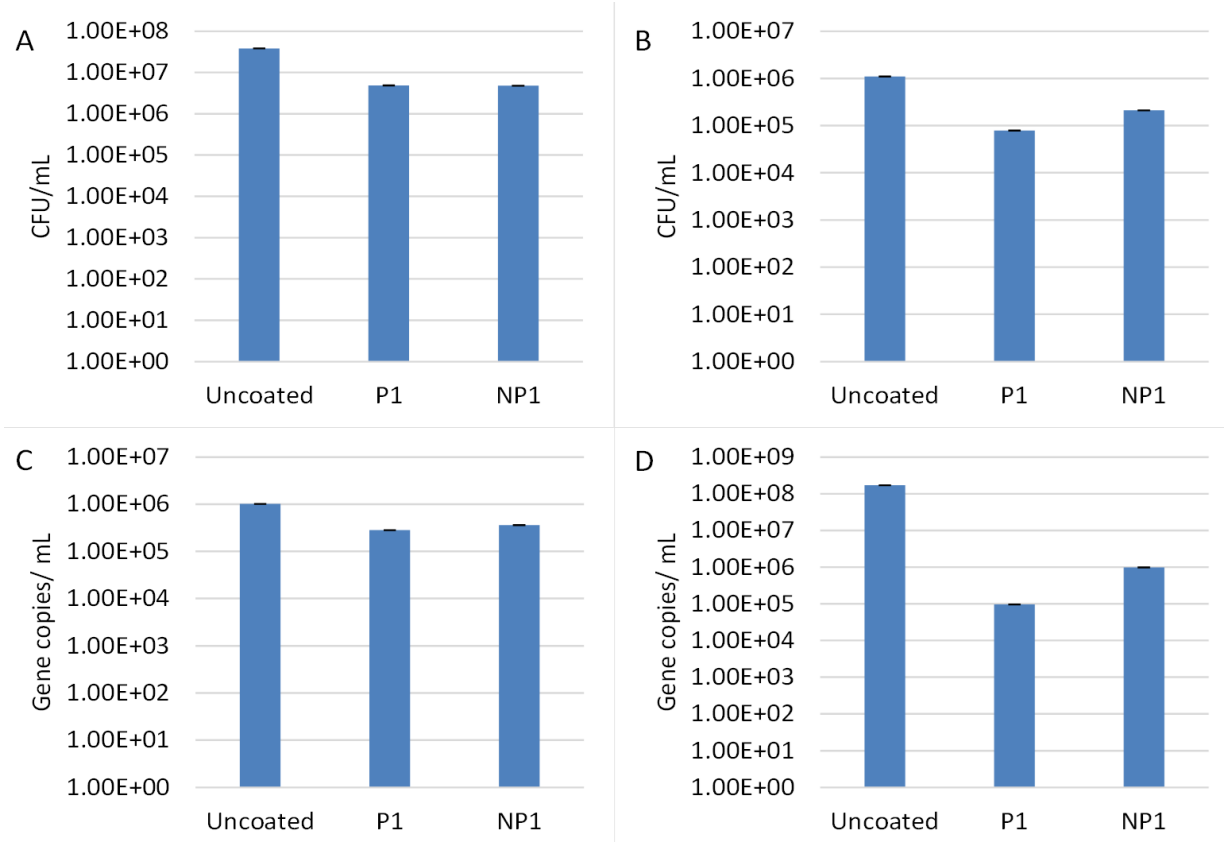

Fig. 4.9 Colony forming units and gene copies/mL of the *P. aeruginosa* S1 68 that were attached to uncoated and crude extract (P1 and NP1) immobilised materials analysed using analysed using plate counts [culture-based analysis; (**A**) HDPE and (**B**) PVC] and EMA-qPCR analysis [(**C**) HDPE and (**D**) PVC].

For the uncoated PVC, an average of 1.09 × 10^6 CFU/mL *P. aeruginosa* S1 68 cells was enumerated in the biofilm suspension using culture-based analysis (**Fig. 4.9B**). For the P1 and NP1 crude extracts immobilised onto PVC, culture-based analysis of the *P. aeruginosa* S1 68 cells in the biofilm suspension indicated that 7.88 × 10^4 (92.8% inhibition) and 2.09 × 10^5 (80.9% inhibition) CFU/mL were recorded, respectively. For the uncoated PVC, an average of 1.71 × 10^8 gene copies/mL was then enumerated in the biofilm suspension using EMA-qPCR analysis (**Fig. 4.9D**). For the P1 and NP1 crude extracts immobilised onto PVC, EMA-qPCR analysis of the

P. aeruginosa S1 68 cells in the biofilm suspension indicated that 9.59×10^4 (99.9% inhibition) and 9.84×10^5 (99.4% inhibition) gene copies/mL were recorded, respectively.

The ability of P1 and NP1 crude extracts immobilised onto PVC and HDPE to prevent *P. aeruginosa* S1 68 biofilm formation was also visualised using the LIVE/DEAD staining assay coupled to CLSM (**Fig. 4.10**). After 20 h of exposure, *P. aeruginosa* S1 68 cells were able to colonise and form a biofilm on the uncoated PVC and HDPE surface (**Fig. 4.10A** and **D**). A reduction in viable biofilm cells was then observed on the surface of the PVC and HDPE immobilised with P1 (**Fig. 4.10B** and **E**) and NP1 (**Fig. 4.10C** and **F**), while an increase in number of dead cells was also apparent, particularly for the PVC immobilised with P1.

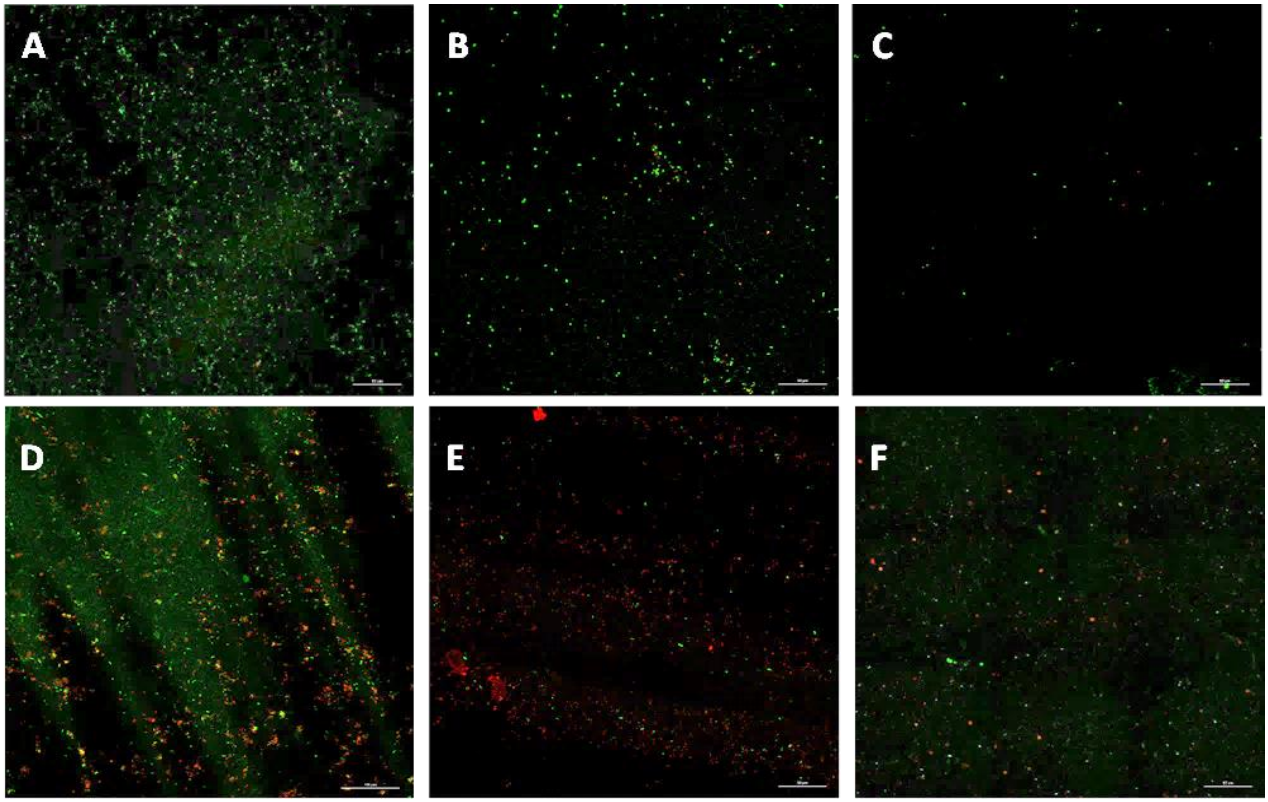

Fig. 4.10 Representative CLSM images (measured at a magnification of 50 µm) of live (green) and dead (red) *P. aeruginosa* S1 68 cells adhering onto uncoated (**A**) HDPE and (**D**) PVC; HDPE immobilised with (**B**) P1 and (**C**) NP1 crude extracts; and PVC immobilised with (**E**) P1 and (**F**) NP1 crude extracts.

4.4. Discussion

As outlined in chapter three, the *S. marcescens* pigmented P1 and non-pigmented NP1 strains produce various secondary metabolites, including serratamolide (serrawettin W1) homologues and glucosamine derivative homologues, while *S. marcescens* P1 also produces prodigiosin. Clements et al. (2019b; chapter two) also demonstrated that the crude extracts from both strains (P1 and

NP1) displayed significant antimicrobial activity against a wide range of Gram-negative and Gram-positive bacteria, including *P. aeruginosa* S1 68 and *E. faecalis* S1. While separating and purifying the individual compounds in the crude extracts is an informative means of determining the antimicrobial and antifouling activity of each compound, the use of the entire complex of secondary metabolites may be a more cost-effective approach for application in various industries (Quinn et al. 2012). The antifouling potential of the complex of secondary metabolites produced by the *S. marcescens* P1 and NP1 strains were thus investigated in the current study.

The susceptibility of preformed single- and dual-species biofilms of *P. aeruginosa* S1 68 and *E. faecalis* S1 to the complex of secondary metabolites detected in the P1 and NP1 crude extracts was firstly investigated using the MBEC Assay®. This assay is advantageous as it provides information on the minimum biofilm eradication concentrations of single-, dual- or mixed- species biofilms, allows for testing of various antimicrobial concentrations in a high-throughput manner, is able to investigate both biofilm disruption and antiadhesive activities of antimicrobial agents and can be combined with culture-based or molecular quantification techniques such as EMA-qPCR, to quantity viable microbial cells within single- or mixed-species biofilms after antimicrobial treatment. The results for the biofilm disruption analysis using the MBEC Assay® then indicated that based on plate counts and gene copies, the minimum concentration of the P1 crude extract required to reduce a single-species *P. aeruginosa* S1 68 biofilm by ≥ 2 logs (equivalent to a ≥ 99% reduction) was 6.25 mg/mL, while a concentration of 1.25 mg/mL was required to reduce a single-species *E. faecalis* S1 biofilm by ≥ 2 logs. Similarly, the plate count and EMA-qPCR analysis indicated that 1.25 mg/mL of the NP1 crude extract was required to disrupt a preformed single-species *E. faecalis* S1 biofilm by ≥ 2 logs. In comparison, based on plate counts, 25 mg/mL of the NP1 crude extract was required to reduce a preformed single-species *P. aeruginosa* S1 68 biofilm by ≥ 2 logs, with only a 1.42 log reduction in *P. aeruginosa* S1 68 gene copies obtained at 25 mg/mL of the NP1 crude extract. Thus, while the single-species *E. faecalis* S1 biofilm was susceptible to both the P1 and NP1 crude extracts, the P1 crude extract was more effective at reducing single-species *P. aeruginosa* S1 68 biofilms. Moreover, a lower concentration of the P1 and NP1 crude extracts was required to disrupt the single-species *E. faecalis* S1 biofilm, suggesting that the serratamolide and glucosamine derivative homologues (and prodigiosin in the P1 crude extract) in both crude extracts were more effective at disrupting single-species *E. faecalis* S1 biofilms.

Further analysis indicated that the minimum concentration of the P1 crude extract required to reduce a dual-species biofilm of *P. aeruginosa* S1 68 and *E. faecalis* S1 by ≥ 2 logs (equivalent to a ≥ 99% reduction) was 6.25 mg/mL based on plate counts and 12.5 mg/mL based on gene copies. Moreover, based on the plate count analysis, the dual-species biofilm of *P. aeruginosa* S1 68 and *E. faecalis* S1 was completely eradicated after exposure to 25 mg/mL of the P1 crude extract. In comparison, 6.25 mg/mL of NP1 crude extract was required to reduce a dual-species biofilm of

P. aeruginosa S1 68 and *E. faecalis* S1 by ≥ 2 logs based on plate counts and gene copies. Interestingly, both the culture-based and molecular analysis indicated that an increase in the concentration of the P1 and NP1 crude extracts was required to reduce *E. faecalis* S1 by ≥ 99% in the dual-species biofilm (6.25 - 12.5 mg/mL), in comparison to the single-species *E. faecalis* S1 biofilm (1.25 mg/mL). This suggests that *E. faecalis* S1 was less susceptible to the P1 and NP1 crude extracts in a dual-species biofilm, while a similar trend in reduction of *P. aeruginosa* S1 68 in the dual-species biofilm and single-species biofilm was observed. Previous research has indicated that interspecies interactions within a biofilm, such as quorum-sensing, the chemical composition of EPS, adaptive stress responses (such as the transfer of antimicrobial resistance genes) and the spatial distribution of individual strains in the biofilm, may affect the susceptibility of a microorganism to an antimicrobial compound (Stewart 2002; Tait and Sutherland 2002; Kocot and Olszewska 2020). Although further research is required to determine the exact interactions observed between *P. aeruginosa* S1 68 and *E. faecalis* S1 strains, a few studies have similarly observed an increase in resistance of dual- or mixed-species biofilms compared to single-species biofilms (Lopes et al. 2012; Ibusquiza et al. 2012). For instance, Lopes et al. (2012) found that the MBEC of several antibiotics (including gentamicin, levoflozacin, chloramphenicol and rifampicin) were significantly higher for two emerging species, *Inquilinus limosus* and *Dolosigranulum pigrum*, when in a dual-species biofilm with *P. aeruginosa* in comparison to the single-species biofilms. In addition, Ibusquiza et al. (2012) found that *L. monocytogenes* was more resistant to benzalkonium chlorine when in the presence of *Pseudomonas putida,* thus suggesting that interactions between the two species affected their susceptibility. Results from this study thus correspond to previous findings and the observed increase in tolerance of *E. faecalis* S1 to P1 and NP1 crude extracts in a dual-species biofilm with *P. aeruginosa* S1 68 is hypothesised to be due to interspecies interactions.

While the exact mechanism involved in the disruption of biofilms by biosurfactants has not fully been elucidated, it has also been proposed that biosurfactants are able to enter the biofilm matrix through water channels and adhere to the surface of the material (Nitschke and Silva 2018). The adhesion of the biosurfactant to a surface reduces the interfacial tensions between the biofilm and the solid substratum and weakens the interactions between bacterial cells, which favours the dispersion of the biofilm. It has additionally been hypothesised that lipopeptides such as serrawettins, act as wetting agents, which solubilise the biofilms extracellular matrix (Nitschke and Silva 2018). Recently, Liu et al. (2019) investigated the ability of surfactin produced by *B. subtilis* to disrupt a preformed *S. aureus* biofilm on different types of materials and investigated the biofilm disruption mechanism of the *S. aureus* biofilm. The authors found that surfactin significantly removed the *S. aureus* biofilm from the surface of glass, polystyrene and stainless steel. Liu et al. (2019) further proposed that the reduced biofilm formation of the *S. aureus* strain was due to the ability of surfactin to effect polysaccharide production, decrease the percentage of alkali-soluble polysaccharide in

biofilms and influence quorum sensing. Thus, while this elucidates the mechanism of biofilm disruption by surfactin, extensive research is still required to investigate the mechanism of biofilm disruption by serratamolides. In addition to the lipopeptides, glucosamine derivative homologues present in the P1 and NP1 crude extracts, as well as the prodigiosin present in the P1 crude extract, have previously been found to display antimicrobial activity (Dwivedi et al. 2008; Clements et al. 2019b), and may have further contributed to the disruption and microbial inhibition of the cells in the single- and dual-species biofilms. A study by Kimyon et al. (2016) also investigated the biofilm disrupting properties of prodigiosin against a *P. aeruginosa* strain. The authors suggested that prodigiosin is able to disrupt preformed biofilms by undergoing oxidation and promoting double-stranded DNA cleavage of extracellular DNA (eDNA), as it is known that eDNA can integrate into the biofilm matrix and may increase the adhesion of bacterial strains to a surface, thus playing a pivotal role in maintaining the biofilm structure and adhesion.

Based on the EMA-qPCR analysis, it was however, interesting to note that in comparison to the culture-based results; the single- and dual-species *P. aeruginosa* S1 68 and *E. faecalis* S1 biofilms were not completely eradicated after treatment with the P1 crude extract at the highest concentration utilised. This was similarly observed for the single-species *E. faecalis* S1 treated with the NP1 crude extract. A major limitation of culture-based analysis is that this technique does not allow for the quantification of cells that have entered a viable but non-culturable state. The use of a nucleic acid-binding dye (such as EMA) coupled with qPCR allows for the differentiation between intact and dead cells, as these dyes penetrate cells with damaged membranes and covalently bind to DNA, preventing qPCR amplification. Thus, once the excess unbound dye has been removed, only the DNA extracted from viable cells is amplified and quantified by qPCR (Qin et al. 2012; Reyneke et al. 2016), which effectively provides a more accurate representation of the viable cells remaining in the biofilm after antimicrobial treatment using the MBEC Assay® (Innovotech).

In addition to biofilm disruption potential, the antiadhesive potential of P1 and NP1 crude extracts was evaluated using the MBEC Assay® against mono- and co-cultures of *E. faecalis* S1 and *P. aeruginosa* S1 68. The results then indicated that pre-coating the pegs of the assay with 50 mg/mL of the P1 crude extract reduced the adhesion of mono-culture *P. aeruginosa* S1 68 cells by 94.4% based on plate counts and 89.5% based on gene copies, while *E. faecalis* S1 cells were reduced by 99.1% based on plate counts and by 82.7% based on gene copies. Similarly, pre-coating the pegs of the assay with 50 mg/mL of the NP1 crude extract reduced the adhesion of mono-culture *P. aeruginosa* S1 68 cells by 93.1% based on plate counts and 85.4% based on gene copies, while *E. faecalis* S1 cells were reduced by 97.3% based on plate counts and by 80.0% based on gene copies. The culture-based and molecular analysis thus indicated that similar reductions in the adhesion of *P. aeruginosa* S1 68 and *E. faecalis* S1 were observed for pegs coated with 50 mg/mL of the P1 and NP1 crude extracts.

For the co-cultures, pre-coating the pegs of the MBEC Assay® with 50 mg/mL of the P1 crude extract reduced the adhesion of *E. faecalis* S1 cells by 96.4% and 89.9%, based on plate counts and gene copies, respectively, while 50 mg/mL of the NP1 crude extract reduced the adhesion of *E. faecalis* S1 cells by 99.8% based on plate counts and by 92.3% based on gene copies. However, for both P1 and NP1, a ≤ 80% reduction in adhesion was obtained for *P. aeruginosa* S1 68 at all concentrations analysed. Thus, a greater reduction in adhesion of the mono-culture *P. aeruginosa* S1 68 cells to the pre-coated P1 and NP1 pegs of the assay was observed in comparison to *P. aeruginosa* S1 68 in co-culture with *E. faecalis* S1 (based on plate counts and gene copies). These results suggest that *P. aeruginosa* S1 68 was more readily able to adhere to the pre-coated peg surface of the MBEC Assay® in the presence of *E. faecalis* S1. A similar phenomenon was observed in a study conducted by do Valle Gomes and Nitschke (2012), where the biosurfactants surfactin and rhamnolipids, were less effective at reducing the adhesion of mixed bacterial cultures when compared to the individual cultures of *S. aureus, L. monocytogenes* and *S.* Enteritidis. The authors hypothesised that the observed effect may be influenced by differing adhesion rates of each individual bacterial strain present in the mixed culture (do Valle Gomes and Nitschke 2012). In addition, the presence of one bacterial genus in a mixed culture may influence the microbial adhesion of another genus (do Valle Gomes and Nitschke 2012). This was corroborated by Rieu et al. (2008), who reported that *S. aureus* facilitated the colonisation of *L. monocytogenes* in a co-culture to stainless steel and revealed that peptide molecules within the cell-free supernatant obtained from *S. aureus* are involved in the stimulation of *L. monocytogenes* biofilm development. It is possible that in the current study, *E. faecalis* S1 may have produced a metabolite that can enhance *P. aeruginosa* S1 68 adhesion to the surface of the pre-coated peg of the MBEC Assay® during co-culture. This hypothesis will however, need to be confirmed.

In order to create a sustainable antimicrobial surface which could be applied in industry, polymeric surfaces with covalently bound antimicrobial agents that reduce microbial adhesion were designed. For this purpose, the serratamolide and glucosamine derivative homologues in the P1 and NP1 crude extracts were immobilised onto surfaces of HDPE and PVC. These two materials were selected as they are frequently utilised in the water, food and medical industries and are suitable for the first step of the material modification process (the addition of hydroxyl groups to the surface of each material via oxidation with the piranha solution). In order to create the biomaterials, the piranha treated HDPE and PVC surfaces were silanized with APTES, followed by the covalent immobilisation of the modified serratamolide and glucosamine derivative homologues. The use of APTES (an organic silane) is intended to act as an intermediate spacer between organic and inorganic constituents during the coating process and provides reactive amine groups that the modified antimicrobial secondary metabolites can covalently attach to. It should however, be noted that the prodigiosin in the P1 crude extract was not immobilised onto the surface of the materials

due to the absence of reactive functional groups within the structure that would covalently attach to the amine groups of the APTES compound. The surfaces of the coated and subsequent control materials were characterised using water contact angle measurements, ATR-FTIR analysis and SEM coupled with BSE-EDX analysis, which confirmed the successful immobilisation of the antimicrobial compounds onto the materials. Moreover, the serratamolide and glucosamine derivative homologues were found to be stable on the surface of HDPE and PVC, as no leaching of the secondary metabolites was observed after 24 h. After the immobilisation was confirmed, the coated and uncoated controls of HDPE and PVC were exposed to mono-cultures of *E. faecalis* S1 and *P. aeruginosa* S1 68 to test antifouling potential of the materials.

Significant reductions in the adhesion of *E. faecalis* S1 cells to the surface of the P1 (98.7% based on plate counts and 87.2% based on gene copies) and NP1 (96.4% based on plate counts and 91.0% based on gene copies) coated HDPE were observed. Comparatively, based on plate counts and gene copies, an 87.3% and 72.1% reduction, respectively, in the adhesion of *P. aeruginosa* S1 68 cells to the surface of the P1 coated HDPE was observed, while the NP1 coated HDPE resulted in reductions of 87.6% based on plate counts and 64.3% based on gene copies for *P. aeruginosa* S1 68. Significant reductions in the adhesion of *P. aeruginosa* S1 68 cells to the surface of the P1 coated PVC were also observed (92.8% based on plate counts and 99.9% based on gene copies), with the NP1 coated PVC resulting in reductions of 80.9% based on plate counts and 99.4% based on gene copies. In contrast, lower reductions in the adhesion of *E. faecalis* S1 cells to the surface of the P1 coated PVC were observed (72.7% based on plate counts and 26.6% based on gene copies), while the NP1 coated PVC resulted in reductions of 76.8% based on plate counts and 8.8% based on gene copies.

The P1 and NP1 coated HDPE were thus effective at reducing the adhesion of both Gram-positive (*P. aeruginosa* S1 68) and Gram-positive bacterial cells (*E. faecalis* S1), while the P1 and NP1 coated PVC were more effective at reducing the adhesion of Gram-negative bacterial cells (*P. aeruginosa* S1 68). The variation in the adhesion of the Gram-negative and Gram-positive bacterial cells to the different polymers may be attributed to a few features involved in the adhesion process, including the surface charge and hydrophobicity of a substratum and of the microbial cell, the surface roughness and texture of each material, the production of the extracellular matrix of each bacterial strain, the presence of fimbriae and flagella, and the proteins and components on the surface of the bacterial cell membrane (Zeraik and Nitschke 2010; Krasowska and Sigler 2014; Oh et al. 2018). Although various factors contribute to the adhesion of microbial cells onto a surface, hydrophobic polymers (such as HDPE and PVC) are potentially more conducive to microbial adhesion (Rodrigues et al. 2006; Rufino et al. 2011). This is due to the removal of interfacial water from between the interacting surfaces, which aids in the adhesion of microbial cells (Rodrigues et al. 2006; Rufino et al. 2011). Thus, coating a material with an agent that makes a surface more

hydrophilic would aid in reducing the adhesion of microbial cells. As previously mentioned, the water contact angle measurements provided a confirmation that the surfaces of coated HDPE and PVC surfaces were modified to become more hydrophilic. The reduction in surface hydrophobicity (change in surface wettability) observed for the coated materials in addition to the antimicrobial activity of the serratamolide and glucosamine derivative homologues, is thus hypothesised to assist with the observed reduction in microbial adhesion to the coated HDPE and PVC surfaces. Moreover, a number of chemical compounds can leach from plastic materials into their surrounding environment, which may affect microbial adhesion and colonisation. Previous research has found that PVC can release chlorinated and organotin compounds, while compounds such as phenols, ketones, aromatic hydrocarbons can be released from HDPE (Robine et al. 2000; Rożej et al. 2015). The release of these toxic compounds may thus have additionally contributed to the variation in adhesion of *P. aeruginosa* S1 68 and *E. faecalis* S1 onto the polymers (Robine et al. 2000).

4.5. Conclusions

The study demonstrated that the complex of secondary metabolites, comprised of serratamolide and glucosamine derivative homologues (and prodigiosin for the P1 crude extract), produced by *S. marcescens* P1 and NP1 strains displayed biofilm disrupting activity. However, the P1 crude extract was more effective at reducing single-species *P. aeruginosa* S1 68 biofilms, while the single-species *E. faecalis* S1 biofilm was equally susceptible to the P1 and NP1 crude extracts. Moreover, based on plate counts, the P1 crude extract eradicated the dual-species *P. aeruginosa* S1 68 and *E. faecalis* S1 biofilm, which was not observed with the NP1 crude extract. As the complex of secondary metabolites produced by the P1 strain displayed pronounced biofilm disrupting activity, it is recommended that this crude extract be applied as a biodetergent solution to reduce pre-existing biofilms on industrial surfaces. Moreover, this work demonstrated that the P1 and NP1 crude extracts, which were pre-adsorbed to the polypropylene surfaces of the MBEC Assay®, delayed the onset or adhesion of biofilm formation by *P. aeruginosa* S1 68 and *E. faecalis* S1. However, after exposure of the P1 and NP1 coated pegs to the co-culture of *P. aeruginosa* S1 68 and *E. faecalis* S1, significant reductions in the adhesion of *E. faecalis* S1 were observed, while a reduced antiadhesive efficiency was observed for *P. aeruginosa* S1 68 in co-culture with *E. faecalis* S1. It is thus recommended that future research investigate the interspecies interactions (production of metabolites, quorum sensing etc.) that may influence the co-adhesion and subsequent biofilm development of *E. faecalis* S1 and *P. aeruginosa* S1 68, as well as the adhesion rates of each individual bacterial strain.

This study then successfully developed non-leaching biomaterials by covalently immobilising serratamolide and glucosamine derivative homologues onto the surface of polymers (HDPE and PVC) commonly used in the food, medical and water industry. The P1 and NP1 coated HDPE were

effectively able to reduce the adhesion of mono-cultures of Gram-negative (*P. aeruginosa* S1 68) and Gram-positive (*E. faecalis* S1) bacterial cells, while the P1 and NP1 coated PVC were only effective at reducing the adhesion of Gram-negative (*P. aeruginosa* S1 68) bacterial cells with minor reductions in adhesion observed for *E. faecalis* S1. Based on these results, it is recommended that the antifouling potential of the P1 and NP1 coated HDPE against mixed microbial communities be investigated. The antimicrobial-based materials developed in this study could thus be utilised for a wide range of industrial applications, such as medical equipment and implant surfaces, food processing system surfaces and water storage and conveyance surfaces. Future research should thus investigate the efficacy of the serratamolide and glucosamine derivative homologues when immobilised onto various other materials, such as stainless steel, which are commonly used in these industries.

Acknowledgements

This work was supported by the Water Research Commission under (grant number K5/2728//3) and the National Research Foundation of South Africa (grant number: 113849). Opinions expressed and conclusions arrived at, are those of the authors and are not necessarily to be attributed to the National Research Foundation. The authors thank the Department of Chemistry and Polymer Science (Stellenbosch University) for the use of the KSV Cam 100 Goniometer and Thermo Scientific Nicolet iS10 ATR-FTIR spectrometer. The authors would also like to thank Dr Rehana Malgas-Enus for laboratory space and reagents. In addition, the authors would like to thank Nonjabulo Gule for financing the SEM and BSE-EDX analysis.

4.6. References

Abdallah, M., Benoliel, C., Drider, D., Dhulster, P., Chihib, N.E. 2014. Biofilm formation and persistence on abiotic surfaces in the context of food and medical environments. Arch Microbiol 196(7), 453–472. https://doi.org/10.1007/s00203-014-0983-1

Abdulkareem, E.H., Memarzadeh, K., Allaker, R.P., Huang, J., Pratten, J., Spratt, D. 2015. Anti-biofilm activity of zinc oxide and hydroxyapatite nanoparticles as dental implant coating materials. J Dent 43(12), 1462–1469. https://doi.org/10.1016/j.jdent.2015.10.010

Alves, D., Pereira, O.M. 2014. Mini-review: Antimicrobial peptides and enzymes as promising candidates to functionalize biomaterial surfaces. Biofouling 30(4), 483–499. https://doi.org/10.1080/08927014.2014.889120

Banat, I.M., De Rienzo, M.A.D., Quinn, G.A. 2014. Microbial biofilms: biosurfactants as antibiofilm agents. Appl Microbiol Biotechnol 98(24), 9915–9929. https://doi.org/10.1007/s00253-014-6169-6

Banerjee, I., Pangule, R.C., Kane, R.S. 2011. Antifouling coatings: recent developments in the design of surfaces that prevent fouling by proteins, bacteria, and marine organisms. Adv Mater 23(6), 690–718. https://doi.org/10.1002/adma.201001215

Bergmark, L., Poulsen, P.H.B., Abu Al-Soud, W., Norman, A., Hansen, L.H., Sørensen, S.J. 2012. Assessment of the specificity of *Burkholderia* and *Pseudomonas* qPCR assays for detection of these genera in soil using 454 pyrosequencing. FEMS Microbiol Let 333, 77–84. https://doi.org/10.1111/j.1574-6968.2012.02601.x

Clements, T., Ndlovu, T., Khan, S., Khan, W. 2019a. Biosurfactants produced by *Serratia* species: Classification, biosynthesis, production and application. Appl Microbiol Biotechnol 103, 589–602. https://doi.org/10.1007/s00253-018-9520-5.

Clements, T., Ndlovu, T., Khan, W. 2019b. Broad-spectrum antimicrobial activity of secondary metabolites produced by *Serratia marcescens* strains. Microbiol Res 229(126329), 1–10. https://doi.org/10.1016/j.micres.2019.126329

Clements, T., Reyneke, B., Strauss, A., Khan, W. 2019c. Persistence of Viable Bacteria in Solar Pasteurised Harvested Rainwater. Water Air Soil Poll 230(130), 1–13. https://doi.org/10.1007/s11270-019-4184-z

De Zoysa, G.H., Sarojini, V. 2017. Feasibility study exploring the potential of novel battacin lipopeptides as antimicrobial coatings. ACS Appl Mater Interfaces 9(2), 1373–1383. https://doi.org/10.1021/acsami.6b15859

Delgado-Viscogliosi, P., Solignac, L., Delattre, J.M. 2009. Viability PCR, a culture-independent method for rapid and selective quantification of viable *Legionella pneumophila* cells in environmental water samples. Appl Environ Microbiol 75, 3502–3512. https://doi.org/10.1128/AEM.02878-08

do Valle Gomes, M.Z., Nitschke, M. 2012. Evaluation of rhamnolipid and surfactin to reduce the adhesion and remove biofilms of individual and mixed cultures of food pathogenic bacteria. Food Control 25(2), 441–447. https://doi.org/10.1016/j.foodcont.2011.11.025

Dobrowsky, P.H., Khan, S., Cloete, T.E. Khan, W. 2016. Molecular detection of *Acanthamoeba* spp., *Naegleria fowleri* and *Vermamoeba* (*Hartmannella*) *vermiformis* as vectors for *Legionella* spp. in untreated and solar pasteurized harvested rainwater. Parasit Vectors 9, 539–552. https://doi.org/10.1186/s13071-016-1829-2

Donlan, R.M. 2002. Biofilms: microbial life on surfaces. Emerg Infect Dis 8(9), 881–890. https://doi.org/10.3201/eid0809.020063

Dusane, D.H., Dam, S., Nancharaiah, Y.V., Kumar, A.R., Venugopalan, V.P., Zinjarde, S.S. 2012. Disruption of *Yarrowia lipolytica* biofilms by rhamnolipid biosurfactant. Aquat Biosyst 8(17), 1–7. https://doi.org/10.1186/2046-9063-8-17

Dusane, D.H., Nancharaiah, Y.V., Zinjarde, S.S., Venugopalan, V.P. 2010. Rhamnolipid mediated disruption of marine *Bacillus pumilus* biofilms. Colloids Surf B Biointerfaces 81(1), 242–248. https://doi.org/10.1016/j.colsurfb.2010.07.013

Dusane, D.H., Pawar, V.S., Nancharaiah, Y.V., Venugopalan, V.P., Kumar, A.R., Zinjarde, S.S. 2011. Anti-biofilm potential of a glycolipid surfactant produced by a tropical marine strain of *Serratia marcescens*. Biofouling 27(6), 645–654. https://doi.org/10.1080/08927014.2011.594883

Dwivedi, D., Jansen, R., Molinari, G., Nimtz, M., Johri, B.N., Wray, V. 2008. Antimycobacterial serratamolides and diacyl peptoglucosamine derivatives from *Serratia* sp. J Nat Prod 71(4), 637–641. https://doi.org/10.1021/np7007126

Eckelmann, D., Spiteller, M., Kusari, S. 2018. Spatial-temporal profiling of prodiginines and serratamolides produced by endophytic *Serratia marcescens* harbored in *Maytenus serrata*. Sci Rep 8, 1–15. https://doi.org/10.1038/s41598-018-23538-5

Epstein, A.K., Pokroy, B., Seminara, A., Aizenberg, J. 2011. Bacterial biofilm shows persistent resistance to liquid wetting and gas penetration. Proc Natl Acad Sci U S A 108(3), 995–1000. https://doi.org/10.1073/pnas.1011033108

Frahm, E., Obst, U. 2003. Application of the fluorogenic probe technique (TaqMan PCR) to the detection of *Enterococcus* spp. and *Escherichia coli* in water samples. J Microbiol Meth 52, 123–131. https://doi.org/10.1016/S0167-7012(02)00150-1

Gudiña, E.J., Rocha, V., Teixeira, J.A., Rodrigues, L.R. 2010. Antimicrobial and antiadhesive properties of a biosurfactant isolated from *Lactobacillus paracasei* ssp. *paracasei* A20. Lett Appl Microbiol 50(4), 419–424. https://doi.org/10.1111/j.1472-765X.2010.02818.x

Ibusquiza, P.S., Herrera, J.J., Vázquez-Sánchez, D., Parada, A., Cabo, M.L. 2012. A new and efficient method to obtain benzalkonium chloride adapted cells of *Listeria monocytogenes*. J Microbiol Methods 91(1), 57–61. https://doi.org/10.1016/j.mimet.2012.07.009

Janek, T., Łukaszewicz, M., Krasowska, A. 2012. Antiadhesive activity of the biosurfactant pseudofactin II secreted by the Arctic bacterium *Pseudomonas fluorescens* BD5. BMC Microbiol 12(24), 1–9. https://doi.org/10.1186/1471-2180-12-24

Kadouri, D.E., Shanks, R.M. 2013. Identification of a methicillin-resistant *Staphylococcus aureus* inhibitory compound isolated from *Serratia marcescens*. Res Microbiol 164(8), 821–826. https://doi.org/10.1016/j.resmic.2013.06.002

Kimyon, Ö., Das, T., Ibugo, A.I., Kutty, S.K., Ho, K.K., Tebben, J., Kumar, N., Manefield, M. 2016. *Serratia* secondary metabolite prodigiosin inhibits *Pseudomonas aeruginosa* biofilm development by producing reactive oxygen species that damage biological molecules. Front Microbiol 7(972), 1–15. https://doi.org/10.3389/fmicb.2016.00972

Kiran, G.S., Sabarathnam, B., Selvin, J. 2010. Biofilm disruption potential of a glycolipid biosurfactant from marine *Brevibacterium casei*. FEMS Immunol Med Microbiol 59(3), 432–438. https://doi.org/10.1111/j.1574-695X.2010.00698.x

Kocot, A.M., Olszewska, M.A. 2020. Interaction of *Pseudomonas aeruginosa* and *Staphylococcus aureus* with *Listeria innocua* in dual species biofilms and inactivation following disinfectant treatments. LWT-Food Sci Technol 118(108736), 1–7. https://doi.org/10.1016/j.lwt.2019.108736

Krasowska, A., Sigler, K. 2014. How microorganisms use hydrophobicity and what does this mean for human needs? Front Cell Infect Microbiol 4, 112. https://doi.org/10.3389/fcimb.2014.00112

Lee, K., Lee, K.M., Kim, D., Yoon, S.S. 2017. Molecular determinants of the thickened matrix in a dual-species *Pseudomonas aeruginosa* and *Enterococcus faecalis* Biofilm. Appl Environ Microbiol 83(21), 1–15. https://doi.org/10.1128/AEM.01182-17

Liu, J., Li, W., Zhu, X., Zhao, H., Lu, Y., Zhang, C., Lu, Z. 2019. Surfactin effectively inhibits *Staphylococcus aureus* adhesion and biofilm formation on surfaces. Appl Microbiol Biotechnol 103(11), 4565–4574. https://doi.org/10.1007/s00253-019-09808-w

Lopes, S.P., Ceri, H., Azevedo, N.F., Pereira, M.O. 2012. Antibiotic resistance of mixed biofilms in cystic fibrosis: impact of emerging microorganisms on treatment of infection. Int J Antimicrob Agents 40(3), 260–263. https://doi.org/10.1016/j.ijantimicag.2012.04.020

Ludensky, M. 2003. Control and monitoring of biofilms in industrial applications. Int Biodeterior Biodegradation 51(4), 255–263. https://doi.org/10.1016/S0964-8305(03)00038-6

Matsuyama, T., Fujita, M., Yano, I. 1985. Wetting agent produced by *Serratia marcescens*. FEMS Microbiol Lett 28, 125–129. https://doi.org/10.1111/j.1574-6968.1985.tb00777.x

Meier, F., Lacroix, C., Meile, L., Jans, C. 2018. Enterococci and pseudomonads as quality indicators in industrial production and storage of mozzarella cheese from raw cow milk. Int Dairy J 82, 28–34. https://doi.org/10.1016/j.idairyj.2018.02.010

Meylheuc, T., Renault, M., Bellon-Fontaine, M.N. 2006. Adsorption of a biosurfactant on surfaces to enhance the disinfection of surfaces contaminated with *Listeria monocytogenes*. Int J Food Microbiol 109(1-2), 71–78. https://doi.org/10.1016/j.ijfoodmicro.2006.01.013

Meylheuc, T., Van Oss, C.J., Bellon-Fontaine, M.N. 2001. Adsorption of biosurfactant on solid surfaces and consequences regarding the bioadhesion of *Listeria monocytogenes* LO28. J Appl Microbiol 91(5), 822–832. https://doi.org/10.1046/j.1365-2672.2001.01455.x

Mohorčič, M., Jerman, I., Zorko, M., Butinar, L., Orel, B., Jerala, R., Friedrich, J. 2010. Surface with antimicrobial activity obtained through silane coating with covalently bound polymyxin B. J Mater Sci-Mater M 21(10), 2775–2782. https://doi.org/10.1007/s10856-010-4136-z

Motley, J.L., Stamps, B.W., Mitchell, C.A., Thompson, A.T., Cross, J., You, J., Powell, D.R., Stevenson, B.S., Cichewicz, R.H. 2016. Opportunistic sampling of roadkill as an entry point to accessing natural products assembled by bacteria associated with non-anthropoidal mammalian microbiomes. J Nat Prod 80, 598–608. https://doi.org/10.1021/acs.jnatprod.6b00772

Nitschke, M., Silva, S.S.E. 2018. Recent food applications of microbial surfactants. Crit Rev Food Sci Nutr 58(4), 631–638. https://doi.org/10.1080/10408398.2016.1208635

Oh, J.K., Yegin, Y., Yang, F., Zhang, M., Li, J., Huang, S., Verkhoturov, S.V., Schweikert, E.A., Perez-Lewis, K., Scholar, E.A., Taylor, T.M. 2018. The influence of surface chemistry on the kinetics and thermodynamics of bacterial adhesion. Sci Rep 8(1), 1–13. https://doi.org/10.1038/s41598-018-35343-1

Pirog, T.P., Konon, A.D., Beregovaya, K.A., Shulyakova, M.A. 2014. Antiadhesive properties of the surfactants of *Acinetobacter calcoaceticus* IMB B-7241, *Rhodococcus erythropolis* IMB Ac-5017, and *Nocardia vaccinii* IMB B-7405. Microbiol 83(6), 732–739. https://doi.org/10.1134/S0026261714060150

Pradel, E., Zhang, Y., Pujol, N., Matsuyama, T., Bargmann, C.I., Ewbank, J.J. 2007. Detection and avoidance of a natural product from the pathogenic bacterium *Serratia marcescens* by *Caenorhabditis elegans*. Proc Natl Acad Sci U S A 104(7), 2295–2300. https://doi.org/10.1073/pnas.0610281104

Qin, T., Tian, Z., Ren, H., Hu, G., Zhou, H., Lu, J., Luo, C., Liu, Z., Shao, Z. 2012. Application of EMA-qPCR as a complementary tool for the detection and monitoring of *Legionella* in different water systems. World J Microbiol Biotechnol 28(5), 1881–1890.

Quinn, G.A., Maloy, A.P., McClean, S., Carney, B., Slater, J.W. 2012. Lipopeptide biosurfactants from *Paenibacillus polymyxa* inhibit single and mixed species biofilms. Biofouling 28(10), 1151–1166. https://doi.org/10.1080/08927014.2012.738292

Reyneke, B., Dobrowsky, P.H., Ndlovu, T., Khan, S., Khan, W. 2016. EMA-qPCR to monitor the efficiency of a closed-coupled solar pasteurization system in reducing *Legionella* contamination of roof-harvested rainwater. Sci Total Environ 553, 662–670. https://doi.org/10.1016/j.scitotenv.2016.02.108

Rieu, A., Lemaître, J.P., Guzzo, J., Piveteau, P. 2008. Interactions in dual species biofilms between *Listeria monocytogenes* EGD-e and several strains of *Staphylococcus aureus*. Int J Food Microbiol 126(1-2), 76–82. https://doi.org/10.1016/j.ijfoodmicro.2008.05.006

Rivardo, F., Turner, R.J., Allegrone, G., Ceri, H., Martinotti, M.G. 2009. Anti-adhesion activity of two biosurfactants produced by *Bacillus* spp. prevents biofilm formation of human bacterial pathogens. Appl Microbiol Biotechnol 83(3), 541–553. https://doi.org/10.1007/s00253-009-1987-7

Rodrigues, L., Banat, I.M., Teixeira, J., Oliveira, R. 2006. Biosurfactants: potential applications in medicine. J Antimicrob Chemother 57(4), 609–618. https://doi.org/10.1093/jac/dkl024

Robine, E., Derangere, D., Robin, D. 2000. Survival of a *Pseudomonas fluorescens* and *Enterococcus faecalis* aerosol on inert surfaces. Int J Food Microbiol, 55(1-3), 229–234. https://doi.org/10.1016/S0168-1605(00)00188-4

Rożej, A., Cydzik-Kwiatkowska, A., Kowalska, B., Kowalski, D. 2015. Structure and microbial diversity of biofilms on different pipe materials of a model drinking water distribution systems. World J Microbiol Biotechnol, 31(1), 37–47. https://doi.org/10.1007/s11274-014-1761-6

Rufino, R.D., Luna, J.M., Sarubbo, L.A., Rodrigues, L.R., Teixeira, J.A., Campos-Takaki, G.M. 2011. Antimicrobial and anti-adhesive potential of a biosurfactant Rufisan produced by *Candida lipolytica* UCP 0988. Colloids Surf B Biointerfaces 84(1), 1–5. https://doi.org/10.1016/j.colsurfb.2010.10.045

Sambanthamoorthy, K., Feng, X., Patel, R., Patel, S., Paranavitana, C. 2014. Antimicrobial and antibiofilm potential of biosurfactants isolated from lactobacilli against multi-drug-resistant pathogens. BMC Microbiol 14(197), 1–9. https://doi.org/10.1186/1471-2180-14-197

Shubina, V., Gaillet, L., Ababou-Girard, S., Gaudefroy, V., Chaussadent, T., Farças, F., Meylheuc, T., Dagbert, C., Creus, J. 2015. The influence of biosurfactant adsorption on the physicochemical behaviour of carbon steel surfaces using contact angle measurements and X-ray photoelectron spectroscopy. Appl Surf Sci 351, 1174–1183. https://doi.org/10.1016/j.apsusc.2015.06.057

Simões, M., Simões, L.C., Vieira, M.J. 2010. A review of current and emergent biofilm control strategies. LWT-Food Sci Technol 43(4), 573–583. https://doi.org/10.1016/j.lwt.2009.12.008

Stewart, P.S. 2002. Mechanisms of antibiotic resistance in bacterial biofilms. Int J Med Microbiol Suppl 292(2), 107–113. https://doi.org/10.1078/1438-4221-00196

Su, C., Xiang, Z., Liu, Y., Zhao, X., Sun, Y., Li, Z., Li, L., Chang, F., Chen, T., Wen, X., Zhou, Y. 2016. Analysis of the genomic sequences and metabolites of *Serratia surfactantfaciens* sp. nov. YD25^{T} that simultaneously produces prodigiosin and serrawettin W2. BMC Genom 17(865), 1–19. https://doi.org/10.1186/s12864-016-3171-7

Tait, K., Sutherland, I.W. 2002. Antagonistic interactions amongst bacteriocin-producing enteric bacteria in dual species biofilms. J Appl Microbiol 93(2), 345–352. https://doi.org/10.1046/j.1365-2672.2002.01692.x

Thies, S., Santiago-Schübel, B., Kovačić, F., Rosenau, F., Hausmann, R., Jaeger, K.E. 2014. Heterologous production of the lipopeptide biosurfactant serrawettin W1 in *Escherichia coli*. J Biotechnol 181, 27–30. https://doi.org/10.1016/j.jbiotec.2014.03.037

Tomas, R.P., Ramoneda, B.M., Lledo, E.G., Pedemonte, M.M., Casas, M.V. 2005. Use of cyclic depsipeptide as a chemotherapeutic agent against cancer. *Patent Number: EP1553080*.

Verma, M., Biswal, A.K., Dhingra, S., Gupta, A., Saha, S. 2019. Antibacterial response of polylactide surfaces modified with hydrophilic polymer brushes. Iran Polym J 28(6), 493–504. https://doi.org/10.1007/s13726-019-00717-3

Wingender, J., Flemming, H.C. 2011. Biofilms in drinking water and their role as reservoir for pathogens. Int J Hyg Environ Health 214(6), 417–423. https://doi.org/10.1016/j.ijheh.2011.05.009

Zeraik, A.E., Nitschke, M. 2010. Biosurfactants as agents to reduce adhesion of pathogenic bacteria to polystyrene surfaces: effect of temperature and hydrophobicity. Curr Microbiol 61(6), 554–559. https://doi.org/10.1007/s00284-010-9652-z

Zhu, L., Pang, C., Chen, L., Zhu, X. 2018. Antibacterial activity of a novel depsipeptide and prodigiosine of *Serratia marcescens* S823. Nat Prod Chem Res 6(2), 1–7. https://doi.org/10.4172/2329-6836.1000312

Chapter 5:

General Conclusions and Recommendations

(UK spelling is employed)

5.1. General Conclusions and Recommendations

Microbial secondary metabolites offer a wide range of structurally diverse, low-molecular weight compounds, with complex biological activity, and have been recognised as a natural source for drug discovery and development (Baral et al. 2018). These bioactive compounds are commonly isolated from microbial species such as *Actinobacteria*, *Streptomyces*, *Myxobacteria*, *Pseudomonas* and *Bacillus,* as well as filamentous fungi (Baral et al. 2018; Niu and Li 2019). The broad-spectrum antimicrobial properties of bioactive metabolites produced by *Serratia* species are however, relatively unexplored and the primary aim of this study was to identify environmental *Serratia* species that produce antimicrobial secondary metabolites, elucidate their metabolic profiles and metabolite structures, and apply these bioactive compounds as antifouling and biofilm disrupting agents.

Various environmental sources, including wastewater treatment plants, an oil refinery, winery and olive oil estates, river water and rainwater, were subsequently screened for pigmented and non-pigmented *Serratia* isolates (chapter two). Preliminary screening for biosurfactant production (including oil spreading methods, emulsification assays and surface tension reduction measurements) and molecular typing resulted in the selection of 11 pigmented and 11 non-pigmented *Serratia marcescens* (*S. marcescens*) strains. These strains were predominantly isolated from wastewater treatment plants, followed by river water and one isolate was obtained from an oil refinery effluent sample. Based on the physico-chemical properties, molecular analysis, and preliminary antimicrobial testing, three *S. marcescens* strains (i.e. P1, NP1 and NP2) were selected for the production and extraction of the secondary metabolites. Following solvent extraction, the P1, NP1 and NP2 crude extracts were subjected to ultra-performance liquid chromatography (UPLC) coupled to electrospray ionisation mass spectrometry (ESI-MS) analysis for the putative identification of the secondary metabolites. The *S. marcescens* P1 and NP1 strains isolated in this study were capable of producing serrawettin W1 homologues (serratamolides A, B, C and E), which corresponded to the identification and production of these lipopeptides by *Serratia* species as described in Dwivedi et al. (2008) and Eckelmann et al. (2018). The co-production of serrawettin W1 homologues with glucosamine derivative A (NP1 strain) or prodigiosin (P1 strain) was also observed. In contrast, while the serrawettin W2 analogues (A to D) detected in the NP2 crude extract corresponded to the detection of these compounds in literature (Su et al. 2016), a novel analogue of serrawettin W2 with a molecular ion at *m/z* 690.41 $[M+H]^+$ was putatively identified. Tandem-mass spectrometry (MS/MS) is thus recommended to elucidate the full chemical structure of this analogue, as well as confirm the chemical structures of the other serrawettin W2 analogues, serrawettin W1 homologues, glucosamine derivative A and prodigiosin. Moreover, while *Serratia* species are well-known producers of serrawettins and prodigiosin, it was interesting to note that of the 22 strains selected and screened for biosurfactant production in chapter two, the *S. marcescens*

NP10 strain was the only isolate that did not contain either the *swrW* (encodes for non-ribosomal serrawettin W1 synthetase) or *swrA* (encoding for non-ribosomal serrawettin W2 synthetase) genes, despite exhibiting surface tension reduction and emulsification activity. This indicates that this strain may be able to produce other types of secondary metabolites and it is recommended that research be conducted on the chemical characterisation and antimicrobial properties of the secondary metabolites produced by NP10.

Previous research has described the antimicrobial activity of the secondary metabolites, serrawettin W1, serrawettin W2 and prodigiosin against for example, *Staphylococcus* species, while glucosamine derivative A displayed activity against *Mycobacterium* species (Dwivedi et al. 2008; Kadouri and Shanks 2013; Darshan and Manonmani 2015; Su et al. 2016). It is however, important to highlight that in chapter two, an extensive investigation into the antimicrobial activity of the P1 and NP1 crude extracts, comprised of serrawettin W1 homologues in combination with prodigiosin (P1) or glucosamine derivative A (NP1) and NP2 (produced serrawettin W2 analogues) was conducted. Subsequently, results indicated that the P1 and NP1 crude extracts displayed broad-spectrum antimicrobial activity against Gram-negative and Gram-positive bacteria, such as multidrug-resistant (MDR) *Pseudomonas aeruginosa* (*P. aeruginosa*) and methicillin-resistant *Staphylococcus aureus*, and fungal opportunistic pathogens, such as clinical *Cryptococcus neoformans* and *Candida albicans* strains. Although the NP2 crude extract exhibited activity against a narrow-spectrum of test microorganisms, in comparison to the other two extracts, activity against MDR *P.* aeruginosa and extensive drug-resistant (XDR) *Acinetobacter baumannii* as well as a clinical *C. neoformans* strain, was recorded. Hage-Hülsmann et al. (2018) investigated the synergism between serrawettin W1 and prodigiosin and indicated that the compounds displayed greater antimicrobial potency in combination against *Corynebacterium glutamicum* in comparison to their individual activities. It is thus hypothesised that as the respective P1 and NP1 crude extracts consisted of at least two classes of secondary metabolites [serrawettin W1 homologues and prodigiosin (P1) or glucosamine derivative A (NP1)], the broad-spectrum activity observed against the test organisms may be due to a synergistic effect displayed between the compounds in these extracts. This could potentially also elucidate the narrow-spectrum activity observed for the NP2 crude extract, where only one class of metabolites (serrawettin W2 analogues) was detected. The production of surface active compounds (i.e. serrawettins) in combination with other antimicrobials may thus enhance the potency of these metabolites (i.e. prodigiosin or glucosamine derivatives) by improving their solubility and aid in their penetration across cell walls (Bhadoriya et al. 2013; Hage-Hülsmann et al. 2018). Although the development of antibiotic formulations containing serrawettin W1 homologues in combination with glucosamine derivatives or prodigiosin may be a promising avenue to explore, future research is required to purify the compounds detected in the crude extracts and analyse the antimicrobial activity displayed by the individual compounds as well as their synergistic effect. Overall, results

from chapter two indicate that *Serratia* species are a reservoir of antibacterial and antifungal compounds of clinical and industrial significance. It should additionally be noted that wastewater treatment plants, river water and oil refinery effluent samples were found to be promising sources for the isolation of pigmented and non-pigmented *S. marcescens* strains capable of producing secondary metabolites with antimicrobial activity. As the secondary metabolites produced by the P1 and NP1 strains exhibited broad-spectrum antimicrobial activity, the extracts produced by these two *S. marcescens* strains were selected for further analysis in chapters three and four.

In chapter three, reverse-phase high performance liquid chromatography (RP-HPLC), ESI-MS, UPLC-MS^e and mass spectrometry-based molecular networking was used to identify secondary metabolites and elucidate the structures of various congeners produced by the pigmented (P1) and a non-pigmented (NP1) *S. marcescens* strains. To achieve this, up-scaled fermentations of the P1 and NP1 strains were completed and the secondary metabolites were extracted. Thereafter, RP-HPLC was used to fractionate the secondary metabolites within the P1 and NP1 crude extracts. The collected fractions were subjected to ESI-MS and UPLC-MS^e and the MS^e data for P1 and NP1 were analysed using molecular networking on the Global Natural Products Social Molecular Networking (GNPS) platform, which enables the detection and visualisation of large groups of natural products that are generated based on structural similarity (Niu and Li 2019). As indicated in chapter two, using UPLC-ESI-MS, the P1 and NP1 crude extracts were comprised of serratamolides (A, B, C and E) with prodigiosin (P1) or glucosamine derivative A (NP1). However in chapter three, the combined use of fractionation by RP-HPLC, ESI-MS, UPLC-MS^e and molecular networking of the secondary metabolites produced by *S. marcescens* P1 and NP1, revealed four major clusters, including the known structures of serratiochelin A, prodigiosin (produced by P1), serratamolide homologues (n = 7) and glucosamine derivative homologues (n = 3). Moreover, based on structural similarity, the molecular network generated using the GNPS platform guided the characterisation of unknown metabolites in combination with the MS^e fragmentation profiles, revealing the putative structures of one novel open-ring serratamolide homologue and eight novel glucosamine derivative congeners. The integrated approach applied in chapter three thus provided new knowledge on the chemical structures of novel serratamolide and glucosamine derivative congeners and is the first report of the co-production of these four secondary metabolic classes (i.e. prodigiosin, serratiochelin A, serratamolides and glucosamine derivatives) by a *Serratia* strain. The use of RP-HPLC and UPLC-MS^e analysis thus proved to be a powerful tool for the detection of minor secondary metabolic constituents produced by *Serratia* strains and may have further contributed to the increased consortium of secondary metabolites identified in the P1 and NP1 crude extracts. Furthermore, the combined use of UPLC-MS^e and molecular networking was found to be a high-throughput method of clustering and characterising known and novel secondary metabolites produced by *Serratia* species.

It should be noted at as the majority of the novel compounds were produced in minor quantities by the P1 and NP1 strains, further structural elucidation (such as nuclear magnetic resonance) could not be conducted to confirm the position of double bonds and hydroxyl groups on the fatty acyl chains. It is thus recommended that further optimisation of the culture conditions, extraction methods or metabolic engineering approaches (heterologous expression of gene clusters in a suitable host) be conducted to increase the production (and ultimately yield) of the minor metabolic constituents detected, effectively allowing for additional structural confirmation. Altering cultivation conditions, such as adjusting media components, temperature or aeration rates used during fermentation (production of secondary metabolites) may also activate certain 'silent' gene clusters in the genome of microbial cells that are involved in secondary metabolism [such as non-ribosomal peptide synthetase (NRPS) gene clusters] (Bode et al. 2002) and lead to the production of different metabolites by the P1 and NP1 strains. Another approach comprises a co-cultivation strategy that involves aseptically culturing two or more microbial strains in solid or liquid media to identify additional secondary metabolites (Romano et al. 2018; Chen et al. 2020). It is hypothesised that the competitive or snergistic relationship between the co-cultured strains may activate biosynthetic gene clusters and produce secondary metabolites that are not typically detected under classical mono-culture conditions (Chen et al. 2020). The co-culturing of the P1 and NP1 strains may thus be a promising future approach to elucidate additional novel natural products produced by these *S. marcescens* strains. A more recent approach involves the use of whole genome sequencing in combination with bioinformatics tools [such as the antibiotics and secondary metabolite analysis shell (antiSMASH)] to analyse a microbial genome for biosynthetic gene clusters responsible for producing secondary metabolites (Villebro et al. 2019). This allows for the detection of all possible NRPS gene clusters within the strains genome that may encode for novel bioactive secondary metabolites and predict the chemical structure of the NRPS products (Medema et al. 2011). The use of genome sequencing and mining for NRPS biosynthetic pathways in the P1 and NP1 strains may thus provide further insight into additional secondary metabolites not actively being produced under typical cultivation conditions and is a promising strategy to pursue in future research.

Following RP-HPLC and ESI-MS analysis (as outlined in chapter three), a disc diffusion assay revealed that a clinical *Enterococcus faecalis* (*E. faecalis*) S1 strain was susceptible to the fractions with the major molecular ions $[M+H]^+$ at *m/z* 324.2073 (prodigiosin), 515.3331, 541.3485 and 543.3644 (serratamolides), 559.3953 and 585.4117 (glucosamine derivatives), with a novel glucosamine derivative homologue (molecular ion at *m/z* 557.3801) also exhibiting antimicrobial activity. The minimum inhibitory concentration (MIC) and minimum bactericidal concentration (MBC) of fractions, selected based on the activity and quantity, was subsequently determined and revealed that the three serratamolides (i.e. *m/z* 515.3331, 541.3485 and 543.3644 $[M+H]^+$) exhibited identical activity against *E. faecalis* S1 with a MIC of 3 mg/mL and MBC of > 3 mg/mL recorded. The

structures of the three serratamolides differed based solely on the length and the presence of a double bond in one of the two fatty acid chains (i.e. lengths of C_{10}; C_{12} and $C_{12:1}$), indicating that the fatty acid modifications of the serratamolide homologues exhibited no additional antimicrobial potency against the Gram-positive strain. Moreover, the glucosamine derivative A (i.e. *m/z* 585.4117) and prodigiosin (i.e. *m/z* 324.2073) were found to be more potent against *E. faecalis* S1 compared to the serratamolides, suggesting that these compounds are promising antimicrobial candidates for future drug development and therapeutic application. However, further tests on the broad-spectrum activity of the individual (RP-HPLC purified) compounds against other Gram-positive bacteria, as well as against Gram-negative bacteria and fungi are recommended. Additional pre-clinical development tests with these compounds, for example testing the chemical stability, solubility in water, safety of the compounds (against mammalian cell lines) and preliminary assessment of spontaneous resistance, are recommended for future studies (Hughes and Karlen 2014). Results obtained in chapter three thus confirmed that the serratamolides, glucosamine derivatives and prodigiosin produced by the *S. marcescens* P1 and NP1 strains exhibited antimicrobial activity and the combination of the respective compounds may have resulted in the broad-spectrum antimicrobial activity observed in chapter two.

While purifying the homologues of serratamolides and glucosamine derivatives via RP-HPLC, and the subsequent antimicrobial testing, provided information regarding the activity of individual compounds, the use of the entire complex of secondary metabolites in the P1 and NP1 crude extracts may be a more cost-effective approach for industrial application as a biodetergent solution or material surface coating agent (Quinn et al. 2012). Moreover, the combination of the secondary metabolites detected in each extract may potentially increase the potency against multi-species biofilms (Quinn et al. 2012). The antifouling and biofilm disrupting activity of the P1 and NP1 crude extracts was thus analysed in chapter four. The P1 and NP1 crude extracts were tested against single- and dual-species *Pseudomonas aeruginosa* (*P. aeruginosa*) S1 68 and *E. faecalis* S1 biofilms using the minimum biofilm eradication concentration (MBEC) Assay®. Results indicated that both the P1 and NP1 extracts significantly reduced the single-species *E. faecalis* S1 biofilm, while the single-species *P. aeruginosa* S1 68 biofilm was more susceptible to the P1 extract. The P1 and NP1 extracts significantly reduced the dual-species *P. aeruginosa* and *E. faecalis* biofilm; however, increased concentrations of both extracts were required to reduce *E. faecalis* by ≥ 2 logs in comparison to the single-species *E. faecalis* biofilm. This provided an indication that *E. faecalis* S1 may have been less susceptible to the compounds in both extracts whilst in a dual-species biofilm with *P. aeruginosa* S1 68. Various factors, including interspecies interactions and spatial distribution of the strains within the biofilm, were hypothesised to have resulted in the observed increase in tolerance of *E. faecalis* S1 to the P1 and NP1 crude extracts in a dual-species biofilm; however, research is required to monitor these factors during antimicrobial treatment in order to

confirm this theory. Overall, the natural compounds in the P1 and NP1 crude extracts were effective at reducing pre-formed single- and dual-species biofilms of bacterial strains (i.e. *E. faecalis* and *P. aeruginosa*) that have been implicated as contaminants of water sources, food processing units and as part of a biofilm community on medical equipment, devices and implants (Wingender and Flemming 2011; Abdallah et al. 2014; Lee et al. 2017; Meier et al. 2018). Moreover, this is the first study to show that an extract comprised of serratamolides and glucosamine derivatives (the NP1 crude extract) as well as prodigiosin in combination with serratamolides and glucosamine derivatives (the P1 crude extract), display biofilm disrupting properties against single- and dual-species biofilms.

Additionally, the pre-adsorption of the P1 and NP1 extracts (at 50 mg/mL) to the pegs of the MBEC Assay® effectively reduced the adhesion of mono-culture *P. aeruginosa* S1 68 and *E. faecalis* S1 cells. For the co-culture analysis, significant reductions in the adhesion of *E. faecalis* S1 to the P1 and NP1 coated pegs were observed, while *P. aeruginosa* S1 68 cells were more readily able to adhere to the pre-coated peg surface of the MBEC Assay® in co-culture with *E. faecalis* S1. Future research is required to investigate the various factors, such as interspecies interactions (production of metabolites, quorum sensing etc.) and adhesion rates, which were hypothesised to facilitate the increased adhesion of *P. aeruginosa* S1 68 to a coated surface in the presence of *E. faecalis* S1. A literature search indicated that the antiadhesive potential of serratamolides and glucosamine derivatives (in the NP1 extract) and prodigiosin in combination with serratamolides and glucosamine derivatives (the P1 crude extract), has not previously been investigated or explored. The antiadhesive properties of the combination of these compounds in the P1 and NP1 crude extracts was thus confirmed in the current study against mono- and co-cultures of bacterial strains. Overall, the MBEC Assay® was advantageous as it allowed for the analysis of two crude extracts at various concentrations in a high-throughput manner against single- and dual-species biofilms, as well as the antiadhesive testing against mono- and co-cultures of bacterial strains. Moreover, the use of the MBEC Assay® with ethidium monoazide bromide quantitative PCR (EMA-qPCR) provided an indication of the viable cells remaining in the biofilm after antimicrobial treatment. Thus, the P1 and NP1 crude extracts have the potential to be developed and applied as biodetergents for controlling bacterial biofilms and preventing biofilm attachment in medical and industrial settings. However, investigation into the effectiveness of the P1 and NP1 crude extracts over extended time intervals is required, to determine the biodetergent dosage frequency as well as the efficacy of the P1 and NP1 crude extracts against mixed microbial communities and a more established biofilm. Additionally, while the mode of biofilm disruption and biofilm prevention (antiadhesive potential) has been described for prodigiosin, future research should explore the mechanisms of biofilm disruption and preventing biofilm formation on surfaces coated with serratamolides and glucosamine derivatives.

Following the use of the MBEC Assay®, the serratamolides and glucosamine derivatives in the P1 and NP1 crude extracts were covalently immobilised onto the surface of high-density polyethylene PE300 (HDPE) and polyvinyl chloride (PVC). The two materials were selected as they are commonly utilised in the food, water and medical industries. The immobilisation process involved pre-modification of the serratamolides and glucosamine derivatives in the P1 and NP1 crude extracts to promote their reactivity with the terminal amine groups of the 3-triethoxysilylpropan-1-amine (APTES) linker, by replacing the hydroxyl groups in the structure of the secondary metabolites with chlorine reactive groups (prodigiosin did not covalently link to APTES due to the absence of reactive functional groups within the structure and was not applied). This was followed by the material modification process, involving the addition of hydroxyl groups to the surface of each material via oxidation with the piranha solution and subsequent silanization with APTES (the organic silane linker). The modified P1 and NP1 crude extracts (i.e. serratamolides and glucosamine derivatives) were then covalently immobilised onto the silanized APTES on the HDPE and PVC surfaces. Surface characterisation methods, including water contact angle measurements, attenuated total reflectance Fourier transform infrared spectroscopy and scanning electron microscope coupled to backscattered electron imaging-energy dispersive x-ray spectroscopy, confirmed the successful immobilisation of the modified compounds onto the materials. The potential leaching of the compounds coated onto the materials was also investigated in the current study by placing the coated HDPE and PVC into milli-Q water for 24 h. The suspension collected after exposure was freeze-dried and UPLC-ESI-MS analysis was conducted on the recovered freeze-dried samples, with results indicating that no leaching of the secondary metabolites was observed. The use of covalent immobilisation to coat the surface of a material is thus advantageous over the methods previously used in chapter four (i.e. simple adsorption of the compounds to the surface of the pegs in the MBEC Assay®) as it prevented leaching and may enhance long-term stability and increase the duration of antimicrobial efficacy (Alves and Pereira 2014; De Zoysa and Sarojini 2017). However, it is recommended that antimicrobial testing with the recovered freeze-dried samples (to confirm that there is no biological activity) and with the coated HDPE and PVC after the 24 h leaching test (to ensure the coated materials still exhibit antimicrobial activity), be conducted.

Antifouling analyses then indicated that the P1 and NP1 coated HDPE were effectively able to reduce the adhesion of mono-cultures of Gram-negative (*P. aeruginosa* S1 68) and Gram-positive (*E. faecalis* S1) bacterial cells, while the P1 and NP1 coated PVC were only effective at reducing the adhesion of the Gram-negative *P. aeruginosa* S1 68, with minor reductions in *E. faecalis* S1 adhesion observed. It was hypothesised that the reduced adhesion was due to the decreased hydrophobicity (became more hydrophilic) of the HDPE and PVC surfaces after coating with the serratamolides and glucosamine derivatives (i.e. less conducive to microbial adhesion) in

combination with the antimicrobial activity exhibited by the secondary metabolites. This is thus one of the first reports of the development of biomaterials, employing secondary metabolites (i.e. serratamolides and glucosamine derivatives) produced by *Serratia* species, that were effectively able to reduce the adhesion of microbial cells. The development of biomaterials with antifouling properties may thus play an important role in the escalating battle against MDR and XDR bacterial contamination in medical, food and water environments. However, potential toxicity analysis of the coated materials is still required prior to the application of these biomaterials in these industries. It is also recommended that the antiadhesive potency of the coated HDPE and PVC be tested against dual- and mixed-species bacterial and fungal biofilms. The coating protocol employed in the current study, to immobilise serratamolides and glucosamine derivatives onto the HDPE and PVC, should also be applied and optimised (if required) on other material types commonly used in the food, water and medical industries.

5.2. References

Abdallah, M., Benoliel, C., Drider, D., Dhulster, P., Chihib, N.E., 2014. Biofilm formation and persistence on abiotic surfaces in the context of food and medical environments. Arch Microbiol 196(7), 453–472. https://doi.org/10.1007/s00203-014-0983-1

Alves, D., Pereira, O.M., 2014. Mini-review: Antimicrobial peptides and enzymes as promising candidates to functionalize biomaterial surfaces. Biofouling 30(4), 483–499. https://doi.org/10.1080/08927014.2014.889120

Baral, B., Akhgari, A., Metsä-Ketelä, M., 2018. Activation of microbial secondary metabolic pathways: Avenues and challenges. Synth Syst Biotechnol 3(3), 163–178. https://doi.org/10.1016/j.synbio.2018.09.001

Bhadoriya, S.S., Madoriya, N., Shukla, K., Parihar, M.S., 2013. Biosurfactants: A new pharmaceutical additive for solubility enhancement and pharmaceutical development. Biochem Pharmacol 2(2), 113. https://doi.org/10.4172/2167-0501.1000113

Bode, H.B., Bethe, B., Höfs, R., Zeeck, A., 2002. Big effects from small changes: possible ways to explore nature's chemical diversity. ChemBioChem 3(7), 619–627. https://doi.org/10.1002/1439-7633(20020703)3:7<619::AID-CBIC619>3.0.CO;2-9

Chen, J., Zhang, P., Ye, X., Wei, B., Emam, M., Zhang, H., Wang, H., 2020. The Structural Diversity of Marine Microbial Secondary Metabolites Based on Co-Culture Strategy: 2009–2019. Mar Drugs 18(9), 449.

Darshan, N., Manonmani, H.K., 2015. Prodigiosin and its potential applications. J Food Sci Technol 52, 5393–5407. https://doi.org/10.1007/s13197-015-1740-4

De Zoysa, G.H., Sarojini, V., 2017. Feasibility study exploring the potential of novel battacin lipopeptides as antimicrobial coatings. ACS Appl Mater Interfaces 9(2), 1373–1383. https://doi.org/10.1021/acsami.6b15859

Dwivedi, D., Jansen, R., Molinari, G., Nimtz, M., Johri, B.N., Wray, V., 2008. Antimycobacterial serratamolides and diacyl peptoglucosamine derivatives from *Serratia* sp. J Nat Prod 71, 637–641. https://doi.org/10.1021/np7007126

Eckelmann, D., Spiteller, M., Kusari, S., 2018. Spatial-temporal profiling of prodiginines and serratamolides produced by endophytic *Serratia marcescens* harbored in *Maytenus serrata*. Sci Rep 8, 5283. https://doi.org/10.1038/s41598-018-23538-5

Hage-Hülsmann, J., Grünberger, A., Thies, S., Santiago-Schübel, B., Klein, A.S., Pietruszka, J., Binder, D., Hilgers, F., Domröse, A., Drepper, T., Kohlheyer, D., 2018. Natural biocide cocktails: Combinatorial antibiotic effects of prodigiosin and biosurfactants. PloS One 13, e0200940. https://doi.org/10.1371/journal.pone.0200940

Hughes, D., Karlén, A., 2014. Discovery and preclinical development of new antibiotics. Ups J Med Sci 119(2), 162–169. https://doi.org/10.3109/03009734.2014.896437

Kadouri, D.E., Shanks, R.M., 2013. Identification of a methicillin-resistant *Staphylococcus aureus* inhibitory compound isolated from *Serratia marcescens*. Res Microbiol 164, 821–826. https://doi.org/10.1016/j.resmic.2013.06.002

Lee, K., Lee, K.M., Kim, D., Yoon, S.S., 2017. Molecular determinants of the thickened matrix in a dual-species *Pseudomonas aeruginosa* and *Enterococcus faecalis* Biofilm. Appl Environ Microbiol 83(21), 1–15. https://doi.org/10.1128/AEM.01182-17

Medema, M.H., Blin, K., Cimermancic, P., de Jager, V., Zakrzewski, P., Fischbach, M.A., Weber, T., Takano, E., Breitling, R., 2011. antiSMASH: rapid identification, annotation and analysis of secondary metabolite biosynthesis gene clusters in bacterial and fungal genome sequences. Nucleic Acids Res 39(suppl_2), W339–W346. https://doi.org/10.1093/nar/gkr466

Meier, F., Lacroix, C., Meile, L., Jans, C., 2018. Enterococci and pseudomonads as quality indicators in industrial production and storage of mozzarella cheese from raw cow milk. Int Dairy J 82, 28–34. https://doi.org/10.1016/j.idairyj.2018.02.010

Niu, G., Li, W., 2019. Next-generation drug discovery to combat antimicrobial resistance. Trends Biochem Sci 44(11), 961–972. https://doi.org/10.1016/j.tibs.2019.05.005

Quinn, G.A., Maloy, A.P., McClean, S., Carney, B., Slater, J.W., 2012. Lipopeptide biosurfactants from *Paenibacillus polymyxa* inhibit single and mixed species biofilms. Biofouling 28(10), 1151–1166. https://doi.org/10.1080/08927014.2012.738292

Romano, S., Jackson, S.A., Patry, S., Dobson, A.D., 2018. Extending the “one strain many compounds” (OSMAC) principle to marine microorganisms. Mar Drugs 16(7), 244. https://doi.org/10.3390/md16070244

Su, C., Xiang, Z., Liu, Y., Zhao, X., Sun, Y., Li, Z., Li, L., Chang, F., Chen, T., Wen, X., Zhou, Y., 2016. Analysis of the genomic sequences and metabolites of *Serratia surfactantfaciens* sp. nov. YD25^{T} that simultaneously produces prodigiosin and serrawettin W2. BMC Genom 17, 865. https://doi.org/10.1186/s12864-016-3171-7

Villebro, R., Shaw, S., Blin, K., Weber, T., 2019. Sequence-based classification of type II polyketide synthase biosynthetic gene clusters for antiSMASH. J Ind Microbiol 46(3-4), 469–475. https://doi.org/10.1007/s10295-018-02131-9

Wingender, J., Flemming, H.C., 2011. Biofilms in drinking water and their role as reservoir for pathogens. Int J Hyg Environ Health 214(6), 417–423. https://doi.org/10.1016/j.ijheh.2011.05.009

Appendices:

Appendix A

Broad-spectrum antimicrobial activity of secondary metabolites produced by *Serratia marcescens* strains

Tanya Clements[a], Thando Ndlovu[a] and Wesaal Khan[a*]

[a]Department of Microbiology, Faculty of Science, Stellenbosch University, Private Bag X1, Stellenbosch, 7602, South Africa

*Corresponding Author: Wesaal Khan; Phone: +27 21 808 5804; E-mail: wesaal@sun.ac.za

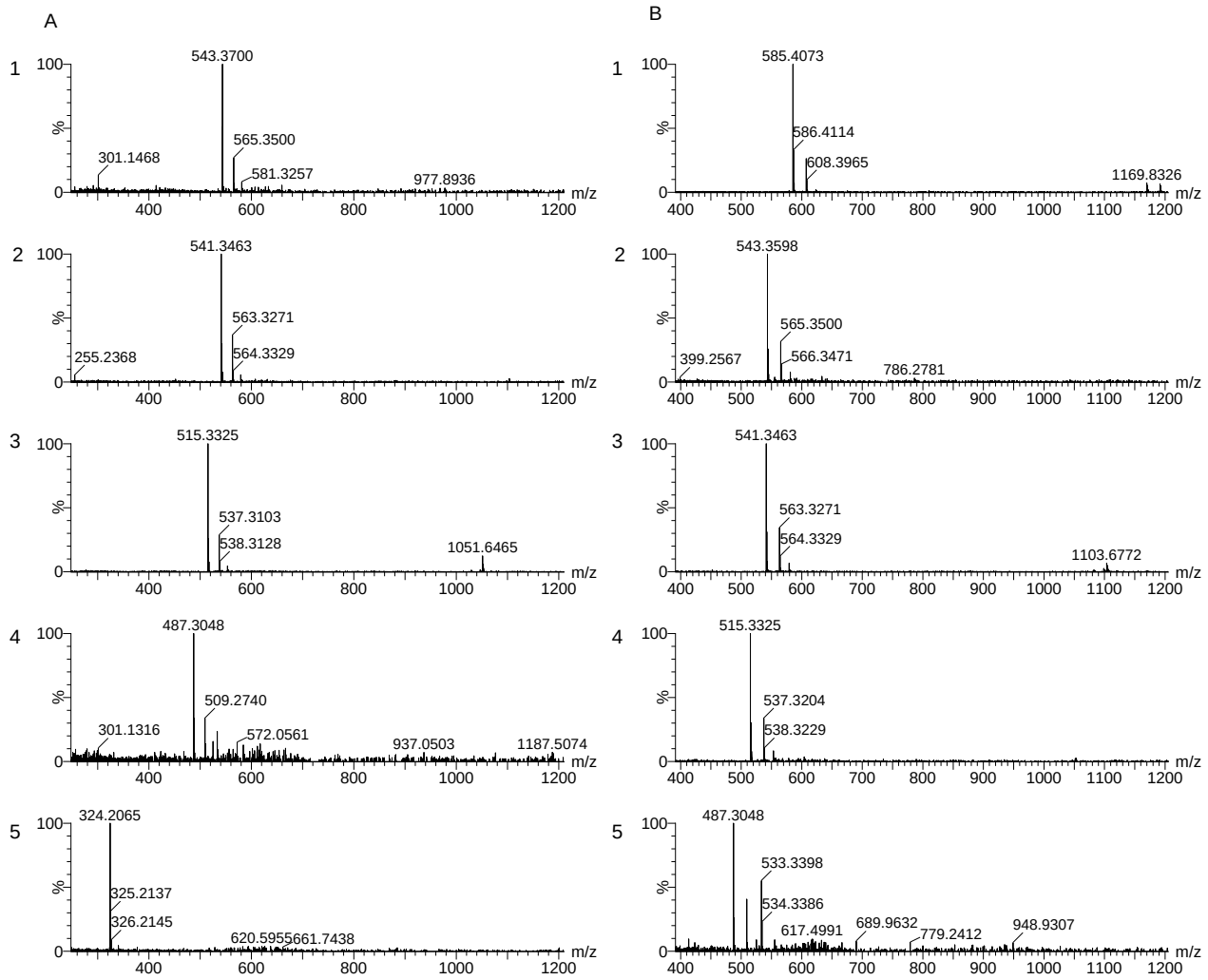

Fig. A1 ESI-MS spectrum of the crude extract obtained from (A) *S. marcescens* P1 and (B) *S. marcescens* NP1. Detected the protonated $[M+H]^+$ singly charged species detected in (A) P1 crude extract corresponded to (1) serratamolide C (*m/z* 543.37), (2) serratamolide B (*m/z* 541.35), (3) serratamolide A (*m/z* 515.33), (4) serratamolide E (*m/z* 487.30) and (5) prodigiosin (*m/z* 324.21); and (B) NP1 crude extract corresponded to (1) glucosamine derivative A (*m/z* 585.41), (2) serratamolide C (*m/z* 543.36), (3) serratamolide B (*m/z* 541.35), (4) serratamolide A (*m/z* 515.33), (5) serratamolide E (*m/z* 487.30).

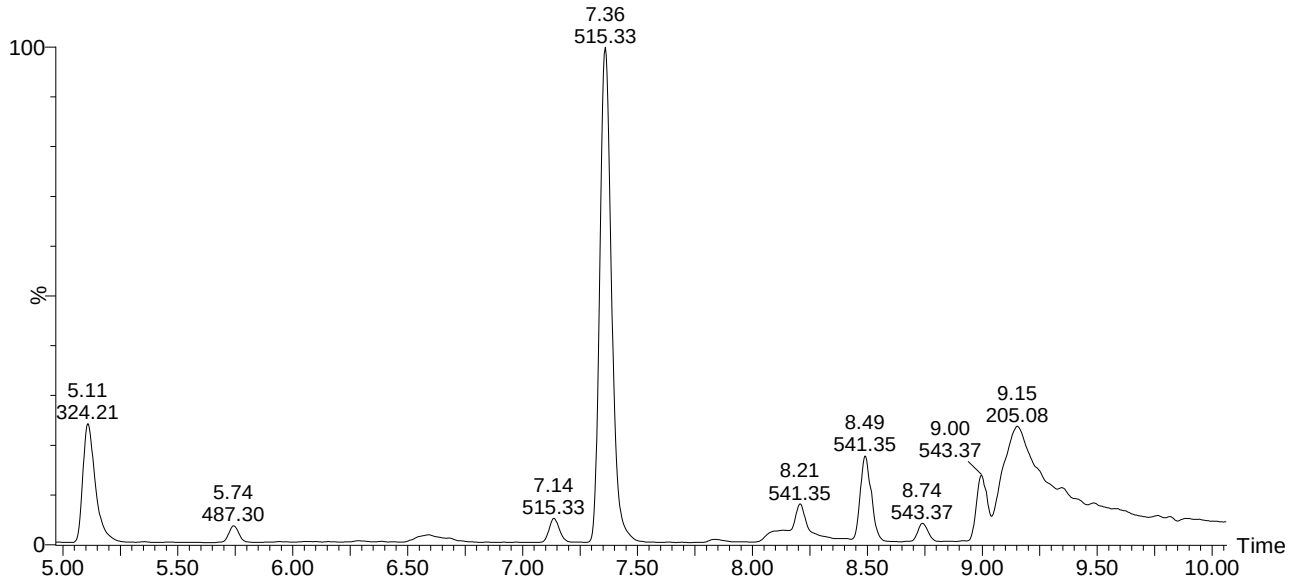

Fig. A2 UPLC-MS chromatogram of the crude extract obtained from *S. marcescens* P1. Five major peaks were observed in both crude extracts. The five peaks correspond to prodigiosin (P) (*m/z* 324.21) and serratamolide homologues: serratamolide A (*m/z* 515.33), serratamolide B (*m/z* 541.35), serratamolide C (*m/z* 543.37) and serratamolide E (*m/z* 487.30).

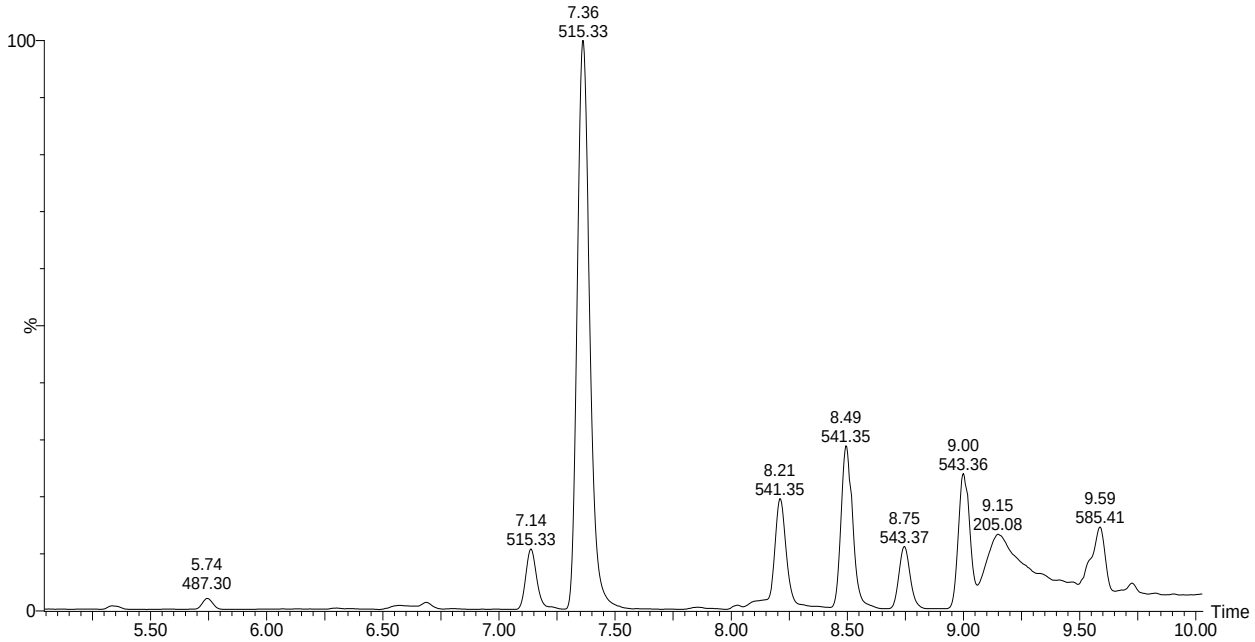

Fig. A3 UPLC-MS chromatogram of the crude extract obtained from *S. marcescens* NP1. Five major peaks are observed in both crude extracts. The five peaks correspond to a glucosamine derivative A (*m/z* 585.41) and serratamolide homologues: serratamolide A (*m/z* 515.33), serratamolide B (*m/z* 541.35), serratamolide C (*m/z* 543.36) and serratamolide E (*m/z* 487.30).

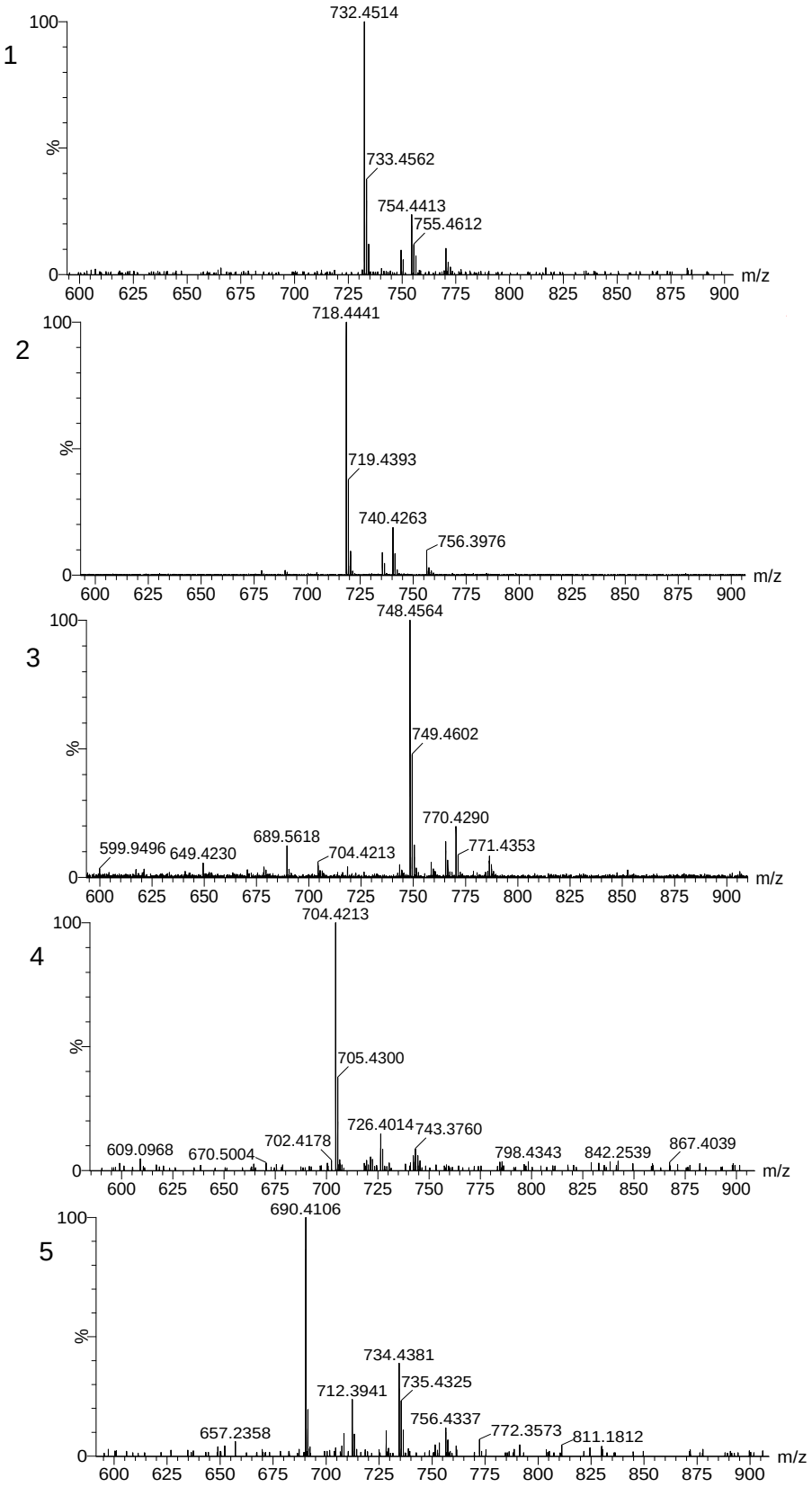

Fig. A4 ESI-MS spectrum of the crude extract obtained from *S. marcescens* NP2. Detected the protonated $[M+H]^+$ singly charged species include (1) serrawettin W2 A (*m/z* 732.45), (2) serrawettin W2 B (*m/z* 718.44), (3) serrawettin W2 D (*m/z* 748.46), (4) serrawettin W2 C (*m/z* 704.42), and (5) serrawettin W2 E (*m/z* 690.41).

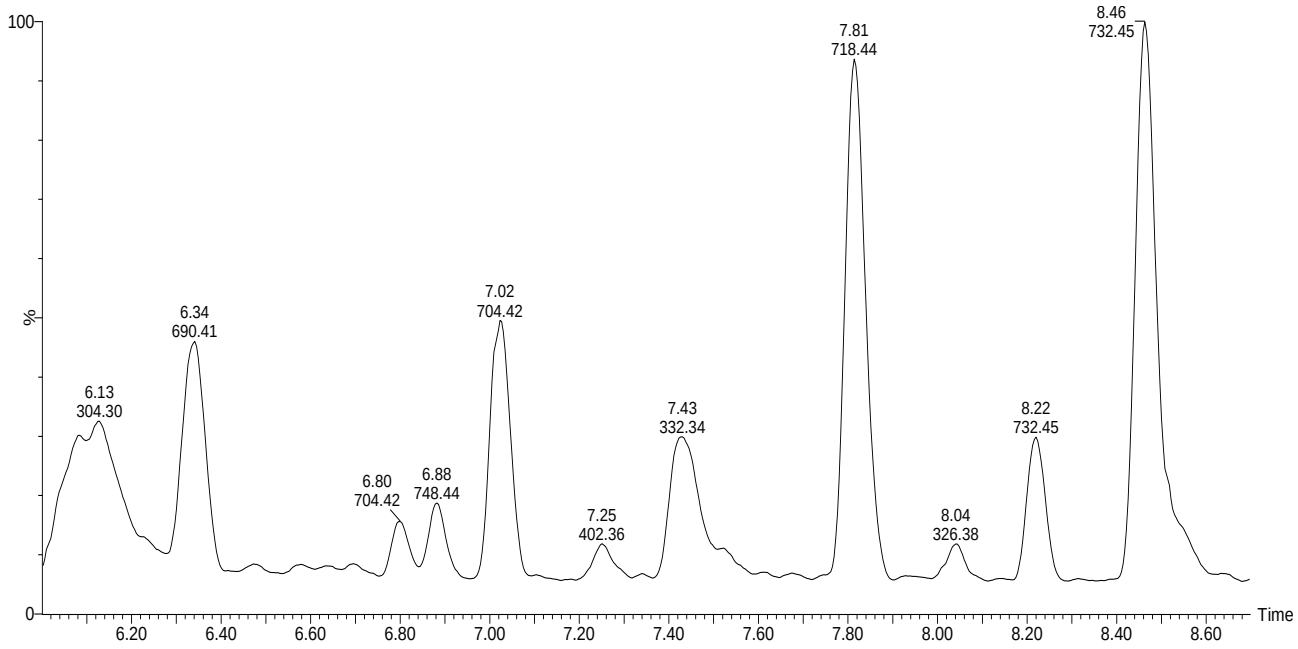

Fig. A5 UPLC-MS chromatogram of the crude extract obtained from *S. marcescens* NP2. Five major peaks are observed in both crude extracts. The five peaks correspond to serrawettin W2 A (*m/z* 732.45), serrawettin W2 B (*m/z* 718.44), serrawettin W2 C (*m/z* 704.42), serrawettin W2 D (*m/z* 748.44) and serrawettin W2 E (*m/z* 690.41).

Table A1 The biosurfactant target genes detected in each *S. marcescens* strain.

Isolate	Gene encoding for the biosynthesis of a biosurfactant	
	swrW	***swrA***
S. marcescens P1	+	-
S. marcescens P2	+	-
S. marcescens P3	+	-
S. marcescens P4	+	-
S. marcescens P5	+	-
S. marcescens P6	+	-
S. marcescens P7	+	-
S. marcescens P8	+	-
S. marcescens P9	+	-
S. marcescens P10	+	-
S. marcescens P11	+	-
S. marcescens NP1	+	-
S. marcescens NP2	-	+
S. marcescens NP3	-	+
S. marcescens NP4	-	+
S. marcescens NP5	-	+
S. marcescens NP6	-	+
S. marcescens NP7	-	+
S. marcescens NP8	-	+
S. marcescens NP9	-	+
S. marcescens NP10	-	-
S. marcescens NP11	-	+

Appendix B

A metabolomics and molecular networking approach to elucidate the structures of the secondary metabolites produced by *Serratia marcescens* strains

Tanya Clements [1], Marina Rautenbach [2], Thando Ndlovu [1], Sehaam Khan [3] and Wesaal Khan [1]*

[1] Department of Microbiology, Faculty of Science, Stellenbosch University, Private Bag X1, Stellenbosch, 7602, South Africa

[2] Department of Biochemistry, Faculty of Science, Stellenbosch University, Private Bag X1, Stellenbosch, 7602, South Africa

[3] Faculty of Health Sciences, University of Johannesburg, PO Box 17011, Doornfontein, 2028, South Africa.

*Corresponding Author: Wesaal Khan; Phone: +27 21 808 5804; E-mail: wesaal@sun.ac.za

Table B1. Summary of the compounds in the P1 and NP1 crude extracts that were identified using RP-HPLC and ESI-MS analysis.

Crude extract	RP-HPLC Rt (min)	Proposed compound identity (literature)	*m/z* $[M+H]^+$	*m/z* $[M+Na]^+$	*m/z* $[M+K]^+$	Reference
P1, NP1	8.8, 8.7	Serratiochelin A/ Serranticin	430.1609	452.1430	468.1061	Seyedsayamdost et al. 2012
P1	20.9	Prodigiosin	324.2073	N/D	N/D	Lee et al. 2011
P1	20.9	Open-ring serratamolide B	559.3600	581.3405	597.3135	Eckelmann et al. 2018
P1, NP1	22.0	Serrawettin W1/ serratamolide A	515.3331	537.3147	553.2894	Dwivedi et al. 2008
P1	22.0	Unidentified	575.3902	597.3736	613.3528	N/D
P1, NP1	22.0	Open-ring serratamolide C	561.3749	583.3563	599.3333	Eckelmann et al. 2018
P1, NP1	24.1	Unidentified	557.3804	579.3623	595.3395	N/D
NP1	24.6	Unidentified	585.3738	607.3548	623.3301	N/D
P1, NP1	24.5, 24.6	Serratamolide B	541.3485	563.3290	579.3591	Dwivedi et al. 2008
NP1	24.6	Unidentified	545.3787	567.3618	583.3265	N/D
NP1	24.6	Open-ring serratamolide 587	587.3908	609.3735	625.3573	Eckelmann et al. 2018
P1, NP1	26.4, 26.5	Unidentified	589.4056	611.3892	627.3608	N/D
P1, NP1	26.4, 26.5	Serratamolide C	543.3644	565.3455	581.3188	Dwivedi et al. 2008
P1, NP1	28.8	Glucosamine derivative C	559.3953	581.3781	597.3525	Dwivedi et al. 2008
P1, NP1	29.7	Unidentified	583.3947	605.3761	621.3491	N/D
P1, NP1	29.8, 29.7	Glucosamine derivative A	585.4117	607.3924	623.3680	Dwivedi et al. 2008
P1	31.1	Unidentified	599.4265	621.4111	637.3778	N/D
P1	31.8	Serratamolide 571	571.3931	593.3783	609.4060	Eckelmann et al. 2018
P1	31.8	Glucosamine derivative B	573.4136	595.3904	611.3514	Dwivedi et al. 2008
P1	31.8	Unidentified	627.4192	649.4021	665.3962	N/D
P1	34.3, 34.5	Unidentified	587.4268	609.4103	625.3834	N/D

N/D – not detected

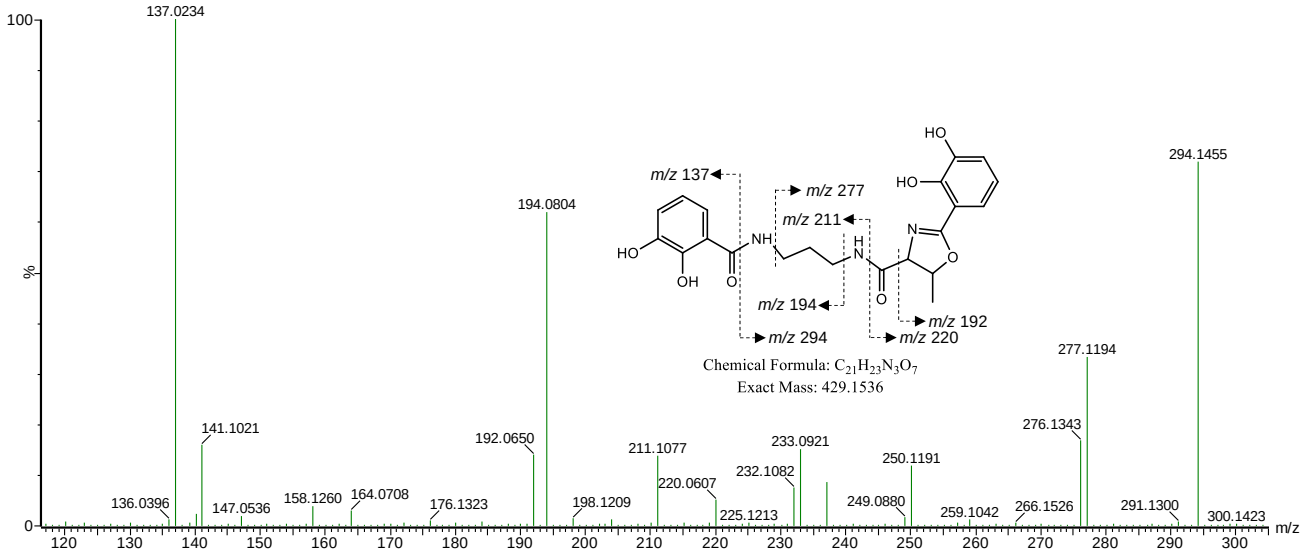

Fig. B1. Fragmentation profile and structure of the compound ion $[M+H]^+$ at *m/z* 430.1609.

Table B2. Summary of the theoretical and experimental fragmentation ions and mass error for the compound ion $[M+H]^+$ at *m/z* 430.1602.

Assigned ion (*m/z* 430.1609)		Theoretical $[M+H]^+$	Experimental $[M+H]^+$	Error (ppm)
	[M + H]	430.1614	430.1609	1.49
1	[M – $C_7H_6O_3$]	294.1454	294.1455	-0.34
2	[M – $C_7H_7NO_3$]	277.1188	277.1194	-2.17
3	[M – $C_{10}H_{14}N_2O_3$]	220.0610	220.0607	1.36
4	[M – $C_{11}H_9NO_4$]	211.1082	211.1077	2.37
5	[M – $C_{13}H_{25}NO_5$]	194.0817	194.0804	6.70
6	[M – $C_{11}H_{12}N_2O_4$]	192.0660	192.0650	5.21
7	[M – $C_{14}H_{19}N_3O_4$]	137.0239	137.0234	3.65

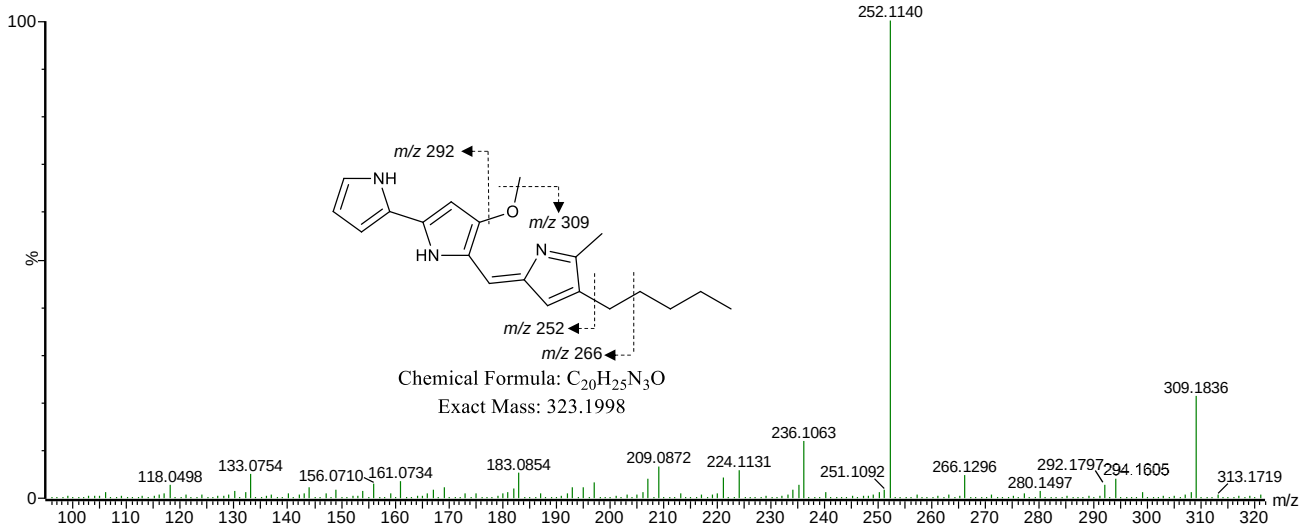

Fig. B2. Fragmentation profile and structure of the compound ion $[M+H]^+$ at *m/z* 324.2073.

Table B3. Summary of the theoretical and experimental fragmentation ions and mass error for the compound ion $[M+H]^+$ at *m/z* 324.2073.

Assigned ion (*m/z* 324.2073)		Theoretical $[M+H]^+$	Experimental $[M+H]^+$	Error (ppm)
	[M + H]	324.2076	324.2073	1.36
1	$[M - CH_4]$	309.1841	309.1836	1.62
2	$[M - CH_4O]$	292.1813	292.1797	5.48
3	$[M - C_5H_{12}]$	252.1137	252.1140	-1.19
4	$[M - C_4H_{10}]$	266.1293	266.1296	-1.13

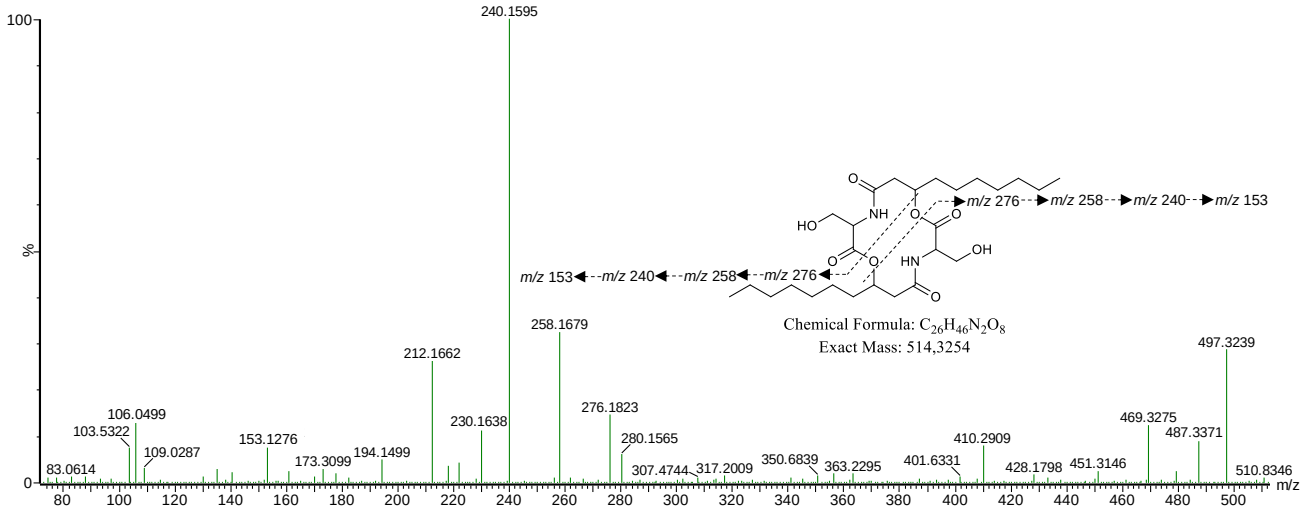

Fig. B3. Fragmentation profile and structure of the compound ion $[M+H]^+$ at *m/z* 515.3331.

Table B4. Summary of the theoretical and experimental fragmentation ions and mass error for the compound ion $[M+H]^+$ at *m/z* 515.3331.

Assigned ion (*m/z* 515.3331)		Theoretical $[M+H]^+$	Experimental $[M+H]^+$	Error (ppm)
	[M + H]	515.3332	515.3331	0.47
1	[M – H, OH]	497.3227	497.3239	-2.41
2	[M – C=O]	487.3383	487.3371	2.46
3	[M – C=O – H, OH]	469.3277	469.3275	0.43
4	[**3** – H, OH]	451.3172	451.3146	5.76
5	[M – Ser – H, OH]	410.2906	410.2909	-0.73
6	[M – $C_{13}H_{25}NO_5$]	276.1811	276.1823	-4.34
7	[**6** – H, OH]	258.1705	258.1679	10.07
8	[**7** – H, OH]	240.1600	240.1595	2.08
9	[**8** – C=O]	212.1650	212.1662	-5.66
10	[**8** – Ser]	153.1279	153.1276	1.96
11	[**6** – $C_{10}H_2O_2$]	106.0504	106.0499	4.71

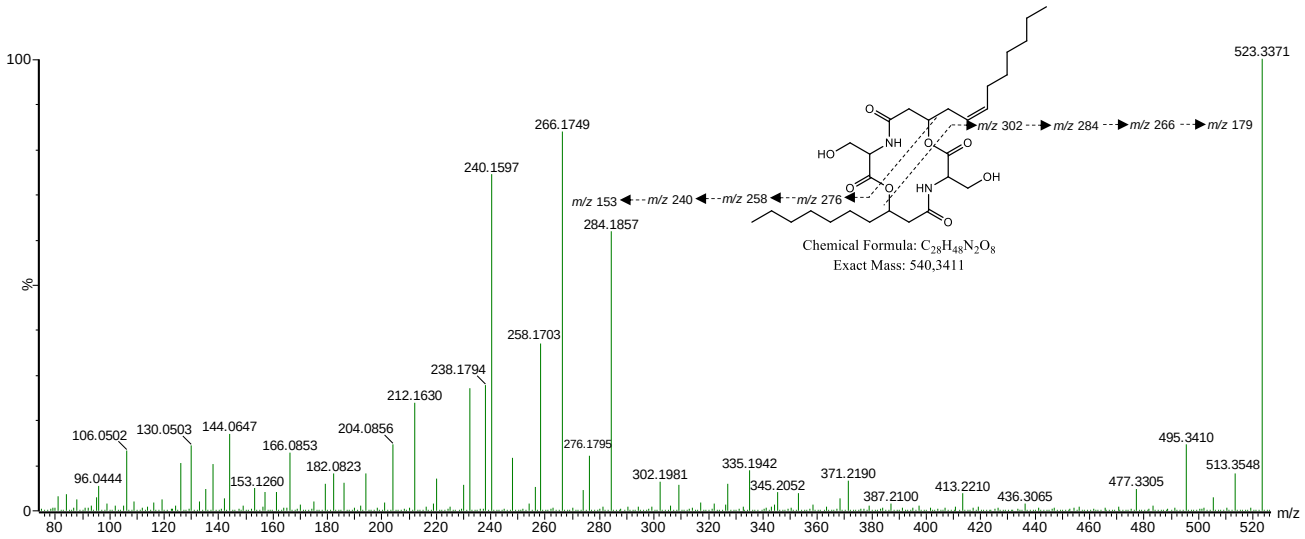

Fig. B4. Fragmentation profile and structure of the compound ion $[M+H]^+$ at *m/z* 541.3485.

Table B5. Summary of the theoretical and experimental fragmentation ions and mass error for the compound *m/z* 541.3485.

Assigned ion (*m/z* 541.3485)		Theoretical $[M+H]^+$	Experimental $[M+H]^+$	Error (ppm)
	[M + H]	541.3488	541.3485	0.55
1	[M – H, OH]	523.3384	523.3371	2.48
2	[M – C=O]	513.3540	513.3548	-1.56
3	[M – Ser – H, OH]	436.3063	436.3065	-0.46
4	[M – $C_{13}H_{25}NO_5$]	302.1967	302.1981	-4.63
5	[**4** – H, OH]	284.1862	284.1857	1.76
6	[**5** – H, OH]	266.1756	266.1749	2.63
7	[M – $C_{15}H_{27}NO_3$]	276.1811	276.1795	5.79
8	[**7** – H, OH]	258.1705	258.1703	0.77
9	[**8** – H, OH]	240.1599	240.1597	0.83
10	[**9** – C=O]	212.1650	212.1630	9.43
11	[**9** – Ser]	153.1279	153.1270	5.88
12	[**7** – $C_{10}H_2O_2$]	106.0504	106.0502	1.89
13	[**6** – Ser]	179.1436	179.1452	-8.93

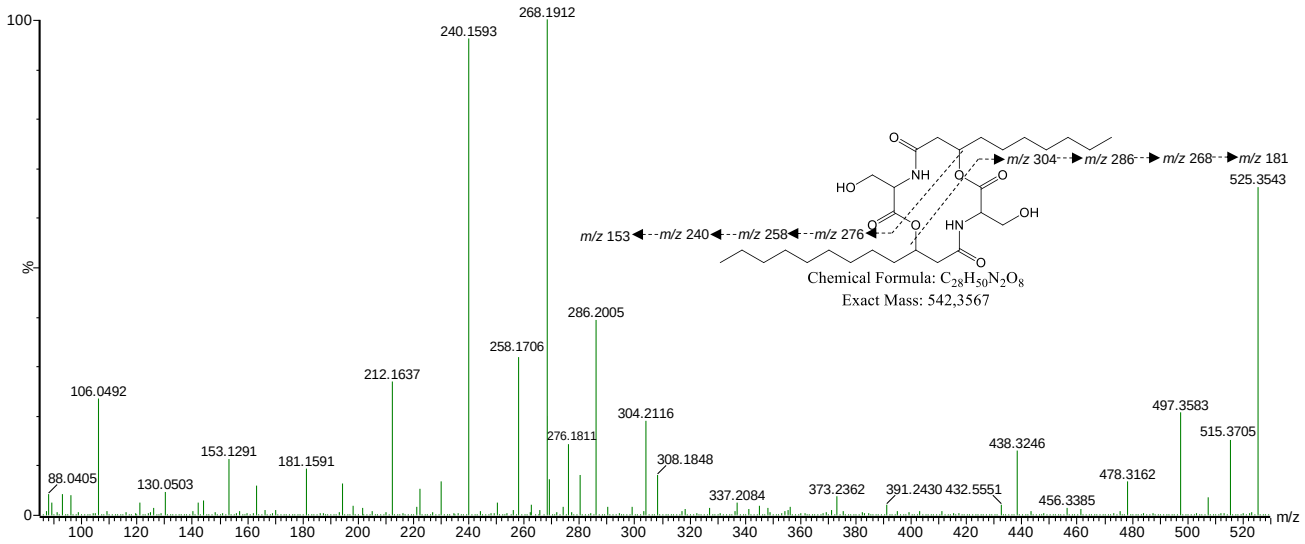

Fig. B5. Fragmentation profile and structure of the compound ion $[M+H]^+$ at *m/z* 543.3644.

Table B6. Summary of the theoretical and experimental fragmentation ions and mass error for the compound ion $[M+H]^+$ at *m/z* 543.3644.

Assigned ion (*m/z* 543.3644)		Theoretical $[M+H]^+$	Experimental $[M+H]^+$	Error (ppm)
	[M + H]	543.3645	543.3644	0.18
1	[M – H, OH]	525.3540	525.3543	-0.57
2	[M – C=O]	515.3696	515.3705	-1.75
3	[M – $C_{13}H_{25}NO_5$]	304.2124	304.2116	2.63
4	[**3** – H, OH]	286.2018	286.2005	4.54
5	[**4** – H, OH]	268.1912	268.1912	0.00
6	[M – $C_{15}H_{29}NO_3$]	276.1811	276.1811	0.00
7	[**6** – H, OH]	258.1705	258.1706	-0.39
8	[**7** – H, OH]	240.1599	240.1593	2.50
9	[**8** – C=O]	212.1650	212.1637	6.13
10	[**8** – Ser]	153.1279	153.1291	-7.84
11	[**6** – $C_{10}H_2O_2$]	106.0504	106.0492	11.32
12	[**5** – Ser]	181.1592	181.1591	0.55

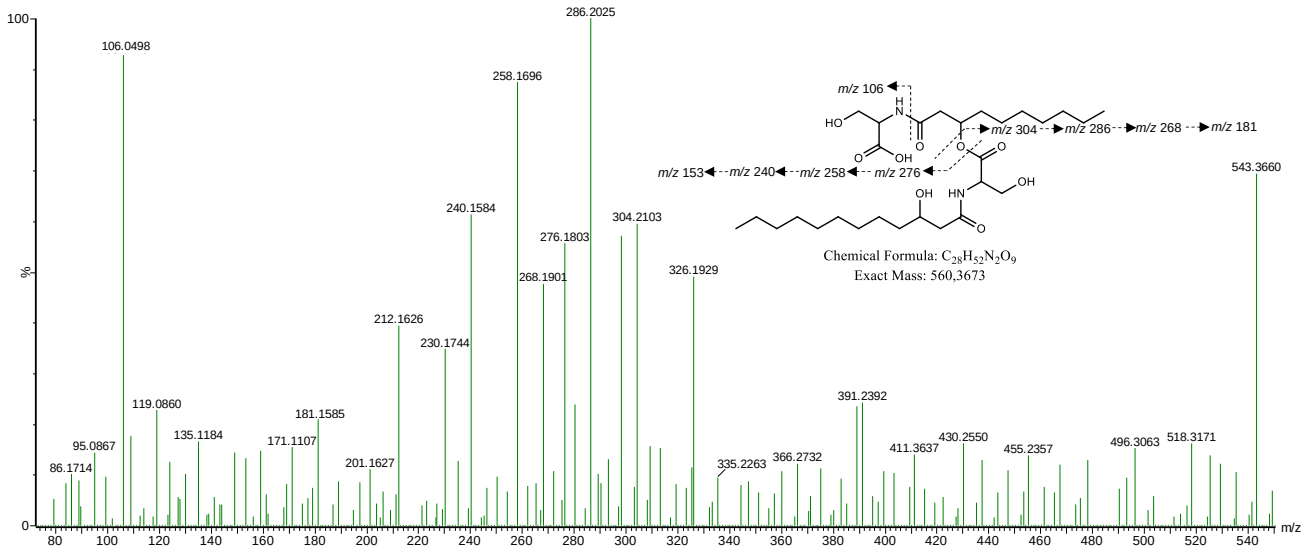

Fig. B6. Fragmentation profile and structure of the compound ion $[M+H]^+$ at *m/z* 561.3749.

Table B7. Summary of the theoretical and experimental fragmentation ions and mass error for the compound ion $[M+H]^+$ at *m/z* 561.3749.

Assigned ion (*m/z* 561.3749)		Theoretical $[M+H]^+$	Experimental $[M+H]^+$	Error (ppm)
	[M + H]	561.3754	561.3749	0.89
1	[M – H, OH]	543.3648	543.3660	-2.21
2	[M – $C_{15}H_{29}NO_5$]	304.2124	304.2103	6.90
3	[**2** – H, OH]	286.2019	286.2025	-2.10
4	[**3** – H, OH]	268.1913	268.1901	4.47
5	[M – $C_{16}H_{29}NO_4$]	276.1811	276.1803	2.90
6	[**5** – H, OH]	258.1706	258.1696	3.87
7	[**6** – H, OH]	240.1600	240.1584	6.66
8	[**8** – C=O]	212.1650	212.1626	11.31
9	[**7** – Ser]	153.1279	153.1275	2.61
10	[**5** – $C_{10}H_2O_2$]	106.0504	106.0498	5.66
11	[**4** – Ser]	181.1592	181.1585	3.86

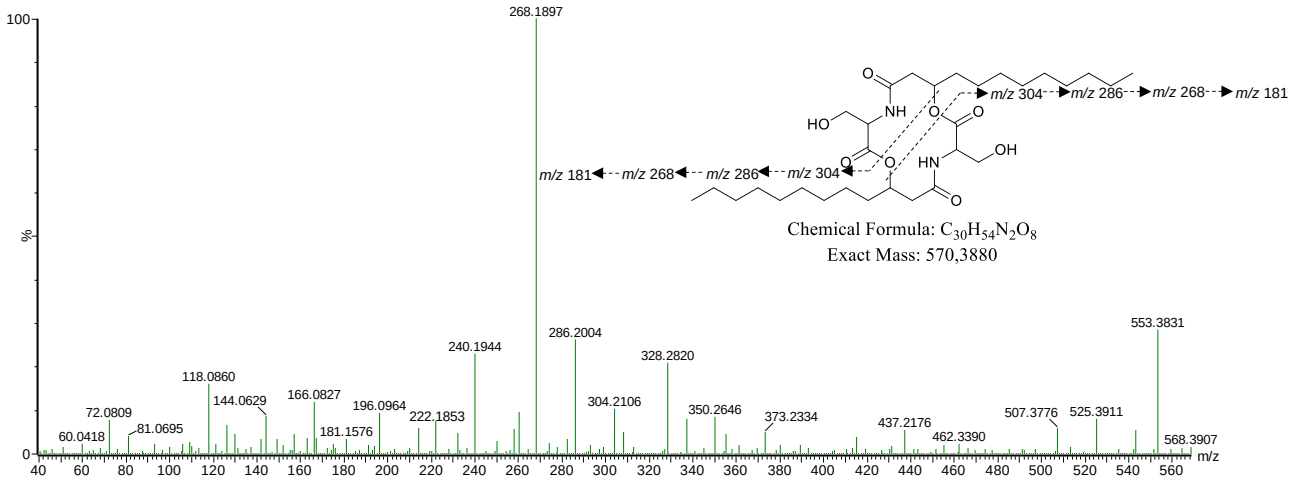

Fig. B7. Fragmentation profile and structure of the compound ion $[M+H]^+$ at *m/z* 571.3931.

Table B8. Summary of the theoretical and experimental fragmentation ions and mass error for the compound ion $[M+H]^+$ at *m/z* 571.3931.

Assigned ion (*m/z* 571.3931)		Theoretical $[M+H]^+$	Experimental $[M+H]^+$	Error (ppm)
	[M + H]	571.3958	571.3931	4.98
1	[M – H, OH]	553.3853	553.3831	3.98
2	[M – C=O – H, OH]	525.3903	525.3911	-1.52
3	[M – $C_{15}H_{29}NO_3$]	304.2124	304.2106	5.92
4	[**3** – H, OH]	286.2019	286.2004	5.24
5	[**4** – H, OH]	268.1913	268.1897	5.97
6	[**5** – C=O]	240.1964	240.1944	8.33
7	[**6** – H, OH]	222.1858	222.1853	2.25

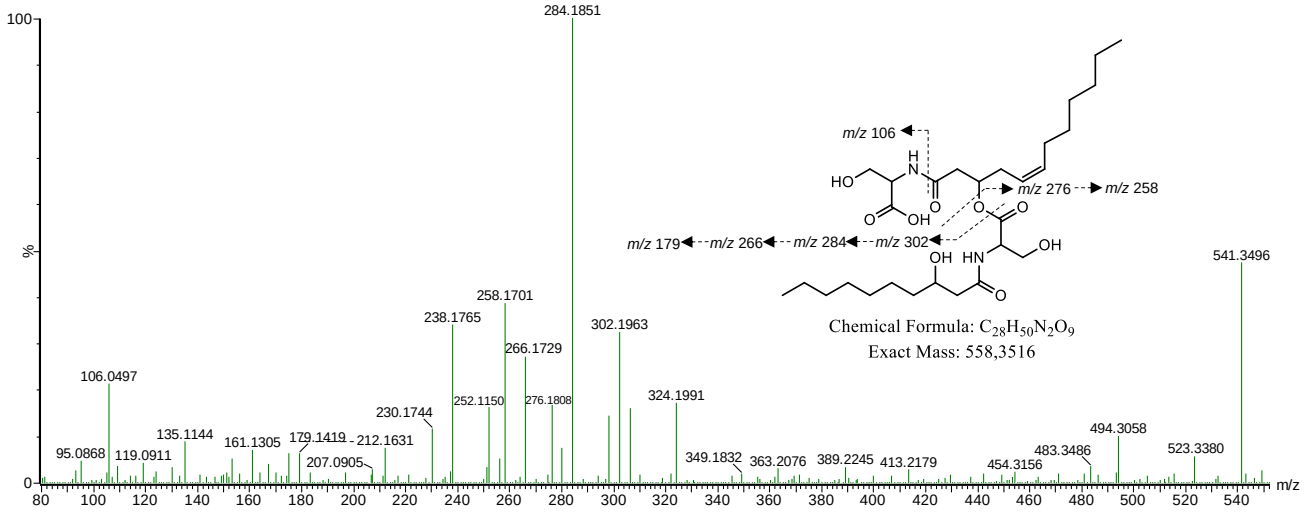

Fig. B8. Fragmentation profile and structure of the compound ion $[M+H]^+$ at *m/z* 559.3600.

Table B9. Summary of the theoretical and experimental fragmentation ions and mass error for the compound ion $[M+H]^+$ at *m/z* 559.3600.

Assigned ion (*m/z* 559.3600)		**Theoretical $[M+H]^+$**	**Experimental $[M+H]^+$**	**Error (ppm)**
	[M + H]	559.3594	559.3600	-1.03
1	[M – H, OH]	541.3489	541.3496	-1.29
2	[**1** – H, OH]	523.3383	523.3380	0.57
3	[M – Ser – H, OH]	454.3168	454.3156	2.64
4	[M – $C_{13}H_{25}NO_4$]	302.1967	302.1963	1.32
5	[**4** – H, OH]	284.1862	284.1851	3.87
6	[**5** – H, OH]	266.1756	266.1729	10.14
7	[M – $C_{15}H_{27}NO_4$]	276.1811	276.1808	1.09
8	[**7** – H, OH]	258.1705	258.1701	1.55
9	[**6** – Ser]	179.1436	179.1419	9.49
10	[**7** – $C_{10}H_2O_2$]	106.0504	106.0497	6.60

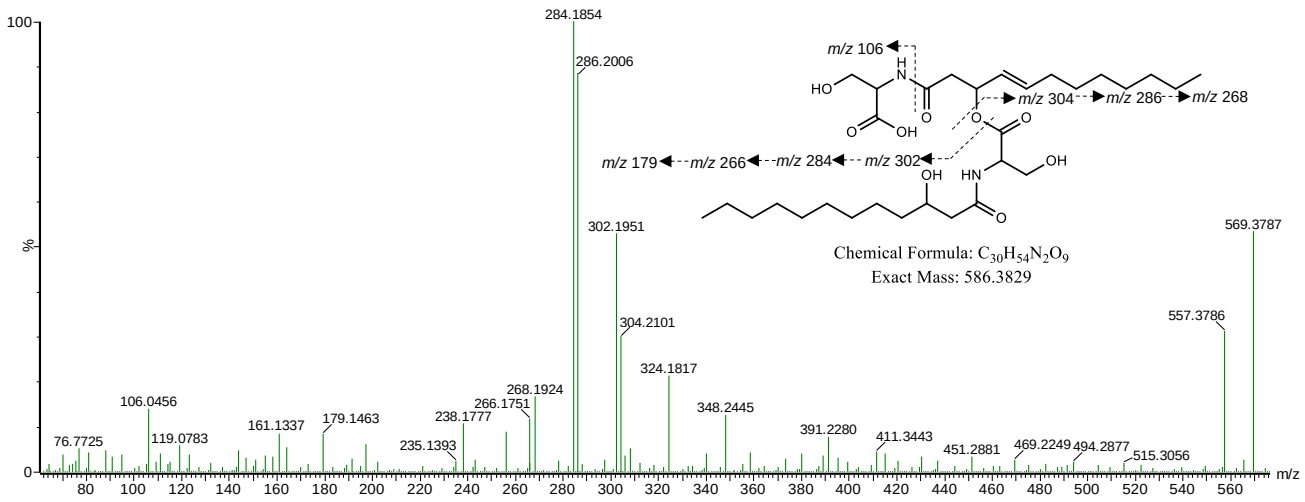

Fig. B9. Fragmentation profile and putative structure of the compound ion $[M+H]^+$ at *m/z* 587.3908.

Table B10. Summary of the theoretical and experimental fragmentation ions and mass error for the compound ion $[M+H]^+$ at *m/z* 587.3908.

Assigned ion (*m/z* 587.3908)		Theoretical $[M+H]^+$	Experimental $[M+H]^+$	Error (ppm)
	[M + H]	587.3907	587.3908	-0.13
1	[M – H, OH]	569.3802	569.3787	2.63
2	[M – $C_{15}H_{29}NO_4$]	302.1967	302.1951	5.29
3	[**2** – H, OH]	284.1862	284.1854	2.82
4	[**3** – H, OH]	266.1756	266.1751	1.88
5	[M – $C_{15}H_{27}NO_4$]	304.2124	304.2101	7.56
6	[**5** – H, OH]	286.2018	286.2006	4.19
7	[**6** – H, OH]	268.1912	268.1924	-4.47
8	[**4** – Ser]	179.1436	179.1463	0.0
9	[**8** – H, OH]	161.1330	161.1337	-4.34

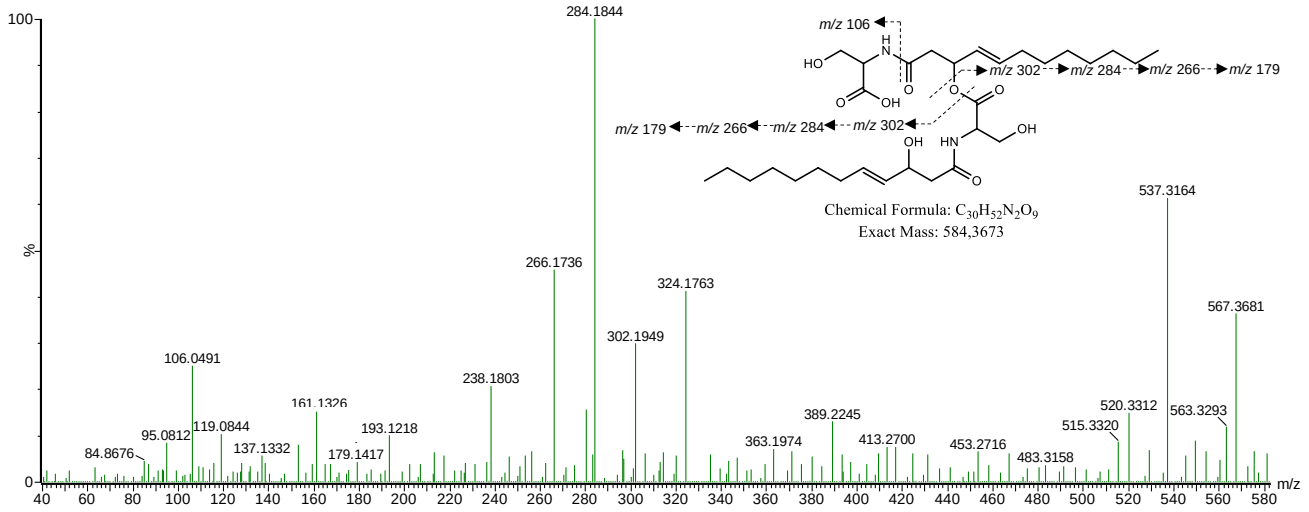

Fig. B10. Fragmentation profile and putative structure of the compound ion $[M+H]^+$ at *m/z* 585.3738.

Table B11. Summary of the theoretical and experimental fragmentation ions and mass error for the compound ion $[M+H]^+$ at *m/z* 585.3738.

Assigned ion (*m/z* 585.3738)		Theoretical $[M+H]^+$	Experimental $[M+H]^+$	Error (ppm)
	[M + H]	585.3751	585.3738	2.26
1	[M – H, OH]	567.3646	567.3681	-6.17
2	[M – $C_{15}H_{27}NO_4$]	302.1967	302.1949	5.96
3	[**2** – H, OH]	284.1862	284.1844	6.33
4	[**3** – H, OH]	266.1756	266.1736	7.51
5	[**4** – Ser]	179.1436	179.1417	10.61
6	[**5** – H, OH]	161.1330	161.1326	2.48

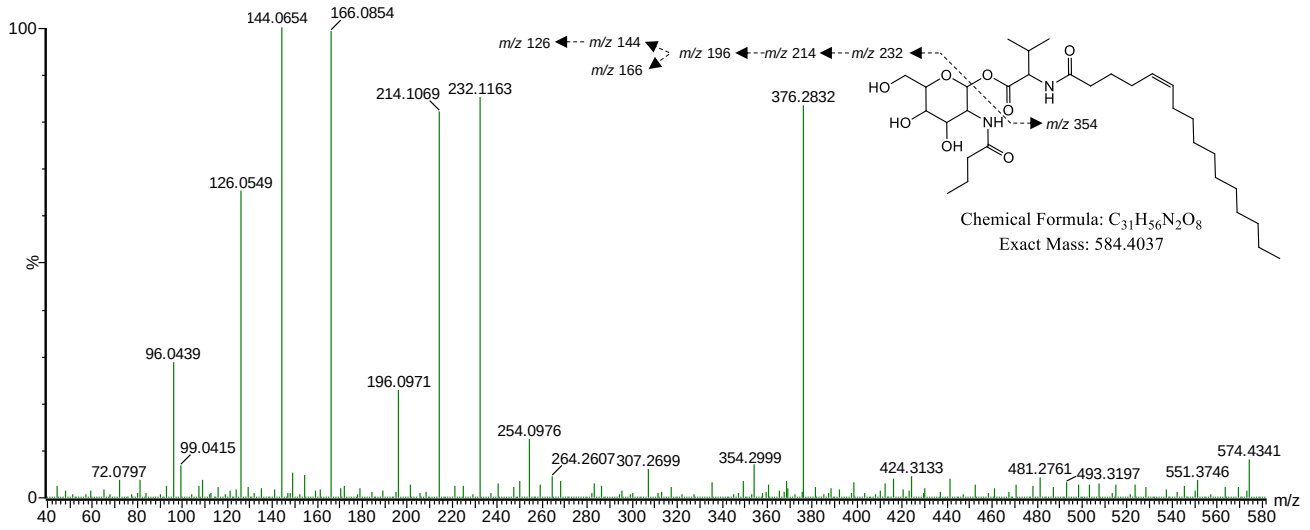

Fig. B11. Fragmentation profile and structure of the compound ion $[M+H]^+$ at *m/z* 585.4117.

Table B12. Summary of the theoretical and experimental fragmentation ions and mass error for the compound ion $[M+H]^+$ at *m/z* 585.4117.

Assigned ion (*m/z* 585.4117)		Theoretical $[M+H]^+$	Experimental $[M+H]^+$	Error (ppm)
	[M + H]	585.4115	585.4117	-0.30
1	[M – $C_{10}H_{17}NO_5$]	354.3008	354.2999	2.54
2	[**1** + Na – H]	376.2828	376.2832	-1.06
3	[M – $C_{21}H_{39}NO_3$]	232.1185	232.1163	9.48
4	[**3** – H, OH]	214.1079	214.1069	4.67
5	[**4** – H, OH]	196.0973	196.0971	1.02
6	[**4** – C_4H_6O]	144.0660	144.0654	4.16
7	[**6** – H, OH]	126.0555	126.0549	4.76
8	[**5** – CH_2O]	166.0868	166.0854	8.43

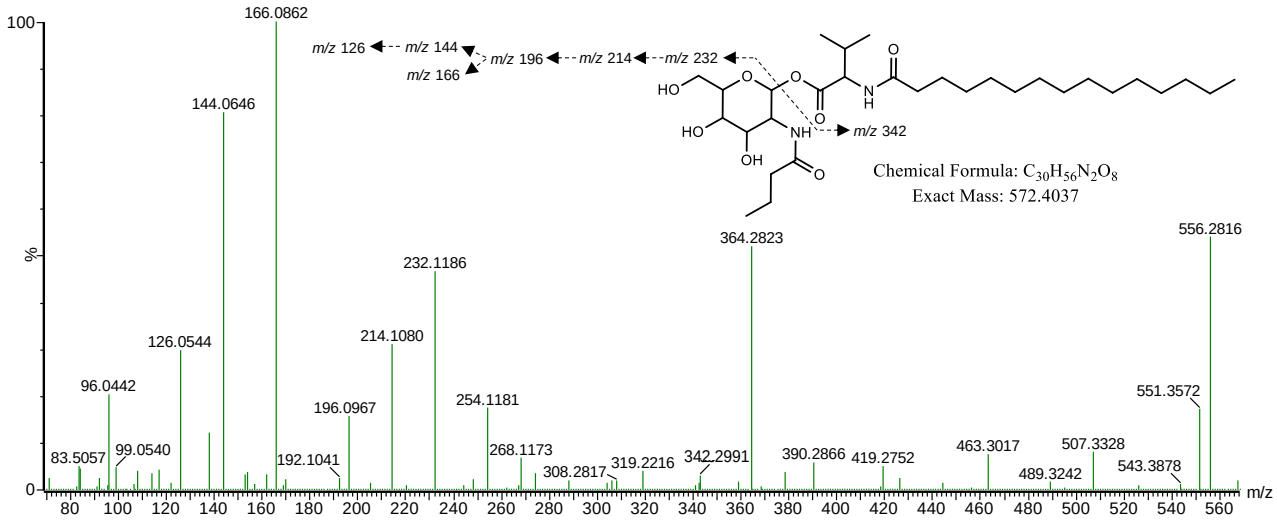

Fig. B12. Fragmentation profile and structure of the compound ion $[M+H]^+$ at *m/z* 573.4136.

Table B13. Summary of the theoretical and experimental fragmentation ions and mass error for the compound ion $[M+H]^+$ at *m/z* 573.4136.

Assigned ion (*m/z* 573.4136)		Theoretical $[M+H]^+$	Experimental $[M+H]^+$	Error (ppm)
	[M]	573.4115	573.4136	-3.66
1	[M - $C_{10}H_{17}NO_5$]	342.3008	342.2991	4.97
2	[**1** + Na - H]	364.2828	364.2823	1.37
3	[M - $C_{20}H_{39}NO_3$]	232.1185	232.1186	-0.43
4	[**3** - H_2O]	214.1079	214.1080	-0.47
5	[**4** - H_2O]	196.0973	196.0967	3.06
6	[**4** – C_4H_6O]	144.0660	144.0646	9.72
7	[**6** – H, OH]	126.0555	126.0544	8.73
8	[**5** – CH_2O]	166.0868	166.0862	3.61

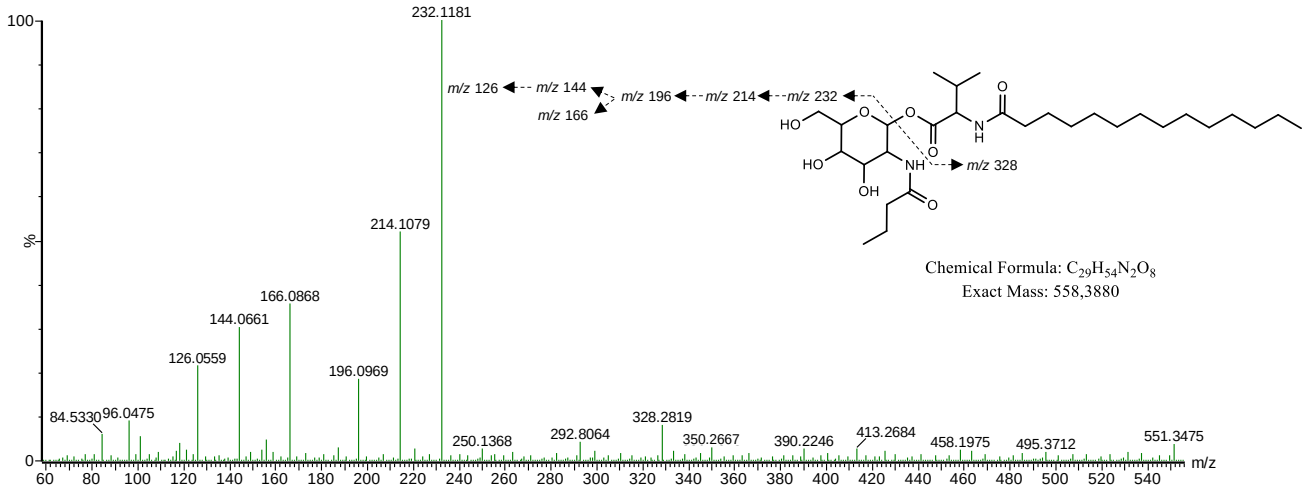

Fig. B13. Fragmentation profile and structure of the compound ion $[M+H]^+$ at *m/z* 559.3953.

Table B14. Summary of the theoretical and experimental fragmentation ions and mass error for the compound ion $[M+H]^+$ at *m/z* 559.3953.

Assigned ion (*m/z* 559.3953)		Theoretical $[M+H]^+$	Experimental $[M+H]^+$	Error (ppm)
	[M + H]	559.3958	559.3953	0.89
1	[M – $C_{10}H_{17}NO_5$]	328.2851	328.2819	9.75
2	[**1** + Na – H]	350.2671	350.2667	1.14
3	[M – $C_{19}H_{37}NO_3$]	232.1185	232.1181	1.72
4	[**3** – H, OH]	214.1079	214.1079	0.00
5	[**4** – H, OH]	196.0973	196.0969	2.04
6	[**4** – C_4H_6O]	144.0660	144.0661	-0.69
7	[**6** – H, OH]	126.0555	126.0559	-3.17
8	[**5** – CH_2O]	166.0868	166.0868	0.00

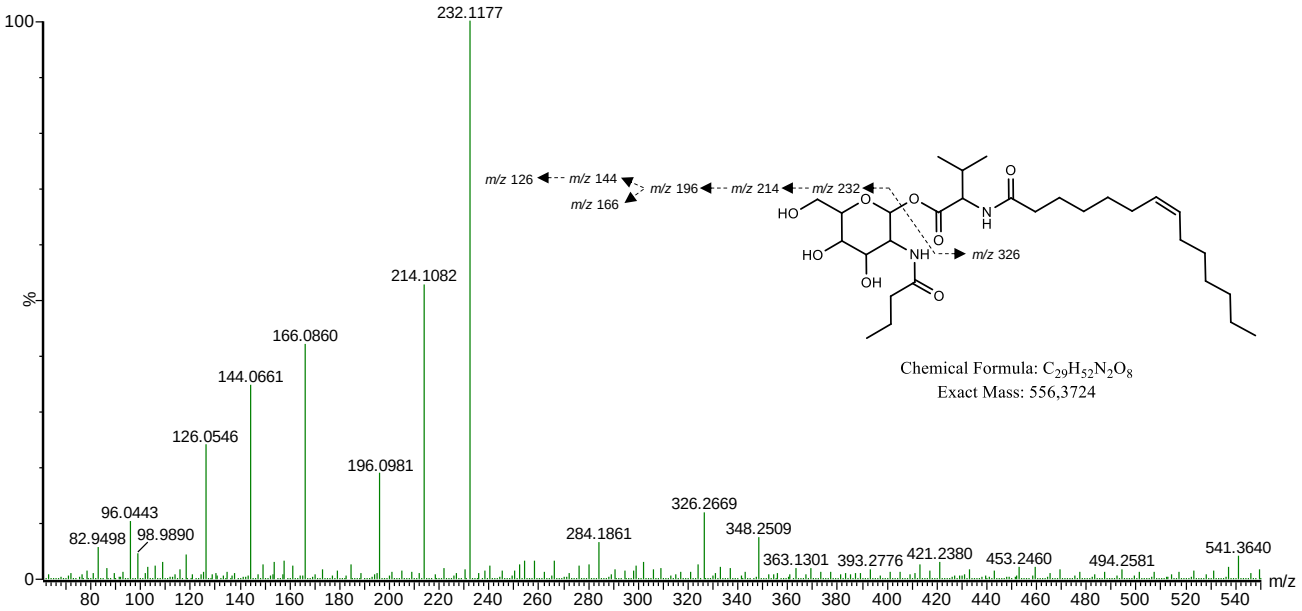

Fig. B14. Fragmentation profile and putative structure of the compound ion $[M+H]^+$ at *m/z* 557.3804.

Table B15. Summary of the theoretical and experimental fragmentation ions and mass error for the compound ion $[M+H]^+$ at *m/z* 557.3804.

Assigned ion (*m/z* 557.3804)		Theoretical $[M+H]^+$	Experimental $[M+H]^+$	Error (ppm)
	[M + H]	557.3802	557.3804	-0.31
1	[M – $C_{10}H_{17}NO_5$]	326.2695	326.2669	7.97
2	[**1** + Na – H]	348.2515	348.2509	1.72
3	[M – $C_{19}H_{35}NO_3$]	232.1185	232.1177	3.45
4	[**3** – H, OH]	214.1079	214.1082	-1.40
5	[**4** – H, OH]	196.0973	196.0981	-4.08
6	[**4** – C_4H_6O]	144.0660	144.0661	-0.69
7	[**6** – H, OH]	126.0555	126.0546	7.14
8	[**5** – CH_2O]	166.0868	166.0860	4.82

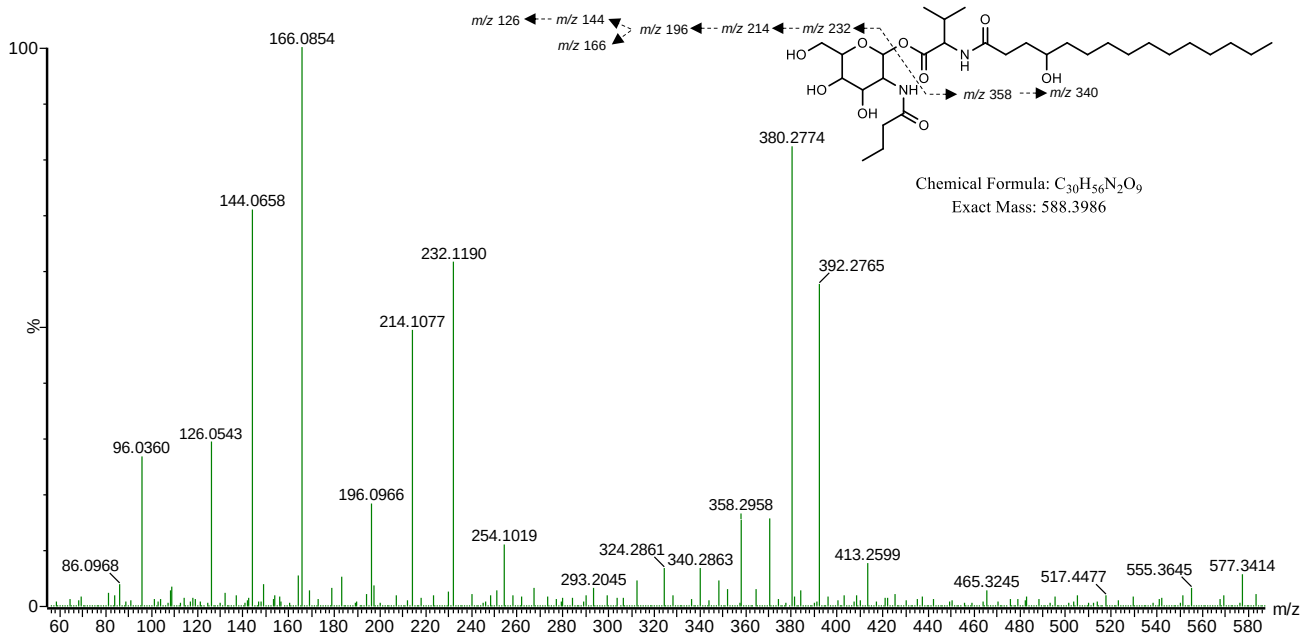

Fig. B15. Fragmentation profile and putative structure of the compound ion $[M+H]^+$ at *m/z* 589.4056.

Table B16. Summary of the theoretical and experimental fragmentation ions and mass error for the compound ion $[M+H]^+$ at *m/z* 589.4056.

Assigned ion (*m/z* 589.4056)		Theoretical $[M+H]^+$	Experimental $[M+H]^+$	Error (ppm)
	[M + H]	589.4064	589.4056	1.40
1	[M – $C_{10}H_{17}NO_5$]	358.2957	358.2958	-0.28
2	[**1** – H, OH]	340.2851	340.2863	-3.53
3	[**1** + Na – H]	380.2777	380.2774	0.79
4	[M – $C_{20}H_{39}NO_4$]	232.1185	232.1190	-2.15
5	[**4** – H, OH]	214.1079	214.1077	0.93
6	[**5** – H, OH]	196.0973	196.0966	3.57
7	[**5** – C_4H_6O]	144.0660	144.0658	1.39
8	[**7** – H, OH]	126.0555	126.0543	9.52
9	[**6** – CH_2O]	166.0868	166.0854	8.43

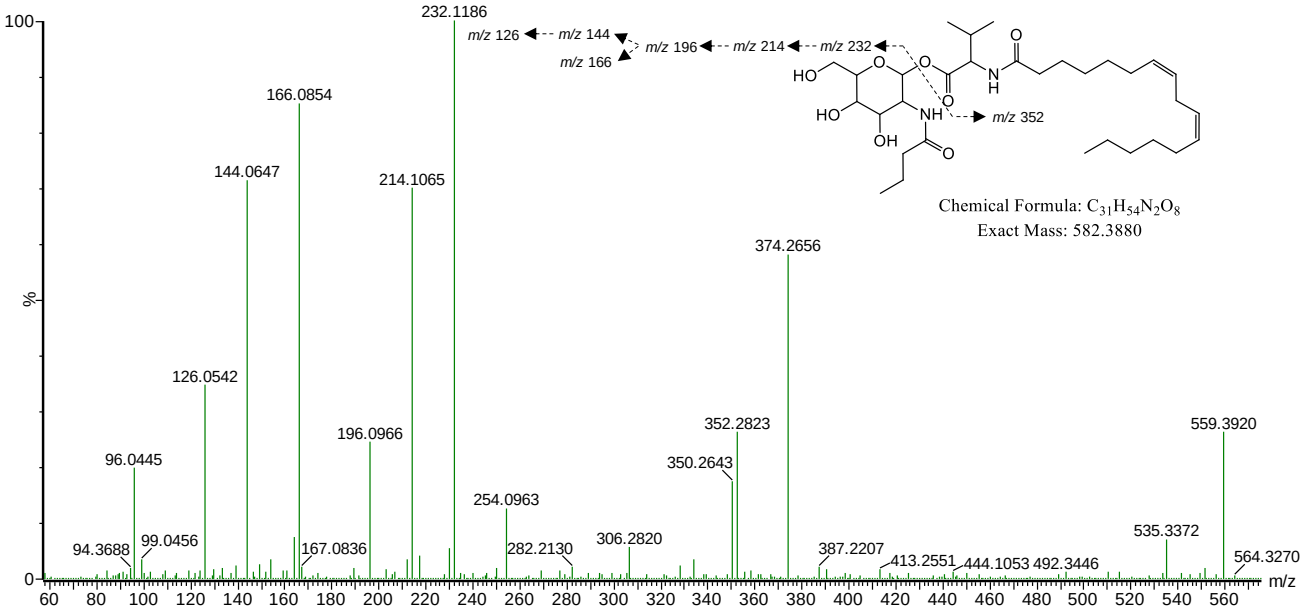

Fig. B16. Fragmentation profile and putative structure of the compound ion $[M+H]^+$ at *m/z* 583.3947.

Table B17. Summary of the theoretical and experimental fragmentation ions and mass error for the compound ion $[M+H]^+$ at *m/z* 583.3947.

Assigned ion (*m/z* 583.3947)		Theoretical $[M+H]^+$	Experimental $[M+H]^+$	Error (ppm)
	[M + H]	583.3958	583.3947	2.13
1	[M – $C_{10}H_{17}NO_5$]	352.2851	352.2823	7.95
2	[**1** + Na – H]	374.2671	374.2656	4.01
3	[M – $C_{21}H_{37}NO_3$]	232.1185	232.1186	-0.43
4	[**3** – H, OH]	214.1079	214.1065	6.54
5	[**4** – H, OH]	196.0973	196.0966	3.57
6	[**4** – C_4H_6O]	144.0660	144.0647	9.02
7	[**6** – H, OH]	126.0555	126.0542	10.31
8	[**5** – CH_2O]	166.0868	166.0854	8.43

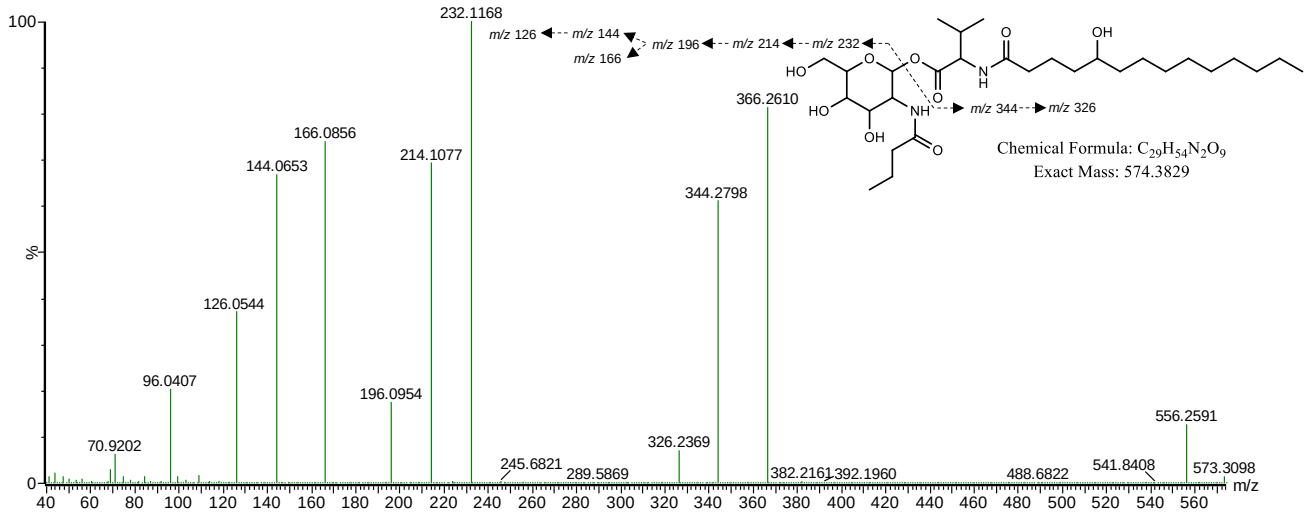

Fig. B17. Fragmentation profile and putative structure of the compound ion $[M+H]^+$ at *m/z* 575.3902.

Table B18. Summary of the theoretical and experimental fragmentation ions and mass error for the compound ion $[M+H]^+$ at *m/z* 575.3902.

Assigned ion (*m/z* 575.3902)		Theoretical $[M+H]^+$	Experimental $[M+H]^+$	Error (ppm)
	[M + H]	575.3907	575.3902	0.91
1	[M – $C_{10}H_{17}NO_5$]	344.2801	344.2798	0.87
2	[**1** + Na – H]	366.2621	366.2610	3.00
3	[M – $C_{19}H_{37}NO_4$]	232.1185	232.1168	7.32
4	[**3** – H, OH]	214.1079	214.1077	0.93
5	[**4** – H, OH]	196.0973	196.0954	9.69
6	[**4** – C_4H_6O]	144.0660	144.0653	4.86
7	[**6** – H, OH]	126.0555	126.0544	8.73
8	[**5** – CH_2O]	166.0868	166.0856	7.23
9	[**1** – H, OH]	326.2695	326.2694	0.38

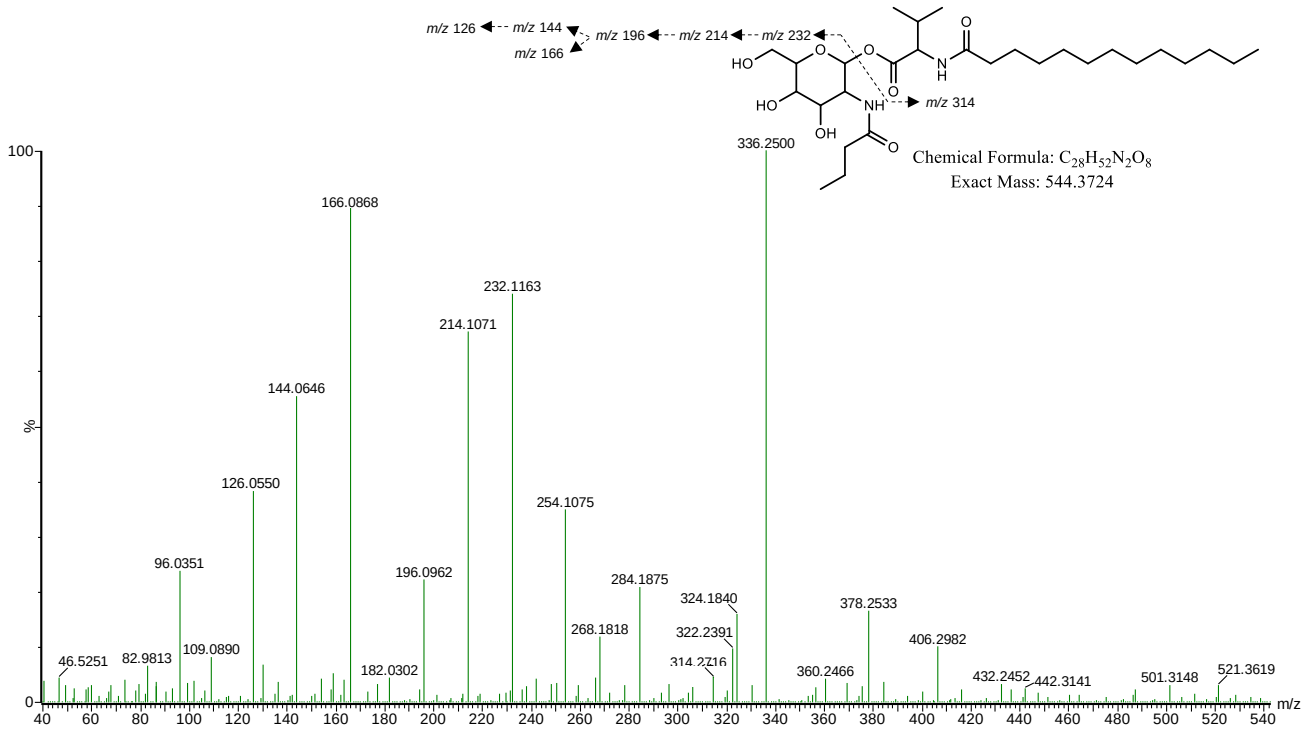

Fig. B18. Fragmentation profile and putative structure of the compound ion $[M+H]^+$ at *m/z* 545.3787.

Table B19. Summary of the theoretical and experimental fragmentation ions and mass error for the compound ion $[M+H]^+$ at *m/z* 545.3787.

Assigned ion (*m/z* 545.3787)		Theoretical $[M+H]^+$	Experimental $[M+H]^+$	Error (ppm)
	[M + H]	545.3802	545.3787	2.75
1	[M – $C_{10}H_{17}NO_5$]	314.2695	314.2716	-6.68
2	[**1** + Na – H]	336.2515	336.2500	4.46
3	[M – $C_{18}H_{35}NO_3$]	232.1185	232.1163	9.48
4	[**3** – H, OH]	214.1079	214.1071	3.74
5	[**4** – H, OH]	196.0973	196.0962	5.61
6	[**4** – C_4H_6O]	144.0660	144.0646	9.72
7	[**6** – H, OH]	126.0555	126.0550	3.97
8	[**5** – CH_2O]	166.0868	166.0868	0.00

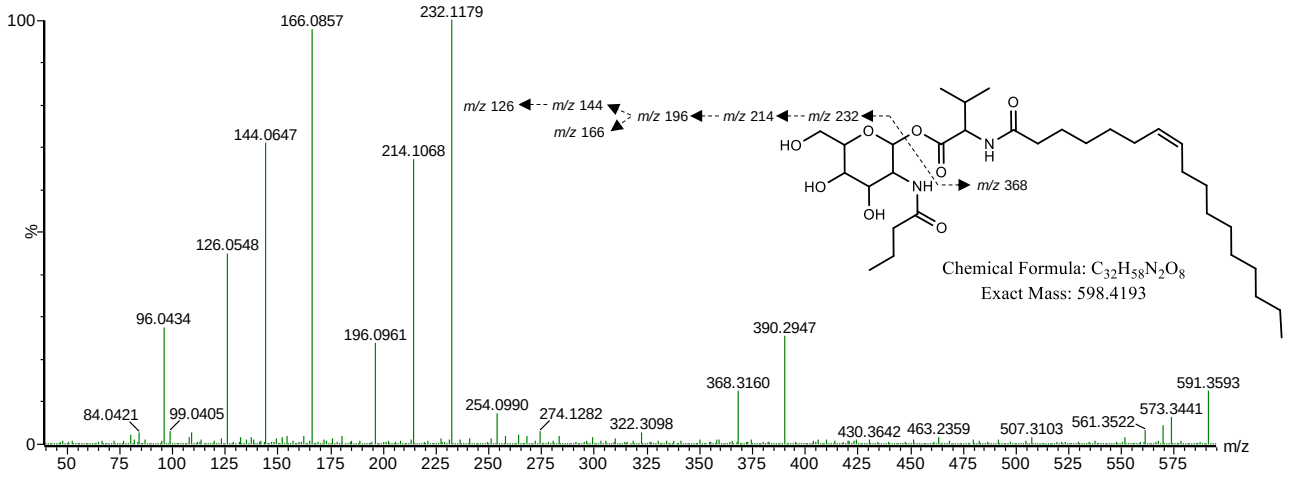

Fig. B19. Fragmentation profile and putative structure of the compound ion $[M+H]^+$ at *m/z* 599.4265.

Table B20. Summary of the theoretical and experimental fragmentation ions and mass error for the compound ion $[M+H]^+$ at *m/z* 599.4265.

Assigned ion (*m/z* 599.4265)		Theoretical $[M+H]^+$	Experimental $[M+H]^+$	Error (ppm)
	[M + H]	599.4271	599.4265	1.04
1	[M – $C_{10}H_{17}NO_5$]	368.3164	368.3160	1.09
2	[**1** + Na – H]	390.2984	390.2947	9.48
3	[M – $C_{22}H_{41}NO_3$]	232.1185	232.1179	2.58
4	[**3** – H, OH]	214.1079	214.1068	5.14
5	[**4** – H, OH]	196.0973	196.0961	6.12
6	[**4** – C_4H_6O]	144.0660	144.0647	9.02
7	[**6** – H, OH]	126.0555	126.0548	5.55
8	[**5** – CH_2O]	166.0868	166.0857	6.62

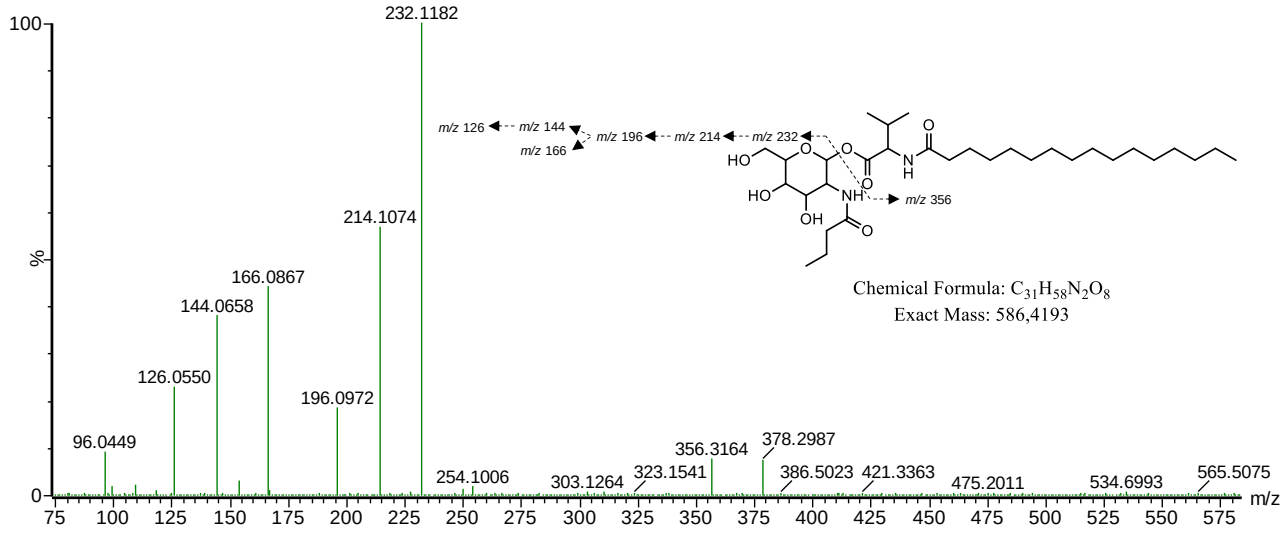

Fig. B20. Fragmentation profile and putative structure of the compound ion $[M+H]^+$ at *m/z* 587.4268.

Table B21. Summary of the theoretical and experimental fragmentation ions and mass error for the compound ion $[M+H]^+$ at *m/z* 587.4268.

Assigned ion (*m/z* 587.4268)		Theoretical $[M+H]^+$	Experimental $[M+H]^+$	Error (ppm)
	[M + H]	587.4271	587.4268	0.55
1	[M – $C_{10}H_{17}NO_5$]	356.3164	356.3164	0.00
2	[**1** + Na – H]	378.2984	378.2987	-0.79
3	[M – $C_{21}H_{41}NO_3$]	232.1185	232.1182	1.29
4	[**3** – H, OH]	214.1079	214.1074	2.34
5	[**4** – H, OH]	196.0973	196.0972	0.51
6	[**4** – C_4H_6O]	144.0660	144.0658	1.39
7	[**6** – H, OH]	126.0555	126.0550	3.97
8	[**5** – CH_2O]	166.0868	166.0867	0.60

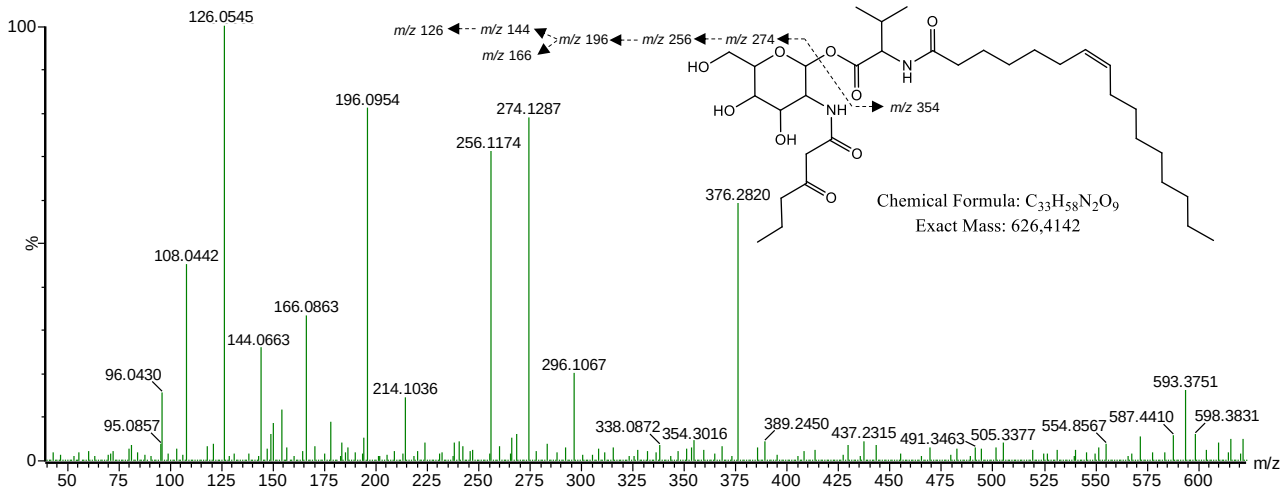

Fig. B21. Fragmentation profile and putative structure of the compound ion $[M+H]^+$ at *m/z* 627.4192.

Table B22. Summary of the theoretical and experimental fragmentation ions and mass error for the compound ion $[M+H]^+$ at *m/z* 627.4192.

Assigned ion (*m/z* 627.4192)		**Theoretical $[M+H]^+$**	**Experimental $[M+H]^+$**	**Error (ppm)**
	[M + H]	627.4220	627.4192	4.46
1	[M – $C_{12}H_{19}NO_6$]	354.3008	354.3016	-2.26
2	[**1** + Na – H]	376.2828	376.2820	2.13
3	[M – $C_{21}H_{39}NO_3$]	274.1290	274.1287	1.09
4	[**3** – H, OH]	256.1185	256.1174	4.29
5	[**4** – C_4H_6O]	144.0660	144.0663	-2.08
6	[**5** – H, OH]	126.0555	126.0545	7.93

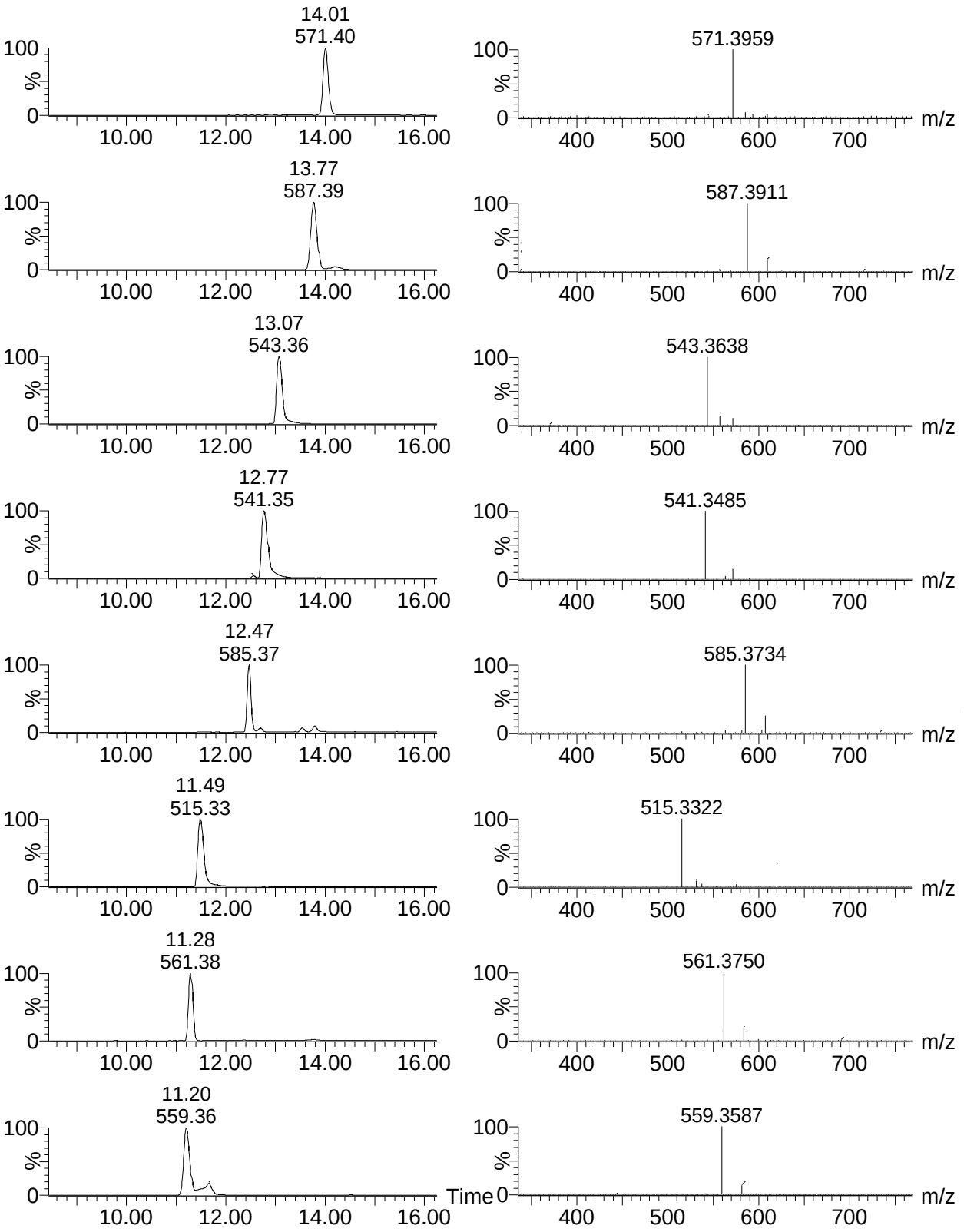

Fig. B22. The UPLC profiles (left panel) and ESI-MS spectra (right panel) of the serratamolide homologues produced by P1 and/or NP1 strains (representatives from both strains).

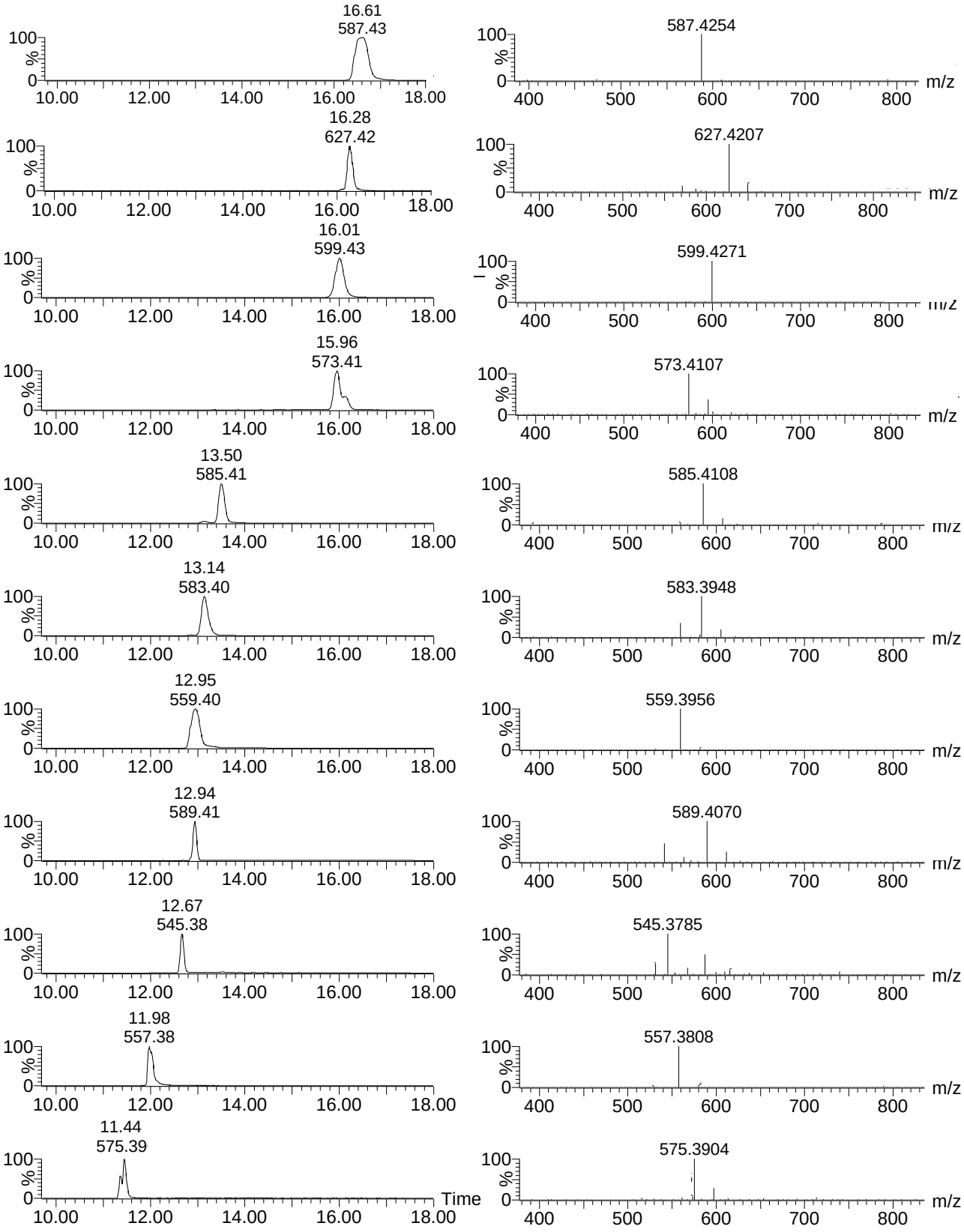

Fig. B23. The UPLC profiles (left panel) and ESI-MS spectra (right panel) of the glucosamine derivative homologues produced by P1 and/or NP1 strains (representatives from both strains).

Appendix C

Biofilm disruption and antiadhesive activity of secondary metabolites produced by *Serratia marcescens* strains

Tanya Clements[a], Thando Ndlovu[a], Nusrat Begum[b] and Wesaal Khan[a*]

[a] Department of Microbiology, Faculty of Science, Stellenbosch University, Private Bag X1, Stellenbosch, 7602, South Africa

[b] Department of Chemistry and Polymer Science, Faculty of Science, Stellenbosch University, Private Bag X1, Stellenbosch, 7602, South Africa

*Corresponding Author: Wesaal Khan; Phone: +27 21 808 5804; E-mail: wesaal@sun.ac.za

Table C1. The efficiency and linear regression coefficient values for the qPCR analysis conducted during the MBEC Assay® analysis and the antifouling analysis of the coated polymers.

Assay used prior to qPCR analysis	**Microorganism**	**qPCR efficiency range for BD and AD***	**Linear regression coefficient (R^2) value**
MBEC Assay® (Innovotech)	*Enterococcus* spp.	2.07 (103.5%) - 2.08 (104%)	1.00
	Pseudomonas spp.	1.88 (94%) - 1.96 (98%)	0.98 - 1.00
Antifouling Activity of Crude Extract-immobilised Polymers	*Enterococcus* spp.	2.03 (101.5%)	1.00
	Pseudomonas spp.	1.96 (98%)	1.00

*BD – biofilm disruption; AD – antiadhesive